



Title	Studies on Cooperative Organometallic Catalysis for Organic Synthesis
Author(s)	Rawat, Vishal Kumar
Citation	北海道大学. 博士(理学) 甲第15197号
Issue Date	2022-09-26
DOI	10.14943/doctoral.k15197
Doc URL	http://hdl.handle.net/2115/87224
Type	theses (doctoral)
File Information	RAWAT_Vishal_Kumar.pdf



[Instructions for use](#)

**Studies on Cooperative Organometallic
Catalysis for Organic Synthesis**

有機合成への応用を指向する協働作用触媒に
関する研究

Vishal Kumar Rawat

2022

Contents

General introduction	1
Chapter 1	31
Use of Imidazo[1,5-a]pyridin-3-ylidene as a Platform for Metal-Imidazole Cooperative Catalysis: Silver-Catalyzed Cyclization of Alkyne-Tethered Carboxylic Acids	
Chapter 2	70
Construction of Heterobimetallic Catalytic Scaffold with a Carbene-Bipyridine Ligand: Gold-Zinc Two-Metal Catalysis for Intermolecular Addition of <i>O</i> -Nucleophiles to Non-activated Alkynes	
Chapter 3	121
Nickel-catalyzed Homo-coupling of Aryl Ethers with Magnesium Anthracene Reductant	
Publications	143
Acknowledgement	144

General Introduction

1. Cooperative Catalysis

Looking at the synthetic point of view, catalytic reactions have gained much attention for the synthesis of organic compounds which has applications in organic, pharmaceutical, agrochemical and material chemistry. Catalysts facilitate the reactivity of non-activated or lower reactive reagents, offering high chemoselective organic transformations which reduce the formation of by-products to achieve high atom economy.

Cooperative catalysts consist of two or more active sites which individually activate multiple sites of a reactant or multiple reactants at the same time.¹ Cooperative catalysts not only increase the rate of reaction but also increase the reactivity of non-activated substrates. Such cooperativity of multiple active sites are common in enzymatic reactions. For example, 'kidney bean acid phosphatase' contains a heterobimetallic Fe-Zn complex which efficiently promotes phosphate hydrolysis reaction (Figure 1).² Coordination of Lewis acidic participation of the zinc metal enhances the electrophilicity of the phosphate ester while the Brønsted base site on the iron atom increases the nucleophilicity of hydroxide anion, facilitating hydrolysis reaction.

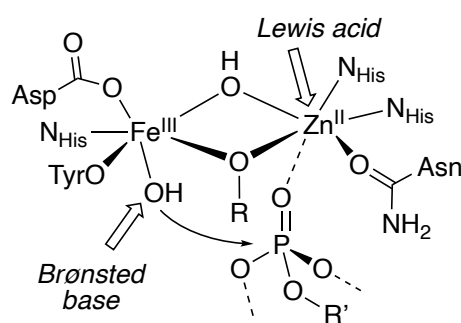


Figure 1. Enzyme cooperativity in hydrolysis reaction.

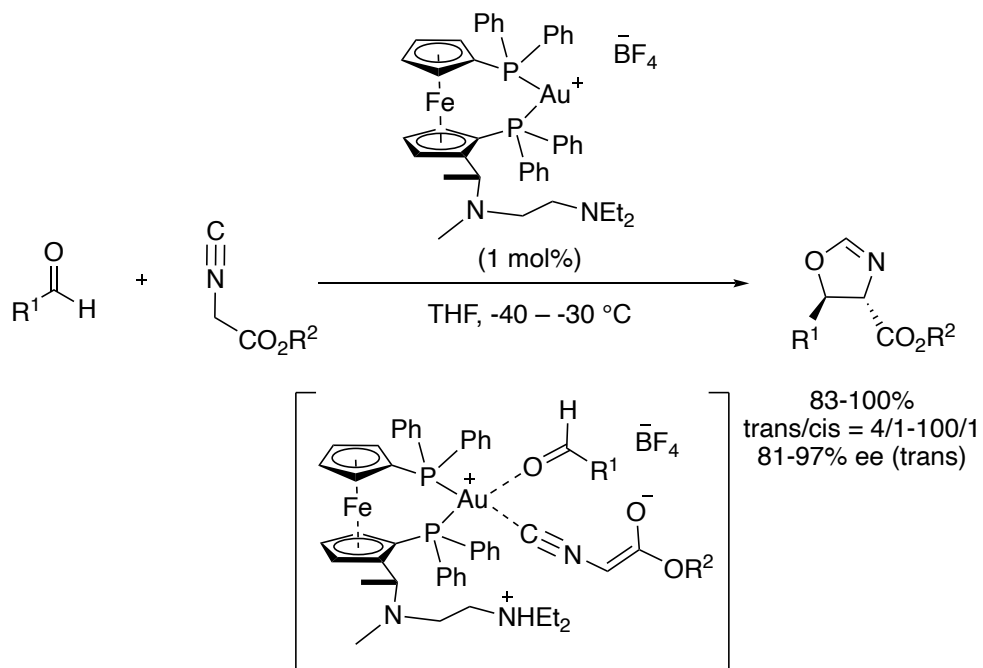
A drawback of enzyme catalysis on the application to organic synthesis is the strictness in the substrate specificity. Hence, it is demanded to design the artificial cooperative systems which is flexible with different diversity of substrates for variety of organic transformation. Various kinds of artificial cooperative organometallic catalysts and organo-catalysts have been explored. In terms of substrate compatibility and versatility of reaction types, organometallic catalysts are attractive for preparing target molecules.

2. Cooperative Organometallic Catalysis

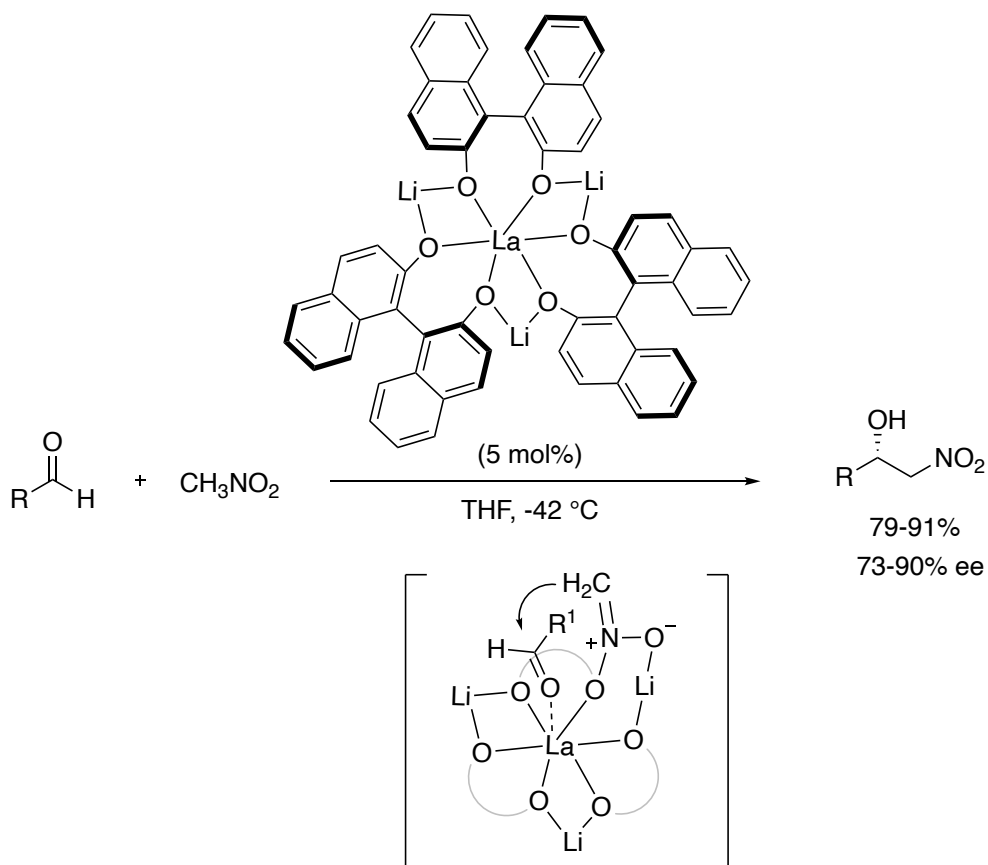
Many of the chemical transformations have been achieved by using cooperative organometallic catalysts. The cooperative organometallic catalysts are categorized into metal-organo cooperative catalysts and bimetallic catalysts. In metal-organo catalysis, one of the active sites is a metal and the other is an organic molecule or a functional group. In bimetallic cooperative catalysis, both active sites are constructed with metals, and they simultaneously activate substrate molecules, individually.

As the pioneering work of cooperative catalysts, Ito, Sawamura, and Hayashi demonstrated asymmetric aldol reaction for synthesizing substituted oxazolines in high enantioselectivity and high yield from aldehydes and isocyanoacetate with designed gold complex bearing the amine group which cooperatively activate the substrates (Figure 2a).³ Shibasaki and his coworkers achieved the broad utility of Lewis acid-Brønsted base cooperative heterobimetallic catalysis by showing variety of catalytic asymmetric transformations.⁴ Especially, the early chemical transformation was asymmetric nitroaldol reaction with heterobimetallic catalysts, which was constructed with La and Li metals on binol ligands (Figure 2b).⁵ In the catalyst system, La promoted the activation of aldehydes and the activation of nitromethane through binol oxygen anion on Li. Shibasaki and co-workers also developed Lewis acid-Lewis base cooperative catalysts that consist of a Lewis acid aluminum metal and a phosphine oxide as a Lewis base. The complex cooperatively promoted the silyl-cyation of aldehydes in high enantioselectivity (Figure 2c).⁶ After these pioneering work, cooperative catalysis has been regarded as one of the most powerful tools for organic transformations, and hence various kinds of cooperative catalysts have been explored by using designed metal-organo and bimetallic catalytic systems.⁷

(a) asymmetric aldol reaction



(b) asymmetric nitroaldol reaction



(c) *asymmetric cyanosilylation*

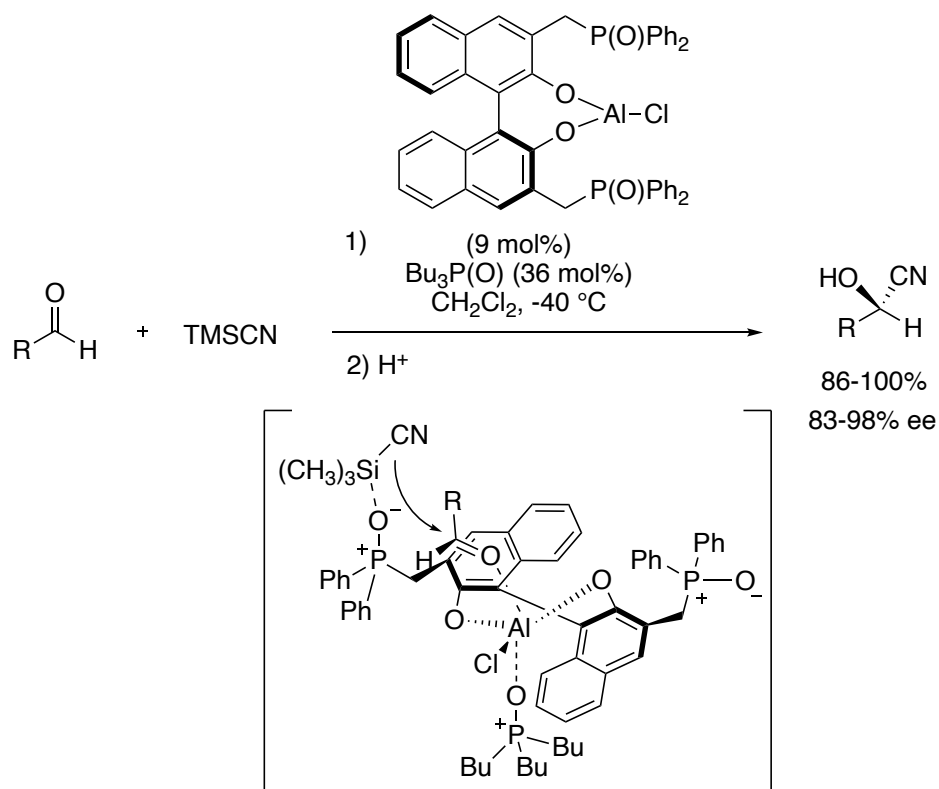


Figure 2. Cooperative catalysis in asymmetric aldol, nitroaldol and cyano-silylation reaction.

3. Cooperative Catalysis in Alkyne Activation

Cooperative catalysis has been proven an outstanding versatility in various types of organic transformations. The organic transformations from the alkyne substrates give valuable synthetic utility products.⁸ Especially, the nucleophilic addition reaction towards alkynes with a designed cooperative system is attractive in terms of achieving high activity and selectivity. The transformation of alkynes is promoted by soft Lewis acids like Pd, Au, Ag, Hg, Co, and Pt, and the simultaneous nucleophilic additions are possible through either Lewis base or Brønsted base catalysts. The cooperative catalysis in nucleophilic addition of alkynes can be divided into two categories:

1. Metal-organo cooperative catalysis
2. Bimetallic cooperative catalysis

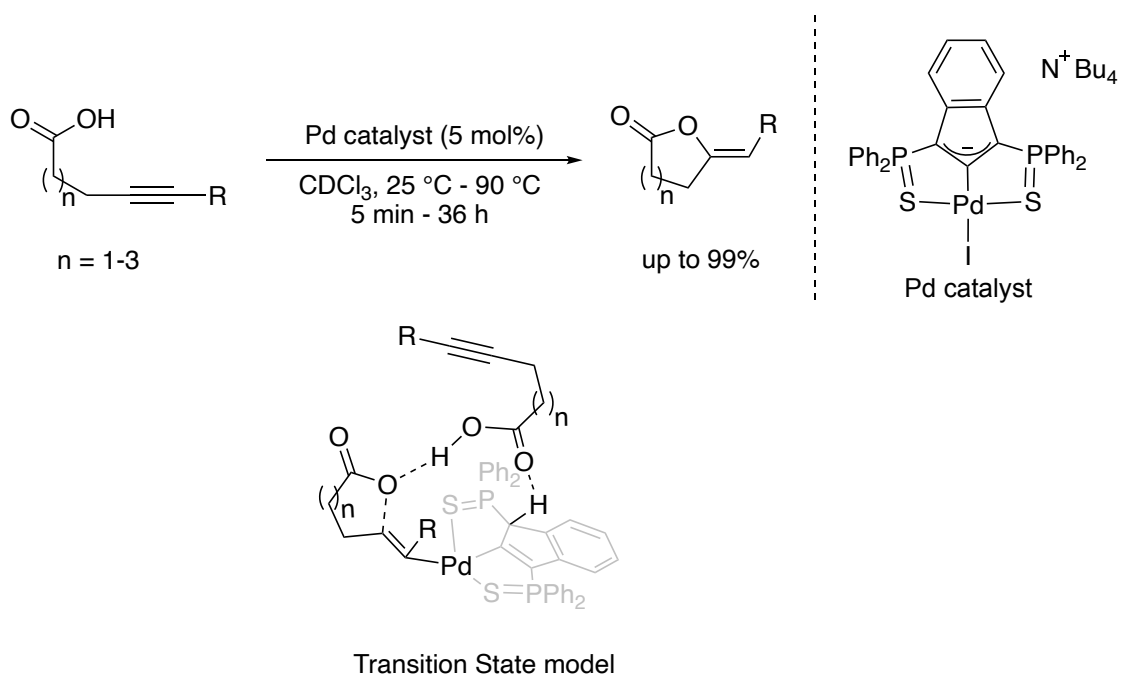
3.1. Metal-organo Catalysis

In metal-organo catalysis, one of the active sites is a Lewis acid metal which promotes the activation of the alkyne substrate and the other active site is a Lewis base which enhances the nucleophilic addition through hydrogen-bonding or deprotonation. Reactions related to nucleophilic addition of alkyne with metal-organo cooperative catalysis are discussed below.

Reactions Related to Metal-organic Cooperative Catalysis

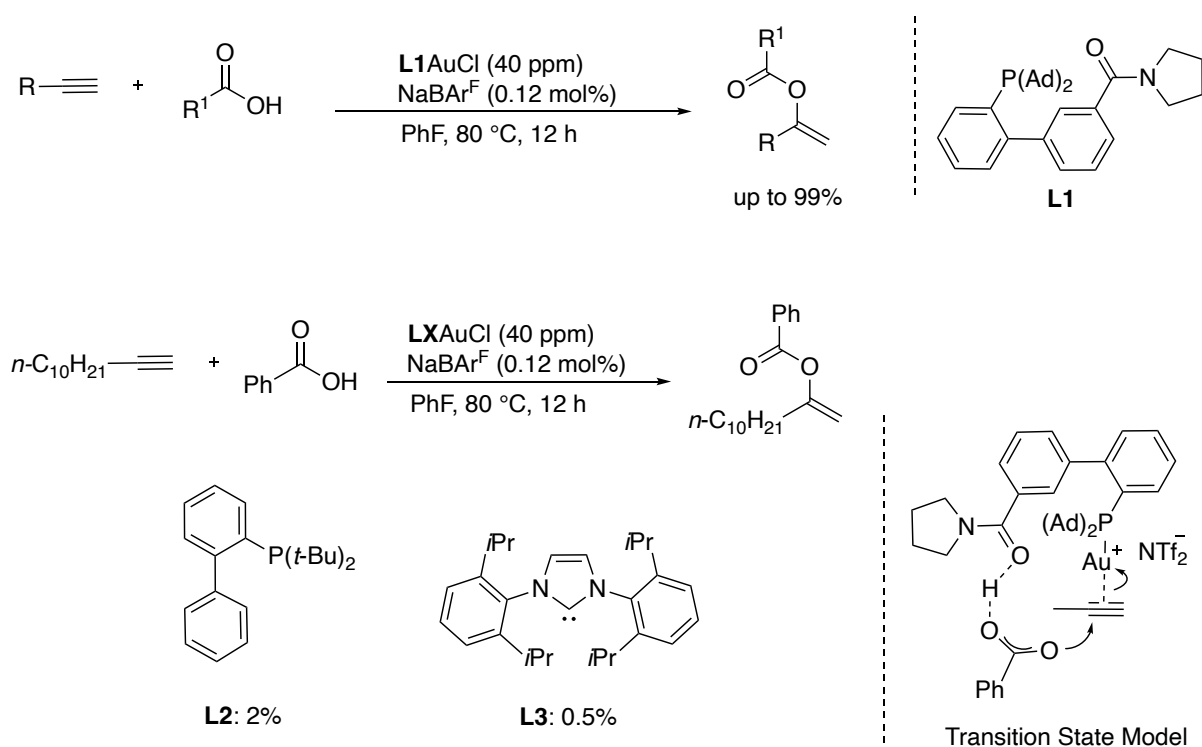
In 2013, Bourissou and his coworkers reported the cycloisomerization of alkynoic acids by using a palladium indenediide cooperative catalytic system (Scheme 1).⁹ The author proposed that the palladium activates the alkyne moiety and the anionic indene ligand deprotonates the carboxy group of the substrate. The utility of palladium indene pincer complexes were also demonstrated in various cycloisomerization reactions.¹⁰ DFT calculations supported the facile nucleophilic attack through the formation of a hydrogen bond network in a transition state involving two molecules of the alkynoic acid.¹¹

Scheme 1. Ligand-cooperated Pd Catalysis for Cyclization of Alkynoic Acids



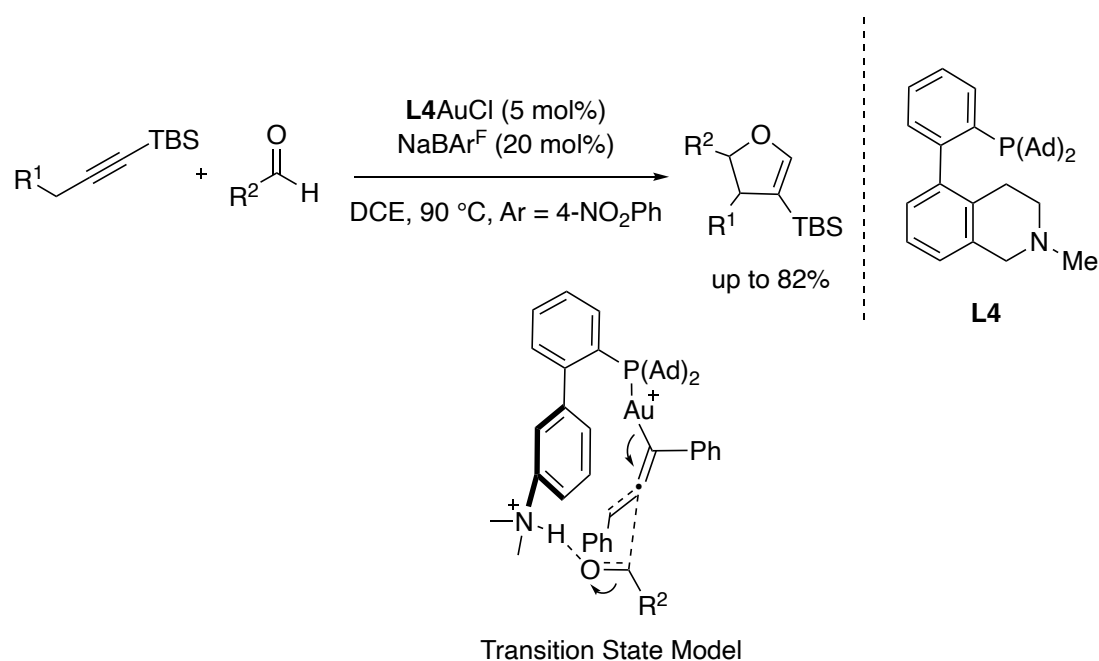
In 2014, Zhang and his coworkers reported the gold-catalyzed anti-nucleophilic addition of alkynes as the further development of highly active catalysts toward challenging intermolecular nucleophilic addition reactions (Scheme 2).¹² The author used a JhonPhos gold complex bearing an amide moiety, which facilitates nucleophilic addition of benzoic acid through hydrogen bond formation. Control experiments with an untailed JhonPhos gold complex and an IPr gold complex showed almost no activity, indicating that the amide moiety facilitates the reactions. DFT calculations supported the hydrogen bond assisted mechanism. Various nucleophiles such as water,¹² amine,¹² *N*-hydroxybenzotriazin,¹³ azide,¹⁴ and naphthol¹⁵ towards nucleophilic addition reactions with alkynes were explored using the amide-containing JhonPhos gold complexes.

Scheme 2. Hydrocarboxylation of Alkynes



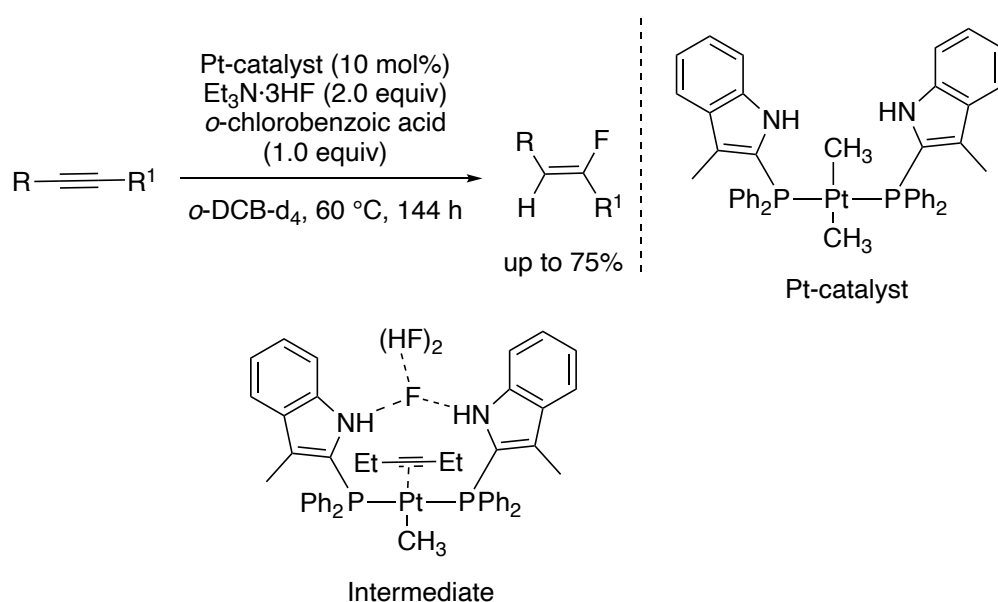
In 2014, Zhang and his coworkers expanded his cooperative catalysis to the efficient bi-functional designed JhonPhos gold complexes bearing an amine moiety which accelerated the propargylation of aldehydes followed by cycloisomerization (Scheme 3).¹⁶ It was proposed that the amine moiety deprotonates the alkyne at the propargylic position. The allenyl gold intermediate thus formed undergoes nucleophilic addition towards the aldehyde through the assistance of hydrogen-bonding with the protonated amine. A control experiment was conducted with an untailed JhonPhos gold complex, showing low activity of the catalyst toward nucleophilic addition to alkynes. The catalytic system demonstrated a broad utility of the JhonPhos gold complexes bearing the amine moiety in hydroalkenylation of alkynes,¹⁷ isomerization of alkynes,¹⁸ propargylic esters,¹⁹ and propargylic alcohol,²⁰ cycloisomerization of alkynoates and ynamides.²¹

Scheme 3. Propargylation of Aldehyde and Silyl-Migrative Cyclization



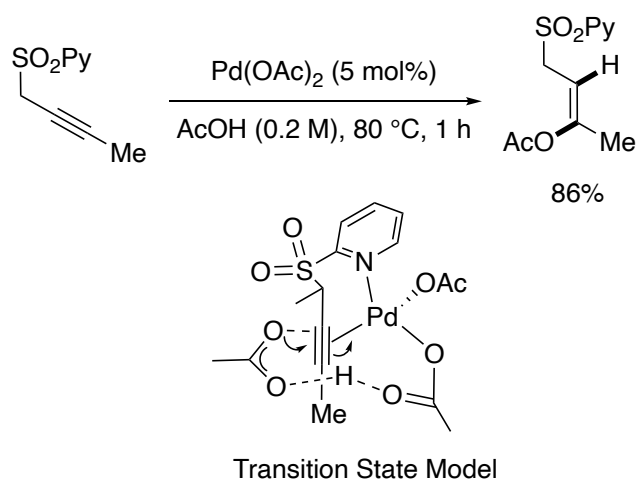
Cooperative catalysis is also beneficial for hydrofluorination of alkynes, while it is challenging to use hydrogen fluoride because of its high pKa value when compared with other halo-acids.²² In 2022, Braun and his coworkers reported platinum-catalyzed hydrofluorination of alkynes with metal-organo cooperative catalysts (Scheme 4)²³, in which the indolylphosphine ligand stabilizes fluorine anion in a platinum polyfluorido complex through hydrogen-bonding. The hydrogen-bonding with polyfluorides in the outer sphere of the indole moiety facilitated the fluorination reaction.

Scheme 4. Hydrofluorination of Internal Alkynes



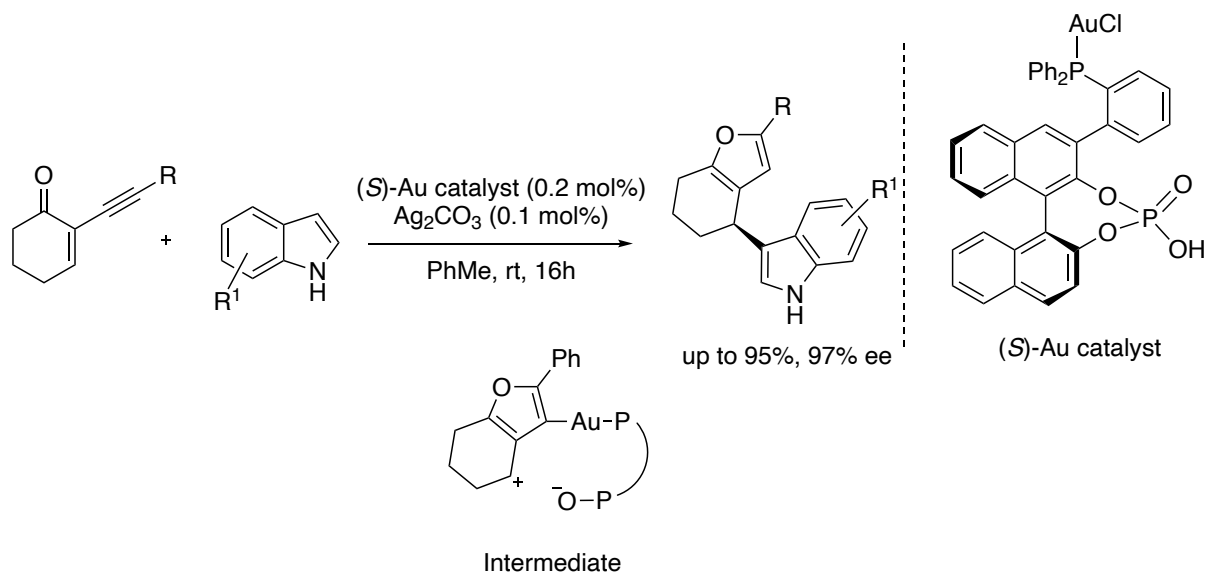
In 2022, Arrayas, Corpas, and their coworkers reported the directing group and cooperative action of acetate ligand assisted *anti*-acetoxylation of unsymmetrical alkynes with a palladium catalyst (Scheme 5).²⁴, in which the acetate ligand acted as a base that deprotonates AcOH for accelerating its nucleophilic attack. The use of deuterated acetic acid instead of normal acetic acid slowed down the reaction rate. DFT calculations supported the cooperative action of the acetate ligand as a base site to increase the nucleophilicity of acetic acid.

Scheme 5. Hydroacetoxylation of an Unsymmetrical Alkyne



In 2020, Guinchard and his coworkers reported the monophosphine gold complexes bearing a phosphate moiety as the counter anion for the cyclization/Indole addition reactions (Scheme 6).²⁵ The phosphate anion was crucial for the high chemo-selectivity of the nucleophilic addition of indoles toward alkynyl-enones. DFT calculations supported the cooperative action of the gold center and the phosphate anion for achieving high selectivity through stabilizing carbocation intermediate.

Scheme 6. Cooperative Catalysis of a Au-Phosphine-Phosphate Complex for Cycloisomerization/Nucleophilic Addition



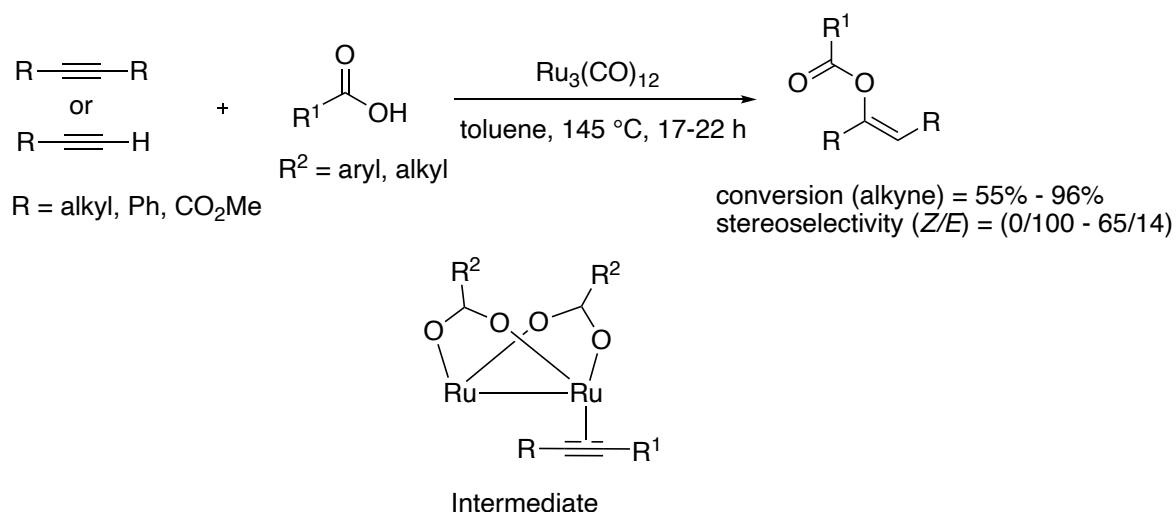
3.2 Bimetallic Cooperative Catalysis

The intermolecular addition of nucleophiles to non-activated internal alkynes was challenging for the metal-organo cooperative catalysis, and hence, there was a requirement for more efficient catalytic systems. Bimetallic catalysts are candidate for the systems. In bimetallic catalysis, one of the active sites is a Lewis acidic metal which promotes the activation of alkynes and the other half of the catalyst has a Brønsted base bound to the other metal which enhances nucleophilicity of the substrate. Reactions related to nucleophilic addition of alkynes through bimetallic cooperative catalysis is discussed below.

Reactions Related to Bimetallic Cooperative Catalysis

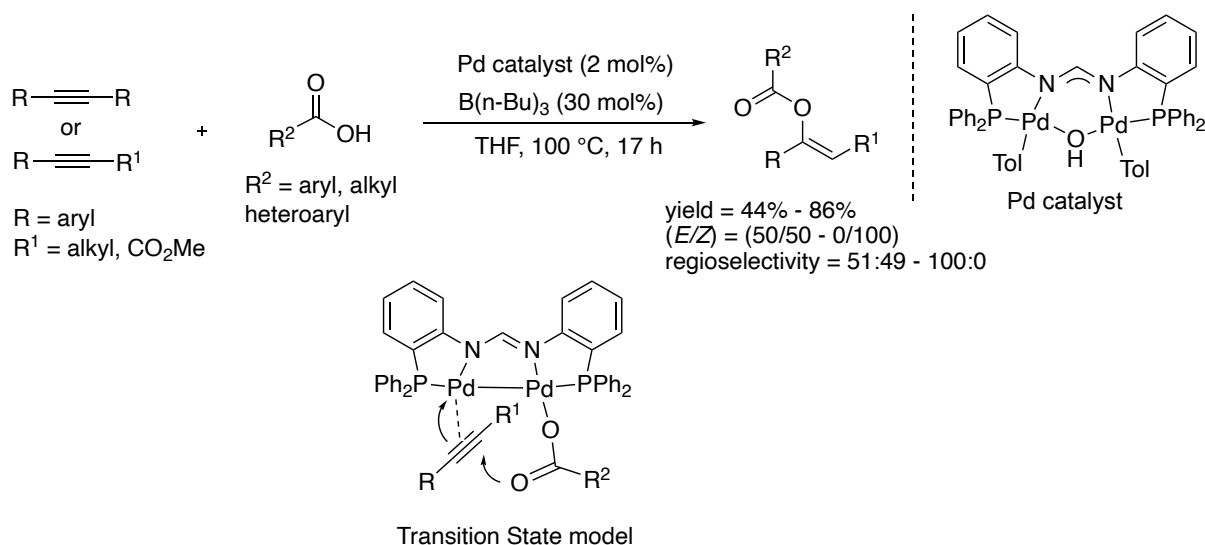
In 1983, Shvo and coworkers reported that a homobimetallic Ru complex accelerated hydrocarboxylation of alkynes (Scheme 7).²⁶ In this reaction, one of the Ru metal center activated the alkyne and the other active site of metal increased nucleophilicity of the carboxylic acid through the formation of a carboxylate anion.

Scheme 7. Homobimetallic Ru-catalyzed Hydrocarboxylation



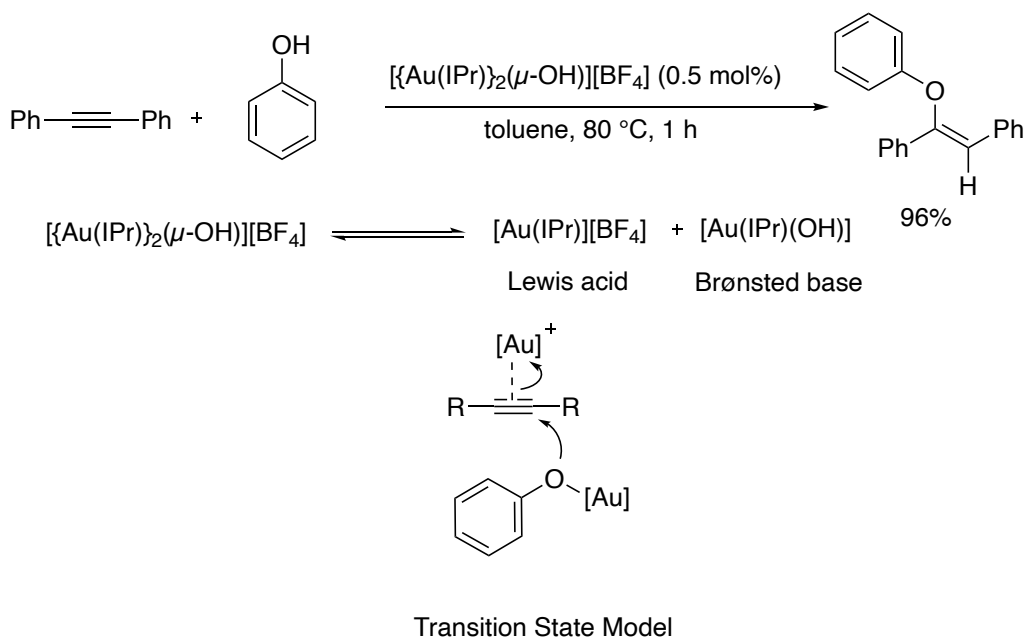
In 2010, Tsukada and his coworkers synthesized dinuclear palladium complexes towards improvement of the scope and efficiency of hydrocarboxylation of internal alkynes (Scheme 8).²⁷ Where two palladium centers were bridged through an amidine moiety. It was proposed that one of the palladium centers activated the alkyne while the other palladium center increased nucleophilicity of the acid through palladium carboxylate formation.

Scheme 8. Hydrocarboxylation Catalyzed by a Dinuclear Pd Complex



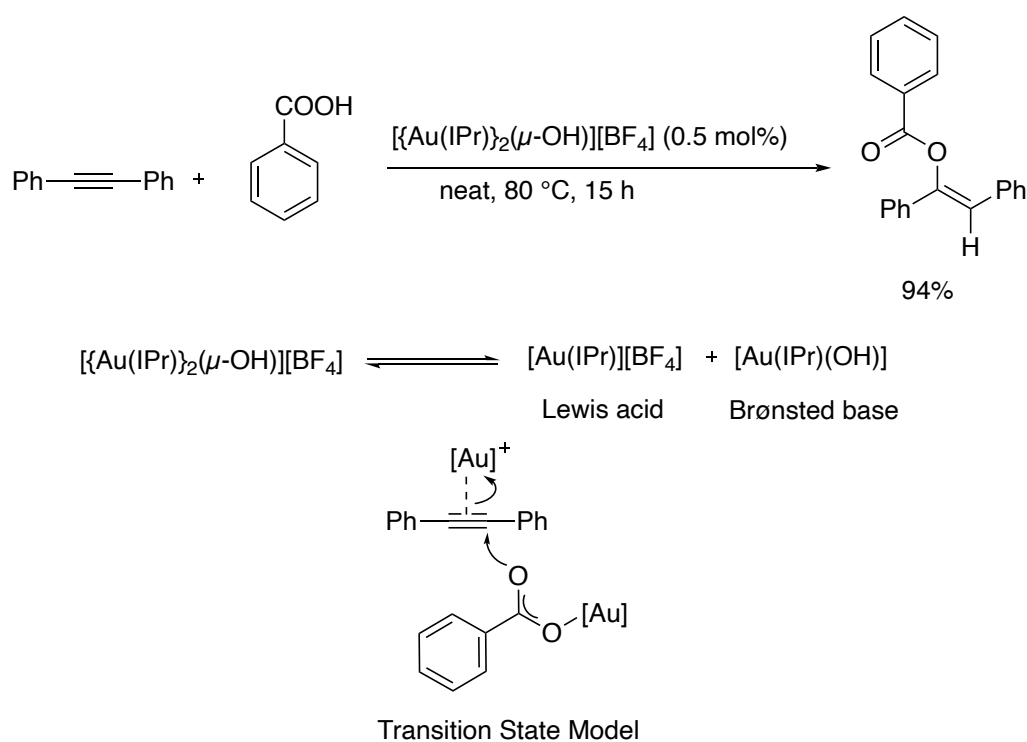
In 2013, Nolan and his coworkers reported the efficient dinuclear gold hydroxide catalytic systems for hydrophenoxylation of internal alkynes (Scheme 9).²⁸ The dinuclear gold species dissociates into two gold complexes in a solution phase. It was proposed that one of the gold complexes activates the alkyne while the other gold complex increases the nucleophilicity of phenol through forming a gold phenoxide species. When the reactions were conducted solely with gold tetrafluoroborate or gold hydroxide, a drastic loss in the activity of the reaction was observed. The author demonstrated a broad utility of the dinuclear gold hydroxy homobimetallic complexes in hydroalkoxylation.²⁹ DFT calculations suggested the cooperative action of the homobimetallic catalyst system in the nucleophilic addition reactions.³⁰

Scheme 9. Homobimetallic Gold Catalysis in Hydrophenoxylation



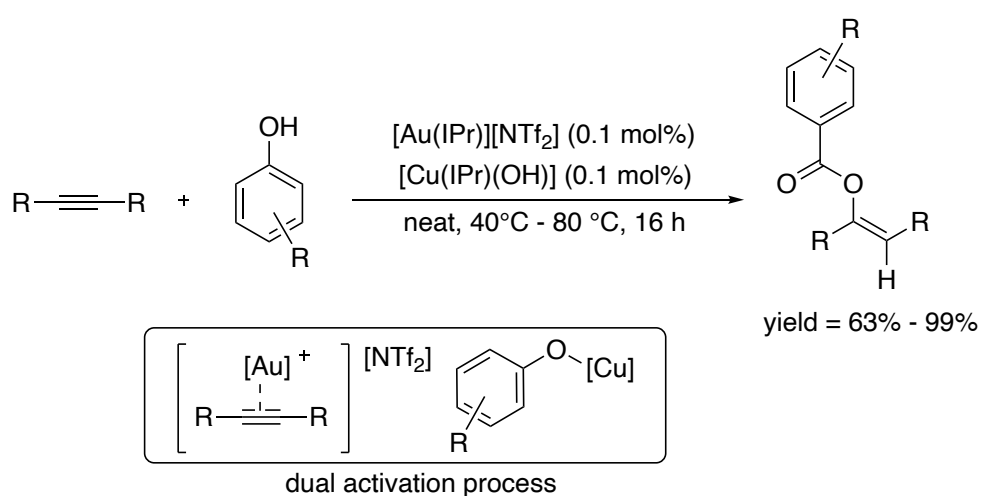
In 2015, Nolan and his coworkers reported the utility of dinuclear gold hydroxide complexes in hydrocarboxylation of internal alkynes (Scheme 10),³¹ in which carboxylic acid is much less reactive nucleophile than phenols. During the reaction, the dinuclear gold species dissociates into two gold complexes. One of the gold complex activates alkyne and the other increases the nucleophilicity of acid by forming a carboxylate species.

Scheme 10. Homobimetallic Gold-catalysis in Hydrocarboxylation



In 2017 Cazin and his coworkers reported heterobimetallic Au-Cu catalyst systems to develop a cost-effective method for hydrophenoxylation of internal alkynes (Scheme 11).³² Where the gold activates the alkyne moiety and the copper increases the nucleophilicity of the phenol by the formation of a copper phenoxide. When only copper hydroxide complex was utilized for the catalytic system, reaction did not occur, indicating that both of the gold and copper complexes were required. DFT calculations suggested the cooperative action of the heterobimetallic catalyst system in the nucleophilic addition reactions.³⁰

Scheme 11. Heterobimetallic Catalysis in Hydrophenoxylation



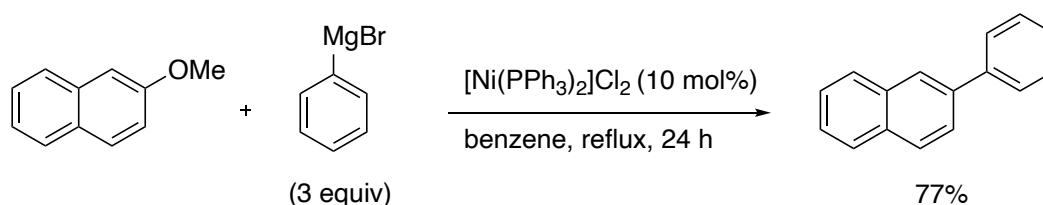
4. Cooperative Catalysis in C-O bond Activation

Coupling reactions are straightforward methods for the preparation of a wide variety of aromatic compounds, which are significant motifs in drugs, optoelectronics, and materials.³³ Aryl halides and sulfonates are the common substrates for the coupling reaction. Extension of a scope of coupling to include aryl ethers, which are attractive substrates in terms of readily availability from nature and less toxicity, is highly demanded. However, chemical stability of C-O bonds have hampered the development of coupling reactions with aryl ethers. For the activation of such a stable bond, the use of strongly nucleophilic metals such as low valent Ni and Rh in conjunction with hard Lewis acid metals such as Mg, Zn, Al, and Li are being recognized to be a general strategy. The role of Lewis acid is to coordinate to the oxygen atom of the ether and make them a better leaving group.

4.1 Effect of Magnesium

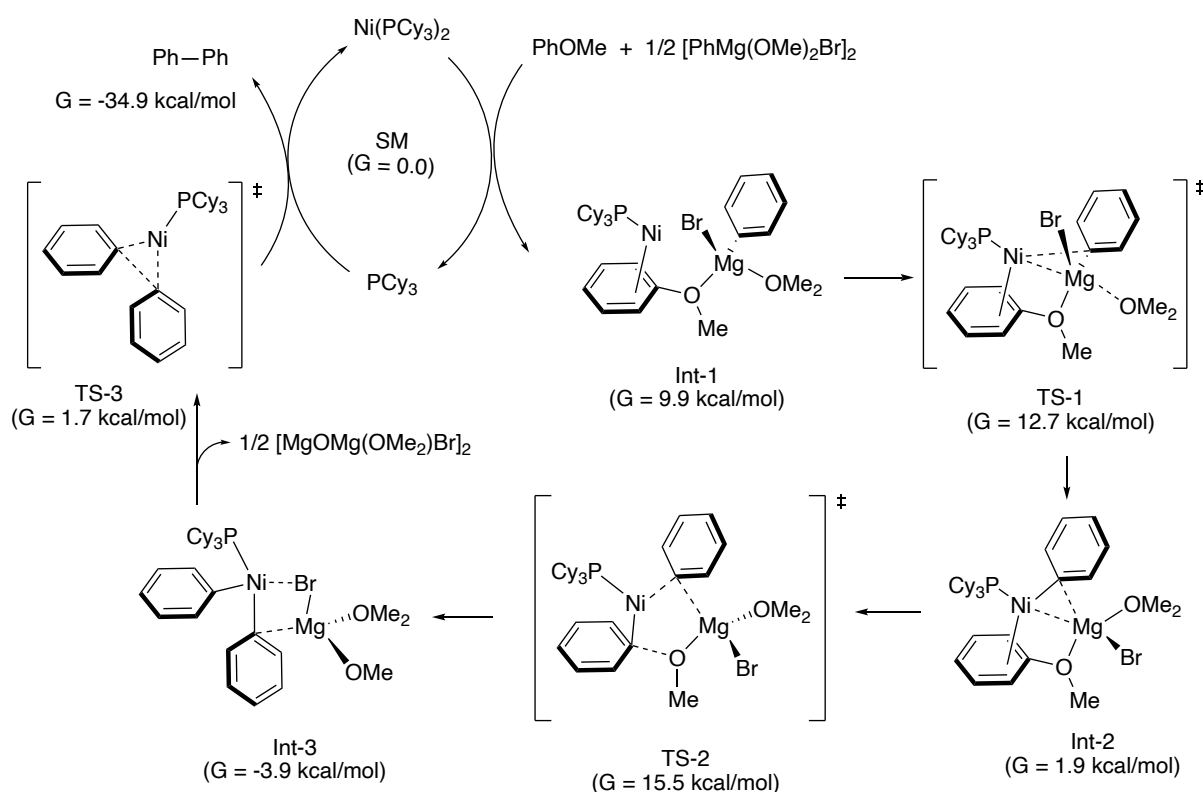
In 1978, Wenkert and his coworkers developed the first-ever nickel catalyzed cross-coupling reaction of aryl ethers by using phenylmagnesium bromide as the coupling partner (Scheme 12).³⁴ The desired coupling product was obtained in good yield under harsh conditions with a prolonged reaction time. The utility of Kumada-coupling reactions was extended to different coupling partners such as aryl,³⁵ alkyl,³⁶ alkyne³⁷ as nucleophiles and phenol as electrophiles.³⁸

Scheme 12. Kumada Coupling in Aryl Ethers



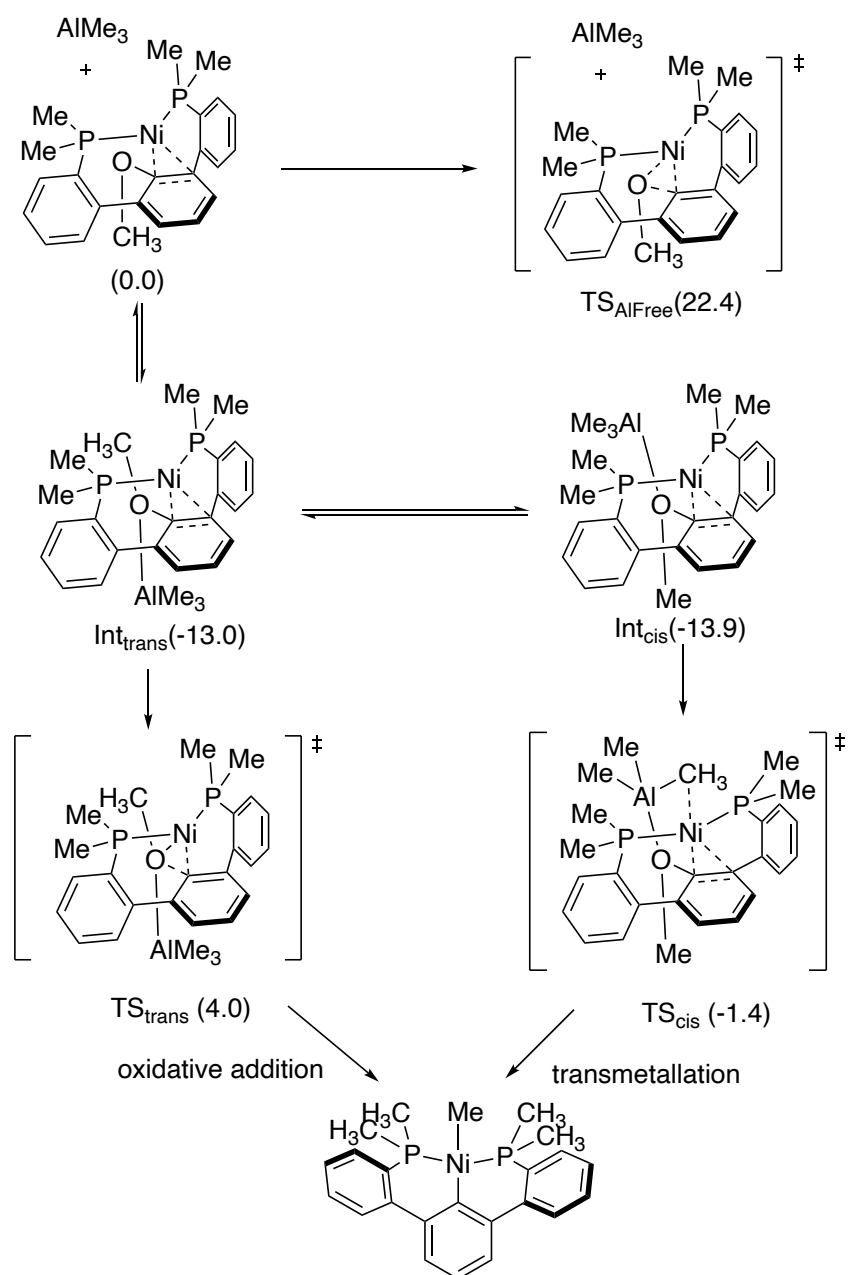
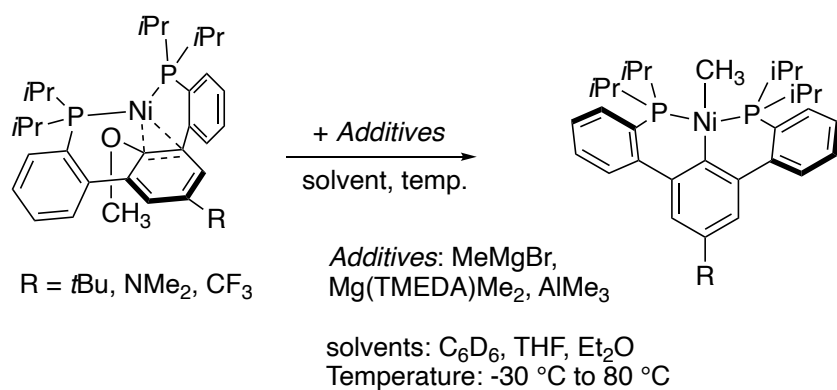
In 2015, Uchiyama and his coworkers studied the mechanism of the Kumada-coupling reaction in aryl ethers with DFT calculations, where cooperative action of Ni and Mg in the cleavage of the C-O bond was revealed. The heterobimetallic Ni(0)-ate complex was the key intermediate for the cleavage of the C-O bond with a reasonable energy barrier (Scheme 13).³⁹

Scheme 13. Reaction Mechanism of Cross-coupling Between PhOMe and PhMgBr



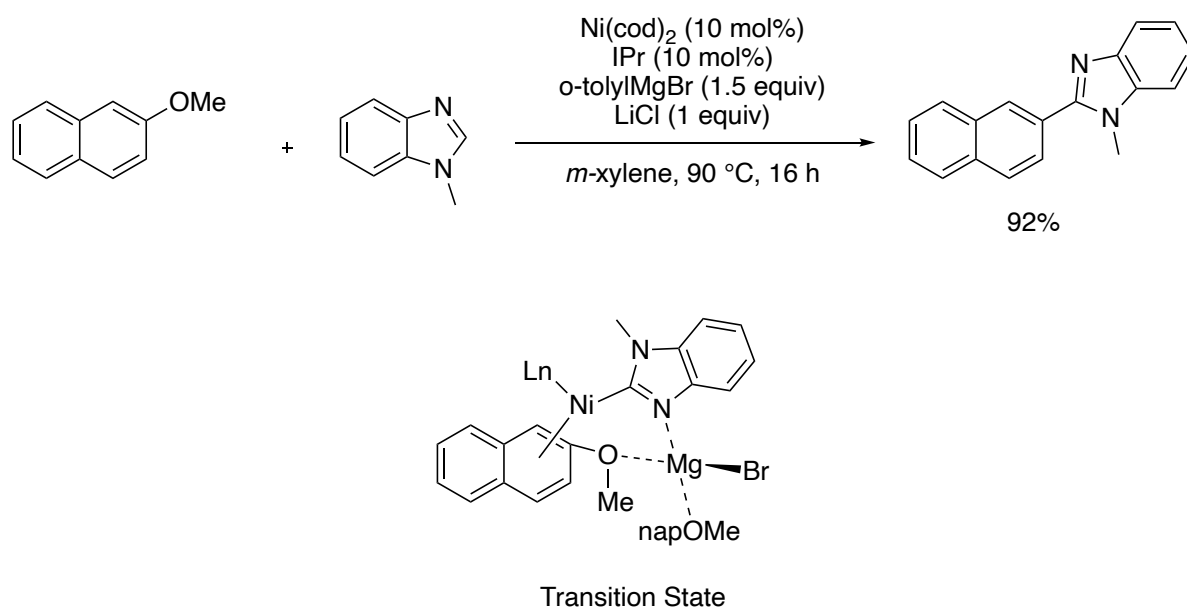
In 2016, Agapie and his coworkers isolated the Ni(II) complex which was formed from the cleavage of the C-O bond in Ni(0) complex after the addition of Lewis acid additives such as MeMgBr, Mg(TMEDA)Me₂ and AlMe₃ (Scheme 14).⁴⁰ DFT calculations were conducted with additive AlMe₃, because of the good solubility in non-polar solvents, to reveal the mechanism. The five-membered Ni(0)-ate complex was reasoned for the cleavage of C-O bond with a low energy barrier instead of three-membered Ni(0) ate complex, which proceeded in a relatively high energy barrier.

Scheme 14. Reactions, DFT Models and Mechanism for AlMe₃ Assisted C-O Bond Cleavage



In 2018, Ong, Zhao and their coworkers revealed the nickel catalyzed cross-coupling of aryl ethers with heteroarene *via* C-O bond activation (Scheme 15).⁴¹ In the presence of a Lewis acid activator, *o*-tolyl-magnesium bromide, benziimidazoles were deprotonated and led to the formation of Ni(I) species. The activation of the C-O bond of aryl ethers were facilitated by the Ni(I) complex through the formation of a heterobimetallic Ni(I)-ate reactive intermediate.

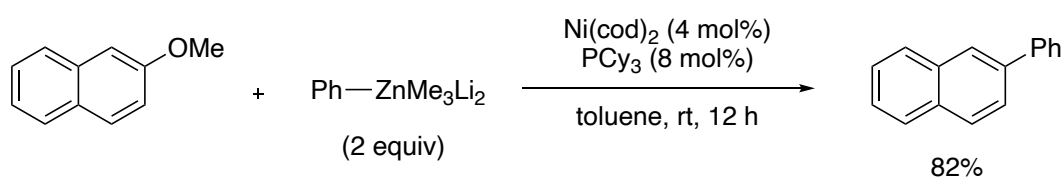
Scheme 15. Cross-coupling of Aryl ethers With Heteroarenes



4.2 Effect of Zinc

In 2012, Uchiyama and his coworkers reported the nickel catalyzed Negishi-type coupling from aryl ethers and aryl zinc reagents under mild conditions (Scheme 16).⁴² The use of dianionic-type Zincate such as $\text{PhZnMe}_3\text{Li}_2$ is crucial for the reaction due to its high nucleophilicity and low basicity.

Scheme 16. Negishi Type Cross-coupling in Aryl Ethers

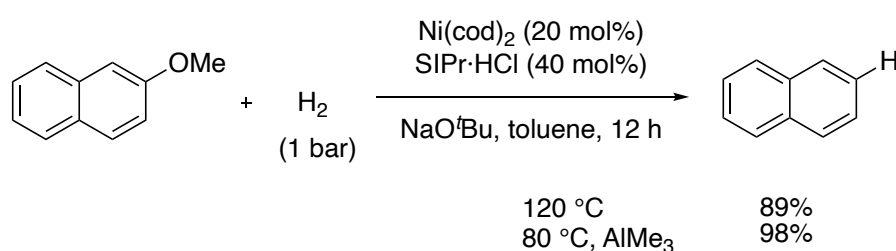


4.3 Effect of Aluminum

Since organoaluminum reagents have high Lewis acidity and oxophilicity.⁴³ The cleavage of the C-O bonds is also promoted through the heterobimetallic Ni-Al cooperative system with the energetically favored Ni(0)-ate complex. The reactions are discussed below for the effect of the aluminum reagent in the cleavage of the C-O bond.

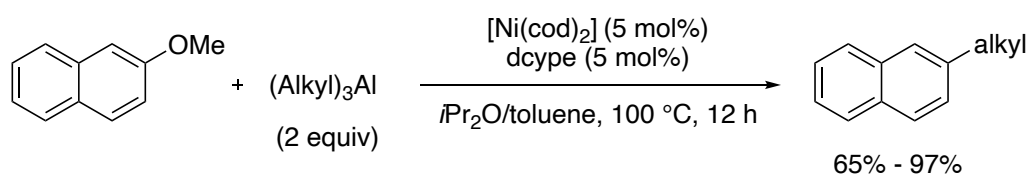
In 2011, Hartwig and his coworkers realized the additive effect of Lewis acid in the nickel-catalyzed reduction of aryl ethers (Scheme 17).⁴⁴ The hydrogenolysis products were obtained in good yield at an elevated temperature of 120 °C. The same reaction was proceeded in better yields at relatively low temperature 80 °C in presence of organometallic trimethylaluminum species, indicating that C-O bond cleavage was promoted by Lewis acidic additives.

Scheme 17. Additive Effect of Aluminum in Hydrogenolysis



In 2016, Rueping, Schoenebeck, and their coworkers developed the nickel catalyzed cross-coupling of aryl ethers using trialkylaluminum as a coupling partner (Scheme 18).⁴⁵ Although the use of Ni and monodentate phosphine ligand is unsuccessful due to the undesired reaction, dealkoxylation through β -hydride elimination. Bidentate phosphine ligand, dcype, realized the desired transformation in high yields. DFT calculations revealed that without Lewis acid a prohibitively high energy barrier was observed during oxidative cleavage of the C-O bond. The utility of the cooperative action of Ni and Al was extended to the reaction of electron-rich heteroaryl ethers.⁴⁶

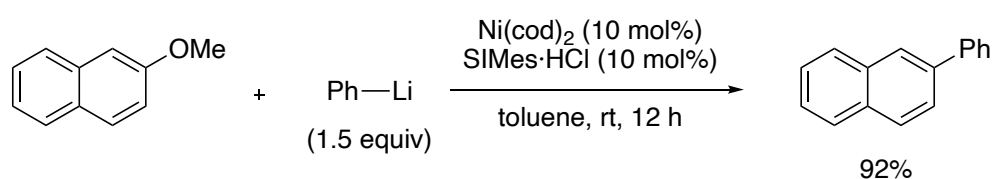
Scheme 18. Aluminum Assisted Kumada Coupling



4.4 Effect of Lithium

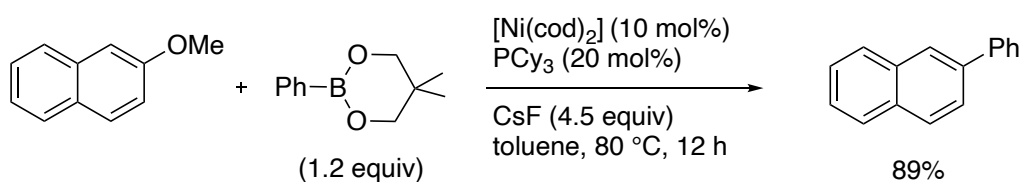
In 2016, Uchiyama, Wang and their coworkers reported the use of an alternative Lewis acid organolithium reagents for the coupling partner in the nickel catalyzed coupling through the C-O bond activation of aryl ethers (Scheme 19).^{47,48} The desired products were obtained in high yield at room temperature.

Scheme 19. Nickel-catalyzed Cross-coupling Between Aryl Ethers and Aryl Lithium



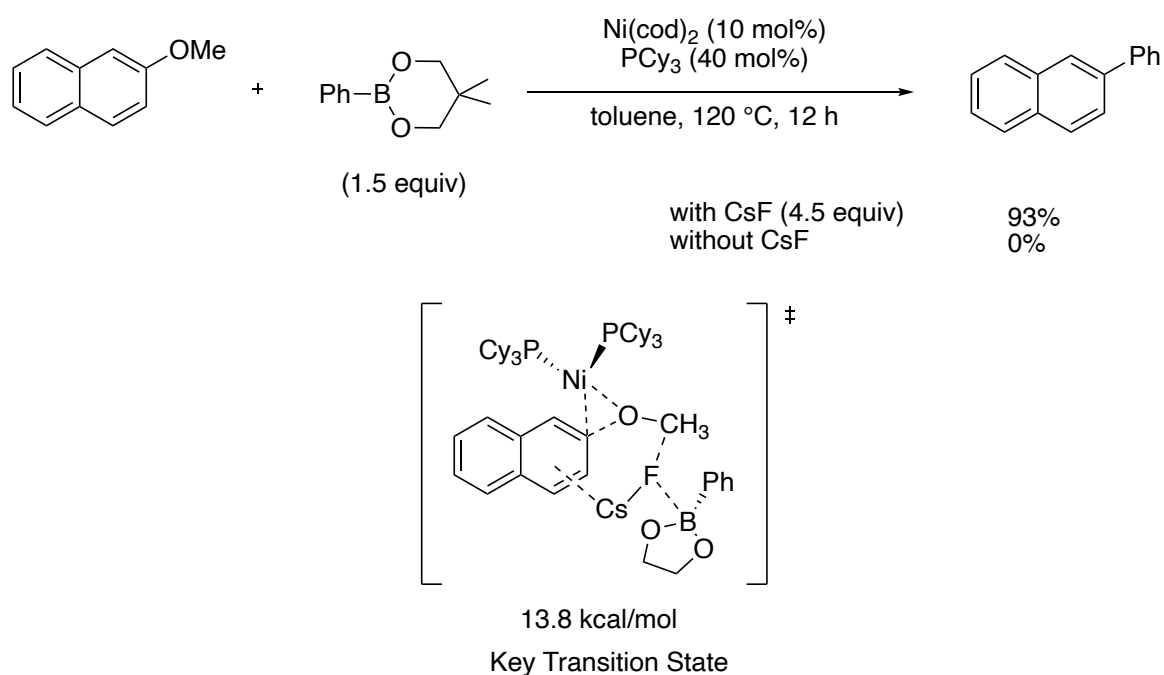
The organometallic reagent is the key to facilitating the C-O bond cleavage in coupling reaction because of the formation of electron-rich nickel(0)-ate complexes. In contrast, metal salt, CsF, also showed acceleration effect in Suzuki-Miyaura coupling of aryl ethers without formation of Ni(0)-ate complexes (Scheme 20).⁴⁹

Scheme 20. Nickel Catalyzed Suzuki Coupling



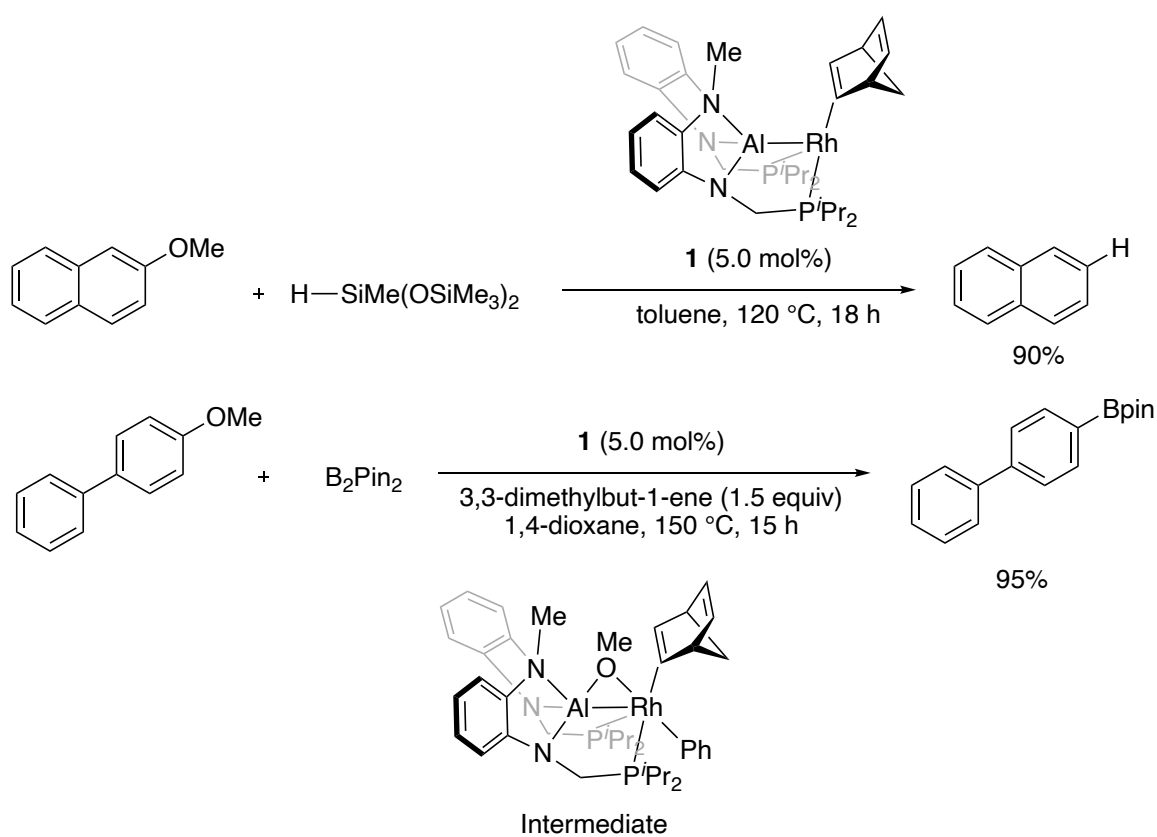
In 2017, Mori, Chatani, Tobisu, and their coworkers disclosed the detailed reaction mechanism by using DFT calculations (Scheme 21),⁵⁰ revealing that the oxidative addition with Ni-PCy₃ system requires high activation energy barrier of 33.0 kcal/mol. The activation energy barrier for C-O cleavage was lowered in the presence of CsF by 4.2 kcal/mol through the formation of a quaternary complex with Ni, PCy₃, CsF, and starting materials.

Scheme 21. Effect of CsF, Metal Salt in Suzuki coupling



In 2021, Nakao and his coworkers reported a Rh-Al heterobimetallic complex for the reduction and selective borylation in aryl ethers (Scheme 22).⁵¹ The desired reduction products and borylated products were obtained in high yields at an elevated temperature of 120 °C and 150 °C, respectively. To gain insight into the reaction mechanism, the intermediate was isolated and characterized, which demonstrated the activation of the C-O bond of anisole through the cooperative action of Rh and Al.

Scheme 22. Heterobimetallic Complex in C-O Bond Cleavage



5. Strategy

Design of Bifunctional Ligand

The author selected a rigid imidazo[1,5-*a*]pyridine-3-ylidene (IPC) ligand framework,⁵² pursuing highly efficient nucleophilic addition towards alkynes (Figure 4a). The substituent at the C5 position of the IPC ligands impacts the catalytic environment around the metal atom, which is bound to the carbene at the C3-position of IPC ligand (Figure 3a). The rigidity of the IPC skeleton places the substituents at the vicinity of the metal centre to introduce a cooperative effect in facilitating the nucleophilic addition (Figure 3b).

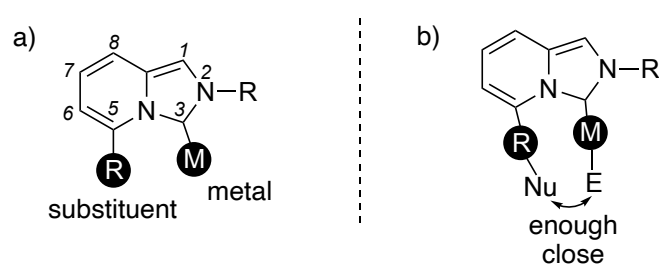


Figure 3. a) Structure of imidazo[1,5-*a*]pyridine-3-ylidene (IPC) ligand, b) Strategy for cooperative catalysis for nucleophilic addition.

6. Overview of the Thesis

Chapter 1 describes the development of highly active catalysts towards intramolecular nucleophilic additions with alkyne. He prepared novel imidazo[1,5-*a*]pyridin-3-ylidene silver complexes including an organic basic site, the imidazole moiety, at C5 position, which enable to form metal-organo cooperative catalysts. The rigid imidazo[1,5-*a*]pyridin-3-ylidene skeleton caused the silver and imidazole, to be placed in close proximity and display a cooperative effect in facilitating intramolecular reactions.

Chapter 2 describes the development of highly active catalysts towards challenging intermolecular nucleophilic additions with non-activated alkyne. He prepared novel imidazo[1,5-*a*]pyridin-3-ylidene gold complexes including bipyridine coordination site at the C5 position, which enable to form the hetero-bimetallic cooperative catalysts through the binding of hard metals at the coordination site. The rigid imidazo[1,5-*a*]pyridin-3-ylidene skeleton caused the two metals, gold and zinc, to be placed in close proximity and display a cooperative effect in facilitating intermolecular reactions.

Chapter 3 describes the application of Lewis acid Mg(anthracene)(thf)₃ reductant in the cleavage of stable C-O bond of aryl ethers for homocoupling reaction to produce symmetrical diaryl ethers. DFT calculations elucidate the behavior of Mg(anthracene)(thf)₃ reductant as a Grignard type of reagent, which participate cooperatively with nickel to facilitate cleavage of the C-O bond.

References

- (1) Book-Cooperative Catalysis: Designing Efficient Catalysts For Synthesis DOI: 10.1002/9783527681020.
- (2) Van Den Beuken, E. K.; Feringa, B. L. *Tetrahedron* **1998**, *54*, 12985-13011.
- (3) Ito, Y.; Sawamura, M.; Hayashi, T. *J. Am. Chem. Soc.* **1986**, *108*, 6405–6406.
- (4) Shibasaki, M.; Sasai, H.; Arai, T. *Angew. Chem. Int. Ed. Engl.* **1997**, *36*, 1236-1256.
- (5) Sasai, H.; Suzuki, T.; Itoh, N.; Tanaka, K.; Date, T.; Okamura, K.; Shibasaki, M. *J. Am. Chem. Soc.* **1993**, *115*, 10372-10373.
- (6) Hamashima, Y.; Sawada, D.; Kanai, M.; Shibasaki, M. *J. Am. Chem. Soc.* **1999**, *121*, 2641-2642.
- (7) a) Cheng, X.; Zhang, L. *CCS Chem.* **2020**, *2*, 1989-2002. b) Matsunaga, S.; Shibasaki, M. *Chem. Commun.* **2014**, *50*, 1044-1057. c) Park, J.; Hong, S. *Chem. Soc. Rev.* **2012**, *41*, 6931-6943.
- (8) a) Hashmi, A. S. K.; Rudolph, M. *Chem. Soc. Rev.* **2008**, *37*, 1766-1775. b) Rudolph, M.; Hashmi, A. S. K. *Chem. Soc. Rev.* **2012**, *41*, 2448-2462.
- (9) Nebra, N.; Monot, J.; Shaw, R.; Martin-Vaca, B.; Bourissou, D. *ACS Catal.* **2013**, *3*, 2930-2934.
- (10) Espinosa-Jalapa, N. A.; Ke, D.; Nebra, N.; Goanvic, L. L.; Mallet-Ladeira, S.; Monot, J.; Martin-Vaca, B.; Bourissou, D. *ACS Catal.* **2014**, *4*, 3605-3611.
- (11) Monot, J.; Brunel, P.; Kefalidis, C. E.; Espinosa-Jalapa, N. A.; Maron, L.; Martin-Vaca, B.; Bourissou, D. *Chem. Sci.* **2016**, *7*, 2179-2187.
- (12) Wang, Y.; Wang, Z.; Yuxue, W.; Wu, G.; Cao, Z.; Zhang, L. *Nat. Commun.* **2014**, *5*, 3470.
- (13) Xu, Y.; Zheng, K.; Zhou, B.; Jin, H.; Liu, Y. *J. Org. Chem.* **2020**, *85*, 6519-6527
- (14) Li, X.; Liao, S.; Wang, Z.; Zhang, L. *Org. Lett.* **2017**, *19*, 3687-3690.
- (15) Li, T.; Yang, Y.; Luo, B.; Li, B.; Zong, L.; Kong, W.; Yang, H.; Cheng, X.; Zhang, L. *Org. Lett.* **2020**, *22*, 6045-6049.
- (16) Li, T.; Zhang, L. *J. Am. Chem. Soc.* **2018**, *140*, 17439-17443.
- (17) Liao, S.; Porta, A.; Cheng, X.; Ma, X.; Zanoni, G.; Zhang, L. *Angew. Chem. Int. Ed.* **2018**, *57*, 8250-8254.
- (18) Wang, Z.; Wang, Y.; Zhang, L. *J. Am. Chem. Soc.* **2014**, *136*, 8887-8890.
- (19) Wang, Z.; Ying, A.; Fan, Z.; Hervieu, C.; Zhang, L. *ACS Catal.* **2017**, *7*, 3676-3680.
- (20) Cheng, X.; Wang, Z.; Quintanilla, C. D.; Zhang, L. *J. Am. Chem. Soc.* **2019**, *141*, 3787-3791.

- (21) Wang, H.; Li, T.; Zheng, Z.; Zhang, L. *ACS Catal.* **2019**, *9*, 10339-10342.
- (22) *J. Chem. Educ.* **2001**, *78*, 1, 116.
- (23) Sander, S.; Braun, T. *Angew. Chem. Int. Ed.* **2022**, e202204678
- (24) Corpas, J.; Arpa, E. M.; Lapierre, R.; Corral, I.; Mauleon, P.; Arrayas, R. G.; Carretro, J. C. *ACS Catal.* **2022**, *12*, 6596-6605.
- (25) Zhang, Z.; Smal, V.; Retailleau, P.; Voituriez, A.; Frison, G.; Marinetti, A.; Guinchard, X. *J. Am. Chem. Soc.* **2020**, *142*, 3797.
- (26) a) Rotem, M.; Shvo, Y. *Organometallics* **1983**, *2*, 1689-1691. b) Rotem, M.; Shvo, Y. *J. Organomet. Chem.* **1993**, *448*, 189-204.
- (27) Tsukada, N.; Takahashi, A.; Inoue, Y. *Tett. Lett.* **2011**, *52*, 248-250.
- (28) Oonishi, Y.; Gomez-Suarez, A.; Martin, A. R.; Nolan, S. P. *Angew. Chem. Int. Ed.* **2013**, *52*, 9767-9771.
- (29) Veenboer, R. M. P.; Dupuy, S.; Nolan, S. P. *ACS Catal.* **2015**, *5*, 1330-1334.
- (30) Gonzalaz-Belman, O. F.; Jimenez-Halla, J. O. C.; Nahra, F.; Cazin, C. S. J.; Poater, A. *Catal. Sci. Technol.* **2018**, *8*, 3638-3648.
- (31) Dupuy, S.; Gasperini, D.; Nolan, S. P. *ACS Catal.* **2015**, *5*, 6918-6921.
- (32) Lazreg, F.; Guidone, S.; Herrera, A. G.; Nahra, F.; Cazin, C. S. J. *Dalton Trans.* **2017**, *46*, 2439-2444.
- (33) (a) Vasconcelos, S. N. S.; Reis, J. S.; de Oliveira, I. M.; Balfour, M. N.; Stefani, H. A. *Tetrahedron* **2019**, *75*, 1865. (b) Hassan, J.; Sévignon, M.; Gozzi, C.; Schulz, E.; Lemaire, M. *Chem. Rev.* **2002**, *102*, 1359.
- (34) Wenkert, E.; Michelotti, E. L.; Swindell, C. S. *J. Am. Chem. Soc.* **1979**, *101*, 2246-2247.
- (35) a) Dankwart, J. W. *Angew. Chem. Int. Ed.* **2004**, *43*, 2428-2432. b) Xie, L. G.; Wang, Z. X. *Chem. Eur. J.* **2011**, *17*, 4972-4975. c) Iglesias, M. J.; Prieto, A.; Nicasio, M. C. *Org. Lett.* **2012**, *14*, 4318-4321. d) Cao, Z. C.; Luo, Q. Y.; Shi, Z. J. *Org. Lett.* **2016**, *18*, 5978-5981. e) Ghorai, D.; Loup, J.; Zannoni, G.; Ackermann, L. *Synlett* **2019**, *30*, 429-432. f) Ambre, R.; Yang, H.; Chen, W. C.; Yap, J. P. A.; Jurca, T.; Ong, T. G. *Eur. J. Inorg. Chem.* **2019**, 3511.
- (36) a) Guan, B. T.; Xiang, S. K.; Wu, T.; Sun, Z. P.; Wang, B. Q.; Zhao, K. Q.; Shi, Z. J. *Chem. Commun.* **2008**, 1437-1439. b) Tobisu, M.; Takahira, T.; Chatani, N. *Org. Lett.* **2015**, *17*, 4352-4355. c) Tobisu, M.; Takahira, T.; Morioka, T.; Chatani, N. *J. Am. Chem. Soc.* **2016**, *138*, 6711-6714.
- (37) Tobisu, M.; Takahira, T.; Ohtsuki, A.; Chatani, N. *Org. Lett.* **2015**, *17*, 680-683.

- (38) Yu, D. G.; Li, B. J.; Zheng, S. F.; Guan, B. T.; Wang, B. Q.; Shi, Z. *J. Angew. Chem. Int. Ed.* **2010**, *49*, 4566-4570.
- (39) Ogawa, H.; Minami, H.; Ozaki, T.; Komagawa, S.; Wang, C.; Uchiyama, M. *Chem. Eur. J.* **2015**, *21*, 13904-13908.
- (40) Kelly, P.; Edouard, G. A.; Lin, S.; Agapie, T. *Chem. Eur. J.* **2016**, *22*, 17173-17176.
- (41) Wang, T. H.; Ambre, R.; Wang, Q.; Lee, W. C.; Wang, P. C.; Liu, Y.; Zhao, L.; Ong, T. G. *ACS Catal.* **2018**, *8*, 11368-11376.
- (42) Wang, C.; Ozaki, T.; Takita, R.; Uchiyama, M. *Chem. Eur. J.* **2012**, *18*, 3482-3485.
- (43) a) *Organomet. Chem.* **2013**, *41*, 173-186. b) Shang, R.; Ilies, L.; Nakamura, E. *J. Am. Chem. Soc.* **2015**, *137*, 7660-7663. c) Groll, K.; Blumke, T. D.; Unsinn, A.; Hass, D.; Knochel, P. *Angew. Chem. Int. Ed.* **2012**, *51*, 11157-11161.
- (44) Sergeev, A. G.; Hartwig, J. F. *Science* **2011**, *332*, 439-443.
- (45) Liu, X.; Hsiao, C. C.; Kalvet, I.; Leiendecker, M.; Guo, L.; Schoenebeck, F.; Rueping, M. *Angew. Chem. Int. Ed.* **2016**, *55*, 6093-6098.
- (46) Liu, C. Y.; Wititsuwannakul, T.; Hsieh, C. H.; Tsai, C. Y.; Wang, T. H.; Ambre, R.; Chen, W. C.; Surawatanawong, P.; Ong, T. G. *J. Chin. Chem. Soc.* **2019**, 1-7
- (47) Leiendecker, M.; Hsiao, C. C.; Guo, L.; Alandini, N.; Rueping, M. *Angew. Chem. Int. Ed.* **2014**, *53*, 12912-12915.
- (48) Yang, Z. K.; Wang, D. Y.; Minami, H.; Ogawa, H.; Ozaki, T.; Saito, T.; Miyamoto, K.; Wang, C.; Uchiyama, M. *Chem. Eur. J.* **2016**, *22*, 15693-15699.
- (49) Tobisu, M.; Shimasaki, T.; Chatani, N. *Angew. Chem. Int. Ed.* **2008**, *47*, 4866-4896.
- (50) Schwarzer, M. C.; Konno, R.; Hojo, T.; Ohtsuki, A.; Nakamura, K.; Yasutome, A.; Takahashi, H.; Shimasaki, T.; Tobisu, M.; Chatani, N.; Mori, S. *J. Am. Chem. Soc.* **2017**, *139*, 10347-10358.
- (51) Seki, R.; Hara, N.; Saito, T.; Nakao, Y. *J. Am. Chem. Soc.* **2021**, *143*, 6388-6394.
- (52) Alcarazo, M.; Roseblade, S. J.; Cowley, A. R.; Fernandez, R.; Lassaletta, J. M. *J. Am. Chem. Soc.* **2005**, *127*, 3290-3291. b) Burstein, C.; Lehmann, C. W.; Glorius, F. *Tetrahedron* **2005**, *61*, 6207-6217.

Chapter 1

Use of Imidazo[1,5-*a*]pyridin-3-ylidene as a Platform for Metal- Imidazole Cooperative Catalysis: Silver-Catalyzed Cyclization of Alkyne-Tethered Carboxylic Acids

Abstract

Silver complexes with 5-(4-(*tert*-butyl)-1*H*-imidazol-1-yl)-imidazo[1,5-*a*]pyridin-3-ylidene ligands were synthesized as metal-imidazole acid- base cooperative catalysts. Single crystal XRD analysis revealed that the silver atom was located in the vicinity of the imidazole ring and that cationic silver complexes formed dimers through coordination between the silver metal and the imidazole pendant. These cationic silver complexes served as catalysts for cyclization of alkyne-tethered carboxylic acids. NMR experiments indicated that the dimeric cationic silver complex dissociated to a monomer upon protonation of the imidazole moiety, resulting in coordination of an acetonitrile to the silver atom. DFT calculations supported the acid- base cooperative action of the silver-imidazole for the efficient alkyne-carboxylic acid cyclization.

Introduction

N-Heterocyclic carbenes (NHCs) are strong σ -donating ligands, and their transition metal complexes have been widely investigated as catalysts for reaction development due to their robustness and tunability.¹ To date, a broad spectrum of NHC ligands with different electronic and steric properties have been synthesized and evaluated. Imidazo[1,5-*a*]pyridin-3-ylidene (Figure 1a) is an NHC scaffold with a rigid bicyclic framework, introduced independently by Lassaletta² and Glorius.³ Since the substituent at the C5 position of the imidazo[1,5-*a*]pyridin-3-ylidene projects into the catalytic environment around the NHC-bound metal centre, it is expected that ligand modification at this position would have great impact on the nature of the catalyst not only through steric effect but also through a coordinative interaction. In fact, imidazo[1,5-*a*]pyridin-3-ylidene ligands have been modified at the C5 position with sterically bulky aromatic rings,⁴ coordinative substituents,⁵ chiral auxiliaries,⁶ and other substituents.⁷

Therefore, the author envisioned that imidazo[1,5-*a*]pyridin-3-ylidene could be used as a robust template for producing acid-base cooperative catalysts⁸ by locating a Lewis acidic transition metal centre and a basic functional group such as imidazole at the C3 carbene carbon and the C5 position, respectively (Figure 1b). More specifically, the 4-(*tert*-butyl)-1*H*-imidazol-1-yl group was chosen as the rigid basic substituent at the C5 position so as to spatially separate the Lewis acidic centre and the basic centre in the catalytic region. This chapter describes the synthesis of protonated precursors for such imidazo[1,5-*a*]pyridin-3-ylidene ligands, their conversion to the corresponding silver(I) complexes, and their application to the silver-catalyzed cyclization of alkyne-tethered carboxylic acids (Figure 1c).^{9,10}

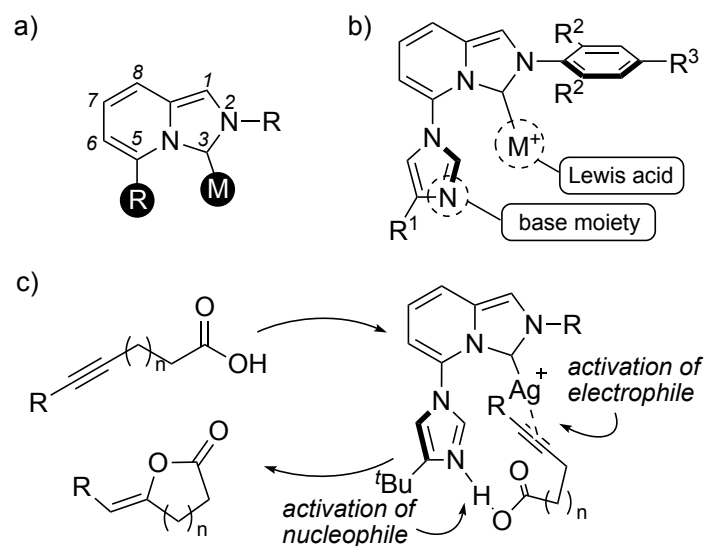


Figure 1. General chemical diagrams for a) imidazo[1,5-*a*]pyridin-3-ylidene metal complexes and b) Lewis acid-base cooperative catalysts with an imidazo[1,5-*a*]pyridin-3-ylidene platform. c) Cyclization of alkyne-tethered carboxylic acids through Lewis acid-base cooperative catalysis.

Synthesis of Ligands & Complexes

The synthesis of 5-(4-(*tert*-butyl)-1*H*-imidazol-1-yl)-imidazo[1,5-*a*]pyridinium salt as an NHC precursor is outlined in Scheme 1. Acetal protection of commercially available 6-bromo-2-pyridinecarboxaldehyde (**1**) gave 2-bromo-6-(diethoxymethyl)pyridine (**2**) in 96% yield. The 4-(*tert*-butyl)-1*H*-imidazolyl substituent was introduced through copper-catalyzed coupling between **2** and 4-(*tert*-butyl)-1*H*-imidazole to give 2-(4-(*tert*-butyl)-1*H*-imidazol-1-yl)-6-(diethoxymethyl)pyridine (**3**) in 79% yield. In this coupling, using benzotriazole¹¹ as a ligand for the copper catalyst was crucial for obtaining **3** in a reasonable yield. After removing the acetal protection under acidic conditions, reductive amination with 2,4,6-trimethylphenylamine or 2,6-diisopropylphenylamine followed by *N*-formylation¹² produced the corresponding *N*-aryl formamides (**4a**: R = 2,4,6-trimethylphenyl; **4b**: R = 2,6-diisopropylphenyl). Next, dehydrative cyclization² of **4a** and **4b** furnished 5-(4-(*tert*-butyl)-1*H*-imidazol-1-yl)-imidazo[1,5-*a*]pyridinium salts **5a** (69%) and **5b** (66%), respectively. The chloride anions on the imidazolium salts **5a** and **5b** were replaced with a weakly coordinating PF₆ anion through salt metathesis with KPF₆, yielding **6a** and **6b** in 86% and 85% yields, respectively.

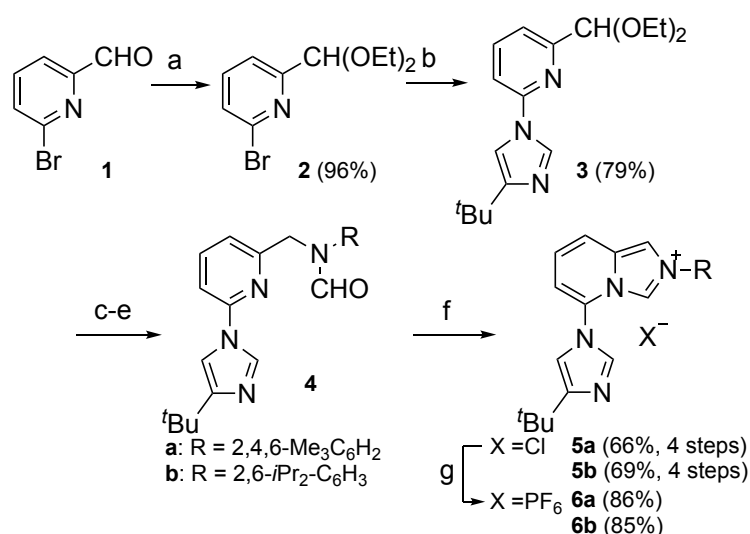


Figure 2. Synthesis of NHC precursors **5** and **6**. (a) TsOH·H₂O (7 mol%), HC(OEt)₃ (1.2 equiv), EtOH, r.t., 3 h; (b) CuI (10 mol%), benzotriazole (20 mol%), 4-(*tert*-butyl)-1*H*-imidazole (1 equiv), KO^tBu (1.4 equiv), DMSO, 110 °C, 14 h; (c) 1 M HCl aq., acetone, 60 °C, 3 h; (d) RNH₂ (1.2 equiv), AcOH (1 equiv), NaBH(OAc)₃ (1.5 equiv), DCM, r.t., 14 h; (e) HCOOH (excess), Ac₂O (excess), THF, 0 °C, 3 h; (f) POCl₃ (1.3 equiv), toluene, 100 °C, 38 h; (g) KPF₆ (2 equiv), H₂O, r.t., 18 h.

Silver(I) chloride complexes **7a** and **7b** bearing the 5-(4-(*tert*-butyl)-1*H*-imidazol-1-yl)-imidazo[1,5-*a*]pyridin-3-ylidene framework were synthesized through the reaction of Ag₂O and imidazolium salts **5a** or **5b** in 84% and 82% yields, respectively (Scheme 2). Single crystals of **7a** and **7b** suitable for XRD analysis were grown from DCM/Et₂O and DCE/Et₂O solutions, respectively. XRD analysis gave the mononuclear structures of complexes **7a** and **7b**. An ORTEP drawing of **7a** is shown in Scheme 2. As expected, the silver atom is located in the vicinity of the imidazole ring uncoordinated to the N(4) atom.

Scheme 1. Synthesis of neutral silver complexes **7a** and **7b**

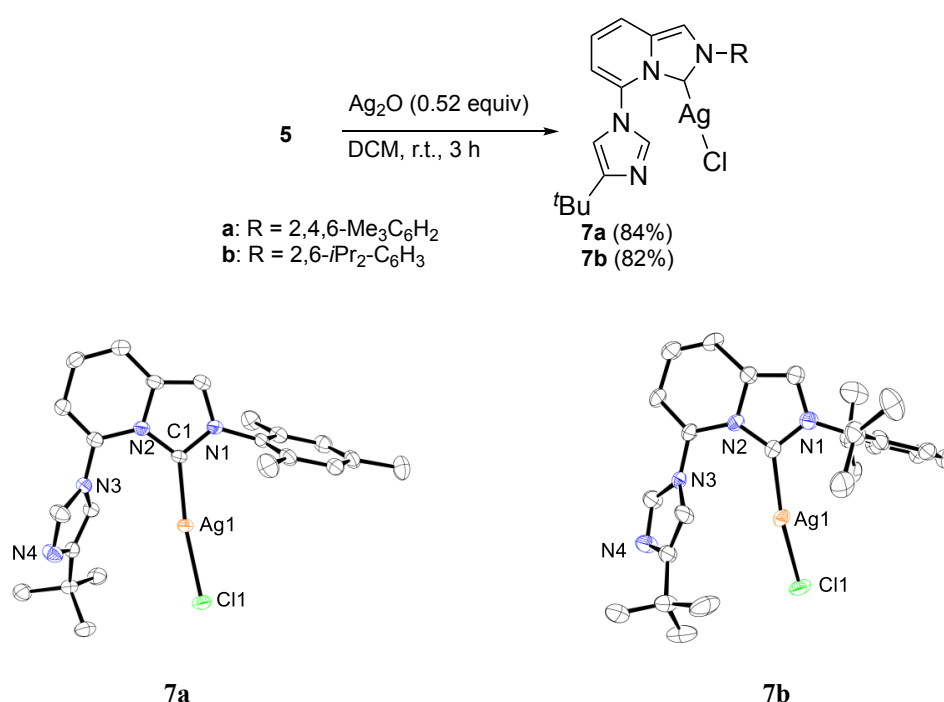


Figure 3. ORTEP drawing of **7a** and **7b** is described with 50% probability thermal ellipsoids. Hydrogen atoms are omitted for clarity.

Cationic silver(I) complexes **8a** and **8b** were prepared from imidazolium salts **6a** and **6b**, respectively. Specifically, the reaction between Ag₂O and the imidazolium salts (**6a** or **6b**) in acetonitrile at 50 °C for 38 hours gave the desired complexes **8a** and **8b** in 69% and 68% yields, respectively (Scheme 3). XRD analysis of single crystals of **8a** and **8b** obtained through recrystallization from a DCM/Et₂O solution indicated that both complexes existed as dimers with intermolecular coordination between the pendant imidazole and the silver atom. The average C_{carbene}-Ag interatomic distance was 2.08 Å for both **8a** and **8b**, which is comparable to those for known silver NHC complexes.¹³ In the ¹³C{¹H} NMR spectra of **8a** and **8b** in

CD₂Cl₂, resonances for the carbene carbon bound to the silver metal were observed as a pair of doublets at 167.3 ppm $\{^1J(^{13}\text{C}-^{107}\text{Ag}) = 287.1 \text{ Hz}, ^1J(^{13}\text{C}-^{109}\text{Ag}) = 248.5 \text{ Hz}\}$ for **8a** and at 167.3 ppm $\{^1J(^{13}\text{C}-^{107}\text{Ag}) = 289.0 \text{ Hz}, ^1J(^{13}\text{C}-^{109}\text{Ag}) = 249.5 \text{ Hz}\}$ for **8b**. The appearance of C–Ag coupling indicated that dissociation of the silver metal from the carbene is much slower than the NMR time scale.^{14,15}

Scheme 2. Synthesis of silver complexes **8a** and **8b**.

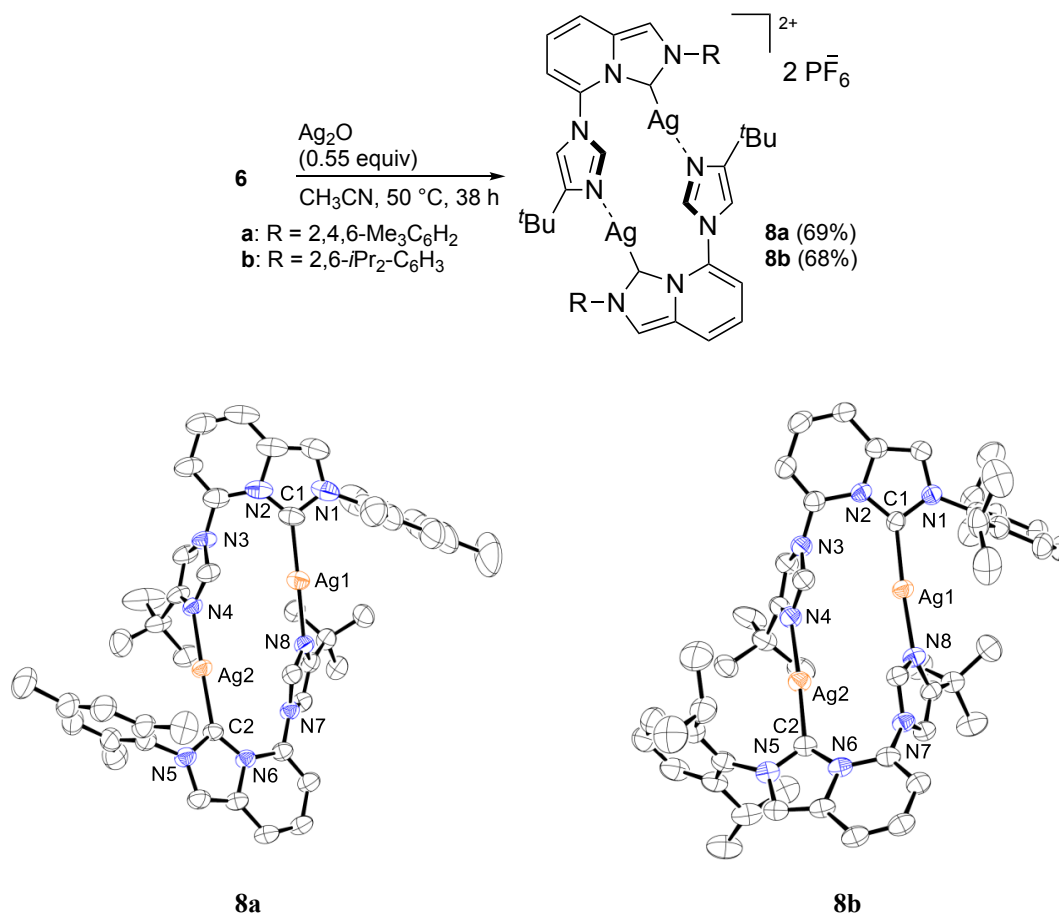


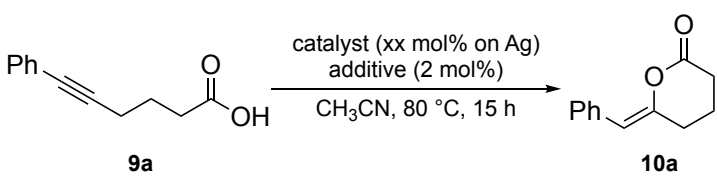
Figure 4. ORTEP drawing of **8a** and **8b** is described with 50% probability thermal ellipsoids. Hydrogen atoms are omitted for clarity.

Investigation of Catalytic Activity

Next, the author evaluated the neutral and cationic silver complexes **7a**, **7b**, **8a**, and **8b** (2 mol% Ag) for catalytic activity in the cyclization of 6-phenylhex-5-ynoic acid (**9a**) in acetonitrile at 80 °C for 15 hours. When he applied the cationic complex (**8a**) with the N(1)-mesityl-substituted NHC ligand, the starting material was fully consumed to afford 6-*exo-dig* lactonization product **10a** in 98% isolated yield with exclusive *Z*-selectivity (Table 1, entry 1). The cationic silver complex (**8b**) having the NHC ligand substituted with a bulkier N(1)-aryl group (2,6-diisopropylphenyl) was much less active, yielding (*Z*)-**10a** in only 21% yield (entry 3). The neutral silver chloride complexes **7a** and **7b** gave only a trace or none of the cyclization product (entries 4 and 5). In accordance with the literature,⁹ Ag₂CO₃ as a basic silver complex also promoted this cyclization to give **10a** (83%), albeit with lower efficiency than **8a** (entry 6). Using ligand-free cationic silver(I) salt AgPF₆ as a catalyst resulted in only 12% yield (entry 8).

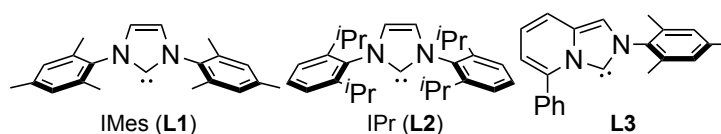
Combinations of AgPF₆ and conventional NHC ligands such as IMes (**L1**)¹⁶ and IPr (**L2**)¹⁷ gave **10a** in 27% and 16% yields, respectively (Table 1, entries 9 and 10). Imidazo[1,5-*a*]pyridin-3-ylidene ligand **L3** with a phenyl group at the C5 position gave even lower yield (13%, entry 11). The addition of 1-phenylimidazole (**11**) as an exogenous organic base to the reaction systems with **L1**, **L2**, or **L3** led to substantial increases in the yield of **10a** to 62%, 44%, or 18%, respectively (entries 12-14). These results suggest cooperative action of the cationic silver centre and the imidazole derivative (**11**) as a Lewis acid and a Brønsted base, respectively. Furthermore, comparison of these results with those for the cationic silver complex (**8a**) with the imidazole-functionalized NHC ligand (entry 1) confirms that the expected acid-base cooperative catalysis with the intramolecularly arranged cationic Ag centre and imidazole moiety has been achieved.

The catalyst loading could be reduced to 1 mol% on the Ag atom using **8a** as the catalyst for the reaction of **9a** over an extended reaction time (50 h) with the product yield nearly unchanged (Table 1, entry 2). In contrast, the reaction of **9a** catalyzed by the reduced amount of Ag₂CO₃ (1 mol% Ag) remained at only 25% even with the extended reaction time (entry 7). A time-course profile for the Ag₂CO₃-catalyzed reaction indicated that Ag₂CO₃ was more active than **8a** but lost its activity at 10 h (see Supporting Information for time-yield profiles). Thus, the NHC ligand (**8a**) with the basic pendant is useful for maintaining the activity of the cationic silver catalyst.

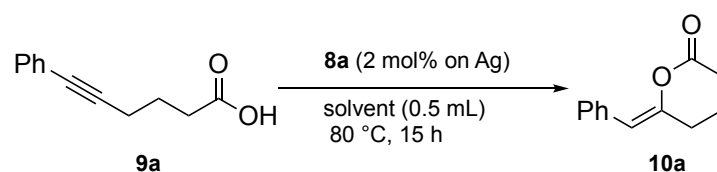
Table 1. Silver-Catalyzed Cyclization of **9a**

entry	catalyst (xx mol% Ag)	additive	yield [%] ^[a]
1	8a (2)	none	98 ^[b]
2	8a (1)	none	94 ^[c]
3	8b (2)	none	21
4	7a (2)	none	trace
5	7b (2)	none	0
6	Ag ₂ CO ₃ (2)	none	83
7	Ag ₂ CO ₃ (1)	none	25 ^[d]
8	AgPF ₆ (2)	none	12
9	AgPF ₆ (2)	L1	27
10	AgPF ₆ (2)	L2	16
11	AgPF ₆ (2)	L3	13
12	AgPF ₆ (2)	L1+11	62
13	AgPF ₆ (2)	L2+11	44
14	AgPF ₆ (2)	L3+11	18

Reaction conditions: **9a** (0.10 mmol) and Ag catalyst (1-2 mol% on Ag atom) in CH₃CN (0.5 mL) at 80 °C for 15 h. **11**: 1-Phenylimidazole. ^[a]Yield was determined by ¹H NMR analysis using 1,3,5-trimethoxybenzene as an internal standard. ^[b]Isolated yield. ^[c]Reaction over 50 h. ^[d]Reaction over 30 h.



Effects of solvents were examined toluene, 1,4-dioxane, and 1,2-dichloroethane (Table 2). When toluene, 1,4-dioxane, and DCE were used as solvent for the cyclization of **9a**, only trace amount of the product was obtained. These results suggested that the use of CH₃CN is crucial for the silver catalyzed cyclization.

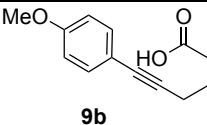
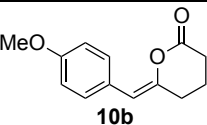
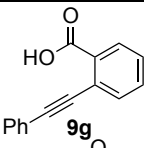
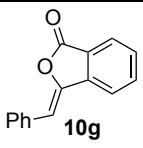
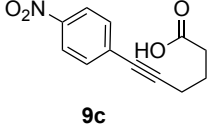
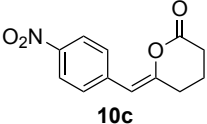
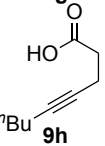
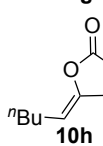
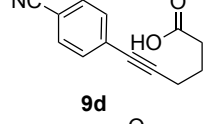
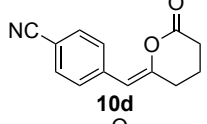
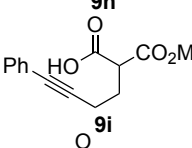
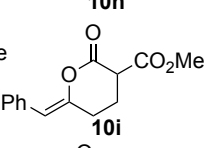
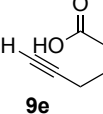
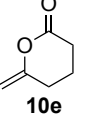
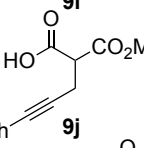
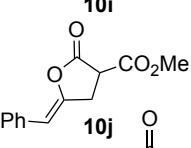
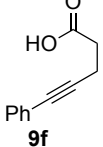
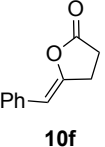
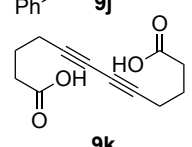
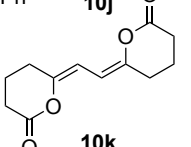
Table 2. Solvent Effects on the Cyclization of Alkynoic Acid

entry	solvent	Yield [%]
1	CH ₃ CN	98 ^a
2	Toluene	trace ^b
3	1,4-dioxane	trace ^b
4	DCE	6 ^b

^aIsolated yield. ^bYield was determined by ¹H NMR analysis using 1,3,5-trimethoxybenzene as an internal standard.

With the optimal conditions in hand using **8a** as the acid-base cooperative catalyst, the scope of alkyne-tethered carboxylic acids (**9**) was explored (Table 2). Both electron-donating (-OMe; **9b**) and withdrawing groups (-NO₂ and -CN: **9c,d**) were competent substituents at the *para* position of the aromatic ring of the phenylacetylene derivatives to afford the cyclized products **10b–d** in high yields (94–99%, entries 1-3). Terminal alkyne **9e** was less reactive (25%, entry 4). 5-Phenyl-4-pentynoic acid (**9f**) underwent 5-*exo-dig* cyclization with exclusive regio- and stereoselectivities to produce (*Z*)-benzylidenebutyrolactone (**10f**) in 93% yield (entry 5). The reaction of 2-(phenylethynyl)benzoic acid (**9g**) occurred preferentially in 5-*exo-dig* cyclization mode to afford (*Z*)-3-benzylideneisobenzofuran-1(3*H*)-one (**10g**) as the major product, while the competitive 6-*endo-dig* cyclization formed the corresponding γ -lactone (1%) as an inseparable by-product (entry 6). 4-Nonynoic acid **9h** was transformed to an *E/Z* mixture (13/87) of the corresponding γ -lactone **10h** in 88% yield (entry 7). Similar erosion of stereoselectivity on the cyclization of **9h** was reported for other silver(I) and gold(I) catalytic systems.^{9b,18} Monomethyl malonate derivatives **9i** and **9j** were suitable substrates for the *exo* cyclization, giving the corresponding six- (**10i**) and five-membered (**10j**) lactones in 87% and 84% yields, respectively (entries 8 and 9). Two-fold cyclization of dodeca-5,7-diynedioic acid **9k** occurred cleanly to furnish the bislactone **10k** in 98% yield (entry 10).

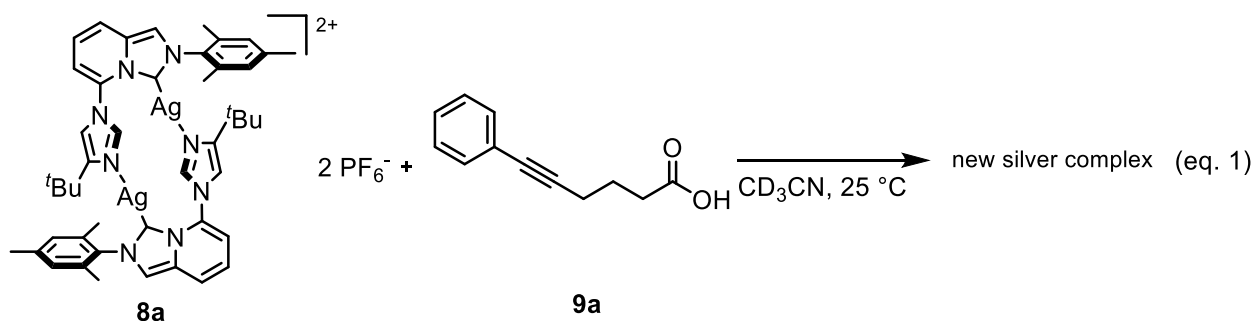
Table 3. Cyclization of Alkyne-Tethered Carboxylic Acids (**9**) Catalyzed by **8a**

entry	substrate	product	yield	entry	substrate	product	yield
1			98%	6			97% ^[b]
2			99%	7			88% (E/Z=13/87)
3			94%	8			87%
4			25% ^[a]	9			84%
5			93%	10			98%

Reaction conditions: **9** (0.1 mmol) and **8a** (0.001 mmol, 2 mol% on Ag atom) in CH₃CN (0.5 mL) at 80 °C for 15 h. ^[a]Determined by ¹H NMR analysis using phenanthrene as an internal standard due to the volatility of the product. ^[b]Including 1% of 3-phenyl-1*H*-isochromen-1-one.

NMR Experiment

To gain insight into the reaction mechanism, the interactions between **8a** and **9a** were investigated by ^1H NMR titration with varying amounts of carboxy-tethered alkyne **9a** (**9a**/Ag: 0–4 equiv) in CD_3CN at $25\text{ }^\circ\text{C}$ (eq. 1). Only a trace of cyclization was observed at this temperature. Upon addition of the alkyne (**9a**), signals for a new species appeared and their intensities increased gradually as the **9a**/Ag ratio increased (Table 7). Figure 5 shows aromatic regions of the spectra of **8a** in CD_3CN and the mixture of **8a** and **9a** at **9a**/Ag = 4, where the ratio between the new species and **8a** is 19:81 (the apparent chemical shift change was observed for H_a^* upon the addition of **9a**). It may be due to weak interaction between H_a^* and **9a**). The most significant spectral change upon addition of **9a** is the downfield shift of the signals arising from the imidazole pendant. This is likely due to protonation of the imidazole at the N(4) atom by the carboxyl group of **9a**, resulting in dissociation of the intermolecular N–Ag interactions and monomerization of the silver complex. Since no significant chemical shift change was observed at the propargylic methylene protons of **9a**, its alkyne moiety should be virtually uncoordinated with the silver atom. Instead, coordination of CD_3CN to the vacant site of the silver atom is reasoned.



^1H NMR titration of **8a** with benzoic acid in CD_3CN produced new signals similar to those detected in the titration of **8a** with **9a** in CD_3CN . In contrast, no new species appeared in the titration of **8a** with benzoic acid in CD_2Cl_2 . This suggests that acetonitrile coordinates to the cationic silver complex, facilitating the monomerization of the complex with simultaneous protonation of the imidazole moiety. This behavior is consistent with low catalytic activity of **8a** in toluene, 1,4-dioxane, or 1,2-dichloroethane.

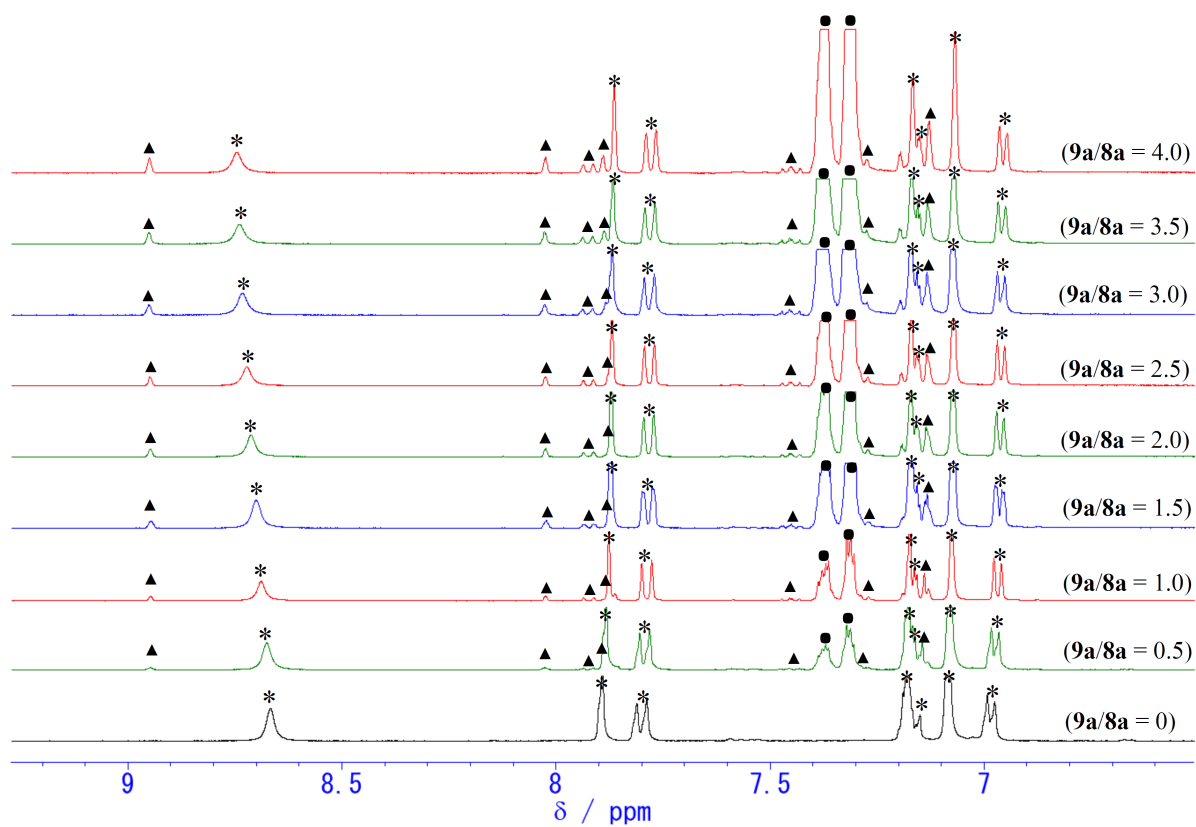


Figure 5. ^1H NMR titration with varying amounts of **9a** ($9\text{a}/8\text{a} = 0\text{-}4$). **8a** = *, **9a** = ●, new silver complex = ▲.

DFT Calculation

Density functional theory (DFT) calculations were conducted to investigate the mechanism of the Ag-catalyzed cyclization. The geometry optimizations as well as frequency calculations were performed at the M06/lanl2dz (for silver) and 6-31+G(d,p) (for other elements) levels of theory^{19,20} using Gaussian 16,²¹ and the solvation effect of acetonitrile was introduced using the CPCM model.²² The relative energies were corrected for the Gibbs free energies and given in kcal mol⁻¹ (Figure 3).

A mononuclear silver-alkyne π complex (**Int-A**) with an interaction between imidazole and the carboxylic acid is proposed as a plausible precursor for the cyclization. Nucleophilic *anti*-attack of the carboxy group to the alkyne moiety in the 6-*exo-dig* mode occurs through **TS-A** to form a six-membered lactone (**Int-B**) hydrogen-bonded with the protonated imidazole moiety. This step has an energy barrier of 21.4 kcal/mol and is 15.7 kcal mol⁻¹ endothermic. After dissociation of the hydrogen bond leading to the more stable intermediate **Int-C**, protonation of the Ag–C bond through **TS-B** gives the lactone (**Int-D**) π -coordinated to the Ag atom at the *exo* alkene moiety. These results support the expectation that the Brønsted base moiety of the NHC ligand would participate cooperatively in the silver-catalyzed cyclization of the alkyne-tethered carboxylic acid.

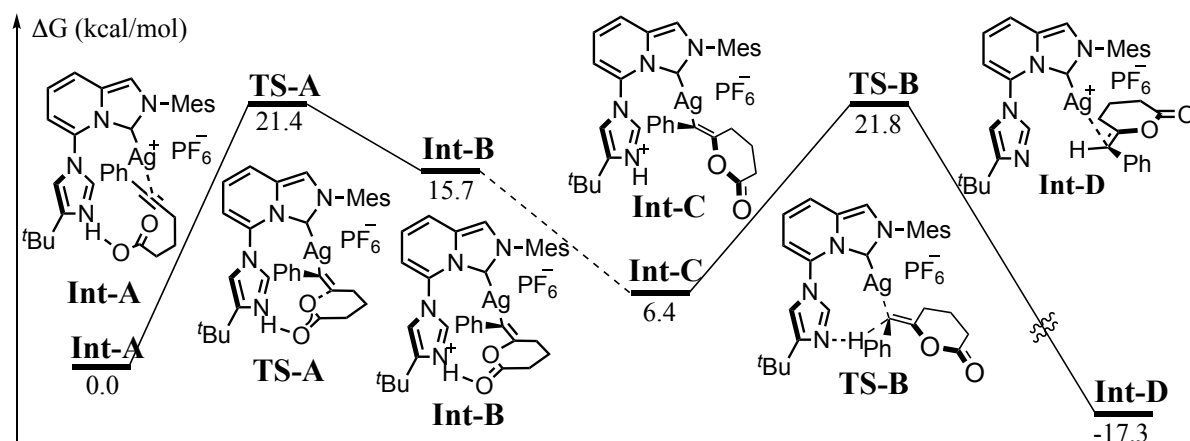


Figure 6. Energy diagram for cyclization of **9a** catalyzed by silver complex **8a**. Calculations were performed at M06/lanl2dz (for silver) and 6-31+G(d,p) (for other elements) levels of theory. The counter anion (PF_6^-) of 3D model of **TS-A** is omitted for clarity.

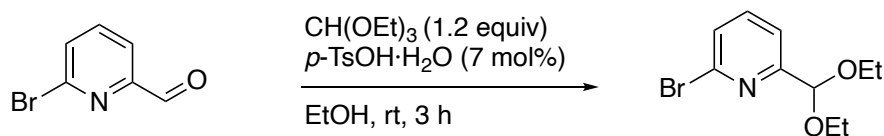
Conclusion

In conclusion, the author synthesized neutral and cationic silver(I) complexes with 5-(4-(*tert*-butyl)-1*H*-imidazol-1-yl)-imidazo[1,5-*a*]pyridin-3-ylidene ligands. Single-crystal XRD analysis showed that the neutral and cationic complexes existed as monomers or dimers. The cationic silver complexes showed catalytic activity for the cyclization of alkyne-tethered carboxylic acids. NMR experiments and DFT calculations indicated that an *in situ* generated monomeric cationic silver complex with an imidazole pendant acts as a cooperative Lewis acid-base catalyst.

Experimental Section

All air and moisture-sensitive reactions were operated using the standard Schlenk techniques or glove box under nitrogen gas atmosphere. THF, DCM, and toluene were dried and deoxygenated by using Grubbs column (Glass Counter Solvent Dispensing System, Nikko Hansen & Co, Ltd.). Dry CH₃CN was purchased from Kanto Chemical Co., Inc.. CD₃CN was distilled with CaH₂ as a drying reagent and degassed by freeze pump thaw cycles. 6-Bromo-2-pyridinecarboxaldehyde was purchased from BLD Pharmatech Ltd.. Other commercially available compounds were purchased from Tokyo Chemical Industry Co., Ltd. (TCI), Sigma-Aldrich Co. LLC, or FUJIFILM Wako Pure Chemical Corporation. ¹H NMR (400 MHz) and ¹³C{¹H} NMR (100 MHz) spectra were measured on JEOL ECZ-400S spectrometer. All ¹H NMR chemical shifts were reported in ppm (δ) relative to the chemical shifts of residual solvent resonances (CDCl₃ at δ 7.26, C₆D₆ at δ 7.16, DMSO-*d*₆ at δ 2.50, and DCM-*d*₂ at δ 5.32). All ¹³C{¹H} NMR chemical shifts were reported in ppm (δ) relative to carbon resonances of CDCl₃ at δ 77.0, C₆D₆ at δ 127.7, DMSO-*d*₆ at δ 39.5, or DCM-*d*₂ at δ 53.8. High-resolution mass spectra were obtained with Thermo Fisher Scientific Exactive, JEOL JMS-T100LP, or JEOL JMS-700TZ at the Instrumental Analysis Division, Equipment Management Center, Creative Research Institution, Hokkaido University. IR spectra were obtained on JASCO FT-IR-4600 spectrometer. Flash column chromatography was performed using silica gel (Wakogel FC-40, 0.020-0.040 mm >70%), and Celite[®] 535 was used for Celite filtration. Silver catalyzed cyclization was conducted using EYELA RCH-1000 of TOKYO RIKAKIKAI CO, LTD as a heating reactor.

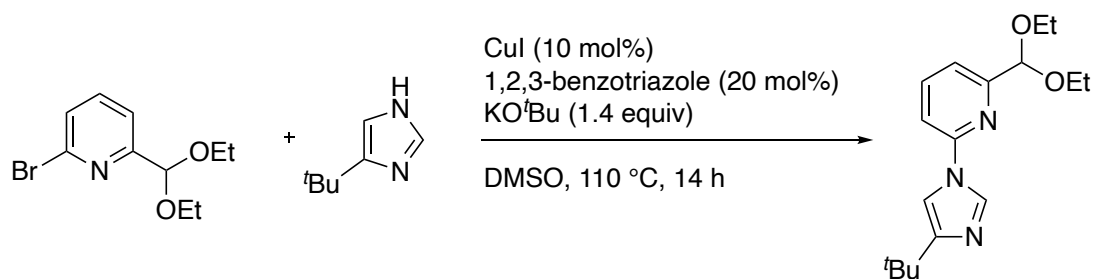
2-Bromo-6-(diethoxymethyl)pyridine (2)²³



6-Bromopicolinaldehyde (5.02 g, 27.0 mmol) and *p*-toluenesulfonic acid monohydrate (380 mg, 2.0 mmol, 7 mol%) were dissolved in EtOH (54 mL) under nitrogen atmosphere. After addition of triethyl orthoformate (5.50 mL, 33.0 mmol, 1.2 equiv), the reaction mixture was stirred for 3 hours at room temperature. The resulting solution was quenched with saturated NaHCO_3 aqueous solution, and the aqueous layer was extracted with EtOAc. The combined organic layer was dried over Na_2SO_4 , filtrated, and evaporated. The crude mixture was purified by silica-gel flash column chromatography (hexane/EtOAc 4:1) to afford the desired product as colorless oil (6.71 g, 25.8 mmol, 96% yield).

Colorless oil. $^1\text{H NMR}$ (400 MHz, CDCl_3 , 25 °C): δ 7.57-7.54 (m, 2H), 7.43 (dd, $J = 6.3$, 2.5 Hz, 1H), 5.38 (s, 1H), 3.77-3.67 (m, 2H), 3.64-3.55 (m, 2H), 1.23 (t, $J = 7.1$ Hz, 1H). $^{13}\text{C}\{^1\text{H}\}$ NMR (100 MHz, CDCl_3 , 25 °C): δ 159.9, 141.1, 139.0, 127.8, 119.8, 102.2, 62.7, 15.1.

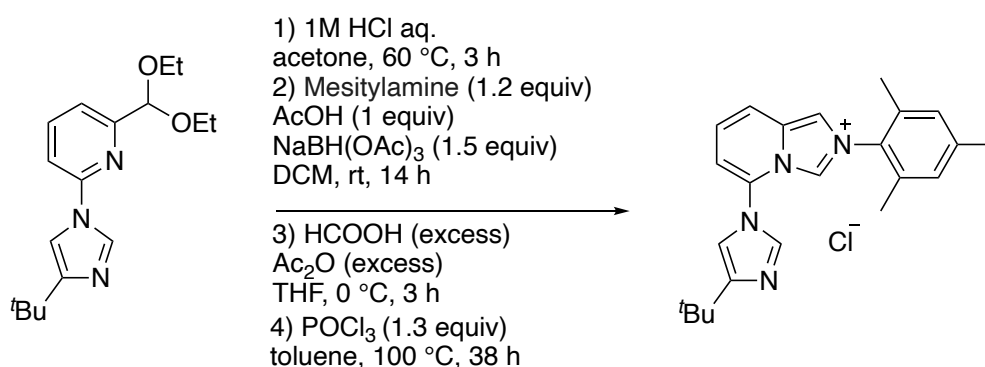
2-(4-(*Tert*-butyl)-1*H*-imidazol-1-yl)-6-(diethoxymethyl)pyridine (3)²⁴



CuI (190 mg, 1.0 mmol, 10 mol%) and 1,2,3-benzotriazole (238 mg, 2.0 mmol, 20 mol%) was dissolved in dry DMSO (10 mL) under nitrogen atmosphere. 2-bromo-6-(diethoxymethyl)pyridine (2.60 g, 10 mmol), 4-(*tert*-butyl)-1*H*-imidazole (1.24 g, 10 mmol, 1.0 equiv), and KO^tBu (1.57 g, 14 mmol, 1.4 equiv) were added to the resulting yellow solution, and the reaction mixture was stirred at 110 °C for 14 hours. After cooling to room temperature, water was poured into the solution, and the aqueous layer was extracted with EtOAc. The combined organic layer was washed with brine twice, dried over Na_2SO_4 , filtrated, and evaporated. The crude mixture was purified by silica-gel flash column chromatography (hexane/EtOAc 4:1 to 1:1) to afford the desired product (2.40 g, 7.9 mmol, 79% yield).

Pale yellow oil. **IR** (ATR, ν/cm^{-1}): 2968 w, 2900 w, 2871 w, 1581 m, 1464 s, 1390 w, 1333 w, 1261 m, 1192 w, 1113 m, 1057 s, 837 w, 802 s, 729 m, 677 w, 619 w. **^1H NMR** (400 MHz, CDCl_3 , 25 °C): δ 8.31 (d, $J = 1.1$ Hz, 1H), 7.80 (t, $J = 7.9$ Hz, 1H), 7.48 (d, $J = 7.8$ Hz, 1H), 7.33 (d, $J = 1.6$ Hz, 1H), 7.27 (d, $J = 8.2$ Hz, 1H), 5.42 (s, 1H), 3.77-3.67 (m, 2H), 3.65-3.57 (m, 2H), 1.32 (s, 9H), 1.24 (t, $J = 7.1$ Hz, 6H). **$^{13}\text{C}\{^1\text{H}\}$ NMR** (100 MHz, CDCl_3 , 25 °C): δ 158.3, 153.5, 148.3, 139.5, 134.1, 118.7, 111.6, 109.8, 102.2, 62.5, 31.8, 29.9, 15.2. **HRMS** (EI^+) m/z calc. for $\text{C}_{17}\text{H}_{25}\text{N}_3\text{O}_2$ 303.19468 found 303.19409.

5-(4-(*Tert*-butyl)-1*H*-imidazol-1-yl)-2-mesitylimidazo[1,5-*a*]pyridin-2-ium Chloride (5a)²⁵

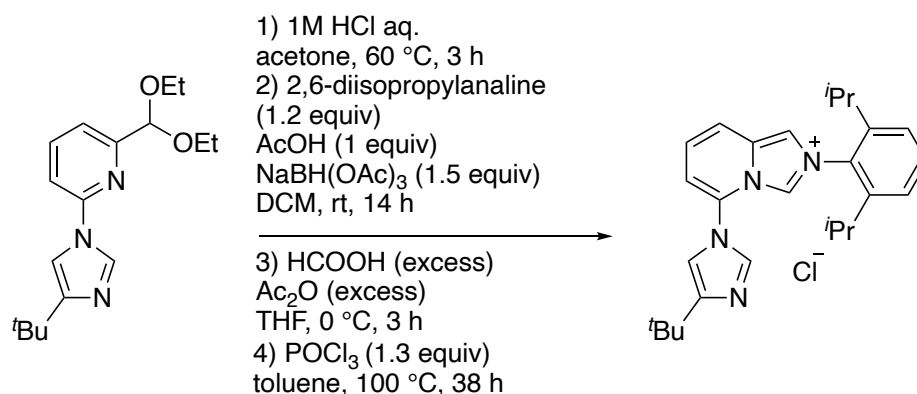


2-(4-(*tert*-butyl)-1*H*-imidazol-1-yl)-6-(diethoxymethyl)pyridine (1.35 g, 4.94 mmol, 1 equiv) was dissolved in the mixed solvent of acetone (11 mL) and 1 M HCl aq (11 mL) under nitrogen atmosphere, and the resulting solution was stirred at 60 °C for 3 hours. After quenching with saturated NaHCO_3 aqueous solution, the aqueous layer was extracted with DCM. The combined organic layer was dried over Na_2SO_4 , filtrated, and evaporated. The crude mixture was dissolved in dry DCM (18 mL) under nitrogen atmosphere, and acetic acid (297 mg, 4.94 mmol, 1 equiv) and 2,4,6-trimethylalanine (802 mg, 5.93 mmol, 1.2 equiv) were added to the solution. After addition of $\text{NaBH}(\text{OAc})_3$ (1.57 g, 7.41 mmol, 1.5 equiv) to the reaction mixture at 0 °C, the resulting suspension was stirred at room temperature for 14 hours. After quenching with saturated NaHCO_3 aqueous solution, aqueous layer was extracted with DCM, and the combined organic layer was dried over Na_2SO_4 , filtrated, and evaporated. The resulting brown oil was dissolved in dry THF (16 mL) under nitrogen atmosphere. Formic acid (1.0 mL) and acetic anhydride (1.0 mL) were stirred for 2 hours at room temperature under nitrogen atmosphere before it was added dropwise to the above THF solution at 0 °C. The resulting mixture was stirred for 3 hours at 0 °C, and the mixture was quenched with saturated

NaHCO₃ aqueous solution. Aqueous layer was extracted with DCM, and the combined organic layer was dried over Na₂SO₄, filtrated, and evaporated. The crude mixture was just pass through silica-gel. The crude product was dissolved in dry toluene (3.0 mL) under nitrogen atmosphere. POCl₃ (0.978 g, 6.42 mmol, 1.3 equiv) was added dropwise to the solution, and the resulting solution was stirred for 38 hours at 100 °C. After quenching with MeOH (1.0 mL), the resulting precipitation was stirred for an additional 1 hour at room temperature. The crude solution was directly purified by basic alumina column chromatography (DCM/MeOH 9:1 to 7:3) to afford the desired product (1.29 g, 3.26 mmol, 66% yield).

Light gray solid. **mp**: 116 °C (decomp.). **IR** (ATR, ν /cm⁻¹): 3359 br, 3063 w, 2959 w, 2902 w, 2862 w, 1665 m, 1551 m, 1485 s, 1259 s, 1196 m, 1151 m, 1036 m, 962 m. **¹H NMR** (400 MHz, DMSO-*d*₆, 25 °C): δ 9.94 (s, 1H), 8.62 (s, 1H), 8.11 (s, 1H), 8.05 (d, *J* = 9.2 Hz, 1H), 7.54-7.41 (m, 3H), 7.17 (s, 2H), 2.35 (s, 3H), 2.03 (s, 6H), 1.27 (s, 9H). **¹³C{¹H} NMR** (100 MHz, DMSO-*d*₆, 25 °C): δ 152.6, 140.5, 137.6, 134.4, 131.7, 131.5, 129.1, 129.0, 125.8, 125.6, 118.2, 116.4, 114.1, 113.3, 31.7, 29.7, 20.6, 17.1. **HRMS** (ESI⁺) *m/z* calc. for C₂₃H₂₇N₄ 359.22302 found 359.22290.

5-(4-(*Tert*-butyl)-1*H*-imidazol-1-yl)-2-(2,6-diisopropylphenyl)imidazo[1,5-*a*]pyridin-2-ium Chloride (**5b**)²⁵

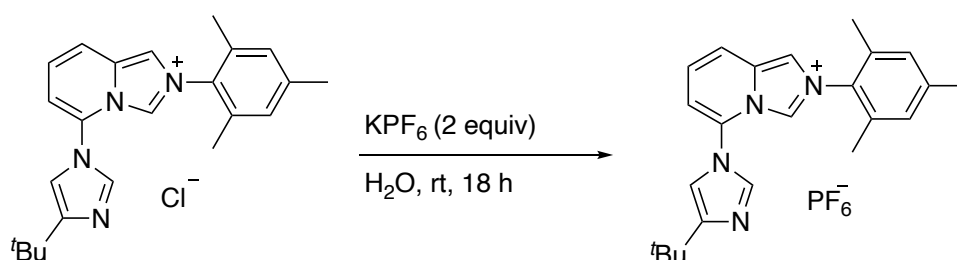


2-(4-(*tert*-butyl)-1*H*-imidazol-1-yl)-6-(diethoxymethyl)pyridine (1.20 g, 3.95 mmol, 1 equiv) was dissolved in mixed solvent of acetone (11 mL) and 1 M HCl aq (11 mL) under nitrogen atmosphere, and the resulting solution was stirred at 60 °C for 3 hours. After quenching with saturated NaHCO₃ aqueous solution, the aqueous layer was extracted with DCM. The combined organic layer was dried over Na₂SO₄, filtrated, and evaporated. The crude mixture was dissolved in dry DCM (18 mL) under nitrogen atmosphere, and acetic acid (237

mg, 3.95 mmol, 1 equiv) and 2,6-diisopropylanaline (840 mg, 4.74 mmol, 1.2 equiv) were added to the solution. After addition of NaBH(OAc)₃ (1.25 g, 5.92 mmol, 1.5 equiv) to the reaction mixture at 0 °C, the resulting suspension was stirred at room temperature for 14 hours. After quenching with saturated NaHCO₃ aqueous solution, aqueous layer was extracted with DCM, and the combined organic layer was dried over Na₂SO₄, filtrated, and evaporated. The resulting brown oil was dissolved in dry THF (16 mL) under nitrogen atmosphere. Formic acid (1.0 mL) and acetic anhydride (1.0 mL) were stirred for 2 hours at room temperature under nitrogen atmosphere before it was added dropwise to the above THF solution at 0 °C. The resulting mixture was stirred for 3 hours at 0 °C, and the mixture was quenched with saturated NaHCO₃ aqueous solution. Aqueous layer was extracted with DCM, and the combined organic layer was dried over Na₂SO₄, filtrated, and evaporated. The crude mixture was just pass through silica-gel. The crude product was dissolved in dry toluene (3.0 mL) under nitrogen atmosphere. POCl₃ (0.792 g, 5.13 mmol, 1.3 equiv) was added dropwise to the solution, and the resulting solution was stirred for 38 hours at 100 °C. After quenching with MeOH (1.0 mL), the resulting precipitation was stirred for an additional 1 hour at room temperature. The crude solution was directly purified by basic alumina column chromatography (DCM/MeOH 9:1 to 7:3) to afford the desired product (1.19 g, 2.72 mmol, 69% yield).

Light gray solid. **mp**: 205 °C (decomp.). **IR** (ATR, ν /cm⁻¹): 3292 w, 3205 w, 3058 m, 2960 m, 1662 m, 1550 m, 1485 s, 1172 s, 1033 s, 802 s, 756 s, 703 m. **¹H NMR** (400 MHz, DMSO-*d*₆, 25 °C): δ 10.00 (d, *J* = 0.8 Hz, 1H), 8.69 (s, 1H), 8.08 (d, *J* = 1.4 Hz, 1H), 8.05 (d, *J* = 9.2 Hz, 1H), 7.65 (t, *J* = 8.0 Hz, 1H), 7.54-7.45 (m, 4H), 7.40 (d, *J* = 0.8 Hz, 1H), 2.27 (sept., *J* = 6.9 Hz, 2H), 1.26 (s, 9H), 1.14 (d, *J* = 6.8, 6H), 1.13 (d, *J* = 6.8 Hz, 6H). **¹³C{¹H} NMR** (100 MHz, DMSO-*d*₆, 25 °C): δ 152.7, 145.0, 137.3, 131.6, 131.5, 131.2, 129.1, 126.11, 126.06, 124.3, 118.1, 117.2, 114.0, 112.8, 31.6, 29.7, 27.6, 24.2, 23.9. **HRMS** (ESI⁺) *m/z* calc. for C₂₆H₃₃N₄ 401.26997 found 401.26975.

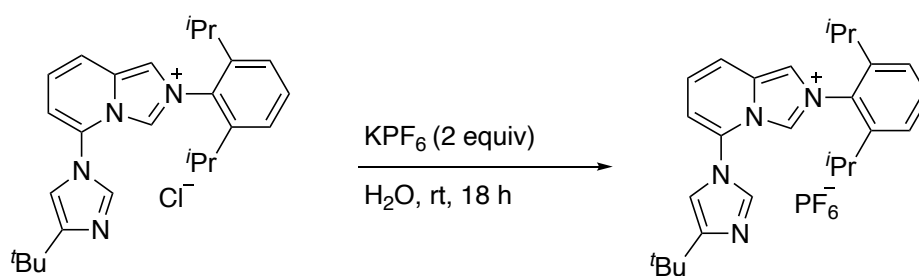
**5-(4-(*Tert*-butyl)-1*H*-imidazol-1-yl)-2-mesitylimidazo[1,5-*a*]pyridin-2-ium
Hexafluorophosphate (6a)**



5-(4-(*Tert*-butyl)-1*H*-imidazol-1-yl)-2-mesitylimidazo[1,5-*a*]pyridin-2-ium chloride (100 mg, 0.25 mmol) was dissolved in deionized water (0.6 mL), and KPF₆ (92.2 mg, 0.5 mmol, 2 equiv) in water (1.0 mL) was added dropwise to the reaction mixture at room temperature. The resulting mixture was stirred at room temperature for 18 hours. The resulting white precipitation was filtered and washed with ether and deionized water. The filtrate was dried in *vacuo* to afford the desired product as a white solid (108 mg, 0.21 mmol, 86% yield).

White solid. **mp**: 193 °C (decomp.). **IR** (ATR, ν /cm⁻¹): 3157 br, 2958 m, 1668 s, 1556 s, 1502 s, 1400 m, 1360 w, 1261 s, 1157 m, 1119 w, 1039 s, 970 w, 833 s. **¹H NMR** (400 MHz, DMSO-*d*₆, 25 °C): δ 9.92 (d, *J* = 0.9 Hz, 1H), 8.53 (d, *J* = 1.8 Hz, 1H), 8.08 (d, *J* = 1.6 Hz, 1H), 8.02 (d, *J* = 9.2 Hz, 1H), 7.51-7.40 (m, 3H), 7.16 (s, 2H), 2.34 (s, 3H), 2.02 (s, 6H), 1.27 (s, 9H). **¹³C{¹H} NMR** (100 MHz, DMSO-*d*₆, 25 °C): δ 152.6, 140.4, 137.5, 134.4, 131.7, 131.5, 129.1, 128.9, 125.8, 125.6, 118.1, 116.2, 114.0, 113.2, 31.6, 29.7, 20.6, 17.0. **HRMS** (ESI⁺) *m/z* calc. for C₂₃H₂₇N₄ 359.22302 found 359.22315.

**5-(4-(*Tert*-butyl)-1*H*-imidazol-1-yl)-2-(2,6-diisopropylphenyl)imidazo[1,5-*a*]pyridin-2-ium
Hexafluorophosphate (6b)**

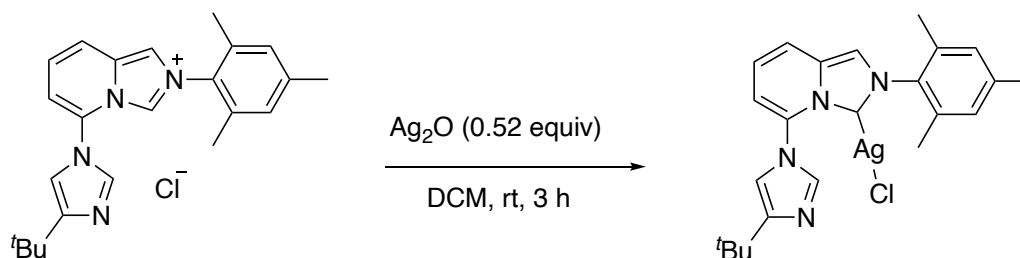


5-(4-(*Tert*-butyl)-1*H*-imidazol-1-yl)-2-(2,6-diisopropylphenyl)imidazo[1,5-*a*]pyridin-2-ium chloride (202 mg, 0.46 mmol, 1 equiv) was dissolved in deionized water (1.3 mL), and KPF₆

(169 mg, 0.92 mmol, 2 equiv) in deionized water (2.0 mL) was added dropwise to the reaction mixture at room temperature. The resulting mixture was stirred at room temperature for 18 hours. The white precipitate was filtered and washed with ether and deionized water. The filtrate was dried in *vacuo* to afford the desired product as a white solid (213.1 mg, 0.39 mmol, 85% yield).

White solid. **mp**: 188 °C (decomp.). **IR** (ATR, ν / cm^{-1}): 3170 w, 3140 m, 2964 s, 1670 m, 1558 m, 1487 s, 1361 w, 1263 s, 1223 w, 1034 m, 845 s, 754 s, 708 w. **$^1\text{H NMR}$** (400 MHz, $\text{DMSO-}d_6$, 25 °C): δ 10.00 (d, $J = 1.2$ Hz, 1H), 8.66 (d, $J = 1.6$ Hz, 1H), 8.07 (d, $J = 1.6$ Hz, 1H), 8.03 (d, $J = 8.8$ Hz, 1H), 7.65 (t, $J = 8.0$ Hz, 1H), 7.54-7.45 (m, 4H), 7.40 (d, $J = 1.2$ Hz, 1H), 2.27 (sept., $J = 6.8$ Hz, 2H), 1.26 (s, 9H), 1.14 (d, $J = 6.8$ Hz, 6H), 1.13 (d, $J = 6.8$ Hz, 6H). **$^{13}\text{C}\{^1\text{H}\}$ NMR** (100 MHz, $\text{DMSO-}d_6$, 25 °C): δ 152.7, 145.0, 137.3, 131.6, 131.5, 131.2, 129.1, 126.2, 126.1, 124.3, 118.1, 117.1, 113.9, 112.9, 31.6, 29.7, 27.6, 24.2, 23.9. **HRMS** (ESI⁺) m/z calc. for $\text{C}_{26}\text{H}_{33}\text{N}_4$ 401.26997 found 401.26988.

(5-(4-(*Tert*-butyl)-1*H*-imidazol-1-yl)-2-mesityl-2,3-dihydroimidazo[1,5-*a*]pyridin-3-yl)silver(I) Chloride (7a)

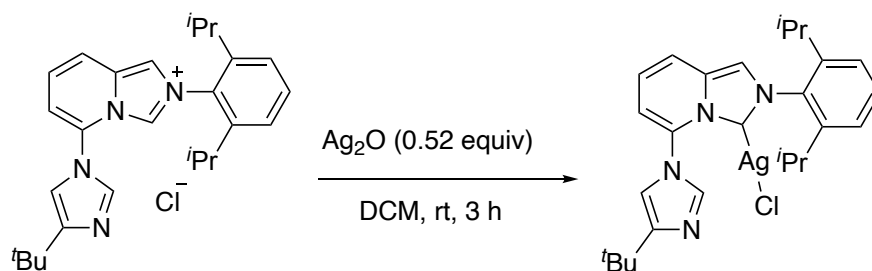


5-(4-(*Tert*-butyl)-1*H*-imidazol-1-yl)-2-mesitylimidazo[1,5-*a*]pyridin-2-ium chloride (48.9 mg, 0.124 mmol, 1 equiv) was dissolved in dry DCM (1.5 mL), and silver(I) oxide (16.2 mg, 0.064 mmol, 0.52 equiv) was added to the reaction mixture. The reaction mixture was stirred at room temperature for 3 hours under the dark. The mixture was then filtered through celite and subsequently eluted with DCM . The filtrate was dried in *vacuo* to afford the desired product as a white solid (52.2 mg, 0.10 mmol, 84% yield). The crystal suitable for X-ray crystallography was grown from $\text{DCM}/\text{Et}_2\text{O}$ solution.

White solid. **mp**: 141 °C (decomp.). **IR** (ATR, ν / cm^{-1}): 3084 w, 2952 m, 1662 m, 1541 w, 1485 s, 1377 m, 1315 w, 1255 s, 1196 s, 1039 s, 960 w, 791 s, 748 w, 708 s, 632 s. **$^1\text{H NMR}$** (400 MHz, CDCl_3 , 25 °C): δ 7.75 (d, $J = 1.4$ Hz, 1H), 7.57 (dd, $J = 9.4, 0.9$ Hz, 1H), 7.47 (s,

1H), 7.13 (d, $J = 1.4$ Hz, 1H), 7.07 (dd, $J = 9.3$ Hz, 6.7 Hz, 1H), 6.98 (s, 2H), 6.76 (dd, $J = 6.7$ Hz, 1.0 Hz, 1H), 2.33 (s, 3H), 1.95 (s, 6H), 1.42 (s, 9H). $^{13}\text{C}\{^1\text{H}\}$ NMR (100 MHz, CDCl_3 , 25 °C): δ 155.3, 140.1, 137.0, 136.0, 133.9, 132.8, 131.9, 129.6, 122.8, 118.7, 114.8, 113.2, 113.0, 32.1, 29.7, 21.1, 17.7. A signal from carbon adjacent to silver was not detected. HRMS (ESI⁺) m/z calc. for $\text{C}_{23}\text{H}_{26}\text{AgClN}_4\text{Na}$ 523.07946 found 523.07868.

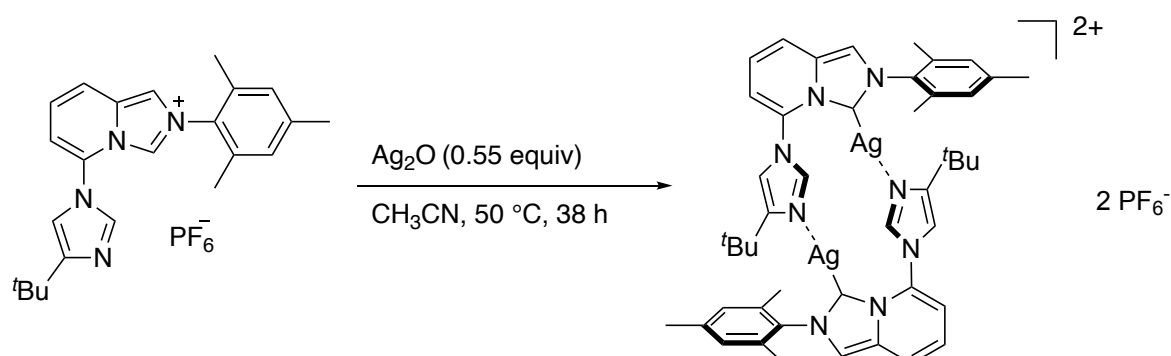
(5-(4-(*Tert*-butyl)-1*H*-imidazol-1-yl)-2-(2,6-diisopropylphenyl)-2,3-dihydroimidazo[1,5-*a*]pyridin-3-yl)silver(I) Chloride (7b)



5-(4-(*Tert*-butyl)-1*H*-imidazol-1-yl)-2-(2,6-diisopropylphenyl)imidazo[1,5-*a*]pyridin-2-ium chloride (60.0 mg, 0.14 mmol, 1 equiv) was dissolved in dry DCM (2.0 mL) and then silver(I) oxide (16.3 mg, 0.07 mmol, 0.52 equiv) was added to the reaction mixture. The reaction mixture was stirred at room temperature for 3 hours under the dark. The mixture was then filtered through celite and subsequently eluted with DCM. The filtrate was dried in *vacuo* to afford the desired product as a white solid (61.0 mg, 0.11 mmol, 82% yield). The crystal suitable for X-ray crystallography was grown from DCE/ Et_2O solution.

White solid. **mp**: 143 °C (decomp.). **IR** (ATR, ν / cm^{-1}): 3114 w, 3076 w, 3076 w, 2958 s, 2866 w, 1664 m, 1543 m, 1485 s, 1383 s, 1315 m, 1257 s, 1178 s, 1113 m, 1041 s, 758 s, 629 s. ^1H NMR (400 MHz, $\text{DCM}-d_2$, 25 °C): δ 7.78 (d, $J = 1.4$ Hz, 1H), 7.61 (d, $J = 9.4$ Hz, 1H), 7.57 (d, $J = 1.2$ Hz, 1H), 7.56 (t, $J = 8.0$ Hz, 1H), 7.33 (d, $J = 7.8$ Hz, 2H), 7.10 (dd, $J = 9.1$, 6.9 Hz, 1H), 7.08 (d, $J = 1.4$ Hz, 1H), 6.80 (dd, $J = 6.9$, 1.1 Hz, 1H), 2.17 (sept., $J = 6.8$ Hz, 2H), 1.34 (s, 9H), 1.22 (d, $J = 6.9$ Hz, 6H), 1.13 (d, $J = 6.9$ Hz, 6H). $^{13}\text{C}\{^1\text{H}\}$ NMR (100 MHz, $\text{DCM}-d_2$, 25 °C): δ 155.2, 145.7, 137.1, 136.0, 133.1, 132.2, 131.2, 124.6, 123.4, 119.0, 116.3, 113.6, 113.4, 32.4, 29.8, 28.7, 24.6, 24.5. A signal from carbon adjacent to silver was not detected. HRMS (ESI⁺) m/z calc. for $\text{C}_{26}\text{H}_{32}\text{AgClN}_4\text{Na}$ 565.12641 found 565.12465.

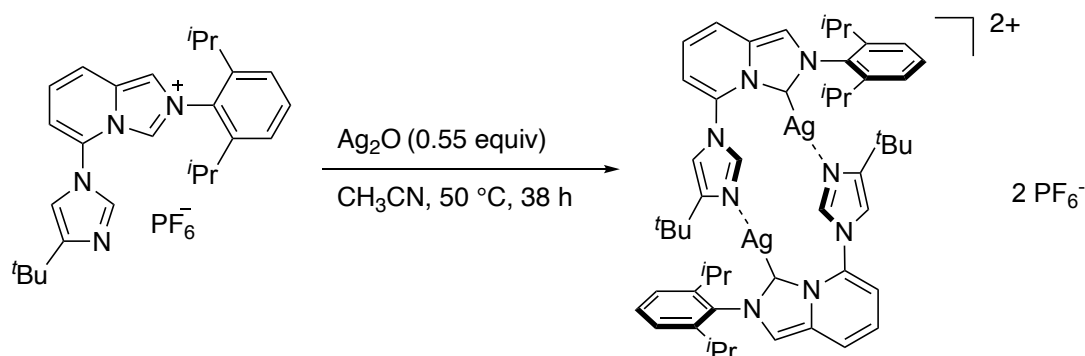
(5-(4-(*Tert*-butyl)-1*H*-imidazol-1-yl)-2-mesityl-2,3-dihydroimidazo[1,5-*a*]pyridin-3-yl)silver(I) Hexafluorophosphate dimer (8a)



5-(4-(*Tert*-butyl)-1*H*-imidazol-1-yl)-2-mesitylimidazo[1,5-*a*]pyridin-2-ium hexafluorophosphate (278.2 mg, 0.55 mmol, 1 equiv) was dissolved in dry CH₃CN (12 mL) under nitrogen atmosphere, and silver(I) oxide (69.5 mg, 0.3 mmol, 0.55 equiv) was added to the reaction mixture. The reaction mixture was stirred at 50 °C for 38 hours under the dark. The mixture was filtered through Celite and subsequently eluted with dry CH₃CN. The filtrate was dried in *vacuo*. Minimum amount of DCM was added to dissolve the residue, and ether was added to the DCM solution until white precipitation was formed. White precipitation was filtered and washed with ether as well as deionized water and dried under the reduced pressure to afford the desired product as a white solid (231.5 mg, 0.19 mmol, 69% yield). The crystal suitable for X-ray crystallography was grown from DCM/Et₂O solution.

White solid. **mp**: 198 °C (decomp.) . **IR** (ATR, ν /cm⁻¹): 3134 br, 2952 m, 1664 m, 1494 s, 1385 m, 1259 s, 1157 w, 1122 w, 835 s, 708 s, 681 m, 646 s. **¹H NMR** (400 MHz, DCM-*d*₂, 25 °C): δ 8.98 (s, 2H), 7.76 (d, J = 9.2 Hz, 2H), 7.72 (s, 2H), 7.17 (t, J = 8.0 Hz, 2H), 7.07 (d, J = 8.2 Hz, 2H), 7.06 (s, 2H), 7.01 (s, 2H), 6.93 (s, 1H), 6.92 (s, 1H), 2.33 (s, 6H), 2.09 (s, 6H), 1.94 (s, 6H), 1.09 (s, 18H). **¹³C{¹H} NMR** (100 MHz, DCM-*d*₂, 25 °C): δ 167.3 ($^1J(^{13}\text{C}—^{107}\text{Ag}) = 287.1$ Hz, $^1J(^{13}\text{C}—^{109}\text{Ag}) = 248.5$ Hz, *C*-carbene), 151.73, 151.70, 141.1, 140.6, 140.5, 136.7, 136.0, 134.3, 134.2, 134.1, 130.20, 130.18, 129.6, 123.2, 120.8, 117.6, 117.5, 116.44, 116.38, 115.0, 31.2, 30.2, 21.2, 17.7, 17.3. **³¹P{¹H} NMR** (162 MHz, DCM-*d*₂, 25 °C): δ -143.9 (quint., J = 711 Hz). **HRMS** (ESI⁺) *m/z* calc. for C₄₆H₅₂Ag₂F₆N₈P 1075.20586 found 1075.20311.

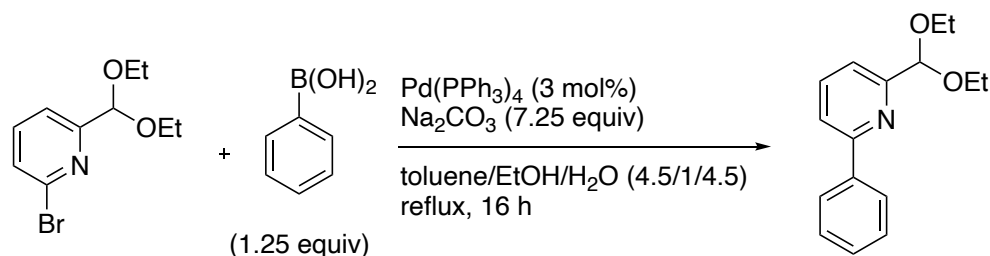
(5-(4-(*Tert*-butyl)-1*H*-imidazol-1-yl)-2-(2,6-diisopropylphenyl)-2,3-dihydroimidazo[1,5-*a*]pyridin-3-yl)silver(I) hexafluorophosphate Dimer (8b)



5-(4-(*Tert*-butyl)-1*H*-imidazol-1-yl)-2-(2,6-diisopropylphenyl)imidazo[1,5-*a*]pyridin-2-ium hexafluorophosphate (120.2 mg, 0.22 mmol, 1 equiv) was dissolved in dry CH₃CN (5.0 mL) under nitrogen atmosphere, and silver(I) oxide (28.1 mg, 0.12 mmol, 0.55 equiv) was added to the reaction mixture. The reaction mixture was stirred at 50 °C for 38 hours under the dark. The mixture was then filtered through Celite and subsequently eluted with dry CH₃CN. The filtrate was dried in *vacuo*. Minimum amount of DCM was added to dissolve the residue and then ether was added to the DCM solution until white precipitation was formed. White precipitation was filtered and washed with ether as well as deionized water and dried under the reduced pressure to afford the desired product as white solid (97.2 mg, 0.074 mmol, 68% yield). The crystal suitable for X-ray crystallography was grown from DCM/Et₂O solution.

White solid. **mp**: 194 °C (decomp.). **IR** (ATR, ν /cm⁻¹): 3157 br, 2962 m, 2871 w, 1668 m, 1495 m, 1363 m, 1257 s, 1124 w, 1053 m, 835 s, 710 s, 648 m. **¹H NMR** (400 MHz, DCM-*d*₂, 25 °C): δ 8.90 (d, J = 1.4 Hz, 2H), 7.80 (d, J = 9.6 Hz, 2H), 7.76 (d, J = 1.8 Hz, 2H), 7.52 (t, J = 7.8 Hz, 2H), 7.33 (dd, J = 10.1, 7.8 Hz, 4H), 7.23 (dd, J = 9.4 Hz, 7.1 Hz, 2H), 7.05 (dd, J = 4.6 Hz, 0.9 Hz, 2H), 7.04 (s, 2H), 2.48 (sept., J = 6.8 Hz, 2H), 2.06 (sept., J = 6.8 Hz, 2H), 1.29 (d, J = 6.9 Hz, 6H), 1.15 (d, J = 6.9 Hz, 6H), 1.13 (d, J = 6.0 Hz, 6H), 1.11 (d, J = 6.4 Hz, 6H), 0.96 (s, 18H). **¹³C{¹H} NMR** (100 MHz, DCM-*d*₂, 25 °C): δ 167.3 ($^1J(^{13}\text{C}—^{107}\text{Ag}) = 289.0$ Hz, $^1J(^{13}\text{C}—^{109}\text{Ag}) = 249.5$ Hz, C-carbene), 151.7, 146.4, 145.5, 140.10, 140.06, 135.8, 133.6, 133.5, 131.4, 129.6, 124.8, 124.2, 123.3, 120.9, 117.53, 117.47, 115.9, 31.0, 29.9, 28.5, 25.3, 24.4, 24.2, 23.8. **³¹P{¹H} NMR** (162 MHz, DCM-*d*₂, 25 °C): δ -143.9 (sept., J = 711 Hz). **HRMS** (ESI⁺) m/z calc. for C₅₂H₆₄Ag₂F₆N₈P 1159.29976 found 1159.29889.

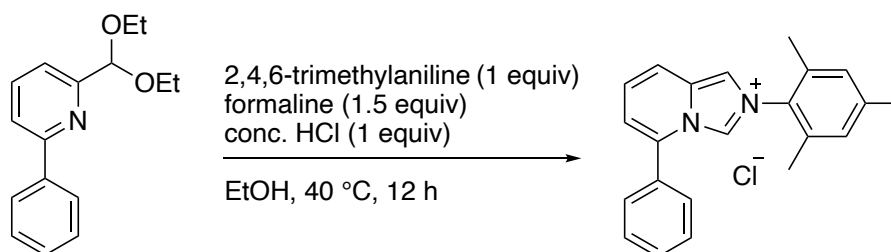
2-(Diethoxymethyl)-6-phenylpyridine²⁶



Phenylboronic acid (1.22 g, 10 mmol, 1.25 equiv) was dissolved in degassed toluene (27 mL), ethanol (6.0 mL), and H₂O (27 mL). Na₂CO₃ (6.11 g, 58.0 mmol, 7.25 equiv), Pd(PPh₃)₄ (347.1 mg, 0.24 mmol, 3 mol%) and 2-bromo-6-(diethoxymethyl)pyridine (1.79 g, 8.0 mmol, 1 equiv) were added to the solution under nitrogen atmosphere. The reaction mixture was refluxed for 16 hours. After filtration through short-pad of silica-gel with DCM, the resulting mixture was poured into water, extracted with DCM, dried over Na₂SO₄, filtrated, and evaporated. The residue was purified by silica-gel flash column chromatography (hexane/EtOAc 97:3) to afford the desired product as colorless oil (1.29 g, 5.02 mmol, 63% yield).

Colorless oil. ¹H NMR (400 MHz, CDCl₃, 25 °C): δ 8.02 (d, *J* = 6.9 Hz, 2H), 7.80 (t, *J* = 7.8 Hz, 1H), 7.68 (dd, *J* = 7.9, 1.0 Hz, 1H), 7.56 (dd, *J* = 7.7, 0.8 Hz, 1H), 7.47 (tt, *J* = 6.8, 1.2, 2H), 7.41 (tt, *J* = 7.6, 1.2 Hz, 1H), 5.56 (s, 1H), 3.83-3.75 (m, 2H), 3.70-3.63 (m, 2H), 1.27 (t, *J* = 7.1 Hz, 6H). ¹³C{¹H} NMR (100 MHz, CDCl₃, 25 °C): δ 158.4, 156.4, 139.2, 137.3, 128.8, 128.6, 127.0, 120.0, 119.2, 103.3, 62.5, 15.2.

2-Mesityl-5-phenylimidazo[1,5-*a*]pyridin-2-ium Chloride²⁷

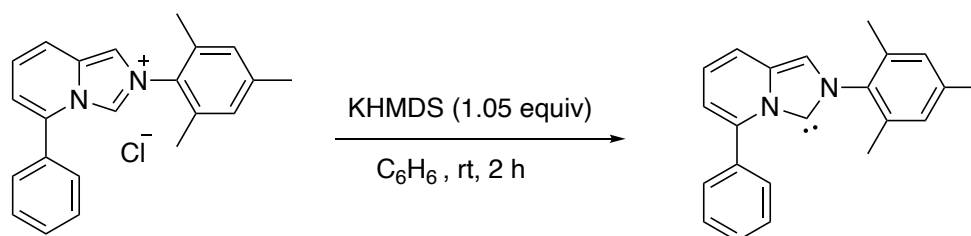


2,4,6-Trimethylaniline (135.2 mg, 1.0 mmol, 1 equiv) was dissolved in ethanol (2.0 mL). Formalin (58.8 μL, 1.5 mmol, 1.5 equiv), 2-(diethoxymethyl)-6-phenylpyridine (257.3 mg, 1.0 mmol, 1 equiv), and 12 N aqueous HCl solution (83.3 μL, 1.0 mmol, 1.0 equiv) were added to the solution under nitrogen atmosphere. The reaction mixture was stirred at 40 °C for 12 hours.

The reaction mixture was concentrated, and the residue was purified by column chromatography with basic alumina (DCM/MeOH 9:1) to afford the desired product as white solid (196.2 mg, 0.562 mmol, 56% yield).

White solid. $^1\text{H NMR}$ (400 MHz, $\text{DMSO-}d_6$, 25 °C): δ 10.02 (s, 1H), 8.53 (s, 1H), 7.99 (d, $J = 9.1$ Hz, 1H), 7.86-7.83 (m, 2H), 7.62-7.61 (m, 3H), 7.49 (dd, $J = 9.3, 7.0$ Hz, 1H), 7.30 (dd, $J = 6.9, 0.9$ Hz, 1H), 7.15 (s, 2H), 2.34 (s, 3H), 2.02 (s, 6H). $^{13}\text{C}\{^1\text{H}\}$ NMR (100 MHz, $\text{DMSO-}d_6$, 25 °C): δ 140.2, 135.8, 134.3, 131.8, 131.3, 131.1, 130.6, 129.4, 129.0, 126.5, 125.7, 118.3, 117.5, 115.5, 20.6, 17.0. HRMS (ESI⁺) m/z calc. for $\text{C}_{22}\text{H}_{21}\text{N}_2$ 313.16993 found 313.16947.

2-Mesityl-5-phenyl-2*H*-imidazo[1,5-*a*]pyridin-3-ylidene



In a nitrogen-filled glove box, potassium bis(trimethylsilyl)amide (28.9 mg, 0.145, 1.05 equiv) was added to 2-mesityl-5-phenylimidazo[1,5-*a*]pyridin-2-ium chloride (48.3 mg, 0.138 mmol, 1.0 equiv) in dry benzene (3.0 mL). After stirring the mixture at room temperature for 2 hours, the resulting mixture was filtrated through dry celite and subsequently eluted with dry benzene. The filtrate was concentrated under reduced pressure. The residue was washed with dry pentane three times, and volatile compounds were removed *in vacuo* to afford the desired product as a light grey solid (36.1 mg, 0.115 mmol, 83% yield).

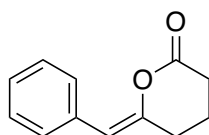
Light grey solid. $^1\text{H NMR}$ (400 MHz, C_6D_6 , 25 °C): δ 8.14 (d, $J = 7.1$ Hz, 2H), 7.22 (t, $J = 7.5$ Hz, 2H), 7.13 (t, $J = 7.3$ Hz, 1H), 6.94 (d, $J = 9.1$ Hz, 1H), 6.76 (s, 2H), 6.73 (s, 1H), 6.43 (dd, $J = 9.1, 6.6$ Hz, 1H), 6.28 (dd, $J = 6.6, 0.9$ Hz, 1H), 2.12 (s, 3H), 1.94 (s, 6H). $^{13}\text{C}\{^1\text{H}\}$ NMR (100 MHz, C_6D_6 , 25 °C): δ 210.9, 142.8, 139.2, 137.2, 136.1, 134.8, 132.1, 130.5, 128.7, 128.4, 128.2, 121.4, 116.4, 111.6, 111.1, 20.6, 17.6.

General Procedure for the Silver-Catalyzed Cyclisation of Alkyne-Tethered Carboxylic Acids

In a nitrogen-filled glove box, alkynoic acid (0.1 mmol) was placed in a screw vial containing a magnetic stirring bar. A solution of cationic silver complex **8a** (2 mol% on Ag) in dry CH₃CN (0.5 mL) was added to the vial, and the vial was sealed with screw-cap and taken out from the glove box. After stirring at 80 °C for 15 hours, the resulting mixture was filtrated through the cotton, and the resulting solution was concentrated under reduced pressure. The residue was purified by silica-gel column chromatography to afford the corresponding product.

Characterization Data for cyclized product 10a–k

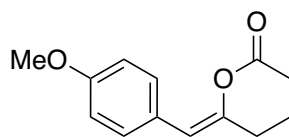
(*Z*)-6-Benzylidenetetrahydro-2*H*-pyran-2-one (**10a**)²⁸



10a

White solid. (18.5 mg, 98% yield). ¹H NMR (400 MHz, CDCl₃, 25 °C): δ 7.61 (d, *J* = 7.3 Hz, 2H), 7.32 (t, *J* = 7.3 Hz, 2H), 7.20 (t, *J* = 7.8 Hz, 1H), 5.50 (s, 1H), 2.72 (t, *J* = 6.9 Hz, 2H), 2.60 (t, *J* = 6.4 Hz, 2H), 1.97 (quint., *J* = 6.4 Hz, 2H). ¹³C{¹H} NMR (100 MHz, CDCl₃, 25 °C): δ 167.6, 148.2, 133.8, 128.9, 128.4, 126.9, 108.4, 30.6, 28.3, 18.8.

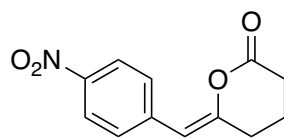
(*Z*)-6-(4-Methoxybenzylidene)tetrahydro-2*H*-pyran-2-one (**10b**)



10b

White Solid. (21.3 mg, 98% yield). mp: 72-77 °C. IR (ATR, ν /cm⁻¹): 2958 w, 2846 w, 1745 s, 1670 m, 1604 w, 1508 m, 1332 w, 1240 s, 1130 s, 1028 s, 767 w. ¹H NMR (400 MHz, CDCl₃, 25 °C): δ 7.57 (d, *J* = 8.7 Hz, 2H), 6.86 (d, *J* = 8.7 Hz, 2H), 5.44 (s, 1H), 3.80 (s, 3H), 2.71 (t, *J* = 6.9 Hz, 2H), 2.57 (t, *J* = 6.4 Hz, 2H), 1.95 (quint., *J* = 6.4 Hz, 2H). ¹³C{¹H} NMR (100 MHz, CDCl₃, 25 °C): δ 167.9, 158.3, 146.6, 130.2, 126.6, 113.8, 107.9, 55.2, 30.6, 28.1, 18.9. HRMS (EI⁺) *m/z* calc. for C₁₃H₁₄O₃ 218.09429 found 218.09360.

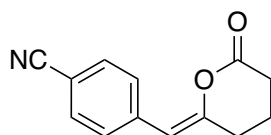
(Z)-6-(4-Nitrobenzylidene)tetrahydro-2H-pyran-2-one (10c)²⁸



10c

Pale yellow Solid. (23.1 mg, 99% yield). ¹H NMR (400 MHz, CDCl₃, 25 °C): δ 8.17 (d, *J* = 7.1 Hz, 2H), 7.76 (d, *J* = 8.7 Hz, 2H), 5.57 (s, 1H), 2.77 (t, *J* = 6.9 Hz, 2H), 2.66 (t, *J* = 6.4 Hz, 2H), 2.01 (quint., *J* = 6.4 Hz, 2H). ¹³C{¹H} NMR (100 MHz, CDCl₃, 25 °C): δ 166.6, 152.0, 145.9, 140.6, 129.3, 123.7, 106.5, 30.5, 28.4, 18.5.

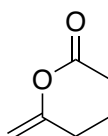
(Z)-4-((6-Oxotetrahydro-2H-pyran-2-ylidene)methyl)benzotrile (10d)



10d

White Solid. (20.1 mg, 94% yield). mp: 113-116 °C . IR (ATR, ν /cm⁻¹): 2920 w, 2224 w, 1749 m, 1657 m, 1410 w, 1203 w, 1126 s, 1043 s, 848 s, 596 w. ¹H NMR (400 MHz, CDCl₃, 25 °C): δ 7.70 (d, *J* = 8.5 Hz, 2H), 7.58 (d, *J* = 8.7 Hz, 2H), 5.50 (s, 1H), 2.75 (t, *J* = 6.9 Hz, 2H), 2.63 (t, *J* = 6.6 Hz, 2H), 1.99 (quint., *J* = 6.4 Hz, 2H). ¹³C{¹H} NMR (100 MHz, CDCl₃, 25 °C): δ 166.7, 151.4, 138.5, 132.1, 129.3, 119.1, 109.8, 106.8, 30.5, 28.3, 18.5. HRMS (EI⁺) m/z calc. for C₁₃H₁₁N₁O₂ 213.07898 found 213.07831.

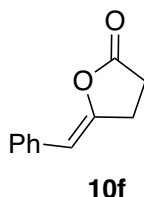
(Z)-6-Ethylidenetetrahydro-2H-pyran-2-one (10e)²⁸



10e

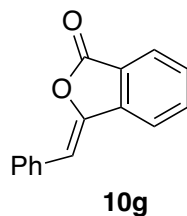
¹H NMR (400 MHz, CDCl₃, 25 °C): δ 4.64 (s, 1H), 4.28 (s, 1H), 2.61 (t, *J* = 6.8 Hz, 2H), 2.45 (t, *J* = 6.4 Hz, 2H), 1.88 (quint., *J* = 6.4 Hz, 2H). Yield was determined by ¹H NMR analysis due to the volatility of **10e**.

(Z)-5-Benzylidenedihydrofuran-2(3H)-one (10f)²⁹



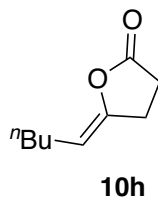
White solid. (16.2 mg, 93% yield). ¹H NMR (400 MHz, CDCl₃, 25 °C): δ 7.55 (d, *J* = 7.3 Hz, 2H), 7.33 (t, *J* = 7.7 Hz, 2H), 7.21 (t, *J* = 7.3 Hz, 1H), 5.55 (t, *J* = 1.6, 1H), 3.03 (t, *J* = 8.6, 2H), 2.71 (t, *J* = 8.5, 2H). ¹³C{¹H} NMR (100 MHz, CDCl₃, 25 °C): δ 174.9, 148.1, 133.9, 128.4, 128.3, 126.7, 104.9, 26.9, 26.3.

(Z)-3-Benzylideneisobenzofuran-1(3H)-one (10g)²⁶



White solid. (21.5 mg, 97% yield). ¹H NMR (400 MHz, CDCl₃, 25 °C): δ 7.94 (d, *J* = 7.8 Hz, 1H), 7.86 (d, *J* = 8.2 Hz, 2H), 7.79-7.69 (m, 2H), 7.55 (t, *J* = 7.3 Hz, 1H), 7.42 (t, *J* = 7.8 Hz, 2H), 7.34-7.30 (m, 1H), 6.43 (s, 1H). ¹³C{¹H} NMR (100 MHz, CDCl₃, 25 °C): δ 167.1, 144.6, 140.6, 134.5, 133.1, 130.1, 129.8, 128.8, 128.4, 125.6, 123.4, 119.8, 107.1. 1% of six-membered lactone, 4-phenyl-1*H*-isochromen-1-one, was detected by ¹H NMR analysis.^[17]

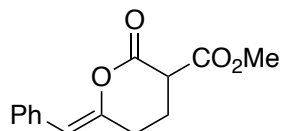
(Z) and (E)-5-Butylidenedihydrofuran-2(3H)-one (10h)³⁰



Colorless oil. (13.6 mg, 88% yield). ¹H NMR (400 MHz, C₆D₆, 25 °C): for (*Z*)-isomer; δ 4.17 (tt, *J* = 7.2, 1.4 Hz, 1H), 2.18-2.12 (m, 2H), 1.88-1.82 (m, 2H), 1.73-1.69 (m, 2H), 1.31-1.22 (m, 4H), 0.90-0.86 (t, *J* = 7.1 Hz, 3H), for (*E*)-isomer; δ 4.40 (t, *J* = 4.4 Hz, 1H), 2.01 (t, *J* = 8.0 Hz, 2H), 1.92-1.90 (m, 2H), 1.55-1.50 (m, 2H), 1.38-1.32 (m, 2H), 1.18-1.12 (m, 2H), 0.80 (t, *J* = 7.2 Hz, 3H). ¹³C{¹H} NMR (100 MHz, C₆D₆, 25 °C): for (*Z*)-isomer; δ 173.6, 148.0,

103.6, 31.8, 27.1, 24.9, 24.4, 22.2, 13.8, for (*E*)-isomer; δ 167.5, 153.5, 98.7, 32.4, 28.4, 28.2, 22.0, 18.4, 13.6.

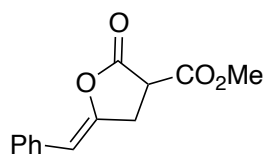
Methyl (*Z*)-6-Benzylidene-2-oxotetrahydro-2*H*-pyran-3-carboxylate (10i)²⁸



10i

Colorless oil. (21.5 mg, 87% yield). ¹H NMR (400 MHz, CDCl₃, 25 °C): δ 7.59 (d, *J* = 7.3 Hz, 2H), 7.33 (t, *J* = 7.8 Hz, 2H), 7.22 (tt, *J* = 7.6, 1.1 Hz, 1H), 5.57 (s, 1H), 3.77 (s, 3H), 3.69 (t, *J* = 7.6 Hz, 1H), 2.76-2.70 (m, 1H), 2.66-2.59 (m, 1H), 2.41-2.32 (m, 1H), 2.24-2.17 (m, 1H). ¹³C{¹H} NMR (100 MHz, CDCl₃, 25 °C): δ 168.6, 164.0, 146.8, 133.4, 129.0, 128.4, 127.2, 110.0, 53.0, 47.7, 26.3, 22.2.

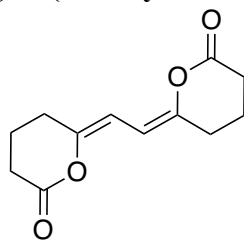
Methyl (*Z*)-5-Benzylidene-2-oxotetrahydrofuran-3-carboxylate (10j)²⁸



10j

Pale yellow oil. (19.6 mg, 84% yield). ¹H NMR (400 MHz, CDCl₃, 25 °C): δ 7.54 (d, *J* = 7.3 Hz, 2H), 7.33 (t, *J* = 8.0 Hz, 2H), 7.22 (tt, *J* = 7.3, 1.4 Hz, 1H), 5.63 (t, *J* = 1.6 Hz, 1H), 3.85 (s, 3H), 3.80 (dd, *J* = 10.4, 7.7 Hz, 1H), 3.48 (ddd, *J* = 16.7, 7.7, 1.9 Hz, 1H), 3.24 (ddd, *J* = 16.6, 10.3, 1.5 Hz, 1H). ¹³C{¹H} NMR (100 MHz, CDCl₃, 25 °C): δ 169.6, 167.2, 145.3, 133.3, 128.49, 128.45, 127.1, 105.9, 53.5, 45.3, 30.6.

(6*Z*,6'*Z*)-6,6'-(Ethane-1,2-diylidene)bis(tetrahydro-2*H*-pyran-2-one) (10k)³⁰



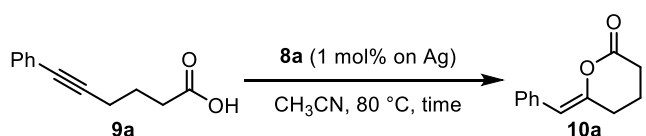
10k

White solid. (21.8 mg, 98% yield). $^1\text{H NMR}$ (400 MHz, CDCl_3 , 25 °C): δ 5.72 (s, 2H), 2.65 (t, $J = 6.6$ Hz, 4H), 2.49 (t, $J = 6.4$ Hz, 4H), 1.88 (quint., $J = 6.4$ Hz, 4H). $^{13}\text{C}\{^1\text{H}\}$ NMR (100 MHz, CDCl_3 , 25 °C): δ 167.7, 147.4, 101.5, 30.6, 27.2, 18.7.

Time Course Experiment with Complex **8a**

In a nitrogen-filled glove box, **9a** (18.8 mg, 0.1 mmol) was placed in a screw vial containing a magnetic stirring bar. A stock solution of cationic silver complex **8a** (2.4 mg, 0.002 mmol) in dry CH_3CN (2.0 mL) was prepared and distributed (0.5 mL) from the stock solution equally into the four screw vials. These vials were sealed with screw-caps and taken out from the glove box. After stirring at 80 °C for 5-50 hours, the resulting mixture was cotton-filtrated, and the resulting solution was concentrated under reduced pressure. The yield was determined by ^1H NMR analysis using 1,3,5-trimethoxybenzene as an internal standard.

Table 4. Time Course Experiment with Complex **8a**



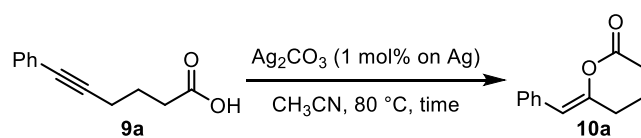
entry	time [h]	yield [%]
1	5	9
2	10	21
3	30	67
4	50	94

Yield was determined by ^1H NMR analysis using 1,3,5-trimethoxybenzene as an internal standard.

Time Course Experiment with Ag₂CO₃

In a nitrogen-filled glove box, Ag₂CO₃ (0.15 mg, 0.0005 mmol, 1 mol% on Ag) was placed in a screw vial containing a magnetic stirring bar. A stock solution of **9a** (75.2 mg, 0.4 mmol) in dry CH₃CN (2.0 mL) was prepared and distributed (0.5 mL) from the stock solution equally into the four screw vials. These vials were sealed with screw-caps and taken out from the glove box. After stirring at 80 °C for 1-30 hours, the resulting mixture was cotton-filtrated, and the resulting solution was concentrated under reduced pressure. The yield was determined by ¹H NMR analysis using 1,3,5-trimethoxybenzene as an internal standard.

Table 5. Time Course Experiment with Ag₂CO₃



entry	time [h]	yield [%]
1	1	8
2	5	23
3	10	25
4	30	25

Yield was determined by ¹H NMR analysis using 1,3,5-trimethoxybenzene as an internal standard.

Single Crystal XRD Analysis

A suitable crystal was mounted with liquid paraffin on a MiTeGen MicroMounts and transferred to the goniometer in a nitrogen stream at 123(2) K. Measurement was made on a RIGAKU XtaLAB Synergy-DW system with 1.2 kW PhotonJet-DW microfocus rotating anode using graphite monochromated Cu-K_α radiation ($\lambda = 1.54184 \text{ \AA}$) and HyPix-6000HE detector. Cell parameters were determined and refined, and raw frame data were integrated using CrysAlis^{Pro} (Agilent Technologies, 2010). The structures were solved by direct methods with SHELXT³¹ and refined by full-matrix least-squares techniques against F^2 with SHELXL-2018/3³² by using Olex2 software package.³³ The non-hydrogen atoms were anisotropically refined, and hydrogen atoms were placed using AFIX instructions. Crystal data and structure refinement parameters are in Table 6. The ORTEP-3 program was used to draw the molecule structures.³⁴

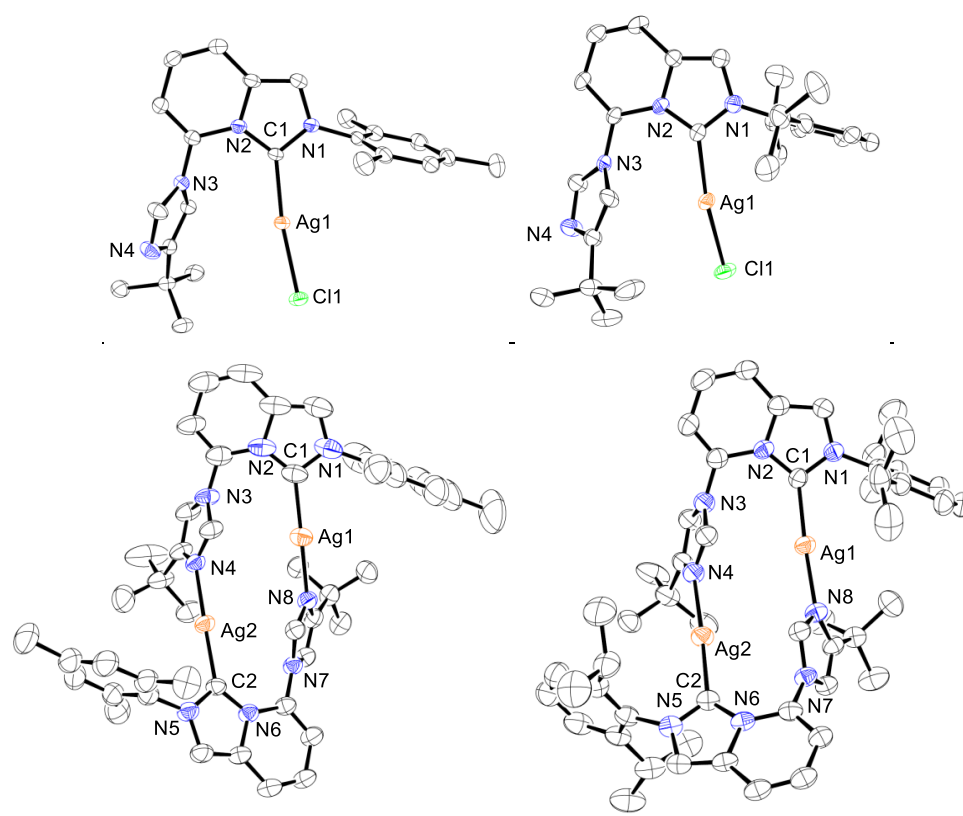


Table 6. Crystal Data and Structure Refinement Parameters

	7a	7b	8a	8b
empirical formula	AgC ₂₃ H ₂₆ ClN ₄	AgC ₂₆ H ₃₂ ClN ₄	Ag ₂ C ₄₆ H ₅₂ F ₁₂ N ₈ P ₂	Ag ₂ C ₅₂ H ₆₄ F ₁₂ N ₈ P ₂
CCDC number	2045685	2045686	2045683	2045684
formula weight	501.80	543.87	1222.63	1391.71
crystal system	orthorhombic	orthorhombic	monoclinic	monoclinic
space group	<i>F d d 2</i> (#43)	<i>P 2₁2₁2₁</i> (#19)	<i>P 2₁/c</i> (#14)	<i>P 2₁/c</i> (#14)
<i>a</i> , Å	38.1544(7)	8.54410(10)	10.12270(10)	17.0036(3)
<i>b</i> , Å	28.2397(4)	14.9720(2)	18.6528(2)	20.1327(2)
<i>c</i> , Å	8.37320(10)	19.7769(2)	30.8647(4)	18.8484(3)
α, deg.	-	-	-	-
β, deg.	-	-	98.8900(10)	100.322(2)
γ, deg.	-	-	-	-
<i>V</i> , Å ³	9021.9(2)	2529.91(5)	5757.76(11)	6347.92(17)
<i>Z</i>	16	4	4	4
<i>D</i> _{calcd} , g/cm ⁻³	1.478	1.428	1.410	1.456
[Cu-Kα], mm ⁻¹	1.54184	1.54184	1.54184	1.54184
<i>T</i> , K	123(2)	123(2)	123(2)	123(2)
crystal size, mm	0.15 x 0.13 x 0.02	0.25 x 0.06 x 0.03	0.15 x 0.10 x 0.03	0.20 x 0.10 x 0.02
range for data collection (deg.)	3.895 to 68.242	3.703 to 76.005	2.777 to 68.248	3.225 to 68.251
no. of reflections measured	7649	15332	57330	59912
unique data (<i>R</i> _{int})	3250 (0.0171)	5136 (0.0356)	10539 (0.0552)	11632 (0.1054)
data/restraints/parameters	3250 / 1 / 268	5136 / 1736 / 588	10539 / 0 / 698	11632 / 0 / 726
<i>R</i> 1 (<i>I</i> > 2.0σ(<i>I</i>))	0.0231	0.0836	0.0481	0.0711
<i>wR</i> 2 (<i>I</i> > 2.0σ(<i>I</i>))	0.0676	0.2206	0.1211	0.2072
<i>R</i> 1 (all data)	0.0234	0.0880	0.0522	0.0740
<i>wR</i> 2 (all data)	0.0677	0.2254	0.1234	0.2109
GOF on <i>F</i> ²	1.121	1.088	1.099	1.051

a) $R1 = (\sum ||F_o| - |F_c||) / (\sum |F_o|)$ b) $wR2 = [(\sum w(F_o^2 - F_c^2)^2) / (\sum w(F_o^4))]^{1/2}$

DFT Calculations

General Information

All calculations of the geometry optimizations were performed using Gaussian 16 package.²¹ The geometry optimizations as well as frequency calculations of all structures were conducted at the M06 functional¹⁹ in conjunction with the lanl2dz (ECP) (for silver) 6-31+G(d,p) (for other elements) basis set.²⁰ The self-consistent reaction field (SCRF) method based on conductor-like polarizable continuum model (CPCM) was introduced to evaluate the effects of solvent (CH₃CN).²² All the transition states were traced with intrinsic reaction coordinate (IRC) analyses by the use of Global Reaction Route Mapping (GRRM) program³⁵ to describe the reaction pathway. For describing energy diagram in the main text, the relative energies were corrected for the Gibbs free energies and given in kcal/mol. The structures of intermediates and transition states were described using GaussView 6.0 package.

Summary of energies

Structure Name	Electronic Energy (EE) [Hartree]	Electronic Energy + Zero-point Energy [Hartree]	Electronic Energy + Thermal Free Energy Correction [Hartree]
Int-A	-2811.159376	-2810.485945	-2810.573946
TS-A	-2811.128881	-2810.454082	-2810.539816
Int-B	-2811.143251	-2810.465934	-2810.548893
Int-C	-2811.154344	-2810.477532	-2810.563754
TS-B	-2811.123991	-2810.452601	-2810.539283
Int-D	-2811.194868	-2810.518532	-2810.601565

NMR Titration of Silver Complex **8a**

Silver complex **8a** (6.1 mg, 0.005 mmol) was dissolved in CD₃CN (0.6 mL), and the sample was monitored on ¹H NMR analysis (eq. 1). After addition of 0.5 M stock solution (10 mL) of **9a** in CD₃CN, the silver complex solution was further recorded ¹H NMR analysis. Addition of alkynoic acid was repeated eight times to add the 8 equivalents of alkynoic acid in total. The result was shown in Figure S1. All the peaks were assigned from the reference point of residual solvent peak DCM (5.44 ppm).

References

- (1) a) Herrmann, W. A.; Köcher, C. *Angew. Chem., Int. Ed. Engl.* **1997**, *36*, 2162–2187; b) Herrmann, W. A. *Angew. Chem., Int. Ed.* **2002**, *41*, 1290–1309; c) Crudden, C. M.; Allen, D. P. *Coord. Chem. Rev.* **2004**, *248*, 2247–2273; d) Köhl, O. *Chem. Soc. Rev.* **2007**, *36*, 592–607; e) Hahn, F. E.; Jahnke, M. C. *Angew. Chem., Int. Ed.* **2008**, *47*, 3122–3172; f) Hopkinson, M. H.; Richter, C.; Schedler, M.; Glorius, F. *Nature* **2014**, *510*, 485–496.
- (2) Alcarazo, M.; Roseblade, S. J.; Cowley, A. R.; Fernández, R.; Brown, J. M.; Lassaletta, J. M. *J. Am. Chem. Soc.* **2005**, *127*, 3290–3291.
- (3) Burstein, C.; Lehmann, C. W.; Glorius, F. *Tetrahedron* **2005**, *61*, 6207–6217.
- (4) a) Espina, M.; Rivilla, I.; Conde, A.; Díaz-Requejo, M. M.; P. Pérez, P. J.; Álvarez, E.; Fernández, R.; Lassaletta, J. M. *Organometallics* **2015**, *34*, 1328–1338; b) Kim, Y.; Kim, Y.; Hur, M. Y.; Lee, E. *J. Organomet. Chem.* **2016**, *820*, 1–7; c) Park, D.-A.; Ryu, J. Y.; Lee, J.; Hong, S. *RSC Adv.* **2017**, *7*, 52496–52502; d) Kashihara, M.; Zhong, R.-L.; Semba, K.; Sakaki, S.; Nakao, Y. *Chem. Commun.* **2019**, *55*, 9291–9294; e) Yi, X.; Chen, K.; Guo, J.; Chen, W.; Chen, W. *Adv. Synth. Catal.* **2020**, *362*, 4373–4377.
- (5) a) Grohmann, C.; Hashimoto, T.; Fröhlich, R.; Ohki, Y.; Tatsumi, K.; Glorius, F. *Organometallics* **2012**, *31*, 8047–8050; b) Tsui, E. Y.; Agapie, T. *Polyhedron* **2014**, *84*, 103–110; c) Nakao, R.; Nozaki, K. *J. Am. Chem. Soc.* **2015**, *137*, 10934–10937; d) Tao, W.; Nakano, R.; Ito, S.; Nozaki, K. *Angew. Chem., Int. Ed.* **2016**, *55*, 2835–2839; e) Tao, W.; Akita, S.; Ito, S.; Hoshimoto, Y.; Ogoshi, S.; Nozaki, K. *Chem. Commun.* **2017**, *53*, 2630–2633; f) Liu, G.; Liu, C.; Han, F.; Wang, Z.; Wang, J. *Tetrahedron Lett.* **2017**, *58*, 726–731; g) Azouzi, K.; Duhayon, C.; Benaissa, I.; Lugan, N.; Canac, Y.; Bastin, S.; César, V. *Organometallics* **2018**, *37*, 4726–4735.
- (6) a) Grande-Carmona, F.; Iglesias-Sigüenza, J.; Álvarez, E.; Díez, E.; Fernández, R.; Lassaletta, J. M. *Organometallics* **2015**, *34*, 5073–5080; b) Check, C. T.; Jang, K. P.; Schwamb, C. B.; Wang, A. S.; Wang, M. H.; Scheidt, K. A. *Angew. Chem., Int. Ed.* **2015**, *54*, 4264–4268; c) Iglesias-Sigüenza, J.; Izquierdo, C.; Díez, E.; Fernández, R.; Lassaletta, J. M. *Dalton. Trans.* **2016**, *45*, 10113–10117; d) Zhang, J.-Q.; Liu, Y.; Wang, X.-W.; Zhang, L. *Organometallics* **2019**, *38*, 3931–3938; e) Swamy P. C. A.; Varenikov, A.; de Ruiter, G. *Chem. Eur. J.* **2020**, *26*, 2333–2337.

- (7) a) Fürstner, A.; Alcarazo, M.; Krause, H.; Lehmann, C. W. *J. Am. Chem. Soc.* **2007**, *129*, 12676–12677; b) Roseblade, S. J.; Ros, A.; Monge, D.; Alcarazo, M.; Álvarez, E.; Lassaletta, J. M.; Fernández, R. *Organometallics* **2007**, *26*, 2570–2578; c) Alcarazo, M.; Stoke, T.; Anoop, A.; Thiel, W.; Fürstner, A. *Angew. Chem., Int. Ed.* **2010**, *49*, 2542–2546; d) Tang, Y.; Benaissa, I.; Huynh, M.; Vendier, L.; Lugan, N.; Bastin, S.; Belmont, P.; César, V.; Michelet, V. *Angew. Chem., Int. Ed.* **2019**, *58*, 7977–7981; Byun, S.; Seo, H.; Choi, J.-H.; Ryu, J. Y.; Lee, J.; Chung, W.; Hong, S. *Organometallics* **2019**, *38*, 4121–4132.
- (8) a) Nogami, H.; Kanai, M.; Shibasaki, M. *Chem. Pharm. Bull.* **2003**, *51*, 702–709; b) Paull, D. H.; Abraham, C. J.; Scerba, M. T.; Alden-Danforth, E.; Lectka, T.; *Acc. Chem. Res.* **2008**, *41*, 655–663; c) Margelefsky, E. L.; Zeidan, R. K.; Davis, M. E. *Chem. Soc. Rev.* **2008**, *37*, 1118–1126; d) Stephan, D. W. *Acc. Chem. Res.* **2015**, *48*, 306–316; e) Afewerki, S.; Córdova, A. *Chem. Rev.* **2016**, *116*, 13512–13570; f) Knox, G. J.; Hutchings-Goetz, L. S.; Pearson, C. M.; Snaddon, T. N. *Top. Curr. Chem.* **2020**, *378*, 16.
- (9) Silver-catalyzed cyclization of alkynoic acids, see: a) Schötz, K.; Clark, T.; Schaller, H.; Von R. Schleyer, P. *J. Org. Chem.* **1984**, *49*, 735–736; b) Pale, P.; Chucho, J.; *Tetrahedron Lett.* **1987**, *28*, 6447–6448; c) Dalla, V.; Pale, P.; *Tetrahedron Lett.* **1994**, *35*, 3525–3528; d) Marshall, J. A.; Wolf, M. A.; Wallace, E. M. *J. Org. Chem.* **1997**, *62*, 367–371; e) Rossi, R.; Bellina, F.; Bechini, C.; Mannina, L.; Vergamini, P. *Tetrahedron* **1998**, *54*, 135–156; f) Dalla, V.; Pale, P. *New. J. Chem.* **1999**, *23*, 803–805; g) Bellina, F.; Ciucci, D.; Vergamini, P.; Rossi, R. *Tetrahedron* **2000**, *56*, 2533–2545; h) Yoshikawa, T.; Shindo, M.; *Org. Lett.* **2009**, *11*, 5378–5381; i) Nolla-Saltiel, R.; Robles-Marín, E.; Porcel, S. *Tetrahedron Lett.* **2014**, *55*, 4484–4488; j) Barve, I. J.; Thikekar, T. U.; Sun, C.-M. *Org. Lett.* **2017**, *19*, 2370–2373.
- (10) For cyclization of alkynoic acids catalyzed by acid-base cooperative catalysts, see: a) Espinosa-Jalapa, N. Á.; Ke, D.; Nebra, N.; Goanvic, L. L.; Mallet-Ladeira, S.; Monot, J.; Martin-Vaca, B.; Bourissou, D. *ACS Catal.* **2014**, *4*, 3605–3611; b) Monot, J.; Brunel, P.; Kefalidis, C. E.; Espinosa-Jalapa, N. Á.; Maron, L.; Martin-Vaca, B.; Bourissou, D. *Chem. Sci.* **2016**, *7*, 2179–2187.
- (11) Verma, A. K.; Singh, J.; Sankar, V. K.; Chaudhary, R.; Chandra, R. *Tetrahedron Lett.* **2007**, *48*, 4207–4210.

- (12) Fürstner, A.; Alcarazo, M.; César, V.; Lehmann, C. W. *Chem. Commun.* **2006**, 2176–2178.
- (13) Garrison, J. C.; Youngs, W. J. *Chem. Rev.* **2005**, *105*, 3978–4008.
- (14) a) De Frémont, P.; Scott, N. M.; Stevens, E. D.; Ramnial, T.; Lightbody, O. C.; Macdonald, C. L. B.; Clyburne, J. A. C.; Abernethy, C. D.; Nolan, S. P. *Organometallics* **2005**, *24*, 6301–6309; b) Su, H.-L.; Pérez, L. M.; Lee, S.-J.; Reibenspies, J. H.; Bazzi, H. S.; Bergbreiter, D. E. *Organometallics* **2012**, *31*, 4063–4071.
- (15) In the $^{13}\text{C}\{^1\text{H}\}$ NMR spectra of the neutral AgCl complexes **7a** and **7b** in CD_2Cl_2 , resonances for the carbene carbon were not observed. This is likely due to line-broadening of the signals, reflecting labile nature of the coordination of the carbene carbon atom to the Cl-bound silver atom. See: Garner, M. E.; Niu, W.; Chen, X.; Ghiviriga, I.; Abboud, K. A.; Tan, W.; Veige, A. S. *Dalton. Trans.* **2015**, *44*, 1914–1923.
- (16) 1,3-Dimesitylimidazol-2-ylidene (IMes) was purchased from Sigma-Aldrich Co. LLC: Arduengo III, A. J.; Dias, H. V. R.; Harlow, R. L.; Kline, M. *J. Am. Chem. Soc.* **1992**, *114*, 5530–5534.
- (17) 1,3-Bis(2,6-diisopropylphenyl)imidazol-2-ylidene (IPr) was purchased from Tokyo Chemical Industry Co.: Arduengo III, A. J.; Krafczyk, R.; Schmutzler, R. *Tetrahedron* **1999**, *55*, 14523–14534.
- (18) a) Harkat, H.; Weibel, J.-M.; Pale, P. *Tetrahedron Lett.* **2006**, *47*, 6273–6276; b) Harkat, H.; Dembelé, A. Y.; Weibel, J.-M.; Blanc, A.; Pale, P. *Tetrahedron* **2009**, *65*, 1871–1879.
- (19) Zhao, Y.; Truhlar, D. G. *Theor. Chem. Acc.* **2008**, *120*, 215–241.
- (20) a) Hay, P. J.; Wadt, W. R.; *J. Chem. Phys.* **1985**, *82*, 299–310; b) Ditchfield, R.; Hehre, W. J.; Pople, J. A. *J. Chem. Phys.* **1971**, *54*, 724–728; c) Hehre, W. J.; Ditchfield, R.; Pople, J. A. *J. Chem. Phys.* **1972**, *56*, 2257–2261; d) Hariharan, P. C.; Pople, J. A. *Theoret. Chim. Acta.* **1973**, *28*, 213–222.
- (21) Gaussian 16, Revision C.01: Frisch, M. J.; Trucks, G. W.; Schlegel, H. B.; Scuseria, G. E.; Robb, M. A.; Cheeseman, J. R.; Scalmani, G.; Barone, V.; Petersson, G. A.; Nakatsuji, H.; Li, X.; Caricato, M.; Marenich, A. V.; Bloino, J.; Janesko, B. G.; Gomperts, R.; Mennucci, B.; Hratchian, H. P.; Ortiz, J. V.; Izmaylov, A. F.; Sonnenberg, J. L.; Williams-Young, D.; Ding, F.; Lipparini, F.; Egidi, F.; Goings, J.; Peng, B.; Petrone, A.; Henderson, T.; Ranasinghe, D.; Zakrzewski, V. G.; Gao, J.; Rega, N.; Zheng, G.; Liang,

- W.; Hada, M.; Ehara, M.; Toyota, K.; Fukuda, R.; Hasegawa, J.; Ishida, M.; Nakajima, T.; Honda, Y.; Kitao, O.; Nakai, H.; Vreven, T.; Throssell, K.; Montgomery, J. A.; Jr., Peralta, J. E.; Ogliaro, F.; Bearpark, M. J.; Heyd, J. J.; Brothers, E. N.; Kudin, K. N.; Staroverov, V. N.; Keith, T. A.; Kobayashi, R.; Normand, J.; Raghavachari, K.; Rendell, A. P.; Burant, J. C.; Iyengar, S. S.; Tomasi, J.; Cossi, M.; Millam, J. M.; Klene, M.; Adamo, C.; Cammi, R.; Ochterski, J. W.; Martin, R. L.; Morokuma, K.; Farkas, O.; Foresman, J. B.; and Fox, D. J. Gaussian, Inc., Wallingford CT, 2019.
- (22) Barone, V.; Cossi, M. *J. Phys. Chem. A* **1998**, *102*, 1995–2001.
- (23) Thomas, S.; Andreas, A. D.; Pierre, B. *Dalton Trans.* **2017**, *46*, 5955–5964.
- (24) Verma, A. K.; Singh, J.; Sankar, V. K.; Chaudhary, R.; Chandra, R. *Tetrahedron Lett.* **2007**, *48*, 4207–4210.
- (25) Alcarazo, M.; Roseblade, S. J.; Cowley, A. R.; Fernandez, R.; Brown, J. M.; Lassaletta, J. M. *J. Am. Chem. Soc.* **2005**, *127*, 3290–3291.
- (26) Park, J.; Chang, S. *Angew. Chem. Int. Ed.* **2015**, *54*, 14103–14107.
- (27) Hutt, J. T.; Aron, Z. D.; *Org. Lett.* **2011**, *13*, 5256–5259.
- (28) Gasperini, D.; Maggi, L.; Dupay, S.; Veenboer, R.; Cordes, D. B.; Slawin, A.; Nolan, S. *P. Adv. Synth. Catal.* **2016**, *358*, 3857–3862.
- (29) Costello, J. P.; Ferreira, E. M. *Org. Lett.* **2019**, *21*, 9934–9939.
- (30) Harkat, H.; Dembele, A. Y.; Weibel, J.-M.; Blanc, A.; Pale, P. *Tetrahedron* **2009**, *65*, 1871–1879.
- (31) Yuan, Q.; Chen, Z.-B.; Zhang, F.-L.; Zhu, Y.-M. *Org. Biomol. Chem.* **2017**, *15*, 1628–1635.
- (32) Dubovtsev, A. Y.; Dar'in, D. V.; Krasavin, M.; Kukushkin, V. Y. *Eur. J. Org. Chem.* **2019**, 1856–1864.
- (33) Sheldrick, G. M. SHTLXT-Integrated space-group and crystal-structure determination. *Acta Cryst.* **2015**, *A71*, 3–8.
- (34) Sheldrick, G. M. Crystal structure refinement with SHELXL. *Acta Cryst.* **2015**, *C71*, 3–8.
- (35) Global Reaction Route Mapping (GRRM) Program, S. Maeda, Y. Harabuchi, Y. Sumiya, M. Takagi, K. Suzuki, K. Sugiyama, Y. Ono, M. Hatanaka, Y. Osada, T. Taketsugu, K. Morokuma, K. Ohno (Version 17-A01).

Chapter 2

Construction of Heterobimetallic Catalytic Scaffold with a Carbene-Bipyridine Ligand: Gold-Zinc Two-Metal Catalysis for Intermolecular Addition of *O*-Nucleophiles to Non-activated Alkynes

Abstract

A gold(I) complex bearing an imidazo[1,5-*a*]pyridin-3-ylidene ligand with a 2,2'-bipyridine moiety at the C5 position was prepared as a template for constructing heterobimetallic cooperative catalysts. *In situ* generated gold-zinc bimetallic systems enabled intermolecular nucleophilic *anti*-addition of *O*-nucleophiles such as carboxylic acids and phenols toward non-activated internal alkynes. DFT calculations supported the proposed cooperative action of the cationic gold atom and the zinc salt site for activating the alkyne and the carboxylic acid, respectively.

Introduction

Cationic gold(I) complexes are well known as effective catalysts for nucleophilic additions toward alkynes with excellent turnover efficiency due to their strong Lewis acidic character and high affinity for alkyne π -systems.¹ Despite the versatile utility of gold catalysts, intermolecular nucleophilic additions of weak oxygen-nucleophiles² such as carboxylic acids³ and phenols⁴ toward non-activated internal alkynes, which form synthetically valuable enol derivatives with high atom economy, are underdeveloped. As a successful precedent, Nolan and co-workers introduced cationic μ^2 -hydroxo-bridged dinuclear gold(I) complexes, which liberate a Lewis acidic cationic gold(I) species and a Brønsted basic hydroxogold(I) complex as components for activating the alkyne and the nucleophile, respectively.^{3c,g,4b,d,e} Zhang and co-workers developed gold(I) catalysts coordinated with a phosphine ligand with an amide pendant for hydrocarboxylation of alkynes and proposed that the carboxylic acid is activated through hydrogen-bonding with the amide moiety, directing the *anti*-attack to the gold-bound alkyne.^{3b} Regardless of the importance of these contributions, further conceptual advances are demanded for intermolecular *O*-nucleophilic addition to alkynes.

The author envisioned that heterobimetallic complexes would be effective catalyst candidates for *O*-nucleophilic addition toward non-activated internal alkynes, expecting cooperative action of the two metal sites for dual activation of electrophiles and nucleophiles as in enzymatic reactions.⁵ As a platform for the heterobimetallic cooperative catalysis, the author synthesized a rigid imidazo[1,5-*a*]pyridin-3-ylidene ligand^{6,7} with a 2,2'-bipyridine moiety at the C5 position and used it for the preparation of a gold(I) carbene complex. The resulting gold complex was converted into heterobimetallic catalysts through *in situ* binding of various hard metals at the bipyridine moiety.⁸ The heterobimetallic catalysts thus formed were examined for catalytic activity in the intermolecular nucleophilic addition of *O*-nucleophiles such as carboxylic acids and phenols towards non-activated internal alkynes. Indeed, the catalytic systems showed apparent bimetallic cooperativity with a strong dependence on the nature of the hard metal site, most favouring Zn(acac)₂ as a Brønsted base site. DFT calculations supported the proposed cooperative action of the Au-Zn bimetallic catalyst system.

Synthesis of Ligand

The synthesis of imidazo[1,5-*a*]pyridinium chloride **3a** bearing a bipyridine moiety at the 5-position is outlined in Figure 1. First, Negishi cross-coupling⁹ between organozinc species prepared from 2-bromo-6-(diethoxymethyl)pyridine **1** and 5-bromo-2,2'-bipyridine gave terpyridine **2a** in 78% yield. The acetal **2a** was hydrolyzed to an aldehyde and subjected to reductive amination with 2,4,6-trimethylaniline. The *N*-formylation of the resulting amino group with acetic formic anhydride followed by dehydrative cyclization with POCl₃ afforded 5-bipyridyl imidazo[1,5-*a*]pyridinium chloride **3a** (73% yield over 4 steps from **2a**). Next, the reaction of **3a** with AuCl·SMe₂ in the presence of K₂CO₃ in acetone at 60 ° C for 3 hours¹⁰ gave, after purification by silica-gel column chromatography, *N*-heterocyclic carbene gold(I) complex **4a** in 82% yield as an air-stable colorless solid. The molecular structure of **4a** was confirmed by single crystal XRD analysis. Similarly, gold(I) complexes with 4-pyridyl or 3-pyridyl pendants (**4b,c**) were also synthesized.

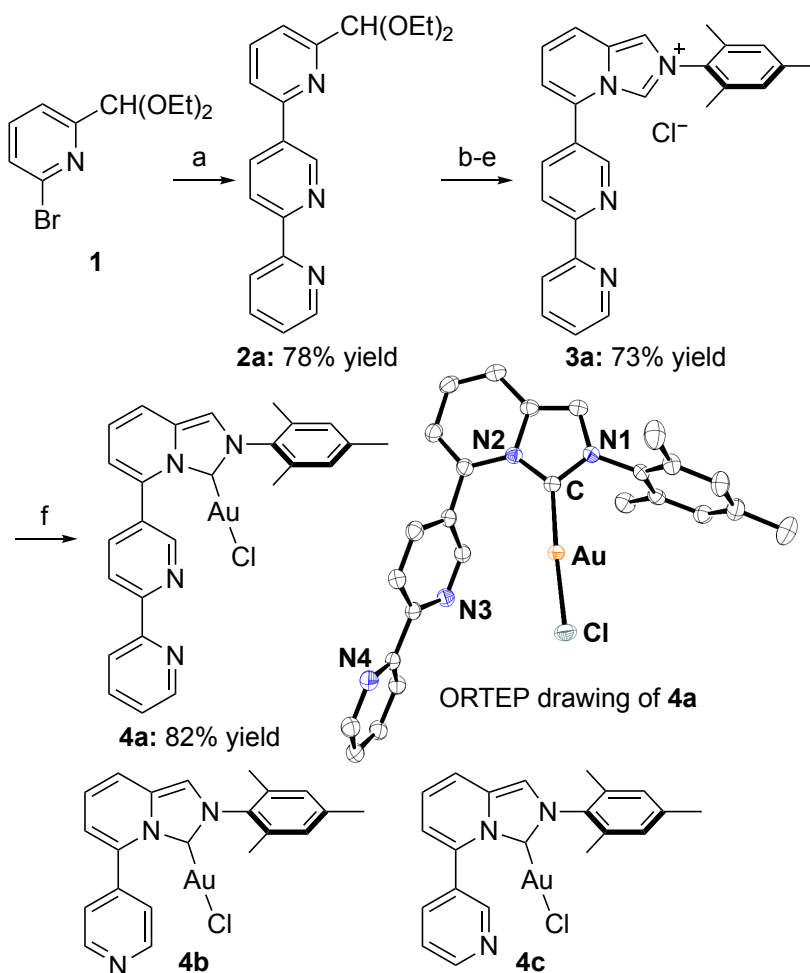


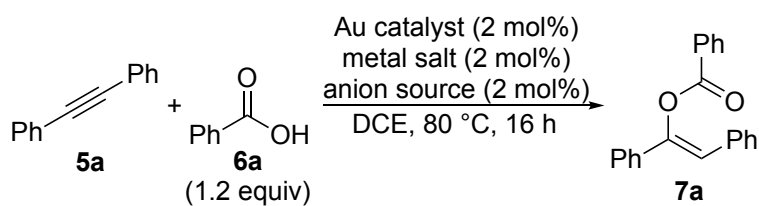
Figure 1. Synthesis of gold complexes **4**. (a) **1** (1.4 equiv), ⁿBuLi (1.5 equiv), ZnCl₂ (1.6 equiv), THF/hexane/Et₂O, -78 °C then 5-bromo-2,2'-bipyridine (1 equiv), Pd(PPh₃)₄ (5 mol%), THF, reflux, 18 h; (b) **2a** (1 equiv), 1 M HCl aq., acetone, 60 °C, 3 h; (c) 2,4,6-trimethylaniline (1.2 equiv), AcOH (1 equiv), NaBH(OAc)₃ (1.5 equiv), DCM, r.t., 14 h; (d) HCOOH (excess), Ac₂O (excess), THF, 0 °C, 3 h; (e) POCl₃ (1.3 equiv), toluene, 100 °C, 21 h; (f) **3a** (1.0 equiv), AuCl·SMe₂ (1.0 equiv), K₂CO₃ (2.0 equiv), acetone, 60 °C, 3 h. All hydrogen atoms were omitted for clarity from ORTEP drawing of **4a** showing 50% probability thermal ellipsoids.

Catalytic Activity Investigation

The author tested the catalytic activity of gold complexes **4** in the hydrocarboxylation of non-activated alkynes. The results are summarized in Table 1. Bimetallic catalysts were prepared *in situ* from **4a**, a hard metal salt, and an anion source. When nucleophilic addition of benzoic acid (**6a**) toward diphenylacetylene (**5a**) as a non-activated alkyne was conducted with **4a**, Zn(acac)₂, and AgNTf₂ in 1,2-dichloroethane (DCE) at 80 °C for 16 h, enol ether **7a** was obtained in 61% yield (entry 1). When the use of other metal zinc salt (Table 1, entry 2-4), resulted into the decreased yield of desired enolate product **7a** (not detected-36%). Employment of different variety of copper salt didn't help the reaction to exceed greater yield than 61% (Table 1, entry 5-8). When other acetylacetonato-metal salts such as Cu(acac)₂, Ni(acac)₂, Pd(acac)₂, Co(acac)₂, Fe(acac)₂, Mn(acac)₃, and Cr(acac)₃ were examined (entries 2-8), the reaction occurred with decreased yield of **7a** (3–23%). The metal alkoxides such as Ti(OⁱPr)₄, Y(OⁱPr)₃, and Mg(OⁱBu)₂ induced almost no reaction (entries 9–11). Additionally, the gold complex **4a** did not cause the reaction in the absence of the metal salt (entry 12). Hence, the hard metal salt had a significant influence on the catalytic activity of **4a**, with Zn(acac)₂ being optimal. In contrast, no reaction was observed with gold complexes (**4b,c**) with the monopyridyl pendant (entries 13 and 14), indicating the necessity of chelation, thus supporting the cooperative participation of the zinc site for the gold catalysis. Similarly, the gold carbene complex **8a** with a phenyl substituent at the C5 position and its phosphine variant **8b** showed almost no catalytic activity (entries 15 and 16). The addition of 2,2'-bipyridine to the reaction system with **8a** and **8b**, expecting it to act as an external ligand for zinc, showed little effect, indicating the importance of the proximity of the gold and zinc metals for the two-metal cooperativity (entries 17 and 18).

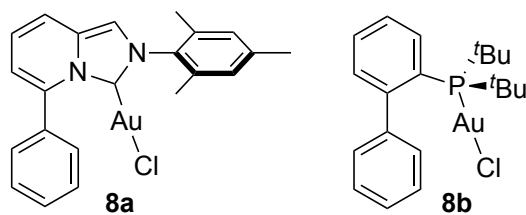
Next, effects of counteranions of the gold complex were investigated. While the replacement of NTf₂⁻ with BF₄⁻, PF₆⁻, or SbF₆⁻ resulted in significant reduction of the product yield (Table 1, entries 19–21), the use of sodium tetrakis[3,5-bis(trifluoromethyl)phenyl]borate (NaBAR^F) as a source of a non-coordinative anion improved the yield to 75% (entry 22). Finally, quantitative yield of **7a** (>99% by ¹H NMR analysis, 98% for the isolated product) was obtained by conducting the reaction under high concentration conditions (12 M in DCE) (entry 23). The reaction at a catalyst loading of 0.5 mol% gave **7a** in 80% yield (entry 24). Based on these results, I employed the reaction conditions of entry 23 as the protocol for subsequent experiments exploring the substrate scope.

Table 1. Screening of Reaction Conditions



entry	Au catalyst	metal salt	anion source	yield of 7a [%] ^a
1	4a	Zn(acac) ₂	AgNTf ₂	61
2	4a	Cu(acac) ₂	AgNTf ₂	18
3	4a	Ni(acac) ₂	AgNTf ₂	8
4	4a	Pd(acac) ₂	AgNTf ₂	23
5	4a	Co(acac) ₂	AgNTf ₂	17
6	4a	Fe(acac) ₂	AgNTf ₂	3
7	4a	Mn(acac) ₃	AgNTf ₂	12
8	4a	Cr(acac) ₃	AgNTf ₂	6
9	4a	Ti(O ⁱ Pr) ₄	AgNTf ₂	2
10	4a	Y(O ⁱ Pr) ₃	AgNTf ₂	1
11	4a	Mg(O ⁱ Bu) ₂	AgNTf ₂	4
12	4a	none	AgNTf ₂	N.D.
13	4b	Zn(acac) ₂	AgNTf ₂	N.D.
14	4c	Zn(acac) ₂	AgNTf ₂	N.D.
15	8a	Zn(acac) ₂	AgNTf ₂	trace
16	8b	Zn(acac) ₂	AgNTf ₂	trace
17 ^b	8a	Zn(acac) ₂	AgNTf ₂	2
18 ^b	8b	Zn(acac) ₂	AgNTf ₂	1
19	4a	Zn(acac) ₂	AgBF ₄	23
20	4a	Zn(acac) ₂	AgPF ₆	40
21	4a	Zn(acac) ₂	AgSbF ₆	26
22	4a	Zn(acac) ₂	NaBAR ^F	75
23 ^c	4a	Zn(acac) ₂	NaBAR ^F	>99 (98) ^d
24 ^{c,e}	4a	Zn(acac) ₂	NaBAR ^F	80

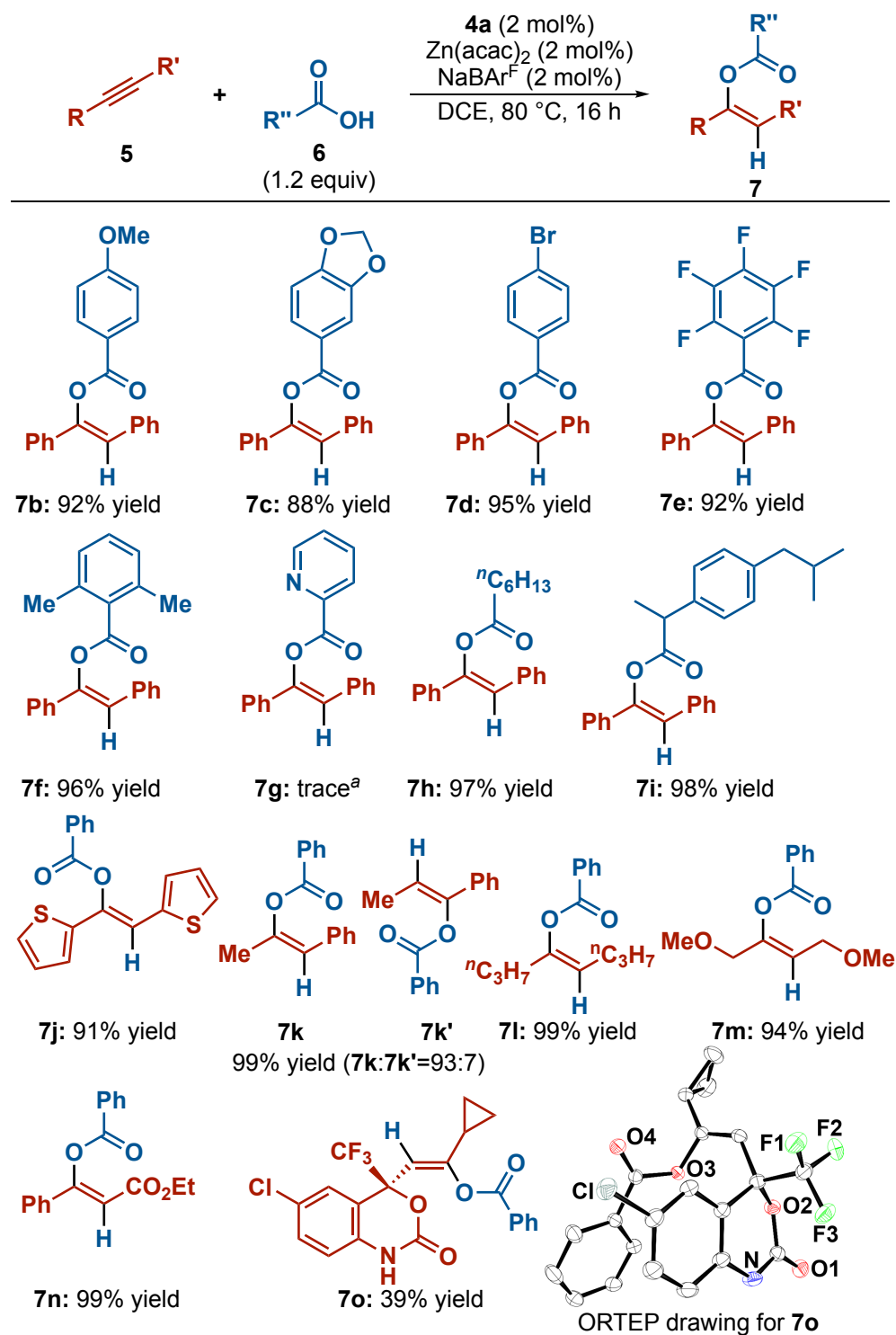
Au catalyst (2 mol%), metal salt (2 mol%), anion source (2 mol%), **5a** (0.10 mmol) and **6a** (0.12 mmol) in DCE (0.1 mL, 1 M). ^aDetermined by ¹H NMR analysis using 1,3,5-trimethoxybenzene as an internal standard. ^b2 mol% of 2,2'-bipyridine was added. ^c**5a** (0.4 mmol) and **6a** (0.48 mmol) in DCE (33 μL, 12 M). ^dIsolated yield. ^e0.5 mol% of **4a**, Zn(acac)₂, and NaBAR^F were used. N.D.=not detected.



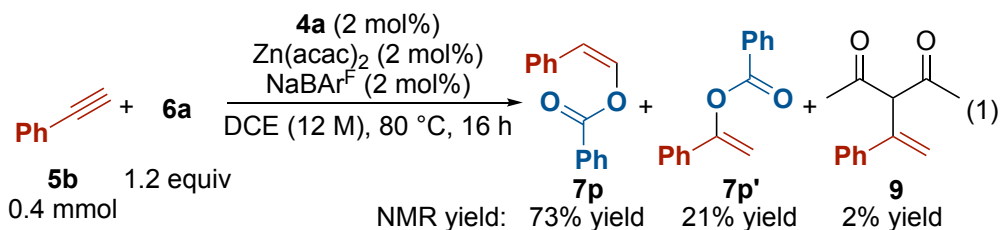
The scope of carboxylic acids and alkynes is summarized in Scheme 1.¹¹ Electron-donating substituents such as methoxy and methylenedioxy groups on the benzoic acid were compatible with the protocol. The corresponding enol esters **7b** and **7c** were obtained in 92% and 88% yields, respectively. Electron-withdrawing substitutions as in 4-bromo and 2,3,4,5,6-pentafluorobenzoic acids were also compatible, affording **7d** and **7e** in 95% and 92% yields, respectively. The reaction with sterically demanding 2,6-dimethylbenzoic acid gave product **7f** in 96% yield. Pyridine-2-carboxylic acid was nearly unreactive probably due to the inhibitory effect of pyridyl *N*-coordination toward zinc or gold. Aliphatic carboxylic acids, heptanoic acid and ibuprofen, were also competent substrates to give **7h** and **7i** in 97% and 98% yields, respectively. The scope of alkynes was investigated for the reaction with benzoic acid (**6a**). The addition of **6a** to 1,2-di(thiophen-2-yl)ethyne proceeded smoothly, giving **7j** in 91% yield. An unsymmetrical alkyne, 1-phenyl-1-propyne, was transformed to an isomeric mixture in 99% yield (**7k/7k'** 93:7). The protocol was applicable to other internal alkynes such as 4-octyne, 1,4-dimethoxy-2-butyne, and ethyl phenylpropiolate, affording *anti*-addition products **7l**, **7m**, and **7n** in 99%, 94%, and 99% yields, respectively. Excellent functional group tolerance of the protocol was demonstrated in the reaction with Efavirenz, a non-nucleoside reverse transcriptase inhibitor, which afforded **7o** in 39% yield as a single constitutional/geometrical isomer. The moderate yield of **7o** was due to a partial conversion of Efavirenz. The molecular structure of **7o** was unambiguously confirmed by single-crystal XRD analysis.

I also investigated the effect of the present gold-zinc heterobimetallic catalyst system toward the reaction of a terminal alkyne, phenylacetylene (**5b**), and benzoic acid (**6a**) as model substrates (eq. 1). Interestingly, when the protocol for the internal alkynes was applied to this reaction, an *anti*-Markovnikov addition product with *Z*-configuration was obtained as the major product in 73% yield (**7p**) along with a Markovnikov addition product (**7p'**, 21% yield) and a product of Markovnikov addition of acetylacetone (**9**, 2% yield). This regioselectivity favoring *anti*-Markovnikov addition contrasts with the reported carboxylation with the PPh₃-AuCl/AgPF₆ catalyst system.^{3a} This interesting regioselectivity is an issue for further investigation.¹²

Scheme 1. Nucleophilic Addition of Carboxylic Acids to Alkynes

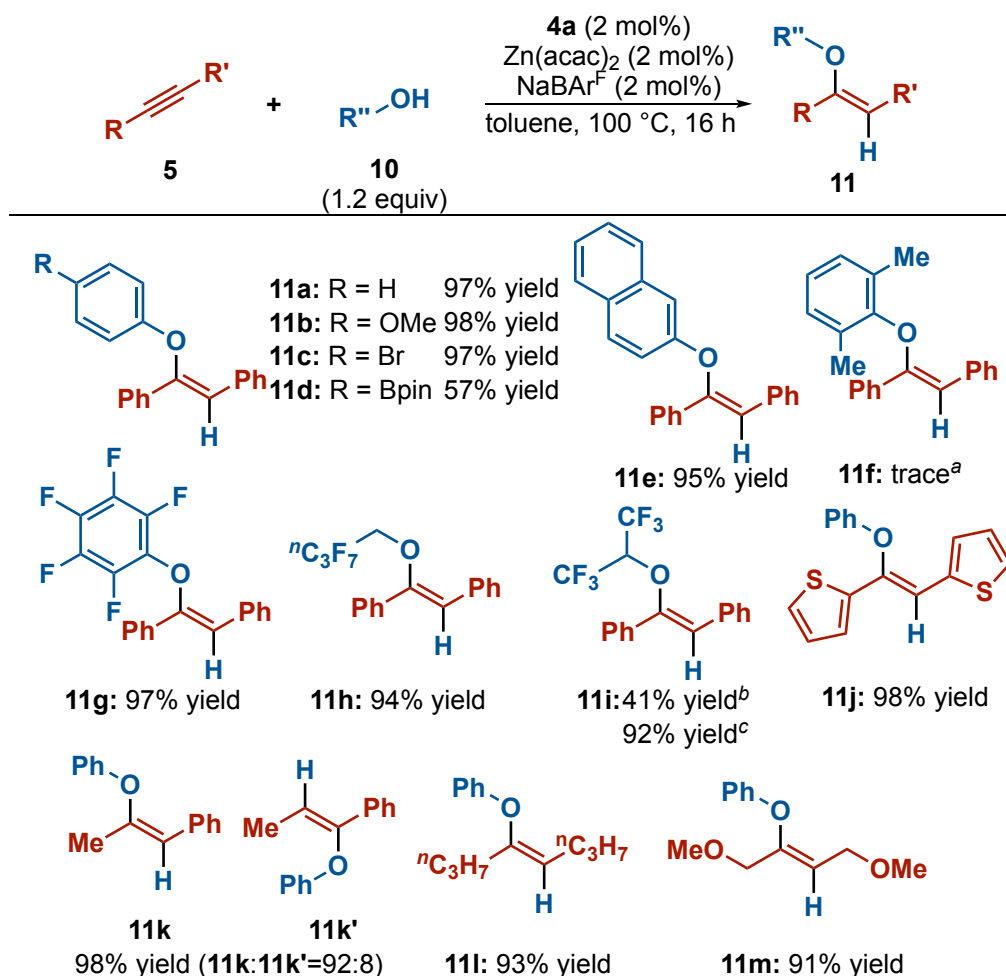


4a (2 mol%), Zn(acac)₂ (2 mol%), NaBAR^F (2 mol%), **5** (0.40 mmol), and **6** (0.48 mmol) in DCE (33 μL). ^aDetected by ¹H NMR analysis.



The addition of phenols and fluorinated alcohols (**10**) to internal alkynes (**5**) was also investigated. After re-optimizing the reaction conditions, the scope of substrates was investigated under the conditions using the gold complex **4a** (2 mol%), Zn(acac)₂ (2 mol%), NaBAr^F (2 mol%) in toluene (12 M) at 100 °C for 16 h (Scheme 2) (see Supporting Information for details). The reaction between phenol (1.2 equiv) and diphenylacetylene (**5a**) gave (*Z*)-(1-phenoxyethene-1,2-diyl)dibenzene **11a** in 97% yield. *p*-Methoxyphenol, *p*-bromophenol, and 2-naphthol were competent with the protocol to afford **11b**, **11c**, and **11e** in 98, 97, and 95% yields, respectively, while a *p*-pinacolatoboron substituent led to a decrease in the yield (57%) of **11d** with the formation of unidentified side products. Sterically hindered 2,6-dimethylphenol gave only a trace amount of **11f**. Pentafluorophenol was a suitable substrate, giving **11g** in 97% yield. The protocol was also applicable to electron-deficient fluorinated alcohols such as 2,2,3,3,4,4,4-heptafluoro-1-butanol and 1,1,1,3,3,3-hexafluoro-2-propanol (HFIP), giving the corresponding fluoroalkyl enol ethers **11h** and **11i** in 94% and 41% yields, respectively. The use of 3 equiv of HFIP improved the yield of the latter (**11i**) to 92%. Thus, the lower yield with the use of 1.2 equiv of HFIP may have been due to its low boiling point (58 °C).¹³ The scope of alkynes was examined using phenol as a model nucleophile. The addition of 1,2-di(thiophen-2-yl)ethyne gave **11j** in 98% yield. 1-Phenyl-1-propyne gave an isomeric mixture (**11k**/**11k'** 92:8) in 98% yield. 4-Octyne and 1,4-dimethoxy-2-butyne produced **11l** and **11m** in 93% and 91% yields, respectively. Efavirenz showed no reactivity with phenol under the optimized conditions.

Scheme 2. Nucleophilic Addition of Alcohols to Alkynes



4a (2 mol%), $\text{Zn}(\text{acac})_2$ (2 mol%), NaBAR^{F} (2 mol%), **5** (0.40 mmol) and **10** (0.48 mmol) in toluene (33 μL). ^aDetected by ^1H NMR analysis. ^bDetermined by ^1H NMR analysis using 1,3,5-trimethoxybenzene as an internal standard. ^c3.0 equiv of HFIP was used.

Characterization of Heterobimetallic Complex

To gain information on the gold-zinc heterobimetallic complexes, the interactions between the neutral gold complex **4a** and zinc salts were investigated both in the solid state and in solution phase. Mixing **4a** and ZnCl_2 in a DCE/THF mixed solvent gave gold-zinc bimetallic complex **4a-ZnCl₂** as a pale yellow powder in 78% yield (Figure 2). Recrystallization of this solid from a DCM/THF solution gave single crystals suitable for XRD analysis. The molecular structure of the gold-zinc bimetallic complex **4a-ZnCl₂** as depicted in Figure 2 shows the existence of a linear two-coordinate gold(I) center and a tetrahedral zinc center in a spatially

independent manner. Interactions between the pyridine moiety of complexes **4** and zinc salts were also observed in the solution phase (THF-*d*₈).

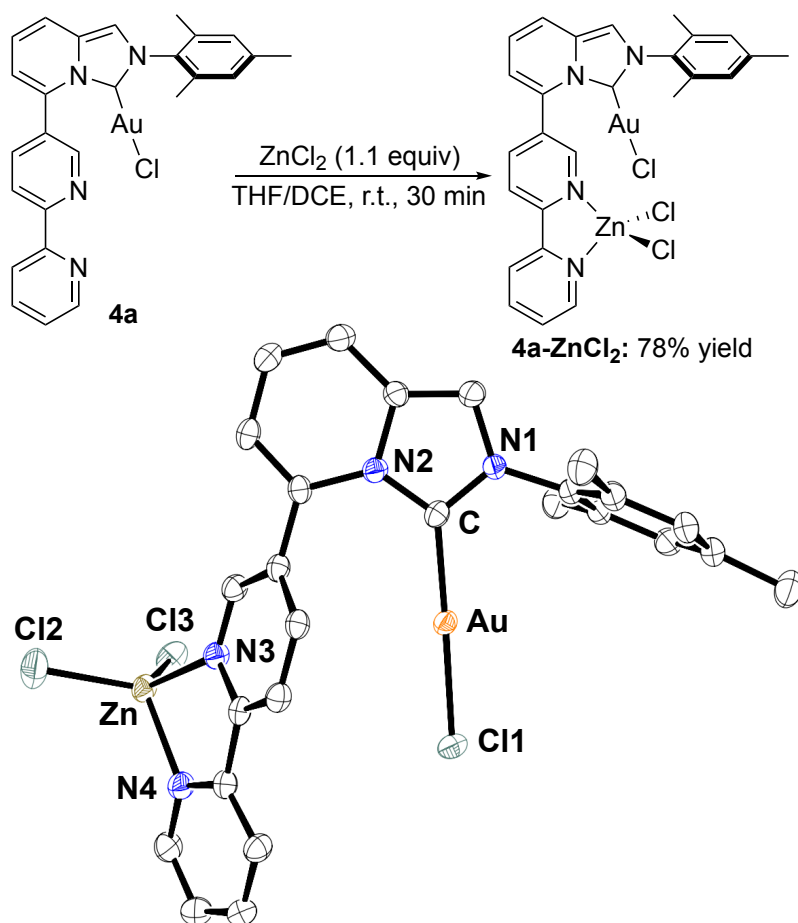


Figure 2. Complexation of gold-zinc bimetallic complex **4a-ZnCl₂**. All hydrogen atoms and a solvent molecule were omitted for clarity from the ORTEP drawing of **4a-ZnCl₂** showing 50% probability thermal ellipsoids. Selected bond lengths (Å) and angles (deg.) of **12**: Au–Cl 2.2951(9); Au–C 1.992(4); Zn–N3 2.066(3); Zn–N4 2.062(3); C–Au–Cl 178.84(12).

Reaction Mechanism

For gaining mechanistic insights into the gold-zinc cooperative catalysis, DFT calculations were conducted at the M06/SDD,6-311+G(d,p)/SMD(DCE)//M06/SDD,6-31G(d) level of theory with the Gaussian 16 package.¹⁵ Gold-zinc complexes were calculated as mono-cationic species without BAr^{F^-} anions. The relative energies were corrected for Gibbs free energy and reported in kcal/mol (Figure 3).

The cationic gold complex **Int-1** including alkyne **5a** is formed through the coordination of the bipyridine moiety of **Int-0** to $\text{Zn}(\text{Obz})_2$ generated from $\text{Zn}(\text{acac})_2$ and benzoic acid. This complexation is an exergonic process by 18.4 kcal/mol. The nucleophilic *anti*-attack of the zinc benzoate toward the alkyne moiety activated by the gold atom proceeds through **TS₁₋₂** with an energy barrier of 24.7 kcal/mol. This step is 15.9 kcal/mol endergonic to afford alkenyl gold(I) intermediate **Int-2**. Alternatively, the benzoate can act as a base to deprotonate benzoic acid. Thus, **Int-1** captures another benzoic acid molecule through hydrogen-bonding at the benzoate oxygen atom to form **Int-3**. The bound benzoic acid undergoes deprotonation coupled with nucleophilic *anti*-attack toward the alkyne moiety through **TS₃₋₄** with an energy barrier of 21.5 kcal/mol, producing alkenyl gold(I) complex **Int-4**. The difference in the relative energies between **TS₁₋₂** and **TS₃₋₄** is only 0.6 kcal/mol indicating that nucleophilic attack could occur through either **TS₃₋₄** or **TS₁₋₂**. **Int-2** is transformed to more stable **Int-4** ($\Delta G = -4.7$ kcal/mol) through ligand exchange on the zinc atom from the enol ester to an external benzoic acid molecule. **Int-4** alters its conformation to **Int-5**, then undergoes protonation at the alkenyl gold moiety through **TS₅₋₆** to form product-bound gold(I) complex **Int-6**. Since **TS₅₋₆** is ca. 4 kcal/mol lower in energy than **TS₁₋₂** and **TS₃₋₄**, the protonation should be faster than the nucleophilic attack.

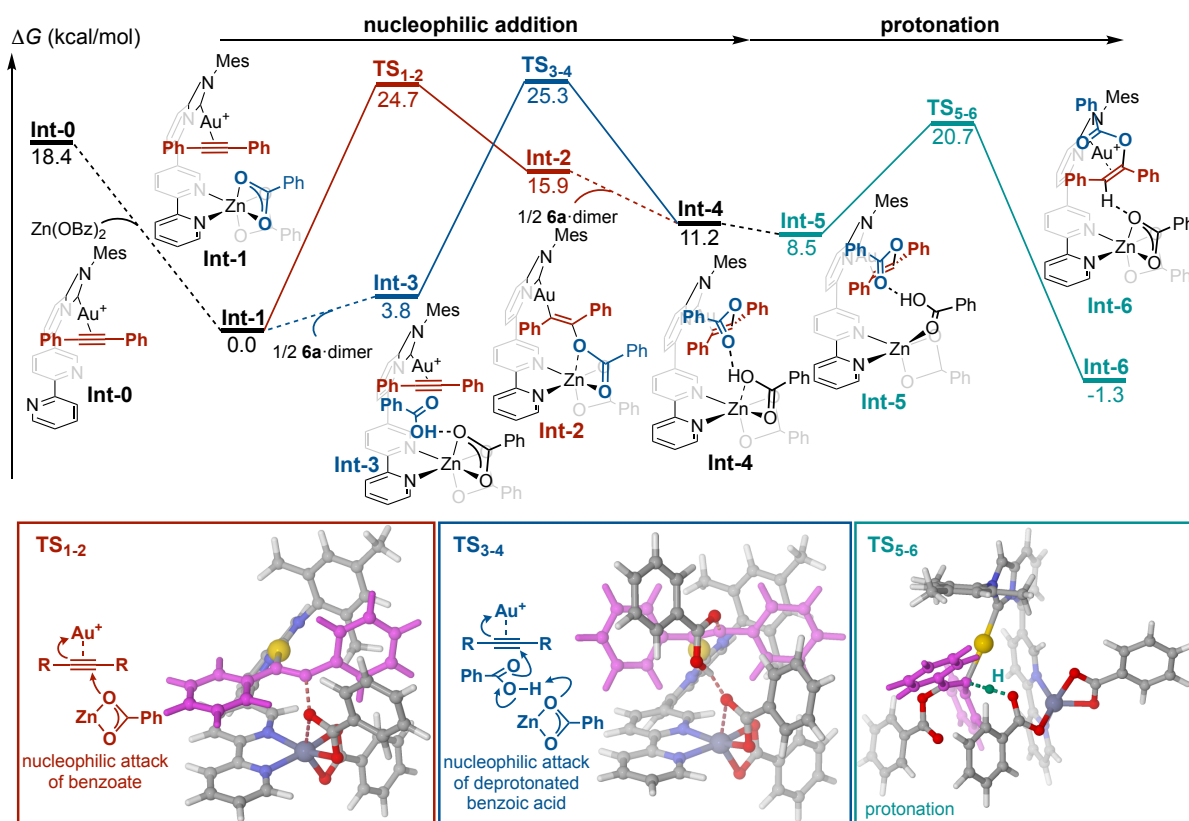


Figure 3. Energy diagram for nucleophilic addition of **6a** toward **5a**. DFT calculations were conducted at the M06/SDD,6-311+G(d,p)/SMD(DCE)//M06/SDD,6-31G(d) level of theory. The relative energies were corrected for the Gibbs free energies and reported in kcal/mol.

Conclusion

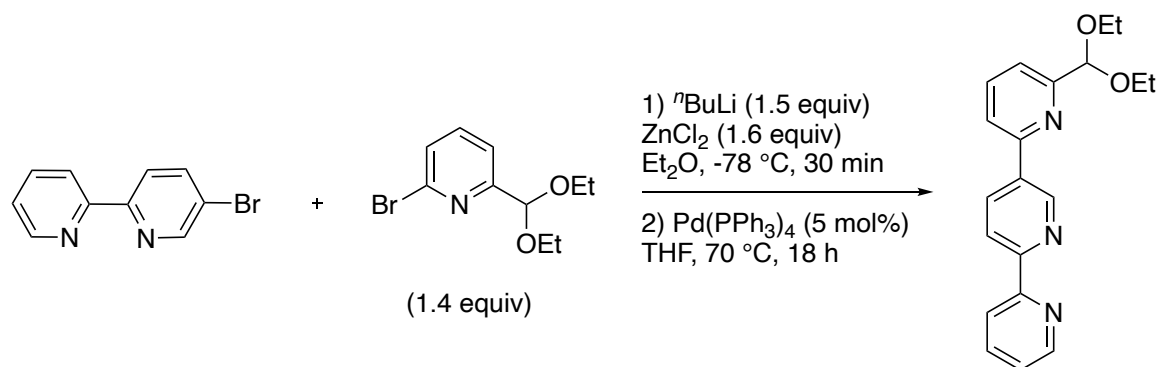
In summary, heterobimetallic cationic gold(I) catalyst systems with a 5-(2,2'-bipyrid-5-yl)imidazo[1,5-*a*]pyridin-3-ylidene ligand allowed intermolecular additions of carboxylic acids and phenols across non-activated internal alkynes. The activity of the heterobimetallic systems was highly dependent on the nature of the hard metal site, with Zn(acac)₂ being optimal. The molecular structure of the heterobimetallic gold-zinc complex was revealed by single-crystal XRD analysis. DFT calculations supported a proposed cooperative action of the cationic gold(I) atom and the zinc site for the intermolecular nucleophilic *anti*-addition of benzoic acid toward diphenylacetylene.

Experimental Section

General

All air and moisture-sensitive reactions were operated using the standard Schlenk techniques and glove box under nitrogen gas atmosphere. THF, DCM, Et₂O, and toluene were dried and deoxygenated by using Grubbs column (Glass Counter Solvent Dispensing System, Nikko Hansen & Co, Ltd.). Anhydrous 1,2-dichloroethane (DCE) was purchased from Sigma-Aldrich Co. LLC. Dry CH₃CN was purchased from Kanto Chemical Co., Inc.. Efavirenz was purchased from Tokyo Chemical Industry Co., Ltd. (TCI). Other commercially available chemicals were purchased from TCI, Sigma-Aldrich, Kanto Chemical, or FUJIFILM Wako Pure Chemical Corporation. ¹H NMR (400 MHz), ¹³C {¹H} NMR (100 MHz), and ¹⁹F NMR (376 MHz) spectra were measured on JEOL ECZ-400S spectrometer. All ¹H NMR chemical shifts were reported in ppm (δ) relative to the chemical shifts of residual solvent resonances (CDCl₃ at δ 7.26 and DCM-*d*₂ at δ 5.32). All ¹³C {¹H} NMR chemical shifts were reported in ppm (δ) relative to carbon resonances of CDCl₃ at δ 77.0 and DCM-*d*₂ at δ 53.8. High-resolution mass spectra were obtained with Thermo Fisher Scientific Exactive, JEOL JMS-T100LP, or JEOL JMS-700TZ at the Instrumental Analysis Division, Equipment Management Center, Creative Research Institution, Hokkaido University. IR spectra were obtained on JASCO FT-IR-4600 spectrometer. Melting points were obtained with OptiMelt (MPA100) of Stanford Research Systems. Flash column chromatography was performed using silica gel (Wakogel FC-40, 0.020-0.040 nm >70%). Gold catalyzed nucleophilic addition was conducted using EYELA RCH-1000 of TOKYO RIKAKIKAI CO, LTD as a heating reactor with screw-cap vial (NN-13) of Maruemu Corporation.

6''-(Diethoxymethyl)-2,2':5',2''-terpyridine (3)

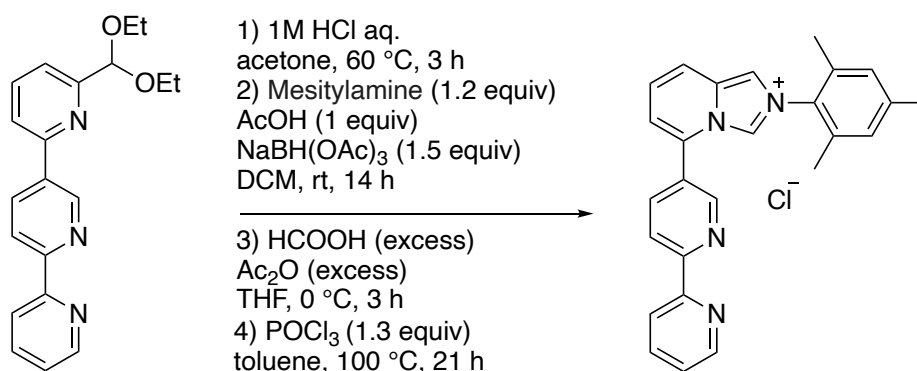


ⁿBuLi (1.57 M in hexane, 16.2 mL, 25.6 mmol, 1.5 equiv) was added dropwise to the solution of 2-bromo-6-(diethoxymethyl)pyridine¹⁵ (6.19 g, 23.8 mmol, 1.4 equiv) in dry Et₂O (28 mL) at -78 °C under nitrogen atmosphere, and the resulting pale yellow mixture was stirred at -78 °C

for 30 minutes. ZnCl_2 (1.0 M in Et_2O , 27.2 mL, 27.2 mmol, 1.6 equiv) was added dropwise to the solution at $-78\text{ }^\circ\text{C}$, and the resulting mixture was stirred for 1 hour at $-78\text{ }^\circ\text{C}$. The resulting organo-zinc solution was added to the solution of 5-bromo-2,2'-bipyridine (3.99 g, 17.0 mmol, 1.0 equiv) and $\text{Pd}(\text{PPh}_3)_4$ (982 mg, 0.85 mmol, 5 mol%) in dry THF (88 mL) at room temperature under nitrogen atmosphere. The mixture was stirred under reflux conditions at $70\text{ }^\circ\text{C}$ for 18 hours. After quenching with $\text{EDTA}\cdot 2\text{Na}$ (21.9 g, 76.5 mmol, 4.5 equiv) and water, the aqueous layer was extracted with CHCl_3 , and the combined organic phase were dried over Na_2SO_4 , filtrated, and evaporated under reduced pressure. The crude mixture was purified by silica-gel flash column chromatography ($\text{EtOAc}/\text{hexane}=2/8$ to $3/7$) to afford the desired product (4.43 g, 13.2 mmol, 78% yield).

Light orange solid. **mp**: $63\text{--}66\text{ }^\circ\text{C}$. **IR** (ATR, ν/cm^{-1}): 2976 w, 2870 w, 1589 w, 1573 w, 1448 w, 1427 w, 1325 m, 1143 m, 1109 m, 1058 s, 1027 m, 914 w, 817 m, 782 m, 745 s, 633 w. **^1H NMR** (400 MHz, CDCl_3 , $25\text{ }^\circ\text{C}$): δ 9.31 (dd, $J = 2.1, 0.9$ Hz, 1H), 8.72 (ddd, $J = 4.8, 1.6, 0.9$ Hz, 1H), 8.54–8.47 (m, 3H), 7.88–7.82 (m, 2H), 7.77 (dd, $J = 7.8, 0.9$ Hz, 1H), 7.62 (dd, $J = 7.7, 1.0$ Hz, 1H), 7.34 (ddd, $J = 7.4, 4.9, 1.1$ Hz, 1H), 5.55 (s, 1H), 3.84–3.77 (m, 2H), 3.72–3.65 (m, 2H), 1.29 (t, $J = 7.1$, 6H). **$^{13}\text{C}\{^1\text{H}\}$ NMR** (100 MHz, CD_2Cl_2 , $25\text{ }^\circ\text{C}$): δ 159.4, 156.6, 156.1, 153.9, 149.6, 148.1, 137.9, 137.2, 135.4, 134.9, 124.2, 121.4, 121.0, 120.40, 120.37, 103.4, 62.8, 15.5. **HRMS** (ESI^+) m/z calc. for $\text{C}_{20}\text{H}_{21}\text{N}_3\text{O}_2\text{Na}$ 358.15260 found 358.15240.

5-([2,2'-Bipyridin]-5-yl)-2-mesitylimidazo[1,5-a]pyridin-2-ium Chloride (5a)

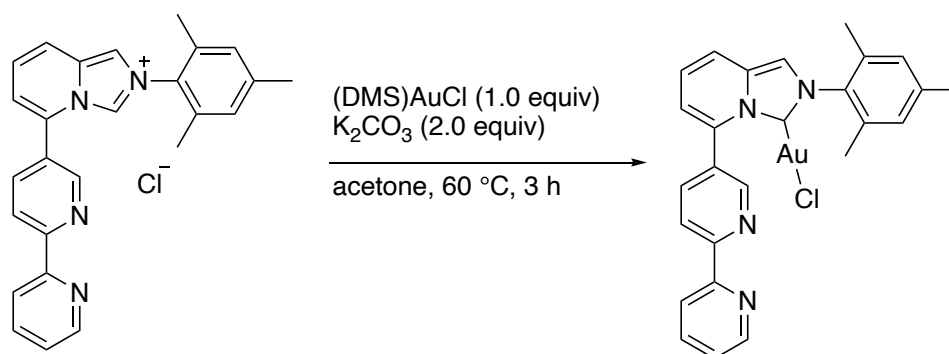


6''-(Diethoxymethyl)-2,2':5',2''-terpyridine (4.43 g, 13.2 mmol, 1 equiv) was dissolved in the mixed solvent of acetone (21 mL) and 1 M HCl aq (21 mL) under nitrogen atmosphere. The resulting solution was stirred at $60\text{ }^\circ\text{C}$ for 3 hours. The reaction mixture was quenched with saturated NaHCO_3 aqueous solution, the aqueous layer was extracted with DCM. Organic layer was dried over Na_2SO_4 , filtrated, and evaporated. The crude was dissolved in dry DCM (36 mL) under nitrogen atmosphere, and acetic acid (0.75 mL, 13.2 mmol, 1 equiv) and 2,4,6-

trimethylaniline (2.2 mL, 15.8 mmol, 1.2 equiv) were added to the solution followed by addition of NaBH(OAc)₃ (4.22 g, 19.8 mmol, 1.5 equiv) to the reaction mixture at 0 °C. The resulting mixture was stirred at room temperature for 14 hours. The reaction mixture was quenched with saturated NaHCO₃ aqueous solution. The aqueous layer was extracted with DCM, and the combined organic layer was dried over Na₂SO₄, filtrated, and evaporated. The resulting brown viscous oil was dissolved in dry THF (42 mL) under nitrogen atmosphere. The mixture of formic acid (3.5 mL) and acetic anhydride (3.5 mL) were stirred for 2 hours at room temperature before adding to the above THF solution at 0 °C under nitrogen atmosphere. The resulting mixture was stirred for 3 hours at 0 °C. The mixture was quenched with saturated NaHCO₃ aqueous solution. Aqueous layer was extracted with DCM, and the combined organic layer was dried over Na₂SO₄, filtrated, and evaporated. The crude mixture was passed through short-pad of silica-gel with EtOAc/DCM = 5/5 to 8/2 to remove highly polar impurity. The crude product was dissolved in dry toluene (20 mL) under nitrogen atmosphere. POCl₃ (1.72 mL, 17.2 mmol, 1.3 equiv) was added dropwise to the solution, and the resulting solution was stirred for 21 hours at 100 °C. After quenching with MeOH (1.5 mL), the reaction mixture was stirred for an additional 1 hour at room temperature. The crude solution was directly purified by basic alumina column chromatography (DCM/MeOH=9/1 to 7/3) to afford the desired product (4.13 g, 9.68 mmol, 73% yield).

Gray Solid. **mp**: 162 °C (decomp.). **IR** (ATR, ν /cm⁻¹): 2911 w, 1648 w, 1586 m, 1537 w, 1458 m, 1434 w, 1358 w, 1229 w, 1194 w, 1150 m, 1080 w, 1036 m, 936 w, 797 s, 768 m, 750 s, 727 s, 679 m, 580 m, 465 w. **¹H NMR** (400 MHz, CD₃OD, 25 °C): δ 9.93 (s, 1H), 9.05 (d, J = 2.3 Hz, 1H), 8.71-8.69 (m, 1H), 8.56 (dd, J = 8.2, 0.7 Hz, 1H), 8.46 (dd, J = 8.0, 0.9 Hz, 1H), 8.41-8.33 (m, 2H), 8.04-7.96 (m, 2H), 7.56 (dd, J = 9.4, 6.9 Hz, 1H), 7.52-7.46 (m, 1H), 7.40 (d, J = 7.1 Hz, 1H), 7.15 (s, 2H), 2.37 (s, 3H), 2.09 (s, 6H). **¹³C{¹H} NMR** (100 MHz, CD₃OD, 25 °C): δ 159.0, 156.2, 150.5, 150.3, 142.8, 138.9, 138.8, 135.7, 134.5, 133.5, 133.1, 130.7, 129.2, 127.6, 127.2, 126.0, 123.0, 122.6, 121.0, 119.5, 117.3, 21.1, 17.3. **HRMS** (ESI⁺) m/z calc. for C₂₆H₂₃N₄ 391.19172 found 391.19137.

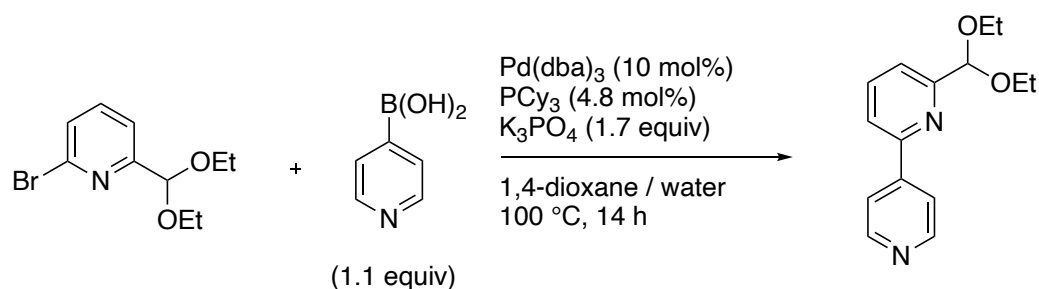
(5-([2,2'-Bipyridin]-5-yl)-2-mesitylimidazo[1,5-a]pyridin-3(2*H*)-ylidene)gold(I) Chloride (7a)



In nitrogen filled glove box, 5-([2,2'-bipyridin]-5-yl)-2-mesitylimidazo[1,5-*a*]pyridin-2-ium chloride (102 mg, 0.24 mmol, 1 equiv), AuCl·SMe₂ (60.7 mg, 0.24 mmol, 1 equiv), dry K₂CO₃ (66.3 mg, 0.48 mmol, 2.0 equiv), and dry acetone (6.0 mL) were filled in a screw vial containing a magnetic stirring bar. The reaction mixture was stirred at 60 °C for 3 hours under dark conditions. The mixture was then filtered through celite and subsequently eluted with DCM. The filtrate was evaporated and purified by silica-gel flash column chromatography (DCM/EtOAc=9/1 to 8/2) to afford the desired product (122 mg, 0.20 mmol, 82% yield). The crystal suitable for X-ray crystallography was grown from DCE/ether solution.

White solid. **mp**: 110 °C (decomp.). **IR** (ATR, ν /cm⁻¹): 2917 w, 1731 w, 1651 w, 1587 w, 1488 w, 1456 s, 1434 m, 1362 m, 1315 w, 1240 m, 1175 m, 1025 m, 851 m, 786 s, 748 s, 684 m, 591 m, 520 w. **¹H NMR** (400 MHz, CD₂Cl₂, 25 °C): δ 8.85 (d, *J* = 2.1 Hz, 1H), 8.70-8.69 (m, 1H), 8.57 (d, *J* = 8.0 Hz, 1H), 8.47 (d, *J* = 8.0 Hz, 1H), 8.00 (dt, *J* = 8.1, 2.0 Hz, 1H), 7.85 (tt, *J* = 7.8, 1.8 Hz, 1H), 7.56 (d, *J* = 9.4 Hz, 1H), 7.41 (s, 1H), 7.35 (t, *J* = 6.2 Hz, 1H), 7.12-7.08 (m, 1H), 7.03 (s, 2H), 6.71 (d, *J* = 6.6 Hz, 1H), 2.35 (s, 3H), 1.99 (s, 6H). **¹³C{¹H} NMR** (100 MHz, CD₂Cl₂, 25 °C): δ 164.8, 157.5, 155.9, 149.7, 149.6, 140.4, 138.7, 137.3, 136.7, 136.5, 134.8, 132.4, 131.0, 129.6, 124.4, 123.4, 121.7, 121.2, 118.5, 118.0, 113.5, 21.3, 17.9. **HRMS** (ESI⁺) *m/z* calc. for C₂₆H₂₂AuN₄ 587.15045 found 587.15048.

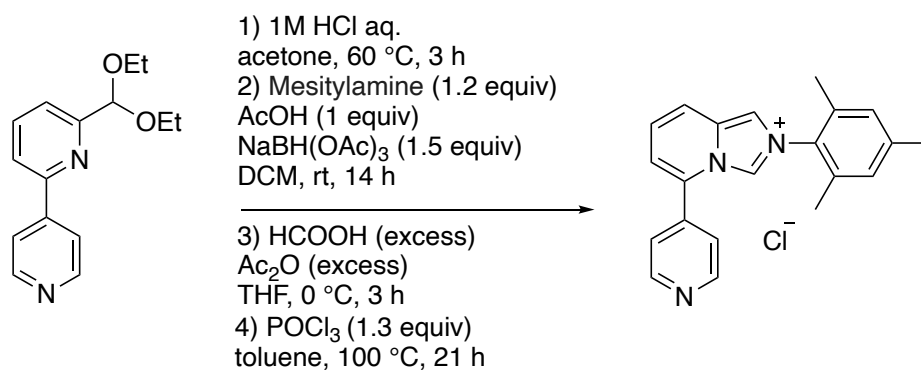
6-(Diethoxymethyl)-2,4'-bipyridine (3)



In a nitrogen filled glove box, Pd₂(dba)₃ (366 mg, 0.40 mmol, 2 mol%) and PCy₃ (269 mg, 0.96 mmol, 4.8 mol%) was dissolved in dry 1,4-dioxane (50 mL). The solution was transferred to the schlenk containing 2-bromo-6-(diethoxymethyl)pyridine (5.20 g, 20.0 mmol, 1 equiv) inside the glove box, and the Schlenk tube was taken out from the glove box. Pyridin-4-ylboronic acid (2.71 g, 22.0 mmol, 1.1 equiv) was added to the reaction solution under nitrogen atmosphere followed by addition of degassed solution of K₃PO₄ (7.22 g, 34.0 mmol, 1.7 equiv) in deionized water (27 mL). The resulting solution was stirred at 100 °C for 14 hours. After cooling to room temperature, water was poured into the solution, and the aqueous layer was extracted with DCM. The combined organic layer was dried over Na₂SO₄, filtrated, and evaporated. The crude mixture was purified by silica-gel flash column chromatography (hexane/EtOAc = 7/3 to 2/8) to afford the desired product (4.56 g, 17.7 mmol, 88% yield).

Orange oil. **IR** (ATR, ν /cm⁻¹): 2975 w, 2879 w, 1589 m, 1551 w, 1453 m, 1334 w, 1110 m, 1054 s, 993 m, 908 w, 800 s, 772 m, 620 s. **¹H NMR** (400 MHz, CDCl₃, 25 °C): δ 8.71 (dd, J = 4.5, 1.7 Hz, 2H), 7.92 (dd, J = 4.5, 1.7 Hz, 2H), 7.85 (t, J = 7.8 Hz, 1H), 7.75 (dd, J = 7.8, 0.9 Hz, 1H), 7.65 (dd, J = 7.8, 0.7 Hz, 1H), 5.53 (s, 1H), 3.82-3.74 (m, 2H), 3.70-3.62 (m, 2H), 1.27 (t, J = 7.1 Hz, 6H). **¹³C{¹H} NMR** (100 MHz, CDCl₃, 25 °C): δ 159.0, 153.6, 150.4, 146.2, 137.7, 121.1, 121.0, 120.4, 103.1, 62.6, 15.2. **HRMS** (ESI⁺) m/z calc. for C₁₅H₁₈N₂O₂Na 281.12605 found 281.12590.

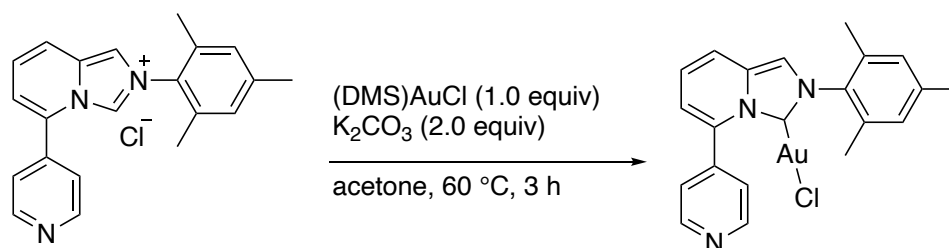
2-Mesityl-5-(pyridin-4-yl)imidazo[1,5-a]pyridin-2-ium Chloride (5a)



6-(Diethoxymethyl)-2,4'-bipyridine (2.07 g, 8.01 mmol, 1 equiv) was dissolved in the mixed solvent of acetone (14 mL) and 1 M HCl aq (14 mL) under nitrogen atmosphere. The resulting solution was stirred at 60 °C for 3 hours. The reaction mixture was quenched with saturated NaHCO₃ aqueous solution, the aqueous layer was extracted with DCM. The combined organic layer was dried over Na₂SO₄, filtrated, and evaporated. The crude was dissolved in dry DCM (23 mL) under nitrogen atmosphere. Acetic acid (0.46 mL, 8.01 mmol, 1 equiv) and 2,4,6-trimethylaniline (1.35 mL, 9.6 mmol, 1.2 equiv) were added to the solution followed by addition of NaBH(OAc)₃ (2.54 g, 12.0 mmol, 1.5 equiv) to the reaction mixture at 0 °C. The resulting mixture was stirred at room temperature for 14 hours. The resultant mixture was quenched with saturated NaHCO₃ aqueous solution, aqueous layer was extracted with DCM, and the combined organic layer was dried over Na₂SO₄, filtrated, and evaporated. The resulting brown viscous oil was dissolved in dry THF (37 mL) under nitrogen atmosphere. The mixture of formic acid (2.3 mL) and acetic anhydride (2.3 mL) were stirred for 2 hours at room temperature before adding dropwise to the above THF solution at 0 °C. The resulting mixture was stirred for 3 hours at 0 °C. The mixture was quenched with saturated NaHCO₃ aqueous solution. Aqueous layer was extracted with DCM, and the combined organic layer was dried over Na₂SO₄, filtrated, and evaporated. The crude mixture was passed through short-pad of silica-gel with EtOAc/hexane = 3/7 to 6/4 to remove highly polar impurity. The crude product was dissolved in dry toluene (7.0 mL) under nitrogen atmosphere. POCl₃ (0.97 mL, 10.4 mmol, 1.3 equiv) was added dropwise to the solution, and the resulting solution was stirred for 21 hours at 100 °C. After quenching with MeOH (1.0 mL), the reaction mixture was stirred for an additional 1 hour at room temperature. The crude solution was directly purified by basic alumina column chromatography (DCM/MeOH = 9/1 to 8/2) to afford the desired product (2.31 g, 6.60 mmol, 82% yield).

Brown oil. **IR** (ATR, ν / cm^{-1}): 3348 w, 3032 w, 2967 w, 1652 w, 1596 s, 1552 w, 1407 m, 1200 w, 1154 m, 1033 w, 849 m, 813 s, 671 s, 613 s. **^1H NMR** (400 MHz, CDCl_3 , 25 °C): δ 9.49 (t, J = 0.8 Hz, 1H), 8.88 (dd, J = 4.6, 1.6 Hz, 2H), 8.53 (d, J = 1.6 Hz, 1H), 8.37 (d, J = 9.4 Hz, 1H), 7.87 (dd, J = 4.3, 1.6 Hz, 2H), 7.44 (dd, J = 9.4, 6.9 Hz, 1H), 7.22 (d, J = 6.9 Hz, 1H), 7.01 (s, 2H), 2.34 (s, 3H), 2.10 (s, 6H). **$^{13}\text{C}\{^1\text{H}\}$ NMR** (100 MHz, CDCl_3 , 25 °C): δ 151.7, 141.7, 138.3, 134.1, 133.4, 132.0, 131.1, 129.8, 125.6, 124.2, 122.8, 120.2, 120.0, 117.1, 21.1, 17.8. **HRMS** (ESI⁺) m/z calc. for $\text{C}_{21}\text{H}_{20}\text{N}_3$ 314.16517 found 314.16499.

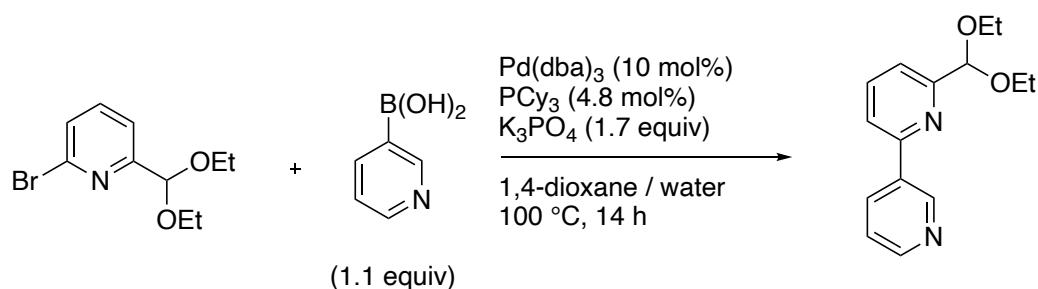
(2-Mesityl-5-(pyridin-4-yl)imidazo[1,5-a]pyridin-3(2H)-ylidene)gold(I) Chloride (7a)



In nitrogen filled glove box, 2-mesityl-5-(pyridin-4-yl)imidazo[1,5-a]pyridin-2-ium chloride (87.4 mg, 0.25 mmol, 1 equiv), $\text{AuCl}\cdot\text{SMe}_2$ (73.6 mg, 0.25 mmol, 1 equiv), dry K_2CO_3 (69.1 mg, 0.51 mmol, 2.0 equiv), and dry acetone (5.0 mL) were filled in a screw vial containing a magnetic stirring bar. The reaction mixture was stirred at 60 °C for 3 hours under dark conditions. The mixture was then filtered through celite and subsequently eluted with DCM. The filtrate was evaporated and was purified by silica-gel flash column chromatography (DCM/EtOAc = 9/1 to 8/2) to afford the desired product as white solid (104 mg, 0.19 mmol, 76% yield). The crystal suitable for X-ray crystallography was grown from DCM/ether solution.

White solid. **mp**: 125 °C (decomp.). **IR** (ATR, ν / cm^{-1}): 3140 w, 2980 w, 2916 w, 1596 m, 1548 w, 1488 w, 1408 m, 1377 m, 1282 w, 1198 m, 994 w, 852 w, 810 m, 791 s, 687 m, 630 m. **^1H NMR** (400 MHz, CD_2Cl_2 , 25 °C): δ 8.75 (dd, J = 4.3, 1.6 Hz, 2H), 7.57-7.53 (m, 3H), 7.41 (s, 1H), 7.07 (dd, J = 9.1, 6.6 Hz, 1H), 7.04 (s, 2H), 6.62 (dd, J = 6.6, 1.1 Hz, 1H), 2.36 (s, 3H), 1.98 (s, 6H). **$^{13}\text{C}\{^1\text{H}\}$ NMR** (100 MHz, CD_2Cl_2 , 25 °C): δ 164.6, 150.6, 142.4, 140.4, 137.1, 136.5, 134.7, 132.3, 129.6, 124.9, 123.4, 118.6, 117.3, 113.5, 21.3, 17.9. **HRMS** (ESI⁺) m/z calc. for $\text{C}_{21}\text{H}_{19}\text{AuClN}_3\text{Na}$ 568.08252 found 568.08493.

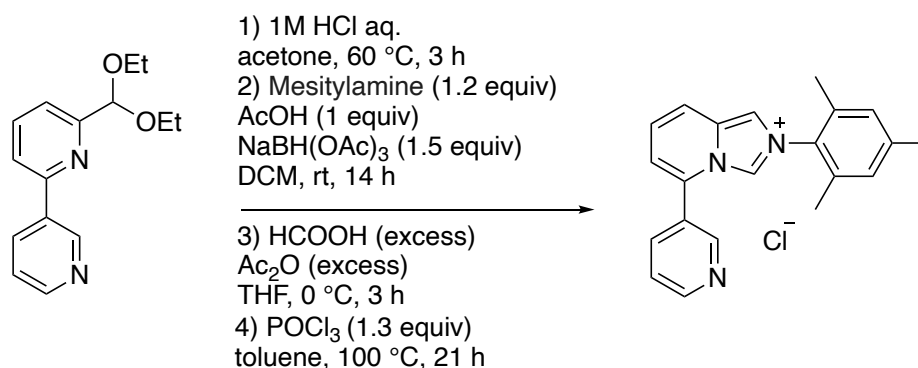
6-(Diethoxymethyl)-2,3'-bipyridine (3)



In a nitrogen filled glove box, Pd₂(dba)₃ (366 mg, 0.40 mmol, 2 mol%) and PCy₃ (269 mg, 0.96 mmol, 4.8 mol%) was dissolved in dry 1,4-dioxane (50 mL). The solution was transferred to the schlenk containing 2-bromo-6-(diethoxymethyl)pyridine (5.20 g, 20.0 mmol) inside the glove box, and the Schlenk tube was taken out from the glove box. Pyridin-3-ylboronic acid (2.70 g, 22.0 mmol, 1.1 equiv) was added to the reaction mixture under nitrogen atmosphere followed by addition of degassed solution of K₃PO₄ (7.22 g, 34.0 mmol, 1.7 equiv) in deionized water (27 mL). The resulting mixture was stirred at 100 °C for 14 hours. After cooling to room temperature, water was poured into the solution, and the aqueous layer was extracted with DCM. The combined organic layer was dried over Na₂SO₄, filtrated, and evaporated. The crude mixture was purified by silica-gel flash column chromatography (EtOAc/hexane = 3/7 to 5/5) to afford the desired product (4.31 g, 16.7 mmol, 83% yield).

Yellow oil. **IR** (ATR, ν /cm⁻¹): 2975 w, 2879 w, 1738 w, 1577 m, 1449 m, 1392 w, 1323 m, 1162 w, 1110 m, 1055 s, 1021 m, 796 s, 767 m, 708 m. **¹H NMR** (400 MHz, CDCl₃, 25 °C): δ 9.21 (d, J = 2.1 Hz, 1H), 8.64 (dd, J = 4.8, 1.6 Hz, 1H), 8.35 (dt, J = 8.0, 1.9 Hz, 1H), 7.83 (t, J = 7.8 Hz, 1H), 7.70 (dd, J = 7.9, 0.8 Hz, 1H), 7.60 (dd, J = 7.7, 0.6 Hz, 1H), 7.39 (dd, J = 7.8, 4.8 Hz, 1H), 5.53 (s, 1H), 3.82-3.74 (m, 2H), 3.70-3.63 (m, 2H), 1.28 (t, J = 7.1 Hz, 6H). **¹³C{¹H} NMR** (100 MHz, CDCl₃, 25 °C): δ 158.9, 153.8, 149.9, 148.4, 137.6, 134.7, 134.4, 123.5, 120.1, 120.0, 103.1, 62.6, 15.2. **HRMS** (ESI⁺) m/z calc. for C₁₅H₁₈N₂O₂Na 281.12605 found 281.12587.

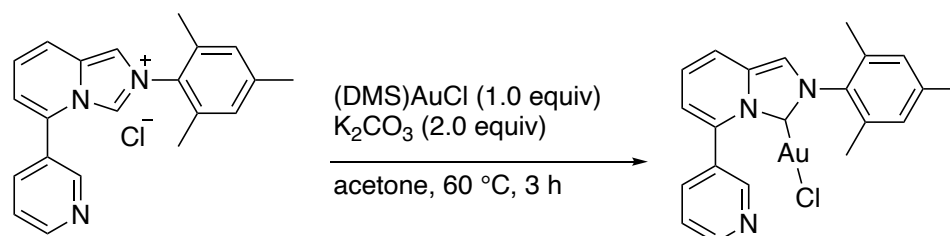
2-Mesityl-5-(pyridin-3-yl)imidazo[1,5-a]pyridin-2-ium Chloride (5a)



6-(Diethoxymethyl)-2,3'-bipyridine (2.07 g, 8.01 mmol, 1 equiv) was dissolved in the mixed solvent of acetone (14 mL) and 1 M HCl aq (14 mL) under nitrogen atmosphere. The resulting solution was stirred at 60 °C for 3 hours. The reaction mixture was quenched with saturated NaHCO₃ aqueous solution, the aqueous layer was extracted with DCM. The combined organic layer was dried over Na₂SO₄, filtrated, and evaporated. The crude was dissolved in dry DCM (23 mL) under nitrogen atmosphere, acetic acid (0.46 mL, 8.01 mmol, 1 equiv) and 2,4,6-trimethylaniline (1.35 mL, 9.59 mmol, 1.2 equiv) were added to the solution followed by addition of NaBH(OAc)₃ (2.55 g, 12.0 mmol, 1.5 equiv) to the reaction solution at 0 °C. The resulting mixture was stirred at room temperature for 14 hours. The reaction mixture was quenched with saturated NaHCO₃ aqueous solution. The aqueous layer was extracted with DCM, and the combined organic layer was dried over Na₂SO₄, filtrated, and evaporated. The resulting brown viscous oil was dissolved in dry THF (37 mL) under nitrogen atmosphere. The mixture of formic acid (2.3 mL) and acetic anhydride (2.3 mL) were stirred for 2 hours at room temperature before adding dropwise to the above THF solution at 0 °C. The resulting mixture was stirred for 3 hours at 0 °C. The mixture was quenched with saturated NaHCO₃ aqueous solution. Aqueous layer was extracted with DCM, and the combined organic layer was dried over Na₂SO₄, filtrated, and evaporated. The crude mixture was just pass-through silica-gel. The crude mixture was passed through short-pad of silica-gel with EtOAc/hexane = 3/7 to 6/4 to remove highly polar impurity. The crude mixture was dissolved in dry toluene (7.0 mL) under nitrogen atmosphere. POCl₃ (0.97 mL, 10.4 mmol, 1.3 equiv) was added slowly to the solution, and the resulting solution was stirred for 21 hours at 100 °C. After quenching with MeOH (1.0 mL), the reaction mixture was stirred for an additional 1 hour at room temperature. The crude solution was directly purified by basic alumina column chromatography (DCM/MeOH = 9/1 to 7/3) to afford the desired product (2.03 g, 5.80 mmol, 72% yield).

Gray Solid. **IR** (ATR, ν/cm^{-1}): 3453 m, 3388 m, 2979 w, 2885 m, 1651 w, 1297 m, 1229 m, 1158 m, 1026 w, 802 s, 774 m, 705 s, 681 m. **^1H NMR** (400 MHz, CDCl_3 , 25 °C): δ 9.60 (dd, $J = 1.6, 0.7$ Hz, 1H), 8.83 (dd, $J = 2.3, 0.9$ Hz, 1H), 8.78 (dd, $J = 5.0, 1.6$ Hz, 1H), 8.69 (dt, $J = 8.0, 1.8$ Hz, 1H), 8.40 (d, $J = 1.6$ Hz, 1H), 8.27 (dd, $J = 9.4$ Hz, 1H), 7.68-7.64 (m, 1H), 7.43 (ddd, $J = 8.5, 6.9, 1.6$ Hz, 1H), 7.17 (d, $J = 7.1$ Hz, 1H), 7.00 (s, 2H), 2.32 (s, 3H), 2.09 (s, 6H). **$^{13}\text{C}\{^1\text{H}\}$ NMR** (100 MHz, CDCl_3 , 25 °C): δ 152.2, 149.0, 141.6, 137.4, 134.1, 133.0, 131.9, 131.1, 129.8, 127.1, 125.7, 124.9, 124.7, 119.8, 119.4, 116.7, 21.1, 17.8. **HRMS** (ESI⁺) m/z calc. for $\text{C}_{21}\text{H}_{20}\text{N}_3$ 314.16517 found 314.16488.

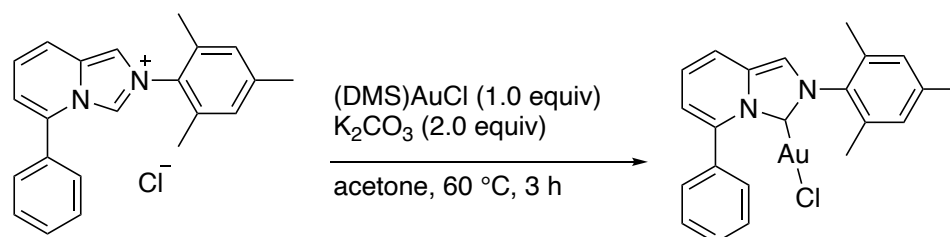
(2-Mesityl-5-(pyridin-3-yl)imidazo[1,5-a]pyridin-3(2H)-ylidene)gold(I) Chloride (7a)



In nitrogen filled glove box, 2-mesityl-5-(pyridin-3-yl)imidazo[1,5-a]pyridin-2-ium chloride (76.4 mg, 0.22 mmol, 1 equiv), $\text{AuCl}\cdot\text{SMe}_2$ (64.7 mg, 0.22 mmol, 1 equiv), dry K_2CO_3 (60.8 mg, 0.44 mmol, 2.0 equiv), and dry acetone (5.0 mL) were filled in a screw vial containing a magnetic stirring bar. The reaction mixture was stirred at 60 °C for 3 hours under dark conditions. The mixture was then filtered through celite and subsequently eluted with DCM. The filtrate was evaporated and was purified by silica-gel flash column chromatography (DCM/EtOAc = 9/1 to 8/2) to afford the desired product (92.7 mg, 0.17 mmol, 77% yield). The crystal suitable for X-ray crystallography was grown from DCM/ether solution.

White solid. **mp**: 118 °C (decomp.). **IR** (ATR, ν/cm^{-1}): 3137 w, 2979 w, 2912 w, 1651 w, 1486 w, 1407 m, 1367 m, 1313 w, 1175 m, 1023 m, 865 m, 784 s, 707 s, 686 m. **^1H NMR** (400 MHz, CD_2Cl_2 , 25 °C): δ 8.78-8.74 (m, 2H), 7.89 (dt, $J = 7.9, 1.9$ Hz, 1H), 7.56 (dd, $J = 9.3, 0.8$ Hz, 1H), 7.48 (ddd, $J = 7.8, 4.9, 0.8$ Hz, 1H), 7.41 (s, 1H), 7.09 (dd, $J = 9.4, 6.6$ Hz, 1H), 7.04 (s, 2H), 6.66 (dd, $J = 6.6, 1.1$ Hz, 1H) 2.36 (s, 3H), 1.98 (s, 6H). **$^{13}\text{C}\{^1\text{H}\}$ NMR** (100 MHz, CD_2Cl_2 , 25 °C): δ 164.6, 151.1, 150.3, 140.4, 137.8, 136.6, 134.7, 132.4, 131.3, 129.6, 123.9, 123.4, 118.5, 118.0, 113.5, 21.3, 17.9. **HRMS** (ESI⁺) m/z calc. for $\text{C}_{21}\text{H}_{19}\text{AuClN}_3\text{Na}$ 568.08252 found 568.08222.

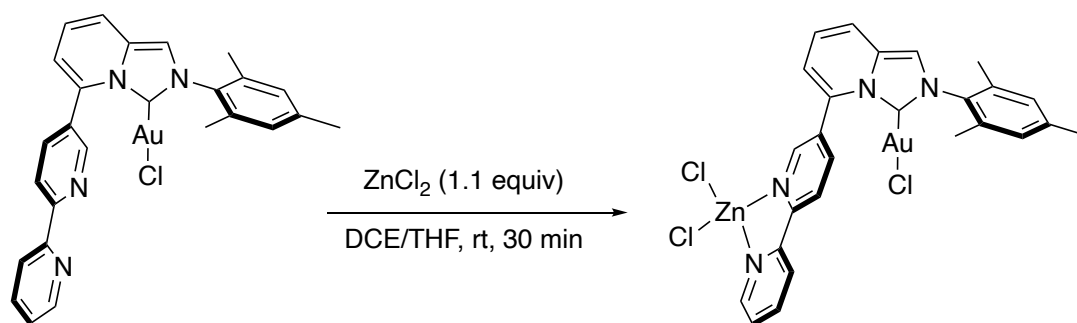
(2-Mesityl-5-phenylimidazo[1,5-a]pyridin-3(2H)-ylidene)gold(I) Chloride (8a)



In nitrogen filled glove box, 2-mesityl-5-phenylimidazo[1,5-*a*]pyridin-2-ium chloride¹ (45.6 mg, 0.13 mmol, 1 equiv), AuCl·SMe₂ (38.6 mg, 0.13 mmol, 1 equiv), dry K₂CO₃ (36.2 mg, 0.26 mmol, 2.0 equiv), and dry acetone (5.0 mL) were filled in a screw vial containing a magnetic stirring bar. The reaction mixture was stirred at 60 °C for 3 hours under dark condition. The mixture was filtered through celite and subsequently eluted with DCM. The filtrate was evaporated and was purified by silica-gel flash column chromatography (only DCM) to afford the desired product (65.4 mg, 0.12 mmol, 92% yield).

White solid. **mp**: 185 °C (decomp.). **IR** (ATR, ν /cm⁻¹): 3145 w, 2913 w, 1651 w, 1542 w, 1486 m, 1442 w, 1365 m, 1315 w, 1282 m, 1200 m, 1160 w, 1030 w, 867 m, 786 s, 760 s, 736 m, 710 m, 694 s, 684 m, 624 m. **¹H NMR** (400 MHz, CD₂Cl₂, 25 °C): δ 7.59-7.48 (m, 6H), 7.36 (s, 1H), 7.07-7.03 (m, 3H), 6.60 (dd, *J* = 6.6, 1.4 Hz, 1H), 2.36 (s, 3H), 1.98 (s, 6H). **¹³C{¹H} NMR** (100 MHz, CD₂Cl₂, 25 °C): δ 164.8, 140.2, 139.9, 136.8, 135.1, 134.8, 132.5, 130.3, 129.5, 129.2, 123.6, 117.6, 116.9, 113.0, 21.3, 17.9. **HRMS** (ESI⁺) *m/z* calc. for C₂₂H₂₀AuClN₂Na 567.08727 found 567.08568.

Hetero-bimetallic Complex



In the glove box, the solution of ZnCl₂ (5.99 mg, 0.044 mmol, 1.1 equiv) in dry THF (1.0 mL) was added to the solution of gold complex (25.1 mg, 0.040, 1 equiv) in dry DCE (2.0 mL) and dry THF (2.0 mL). The yellow solution was stirred for 30 minutes at room temperature, and the pale-yellow precipitate was formed. The resulting mixture was cooled to -20 °C, and the precipitate was filtrated, washed with cold THF, and dried under reduced pressure to afford

the bimetallic complex (23.7 mg, 0.031 mmol, 78%). The crystal suitable for X-ray crystallography was grown from DCM/THF solution.

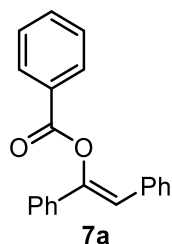
Pale yellow solid. **IR** (ATR, ν / cm^{-1}): 3500 w, 3143 w, 3054 w, 2920 w, 2852 w, 1652 w, 1489 m, 1470 s, 1439 s, 1365 m, 1316 m, 1282 w, 1199 w, 1051 w, 854 m, 787 s, 735 s, 685 m. **^1H NMR** (400 MHz, CD_2Cl_2 , 25 °C): δ 8.89 (brs, 1H), 8.74 (brs, 1H), 8.52 (d, J = 6.6 Hz, 1H), 8.42 (d, J = 8.2 Hz, 1H), 8.34 (d, J = 7.8 Hz, 1H), 8.16 (brs, 1H), 7.69 (brs, 1H), 7.61 (d, J = 9.6 Hz, 1H), 7.44 (s, 1H), 7.14 (brs, 1H), 7.03 (s, 2H), 6.88 (brs, 1H), 2.33 (s, 3H), 1.99 (brs, 3H), 1.93 (brs, 3H). Sharp $^{13}\text{C}\{^1\text{H}\}$ NMR chart was not obtained due to its poor solubility. $^{13}\text{C}\{^1\text{H}\}$ NMR analysis with saturated DCM- d_2 solution for 39 hours showed only few signals: **$^{13}\text{C}\{^1\text{H}\}$ NMR** (400 MHz, CD_2Cl_2 , 25 °C): δ 149.7, 140.6, 136.3, 129.7, 122.5, 114.2, 21.3, 18.0. **HRMS** (ESI⁺) m/z calc. for $\text{C}_{26}\text{H}_{22}\text{AuCl}_2\text{N}_4\text{Zn}$ 721.01785 found 721.01706.

General Procedure for the Gold-catalyzed Hydrocarboxylation of Alkynes

In a nitrogen-filled glove box, Au catalyst (5.0 mg, 0.008 mmol, 2 mol%) and NaBAR^{F} (7.1 mg, 0.008 mmol, 2 mol%) were placed in a screw vial containing a magnetic stirring bar. After addition of dry DCE (0.3 mL), the reaction mixture was stirred for 10 minutes. The resulting solution was filtrated through a glass-fiber pad packed into a pipet, and the filtrate was added to $\text{Zn}(\text{acac})_2$ (2.1 mg, 0.008 mmol, 2 mol%) and alkyne (0.40 mmol, if boiling point of alkyne is higher than 220 °C) in a screw vial containing a magnetic stirring bar. After stirring 30 minutes, all volatile compounds were removed under reduced pressure. Carboxylic acid (0.48 mmol), alkyne (0.40 mmol, if boiling point of alkyne is lower than 220 °C), and dry DCE (33 μL) was added to the mixture, and the reaction vial was sealed with screw-cap and taken out from the glove box. After stirring at 80 °C for 16 hours, the resulting mixture was quenched through a short pad of silica-gel. The crude mixture was purified by silica-gel column chromatography to give the desired compound.

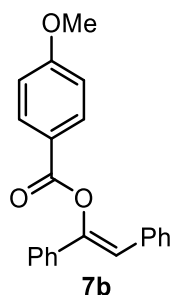
Characterization Data for Hydrocarboxylation products

(Z)-1,2-Diphenylvinyl Benzoate (7a)¹⁶



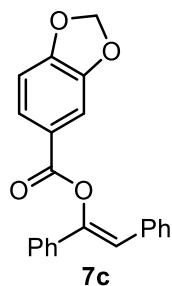
White solid. (117.4 mg, 0.391 mmol, 98% yield). ¹H NMR (400 MHz, CDCl₃, 25 °C): δ 8.28-8.23 (m, 2H), 7.70-7.66 (m, 1H), 7.61-7.58 (m, 2H), 7.57-7.53 (m, 4H), 7.40-7.35 (m, 2H), 7.35-7.26 (m, 2H), 7.23-7.19 (m, 1H), 6.82 (s, 1H). ¹³C{¹H} NMR (100 MHz, CDCl₃, 25 °C): δ 164.3, 146.6, 135.7, 134.2, 133.8, 130.3, 129.2, 128.75, 128.68, 128.63, 128.56, 127.6, 124.8, 117.1.

(Z)-1,2-Diphenylvinyl 4-Methoxybenzoate (7b)¹⁶



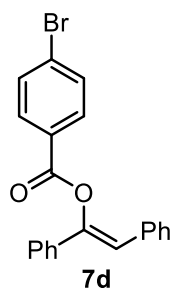
White solid (122.0 mg, 0.369 mmol, 92%). ¹H NMR (400 MHz, CDCl₃, 25 °C): δ 8.22-8.19 (m, 2H), 7.61-7.58 (m, 2H), 7.57-7.54 (m, 2H), 7.39-7.35 (m, 2H), 7.34-7.28 (m, 2H), 7.22-7.19 (m, 1H), 7.04-7.00 (m, 2H), 6.80 (s, 1H), 3.91 (s, 3H). ¹³C{¹H} NMR (100 MHz, CDCl₃, 25 °C): δ 164.1, 164.0, 146.7, 135.9, 134.4, 132.4, 128.75, 128.65, 128.5, 127.5, 124.8, 121.6, 117.0, 114.0, 55.5.

(Z)-1,2-Diphenylvinyl Benzo[d][1,3]dioxole-5-carboxylate (7c)



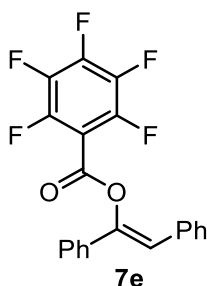
White solid. (121.2 mg, 0.352 mmol, 88% yield). **mp**: 127-128 °C. **IR** (ATR, ν / cm^{-1}): 1736 m, 1484 m, 1435 w, 1368 w, 1255 s, 1218 m, 1038 m, 922 m, 761 s, 746 m, 690 s, 511 m, 438 w. **^1H NMR** (400 MHz, CDCl_3 , 25 °C): δ 7.89-7.87 (m, 1H), 7.66-7.65 (m, 1H), 7.59 (d, J = 8.2 Hz, 2H), 7.55 (d, J = 8.2 Hz, 2H), 7.40-7.33 (m, 3H), 7.30 (t, J = 7.7 Hz, 2H), 7.22 (t, J = 7.3 Hz, 1H), 6.94 (d, J = 8.0 Hz, 1H), 6.80 (s, 1H), 6.09 (s, 2H). **$^{13}\text{C}\{^1\text{H}\}$ NMR** (100 MHz, CDCl_3 , 25 °C): δ 163.6, 152.4, 148.1, 146.6, 135.7, 134.3, 128.73, 128.66, 128.6, 128.5, 127.6, 126.4, 124.7, 123.1, 117.1, 110.0, 108.3, 102.0. HRMS (EI) m/z calc. for $\text{C}_{22}\text{H}_{16}\text{O}_4$ 344.10486 found 344.10427.

(Z)-1,2-Diphenylvinyl 4-Bromobenzoate (7d)¹⁶



White solid. (144.5 mg, 0.381 mmol, 95% yield). **^1H NMR** (400 MHz, CDCl_3 , 25 °C): δ 8.10-8.07 (m, 2H), 7.70-7.67 (m, 2H), 7.58-7.55 (m, 2H), 7.52-7.48 (m, 2H), 7.40-7.33 (m, 3H), 7.30-7.27 (m, 2H), 7.24-7.21 (m, 1H), 6.81 (s, 1H). **$^{13}\text{C}\{^1\text{H}\}$ NMR** (100 MHz, CDCl_3 , 25 °C): δ 163.6, 146.4, 135.4, 134.1, 132.2, 131.7, 129.1, 128.73, 128.69, 128.6, 128.1, 127.7, 124.8, 117.2.

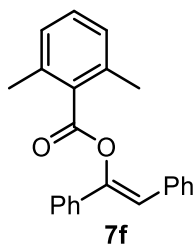
(Z)-1,2-Diphenylvinyl 2,3,4,5,6-Pentafluorobenzoate (7e)



Orange solid. (143.9 mg, 0.369 mmol, 92% yield). **mp**: 119-121 °C. **IR** (ATR, ν / cm^{-1}): 3070 w, 3030 w, 1749 s, 1653 w, 1523 m, 1503 s, 1450 w, 1422 m, 1327 m, 1194 s, 1095 m, 987 s, 844 w, 756 s, 687 s. **^1H NMR** (400 MHz, CDCl_3 , 25 °C): δ 7.65-7.62 (m, 2H), 7.51 (d, J = 8.0 Hz, 2H), 7.46-7.38 (m, 3H), 7.38-7.34 (m, 2H), 7.31-7.27 (m, 1H), 6.83 (s, 1H). **$^{13}\text{C}\{^1\text{H}\}$ NMR** (100 MHz, CDCl_3 , 25 °C): δ 156.7, 147.5-146.7 (m), 146.0, 145.3-144.7 (m), 144.7-144.2 (m),

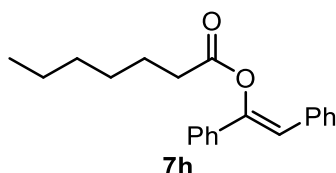
142.7-142.1 (m), 139.4-138.8 (m), 136.9-136.3 (m), 134.6, 133.6, 129.5-127.7 (m), 125.4-124.7 (m), 118.7-117.2 (m), 107.6-107.0 (m). **¹⁹F NMR** (376 MHz, CDCl₃, 25 °C): δ -136.5 - -136.6 (m, 2F), -146.8 (tt, *J* = 20.9, 4.8 Hz, 1F), -159.4 - -159.6 (m, 2F). **HRMS** (EI) *m/z* calc. for C₂₁H₁₁F₅O₂ 390.06792 found 390.06797.

(Z)-1,2-Diphenylvinyl 2,6-Dimethylbenzoate (7f)¹⁶



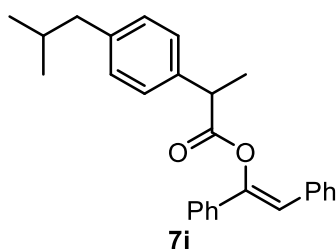
Colourless oil. (125.8 mg, 0.383 mmol, 96% yield). **¹H NMR** (400 MHz, CDCl₃, 25 °C): δ 7.70-7.68 (m, 2H), 7.54-7.52 (m, 2H), 7.46-7.42 (m, 2H), 7.40-7.38 (m, 1H), 7.33-7.27 (m, 3H), 7.25-7.23 (m, 1H), 7.06 (d, *J* = 7.5 Hz, 2H), 6.72 (s, 1H), 2.25 (s, 6H). **¹³C{¹H} NMR** (100 MHz, CDCl₃, 25 °C): δ 167.7, 147.7, 136.5, 136.4, 134.2, 132.1, 130.0, 129.0, 128.7, 128.5, 128.4, 128.1, 127.6, 126.0, 118.3, 20.6.

(Z)-1,2-Diphenylvinyl Heptanoate (7h)¹⁷



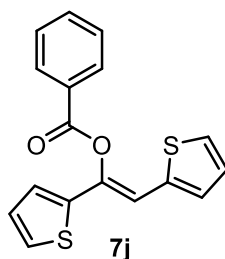
White solid. (119.4 mg, 0.387 mmol, 97% yield). **¹H NMR** (400 MHz, CDCl₃, 25 °C): δ 7.54-7.50 (m, 4H), 7.40-7.31 (m, 5H), 7.28-7.24 (m, 1H), 6.69 (s, 1H), 2.58 (t, *J* = 7.5 Hz, 2H), 1.71 (q, *J* = 7.5, 2H), 1.38-1.28 (m, 6H), 0.90 (t, *J* = 6.7 Hz, 3H). **¹³C{¹H} NMR** (100 MHz, CDCl₃, 25 °C): δ 171.3, 146.7, 135.8, 134.4, 128.7, 128.61, 128.56, 128.5, 127.6, 124.8, 116.8, 34.4, 31.4, 28.8, 24.7, 22.5, 14.0.

(Z)-1,2-Diphenylvinyl 2-(4-Isobutylphenyl)propanoate (7i)



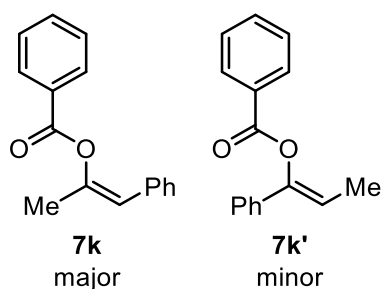
White solid. (151.1 mg, 0.393 mmol, 98% yield). **mp**: 106-107 °C. **IR** (ATR, ν / cm^{-1}): 2949 w, 2865 w, 1751 s, 1640 w, 1495 w, 1448 m, 1256 w, 1127 s, 1087 s, 1014 m, 865 m, 797 m, 764 s, 751 s, 585 m, 548 s, 515 s. $^1\text{H NMR}$ (400 MHz, CDCl_3 , 25 °C): δ 7.35-7.17 (m, 14H), 6.63 (s, 1H), 3.99 (q, $J = 7.1$ Hz, 1H), 2.53 (d, $J = 7.1$ Hz, 2H), 1.96-1.89 (m, 1H), 1.59 (d, $J = 7.2$, Hz, 3H), 0.96 (dd, $J = 6.6, 0.7$ Hz, 6H). $^{13}\text{C}\{^1\text{H}\}$ NMR (100 MHz, CDCl_3 , 25 °C): δ 171.9, 146.6, 141.0, 136.4, 135.7, 134.2, 129.5, 128.7, 128.43, 128.40, 128.3, 127.7, 127.4, 124.7, 116.9, 45.4, 45.1, 30.3, 22.4, 17.9. **HRMS** (ESI $^+$) m/z calc. for $\text{C}_{27}\text{H}_{28}\text{O}_2\text{Na}$ 407.19815 found 407.19715.

(Z)-1,2-Di(thiophen-2-yl)vinyl Benzoate (7j)



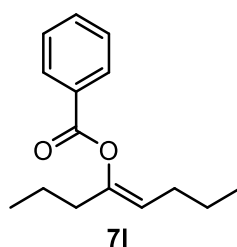
Light Yellow solid. (113.7 mg, 0.364 mmol, 91% yield). **mp**: 162-164 °C. **IR** (ATR, ν / cm^{-1}): 1741 m, 1450 w, 1436 w, 1231 s, 1211 m, 1173 w, 1071 w, 1053 s, 1022 s, 849 m, 722 m, 697 s, 598 w, 509 w. $^1\text{H NMR}$ (400 MHz, CDCl_3 , 25 °C): δ 8.34-8.31 (m, 2H), 7.70 (tt, $J = 7.6, 1.1$ Hz, 1H), 7.58 (t, $J = 7.7$ Hz, 2H), 7.24 (dd, $J = 5.0, 1.1$ Hz, 1H), 7.20 (d, $J = 5.0$ Hz, 1H), 7.14 (d, $J = 3.4$ Hz, 1H), 7.12 (dd, $J = 3.7, 1.1$ Hz, 1H), 7.04 (s, 1H), 6.99 (d, $J = 3.7$ Hz, 1H), 6.98 (d, $J = 3.7$ Hz, 1H). $^{13}\text{C}\{^1\text{H}\}$ NMR (100 MHz, CDCl_3 , 25 °C): δ 164.1, 139.8, 138.9, 136.4, 133.9, 130.5, 129.2, 128.7, 128.4, 127.8, 126.8, 125.4, 124.3, 110.7. **HRMS** (EI) m/z calc. for $\text{C}_{17}\text{H}_{12}\text{O}_2\text{S}_2$ 312.02787 found 312.02716.

(Z)-1-Phenylprop-1-en-2-yl Benzoate (7k) and (Z)-1-Phenylprop-1-en-1-yl Benzoate (7k')¹⁷



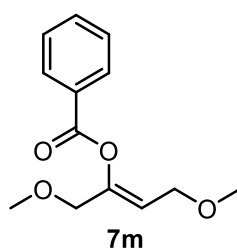
Colourless oil. (94.6 mg, 0.397 mmol, 99% yield). $^1\text{H NMR}$ (400 MHz, CDCl_3 , 25 °C): δ 8.29-8.27 (m, 2H, minor), 8.20-8.17 (m, 2H, major), 7.66-7.60 (m, 1H, major and minor), 7.56-7.49 (m, 2H, major and minor), 7.44 (d, $J = 7.8$ Hz, 2H, major), 7.36-7.30 (m, 3H, minor), 7.29-7.24 (m, 2H, major), 7.20-7.16 (m, 1H, major), 6.10 (s, 1H, major), 6.05 (q, $J = 7.0$ Hz, 1H, minor), 2.25 (d, $J = 0.9$ Hz, 3H, major), 1.81 (d, $J = 6.9$ Hz, 3H, minor). $^{13}\text{C}\{^1\text{H}\}$ NMR (100 MHz, CDCl_3 , 25 °C): δ 164.0, 146.3, 134.3, 133.4, 130.0, 129.5, 128.5, 128.3, 128.1, 126.9, 116.8, 20.7 for major isomer; 164.1, 147.0, 134.9, 130.1, 129.3, 128.0, 112.8, 11.6 for minor isomer, some signals were overlapped to the signals for major isomer.

(Z)-Oct-4-en-4-yl Benzoate (7l)¹⁶



Colourless oil. (91.8 mg, 0.395 mmol, 99% yield). $^1\text{H NMR}$ (400 MHz, CDCl_3 , 25 °C): δ 8.13-8.10 (m, 2H), 7.60 (tt, $J = 7.6, 1.4$ Hz, 1H), 7.48 (t, $J = 7.7$ Hz, 2H), 5.11 (t, $J = 7.3$ Hz, 1H), 2.30-2.26 (m, 2H), 1.96 (q, $J = 7.3$ Hz, 2H), 1.52 (sext., $J = 7.5$ Hz, 2H), 1.38 (sext., $J = 7.2$ Hz, 2H), 0.95 (t, $J = 7.3$ Hz, 3H), 0.88 (t, $J = 7.4$ Hz, 3H). $^{13}\text{C}\{^1\text{H}\}$ NMR (100 MHz, CDCl_3 , 25 °C): δ 164.4, 148.5, 133.1, 129.9, 128.4, 116.5, 35.5, 27.4, 22.3, 20.0, 13.7, 13.5.

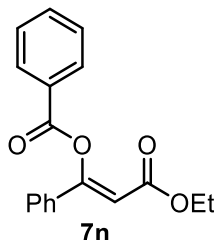
(Z)-1,4-Dimethoxybut-2-en-2-yl Benzoate (7m)



Colourless oil. (88.8 mg, 0.376 mmol, 94% yield). IR (ATR, ν/cm^{-1}): 1731 m, 1601 w, 1451 w, 1243 s, 1195 m, 1170 m, 1087 s, 1062 s, 1025 m, 912 w, 708 s. $^1\text{H NMR}$ (400 MHz, CDCl_3 , 25 °C): δ 8.12-8.09 (m, 2H), 7.61 (tt, $J = 7.3, 1.4$ Hz, 1H), 7.48 (t, $J = 7.7$ Hz, 2H), 5.62 (tt, $J = 6.5, 0.9$ Hz, 1H), 4.10 (d, $J = 0.9$ Hz, 2H), 3.99 (dt, $J = 6.4, 0.8$ Hz, 2H), 3.38 (s, 3H), 3.30 (s, 3H). $^{13}\text{C}\{^1\text{H}\}$ NMR (100 MHz, CDCl_3 , 25 °C): δ 164.1, 146.7, 133.6, 130.1, 129.0, 128.5,

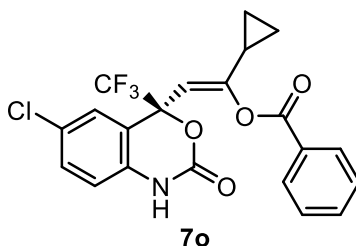
116.8, 71.5, 66.3, 58.2, 58.1. **HRMS** (ESI⁺) *m/z* calc. for C₁₃H₁₆O₄Na 259.09408 found 259.09359.

(Z)-3-Ethoxy-3-oxo-1-phenylprop-1-en-1-yl Benzoate (7n)¹⁶



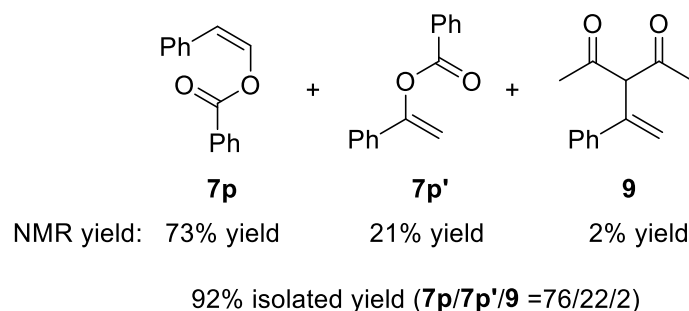
White Solid. (117.2 mg, 0.396 mmol, 99% yield). **¹H NMR** (400 MHz, CDCl₃, 25 °C): δ 8.25-8.22 (m, 2H), 7.67-7.63 (m, 3H), 7.55-7.51 (m, 2H), 7.44-7.38 (m, 3H), 6.38 (s, 1H), 4.13 (q, *J* = 7.2 Hz, 2H), 1.15 (t, *J* = 7.1 Hz, 3H). **¹³C{¹H} NMR** (100 MHz, CDCl₃, 25 °C): δ 164.1, 163.8, 157.8, 133.7, 133.5, 131.0, 130.4, 129.1, 128.9, 128.7, 126.0, 106.9, 60.4, 14.1.

(S,Z)-2-(6-Chloro-2-oxo-4-(trifluoromethyl)-1,4-dihydro-2H-benzo[d][1,3]oxazin-4-yl)-1-cyclopropylvinyl Benzoate (7o)



White solid. (68.6 mg, 0.157 mmol, 39% yield). **IR** (ATR, ν /cm⁻¹): 3331 w, 1747 s, 1709 m, 1684 w, 1602 w, 1497 m, 1310 m, 1195 s, 1143 m, 1090 m, 951 w, 822 m, 707 s, 695 m, 682 m. **¹H NMR** (400 MHz, CDCl₃, 25 °C): δ 9.25 (brs, 1H), 7.67-7.65 (m, 2H), 7.52 (tt, *J* = 7.5, 1.1 Hz, 1H), 7.31 (t, *J* = 7.9 Hz, 2H), 7.21 (s, 1H), 6.96 (dd, *J* = 8.5, 2.3 Hz, 1H), 6.33 (d, *J* = 8.5 Hz, 1H), 5.72 (s, 1H), 1.87-1.81 (m, 1H), 0.95-0.85 (m, 2H), 0.85-0.76 (m, 2H). **¹³C{¹H} NMR** (100 MHz, CDCl₃, 25 °C): δ 162.7, 161.2, 149.4, 133.9, 133.3, 130.5, 129.6, 128.7, 128.3, 127.7, 127.4, 123.3 (q, *J* = 286 Hz), 115.7, 115.3, 107.8, 82.1 (q, *J* = 31.8 Hz), 14.9, 7.2, 6.9. **HRMS** (ESI⁺) *m/z* calc. for C₂₁H₁₅O₄NCIF₃Na 460.05339 found 460.05500. The crystal suitable for X-ray crystallography was grown by slow evaporation of DCM/Et₂O solution.

(Z)-Styryl Benzoate (**7p**)¹⁸ and 1-Phenylvinyl Benzoate (**7p'**)¹⁹



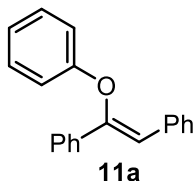
Orange oil. (84.5 mg, **7p/7p'/8** = 76/22/2, 92% yield as carboxylation products including 2% of **9**²⁰). ¹H NMR (400 MHz, CDCl₃, 25 °C): δ 8.19-8.15 (m, 2H), 7.71-7.61 (m, 3H), 7.58-7.49 (m, 3H), 7.45-7.38 (m, 2H), 7.29 (tt, *J* = 7.32, 1.4 Hz, 1H), 5.87 (d, *J* = 7.0 Hz, 1H) for (**7p**)-isomer; 8.23-8.19 (m, 2H), 7.71-7.61 (m, 1H), 7.58-7.49 (m, 4H), 7.45-7.30 (m, 3H), 5.60 (d, *J* = 2.2 Hz, 1H), 5.18 (d, *J* = 2.2 Hz, 1H) for (**7p'**)-isomer. ¹³C{¹H} NMR (100 MHz, CDCl₃, 25 °C): δ 163.4, 134.2, 133.7, 130.1, 129.2, 128.7, 128.5, 127.3, 124.9, 112.6 for (**7p**) isomer; 164.8, 153.1, 134.1, 133.6, 129.4, 128.95, 128.92, 128.6, 128.5, 125.9, 102.3 for (**7p'**) isomer.

General Procedure for the Gold-catalyzed Hydrocarboxylation of Alkynes

In a nitrogen-filled glove box, Au catalyst (5.0 mg, 0.008 mmol, 2 mol%) and NaBAR^F (7.1 mg, 0.008 mmol, 2 mol%) were placed in a screw vial containing a magnetic stirring bar. After addition of dry DCE (0.3 mL), the reaction mixture was stirred for 10 minutes. The resulting solution was filtrated through a glass-fiber pad packed into a pipet, and the filtrate was added to Zn(acac)₂ (2.1 mg, 0.008 mmol, 2 mol%) and alkyne (0.40 mmol, if boiling point of alkyne is higher than 220 °C) in a screw vial containing a magnetic stirring bar. After stirring 30 minutes, all volatile compounds were removed under reduced pressure. Alcohol (0.48 mmol), alkyne (0.40 mmol, if boiling point of alkyne is lower than 220 °C), and dry toluene (33 μL) was added to the mixture, and the reaction vial was sealed with screw-cap and taken out from the glove box. After stirring at 100 °C for 16 hours, the resulting mixture was quenched through a short pad of silica-gel. The crude mixture was purified by silica-gel column chromatography to give the desired compound.

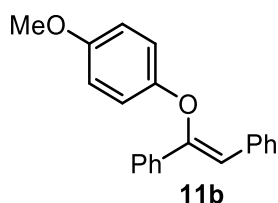
Characterization Data for Hydrophenoxylation Products

(Z)-(1-Phenoxyethene-1,2-diyl)dibenzene (11a)²¹



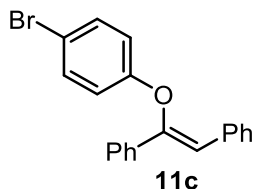
White solid. (105.5 mg, 0.387 mmol, 97% yield). ¹H NMR (400 MHz, CDCl₃, 25 °C): δ 7.65 (d, *J* = 8.0 Hz, 2H), 7.60 (d, *J* = 8.2 Hz, 2H), 7.34-7.27 (m, 5H), 7.25-7.19 (m, 3H), 7.04-7.02 (m, 2H), 6.95 (td, *J* = 7.3, 0.9 Hz, 1H), 6.67 (s, 1H). ¹³C{¹H} NMR (100 MHz, CDCl₃, 25 °C): δ 156.3, 149.6, 136.0, 134.7, 129.6, 128.9, 128.54, 128.50, 128.3, 127.3, 126.0, 122.0, 116.7, 116.3.

(Z)-(1-(4-Methoxyphenoxy)ethene-1,2-diyl)dibenzene (11b)²¹



White solid. (118.9 mg, 0.393 mmol, 98% yield). ¹H NMR (400 MHz, CDCl₃, 25 °C): δ 7.67 (d, *J* = 8.0 Hz, 2H), 7.60 (d, *J* = 8.2 Hz, 2H), 7.34-7.27 (m, 5H), 7.24-7.20 (m, 1H), 6.97-6.95 (m, 2H), 6.78-6.75 (m, 2H), 6.62 (s, 1H), 3.72 (s, 3H). ¹³C{¹H} NMR (100 MHz, CDCl₃, 25 °C): δ 154.6, 150.2, 150.1, 136.1, 134.9, 128.9, 128.5, 128.3, 127.3, 126.2, 117.1, 116.5, 114.7, 55.5.

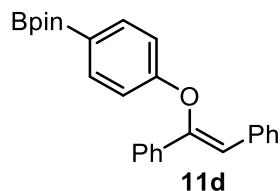
(Z)-(1-(4-Bromophenoxy)ethene-1,2-diyl)dibenzene (11c)



White solid. (136.0 mg, 0.387 mmol, 97% yield). mp: 107-109 °C. IR (ATR, ν/cm⁻¹): 3052 w, 1631 w, 1585 w, 1480 s, 1447 m, 1342 w, 1280 w, 1221 s, 1165 m, 1070 w, 1019 m, 1007 m, 916 w, 810 m, 761 s, 690 s, 561 w, 515 s, 498 m, 443 w. ¹H NMR (400 MHz, CDCl₃, 25 °C): δ 7.62-7.60 (m, 2H), 7.58-7.56 (m, 2H), 7.36-7.29 (m, 7H), 7.25-7.21 (m, 1H), 6.93-6.90 (m, 2H), 6.68 (s, 1H). ¹³C{¹H} NMR (100 MHz, CDCl₃, 25 °C): δ 155.5, 149.3, 135.5, 134.4,

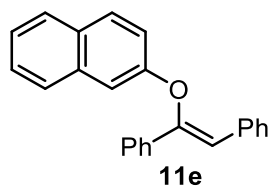
132.6, 128.9, 128.7, 128.6, 127.6, 125.9, 118.0, 116.9, 114.4. **HRMS** (EI) m/z calc. for $C_{20}H_{15}Br_1O_1$ 350.03063 found 350.03039.

(Z)-2-(4-((1,2-Diphenylvinyl)oxy)phenyl)-4,4,5,5-tetramethyl-1,3,2-dioxaborolane (11d)²²



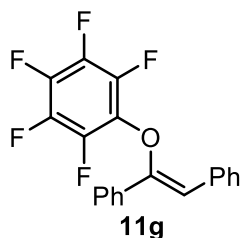
White solid. (90.5 mg, 0.227 mmol, 57% yield). **¹H NMR** (400 MHz, $CDCl_3$, 25 °C): δ 7.71-7.66 (m, 2H), 7.62-7.59 (m, 2H), 7.58-7.56 (m, 2H), 7.32-7.26 (m, 4H), 7.27-7.22 (m, 1H), 7.20 (tt, $J = 8.0, 1.4$ Hz, 1H), 7.03-6.99 (m, 2H), 6.67 (s, 1H), 1.29 (s, 12H). **¹³C{¹H} NMR** (100 MHz, $CDCl_3$, 25 °C): δ 159.0, 149.3, 136.6, 135.7, 134.5, 128.9, 128.6, 128.5, 128.4, 127.4, 125.9, 116.8, 115.7, 83.6, 24.8.

(Z)-2-((1,2-Diphenylvinyl)oxy)naphthalene (11e)²³



White solid. (122.5 mg, 0.380 mmol, 95% yield). **¹H NMR** (400 MHz, $CDCl_3$, 25 °C): δ 7.80-7.75 (m, 2H), 7.71-7.66 (m, 4H), 7.63 (d, $J = 8.2$ Hz, 1H), 7.41-7.38 (m, 2H), 7.35-7.26 (m, 7H), 7.25-7.20 (m, 1H), 6.77 (s, 1H). **¹³C{¹H} NMR** (100 MHz, $CDCl_3$, 25 °C): δ 154.2, 149.6, 135.8, 134.7, 134.3, 129.9, 129.6, 128.9, 128.6, 128.5, 128.4, 127.6, 127.4, 127.0, 126.4, 126.0, 124.1, 118.2, 116.9, 111.0.

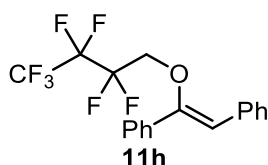
(Z)-2-(1-(Perfluorophenoxy)ethene-1,2-diyl)dibenzene (11g)



White solid. (140.1 mg, 0.387 mmol, 97% yield). **mp**: 86-89 °C. **IR** (ATR, ν /cm^{-1}): 3057 w, 3025 w, 1638 w, 1509 s, 1466 m, 1449 m, 1280 w, 1199 w, 1157 w, 1046 s, 1028 m, 994 s, 971 s, 864 w, 766 s, 692 s, 571 m, 515 m. **¹H NMR** (400 MHz, $CDCl_3$, 25 °C): δ 7.63 (d, $J =$

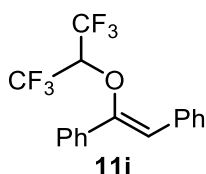
7.5 Hz, 2H), 7.50-7.47 (m, 2H), 7.37-7.32 (m, 5H), 7.26 (t, $J = 7.4$ Hz, 1H), 6.25 (s, 1H). $^{13}\text{C}\{^1\text{H}\}$ NMR (100 MHz, CDCl_3 , 25 °C): δ 152.1, 142.0-141.5 (m), 139.5-138.3 (m), 136.8-135.9 (m), 134.6, 134.3, 131.2-130.7 (m), 129.3, 129.0, 128.7, 128.5, 127.5, 126.6, 114.2. ^{19}F NMR (376 MHz, CDCl_3 , 25 °C): δ -156.2 (d, $J = 21.7$ Hz, 1H), -162.5 (dd, $J = 23.3, 20.1$ Hz, 1H), -162.8 (t, $J = 22.2$ Hz, 1H). HRMS (EI) m/z calc. for $\text{C}_{20}\text{H}_{11}\text{F}_{19}\text{O}_1$ 362.07301 found 362.07290.

(Z)-(1-(2,2,3,3,4,4,4-Heptafluorobutoxy)ethene-1,2-diyl)dibenzene (11h)



Colourless oil (142.6 mg, 0.377 mmol, 94%). IR (ATR, ν/cm^{-1}): 3063 w, 3025 w, 1644 w, 1600 w, 1494 w, 1448 m, 1332 w, 1228 s, 1183 m, 1127 m, 1017 m, 959 w, 915 m, 768 m, 696 m. ^1H NMR (400 MHz, CDCl_3 , 25 °C): δ 7.74 (d, $J = 8.0$ Hz, 2H), 7.62-7.60 (m, 2H), 7.49-7.45 (m, 2H), 7.44-7.40 (m, 3H), 7.32-7.28 (m, 1H), 6.25 (s, 1H), 4.24-4.15 (m, 2H). $^{13}\text{C}\{^1\text{H}\}$ NMR (100 MHz, CDCl_3 , 25 °C): δ 153.3, 134.9, 134.7, 129.0, 128.8, 128.5, 127.3, 126.6, 114.6, 65.8 (t, $J = 25.0$ Hz). $^{13}\text{C}\{^1\text{H}\}$ NMR signals of fluorinated carbon chain were detected at 122-104 ppm as multiplets. ^{19}F NMR (376 MHz, CDCl_3 , 25 °C): δ -80.7 (t, $J = 9.2$ Hz), -120.4 - -120.7 (m), -127.1 - -127.2 (m). HRMS (EI) m/z calc. for $\text{C}_{18}\text{H}_{13}\text{F}_7\text{O}$ 378.08546 found 378.08548.

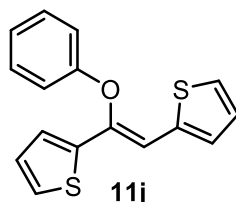
(Z)-(1-((1,1,1,3,3,3-Hexafluoropropan-2-yl)oxy)ethene-1,2-diyl)dibenzene (11i)



White solid (127.4 mg, 0.368 mmol, 92%). mp: 52-53 °C. IR (ATR, ν/cm^{-1}): 3060 w, 3035 w, 1643 w, 1496 w, 1449 w, 1375 m, 1360 w, 1272 m, 1225 m, 1186 s, 1105 s, 1013 m, 920 w, 901 m, 868 m, 768 s, 748 m, 735 s, 652 m. ^1H NMR (400 MHz, CDCl_3 , 25 °C): δ 7.70 (d, $J = 8.2$ Hz, 2H), 7.54-7.45 (m, 5H), 7.39-7.34 (m, 2H), 7.29-7.25 (m, 1H), 5.98 (s, 1H), 4.64-4.58 (m, 1H). $^{13}\text{C}\{^1\text{H}\}$ NMR (100 MHz, CDCl_3 , 25 °C): δ 151.7, 134.2, 133.3, 131.6, 129.6, 129.1, 128.4, 128.3, 128.0, 127.4, 121.1 (q, $J = 286.1$ Hz), 115.6, 72.5 (sept, $J = 32.7$ Hz). ^{19}F NMR

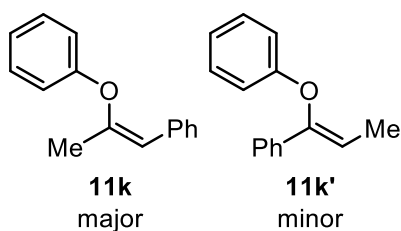
(376 MHz, CDCl₃, 25 °C): δ -72.6 (d, J = 6.0 Hz). HRMS (EI) m/z calc. for C₁₇H₁₂F₆O 346.07923 found 346.07873.

(Z)-2,2'-(1-Phenoxyethene-1,2-diyl)dithiophene (11j)²³



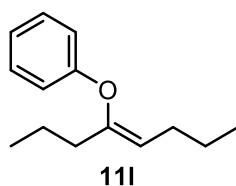
Light green solid. (111.8 mg, 0.393 mmol, 98% yield). ¹H NMR (400 MHz, CDCl₃, 25 °C): δ 7.30-7.26 (m, 2H), 7.22 (d, J = 5.3 Hz, 1H), 7.19 (dd, J = 5.0, 1.1 Hz, 1H), 7.16 (dt, J = 3.7, 0.5 Hz, 1H), 7.09-7.07 (m, 3H), 7.04-6.97 (m, 3H), 6.93 (dd, J = 5.0, 3.7 Hz, 1H). ¹³C{¹H} NMR (100 MHz, CDCl₃, 25 °C): δ 155.9, 142.6, 139.0, 136.9, 129.6, 127.7, 127.6, 126.9, 126.5, 125.4, 125.3, 122.4, 115.8, 110.5.

(Z)-(2-Phenoxyprop-1-en-1-yl)benzene (11k) and (Z)-(1-phenoxyprop-1-en-1-yl)benzene (11k')²¹



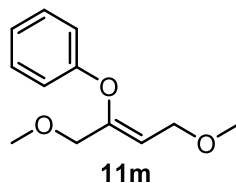
Colourless oil. (82.4 mg, 0.392 mmol, 98% yield). ¹H NMR (400 MHz, CDCl₃, 25 °C): δ 7.57 (d, J = 7.8 Hz, 2H, major), 7.53-7.51 (m, 2H, minor), 7.38-7.32 (m, 2H, major and minor), 7.30-7.24 (m, 2H, major and minor), 7.18 (tt, J = 7.3, 1.1 Hz, 1H, major), 7.12-7.04 (m, 3H, major), 7.01-6.94 (m, 3H, minor), 5.97 (q, J = 6.9 Hz, 1H, minor), 5.91 (s, 1H, major), 2.00 (s, 3H, major), 1.79 (d, J = 6.9 Hz, 3H, minor). ¹³C{¹H} NMR (100 MHz, CDCl₃, 25 °C): δ 155.3, 149.2, 135.2, 129.6, 128.3, 128.1, 126.4, 122.6, 117.6, 114.8, 19.6 for major isomer; 157.3, 149.6, 135.5, 129.5, 128.4, 127.8, 125.1, 121.3, 115.3, 112.4, 11.4. for minor isomer.

(Z)-(Oct-4-en-4-yloxy)benzene (11l)²¹



Colorless oil. (76.2 mg, 0.373 mmol, 93% yield). $^1\text{H NMR}$ (400 MHz, CDCl_3 , 25 °C): δ 7.31-7.27 (m, 2H), 7.00-6.94 (m, 3H), 5.04 (t, $J = 7.2$ Hz, 1H), 2.12 (t, $J = 7.4$ Hz, 2H), 2.02 (q, $J = 7.3$ Hz, 2H), 1.54-1.45 (m, 2H), 1.41-1.34 (m, 2H), 0.96-0.88 (m, 6H). $^{13}\text{C}\{^1\text{H}\}$ NMR (100 MHz, CDCl_3 , 25 °C): δ 156.8, 150.4, 129.4, 121.2, 116.1, 115.9, 34.3, 27.2, 22.7, 20.1, 13.8, 13.6.

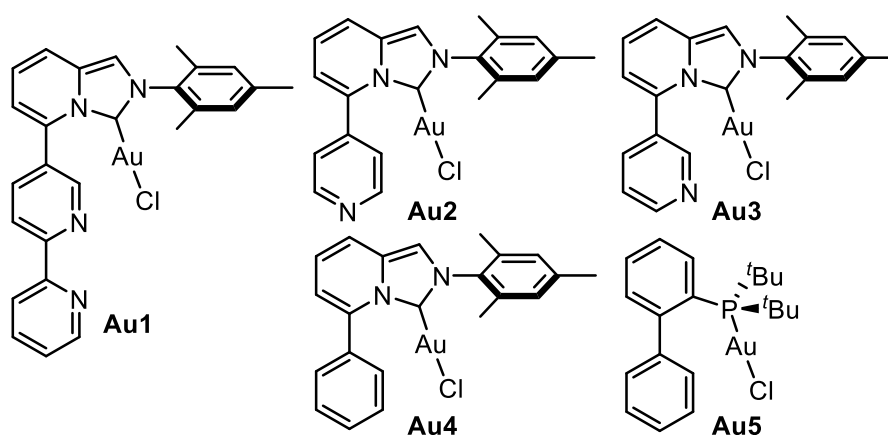
(Z)-((1,4-Dimethoxybut-2-en-2-yl)oxy)benzene (11m)²³



11m was isolated by column chromatography with basic alumina (EtOAc/hexane = 8/92). Colorless oil. (76.0 mg, 0.365 mmol, 91% yield). $^1\text{H NMR}$ (400 MHz, CDCl_3 , 25 °C): δ 7.31-7.27 (m, 2H), 7.03 (tt, $J = 7.3, 1.1$ Hz, 1H), 6.99-6.96 (m, 2H), 5.51 (tt, $J = 6.6, 0.8$ Hz, 1H), 4.02 (d, $J = 6.6$ Hz, 2H), 3.91 (d, $J = 0.9$ Hz, 2H), 3.35 (s, 3H), 3.31 (s, 3H). $^{13}\text{C}\{^1\text{H}\}$ NMR (100 MHz, CDCl_3 , 25 °C): δ 156.2, 149.7, 129.6, 122.4, 116.4, 114.8, 70.5, 66.2, 58.3, 58.1.

Screening of Reaction Conditions

Scheme S1. Structures of gold complexes.



Screening of Reaction Conditions for Nucleophilic Addition of Carboxylic Acids

General Procedure for Screening of Reaction Conditions: In a nitrogen-filled glove box, Au catalyst (2 mol%) and anion source (2 mol%) were placed in a screw vial containing a magnetic stirring bar. After addition of dry DCE (0.1 mL), the reaction mixture was stirred for 10 minutes. The resulting solution was filtrated through a glass-fiber pad packed into a pipet, and the filtrate

was added to metal salt (2 mol%) and diphenylacetylene (17.8 mg, 0.10 mmol) in a screw vial containing a magnetic stirring bar. After stirring 30 minutes, benzoic acid (14.7 mg, 0.12 mmol, 1.2 equiv) was added to the mixture, and the reaction vial was sealed with screw-cap and taken out from the glove box. After stirring at 80 °C for 16 hours, the resulting mixture was quenched through a short pad of silica-gel. Yield was determined by ¹H NMR analysis using 1,3,5-trimethoxybenzene as an internal standard.

NMR Experiments

General Procedure for Titration with ^1H NMR Analysis

Gold complex (0.01 mmol) was dissolved in THF- d_8 (0.63 mL), and the sample was monitored on ^1H NMR analysis at 25 °C. After addition of $\text{Zn}(\text{acac})_2$ as a solid, the gold complex solution was further recorded ^1H NMR analysis. Addition of $\text{Zn}(\text{acac})_2$ was repeated to add the 10 equivalents of $\text{Zn}(\text{acac})_2$ in total. The result was shown in Figure S2-4. All the peaks were assigned from the reference point of residual solvent peak for THF- d_8 (1.73 ppm).

THF- d_8 was selected for the titration in terms of solubility of $\text{Zn}(\text{acac})_2$. Titration with ZnCl_2 and $\text{Zn}(\text{OTf})_2$ was failed, because insoluble materials were formed from THF solution. When over 10 equivalents of $\text{Zn}(\text{acac})_2$ were added, $\text{Zn}(\text{acac})_2$ was partially not soluble. Hence, I performed the titration using 0-10 equivalent of $\text{Zn}(\text{acac})_2$ for monitoring the homogeneous mixture. According to the titrations, $\text{Zn}(\text{acac})_2$ interacted with pyridine moiety of gold complexes **4**. The equilibrium between gold complexes **4** and bimetallic complexes was much faster than NMR time-scale, indicating that coordination abilities of pyridine moieties are not so high in the THF solution. Such poor coordination abilities might be arisen from coordination of THF molecules toward $\text{Zn}(\text{acac})_2$. However, the actual catalytic reactions were conducted in non-coordinative solvents such as DCE and toluene, and binding constants in these solvents might be much higher than that in THF.

¹H NMR Charts for Titration

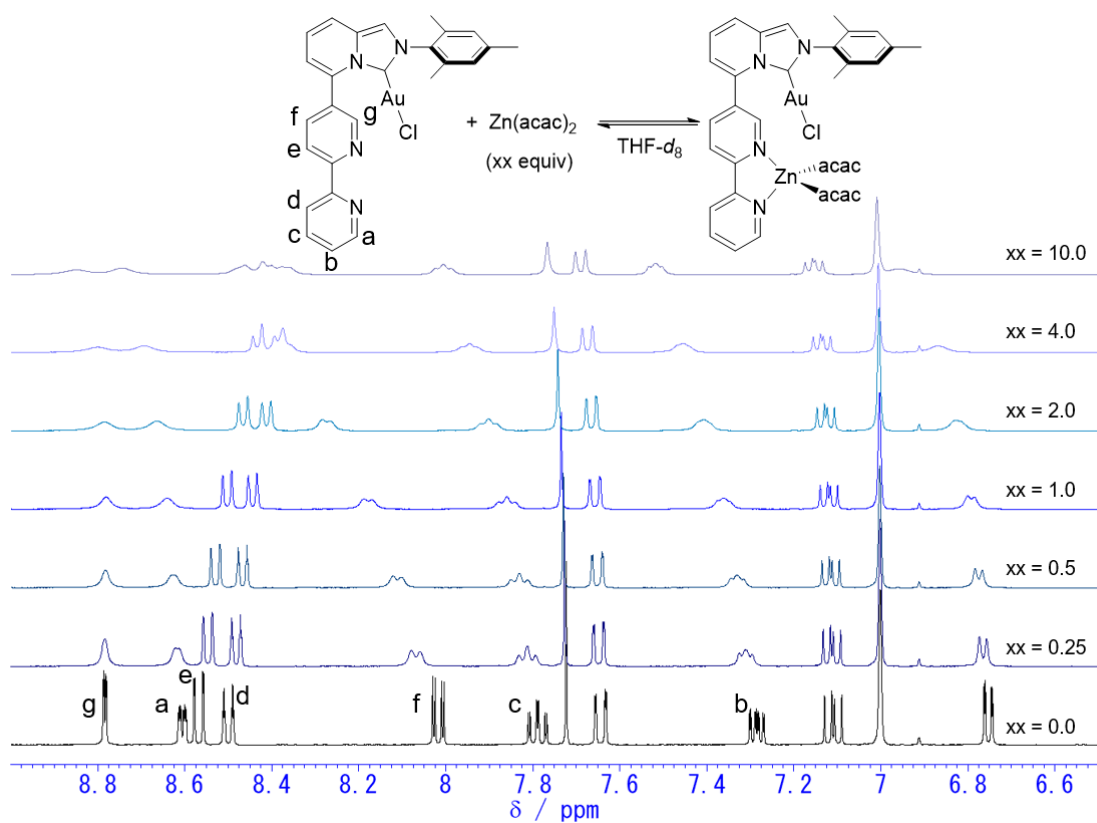


Figure S2. ¹H NMR titration with Au1 and Zn(acac)₂.

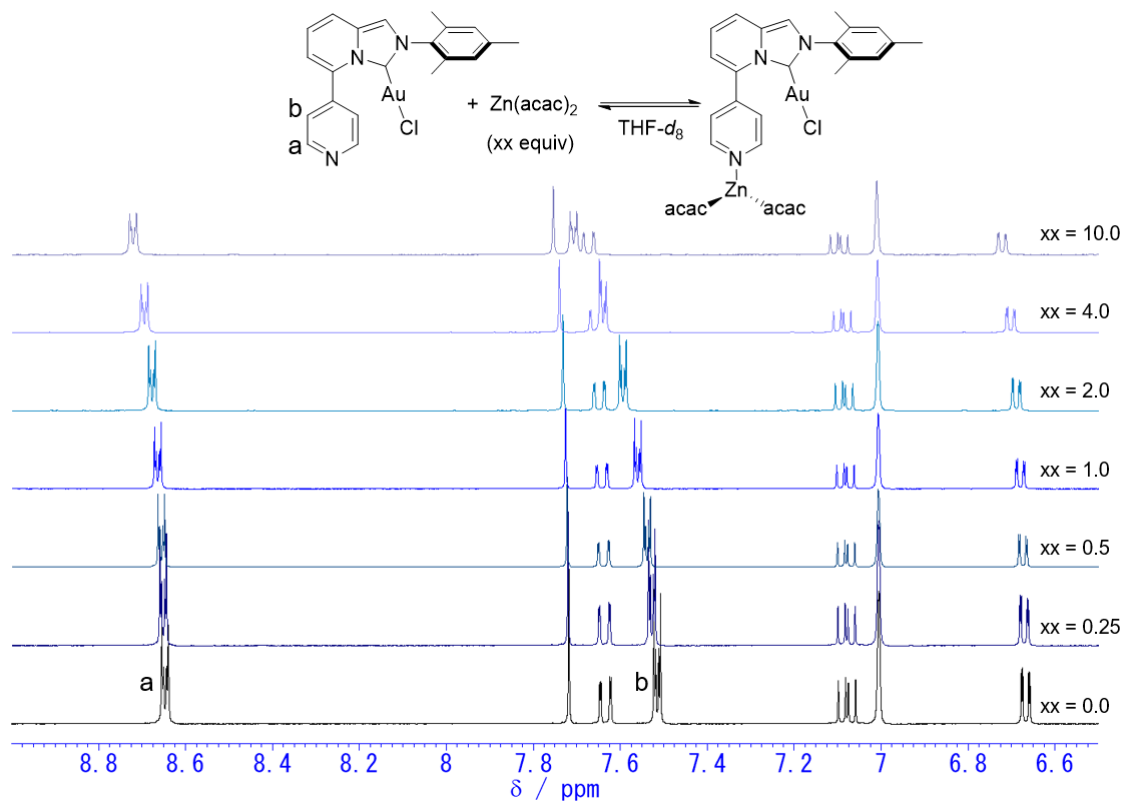


Figure S3. ¹H NMR titration with Au2 and Zn(acac)₂.

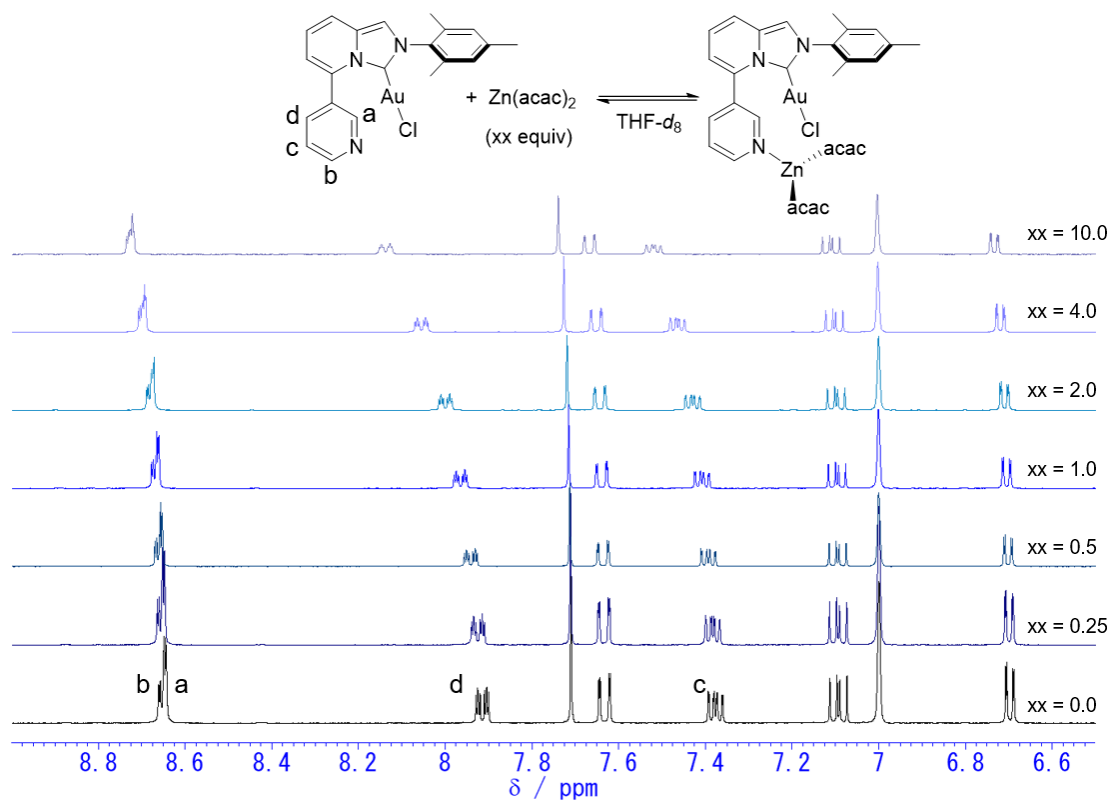


Figure S4. ^1H NMR titration with Au^3 and $\text{Zn}(\text{acac})_2$.

XRD Analysis

General Procedure

A suitable crystal was mounted with liquid paraffin on a MiTeGen MicroMounts and transferred to the goniometer in a nitrogen stream at 123(2) K. Measurement was made on a RIGAKU XtaLAB Synergy-DW system with 1.2 kW PhotonJet-DW microfocus rotating anode using graphite monochromated Mo-K_a radiation ($\lambda = 0.71073 \text{ \AA}$) or Cu-K_a radiation ($\lambda = 1.54184 \text{ \AA}$) and HyPix-6000HE detector. Cell parameters were determined and refined, and raw frame data were integrated using CrysAlis^{Pro} (Agilent Technologies, 2010). The structures were solved by direct methods with SHELXT²⁴ and refined by full-matrix least-squares techniques against F^2 with SHELXL-2018/3²⁵ by using Olex2 software package.²⁶ The non-hydrogen atoms were anisotropically refined, and hydrogen atoms were placed using AFIX instructions. Crystal data and structure refinement parameters are in Table S1. The ORTEP-3 program was used to draw the molecule structures.²⁷

ORTEP Drawing

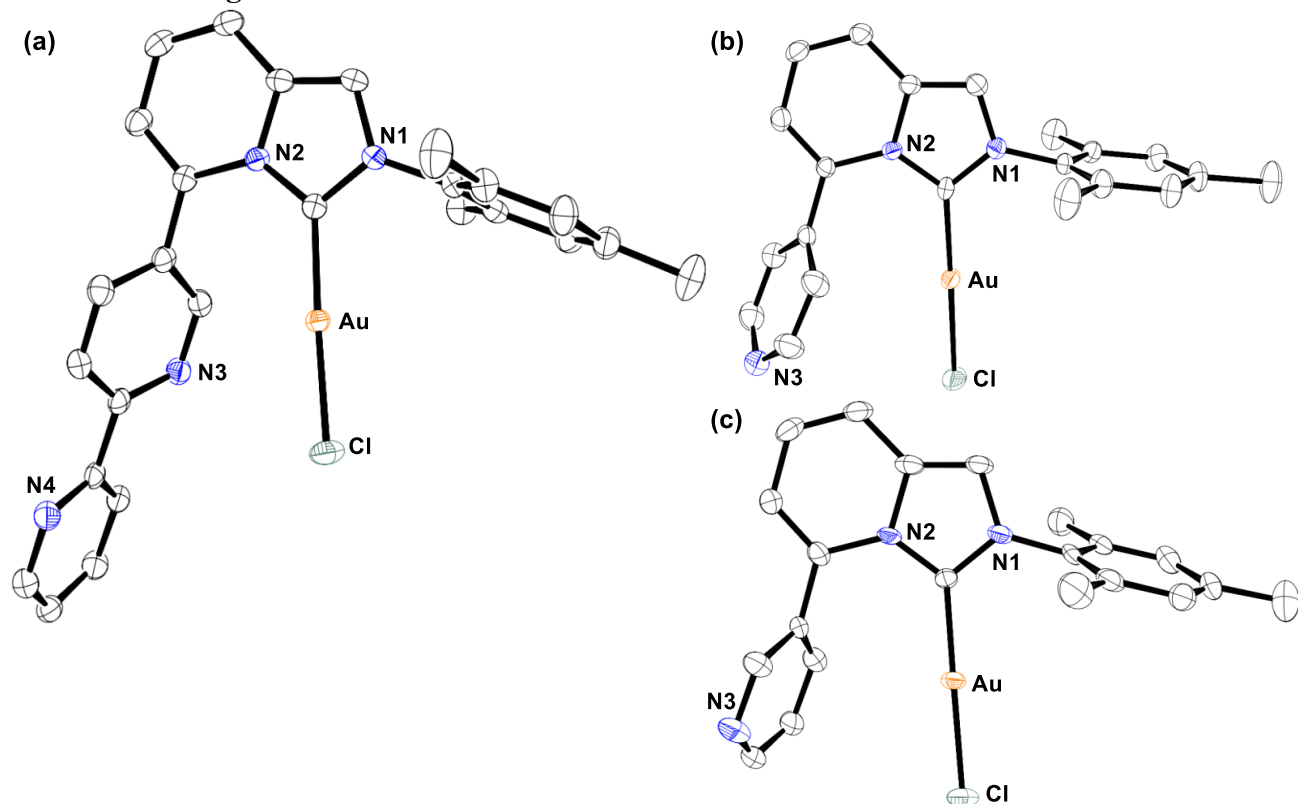


Figure S5. ORTEP drawing of (a) **4a**, (b) **4b**, and (c) **4c** showing 50% probability thermal ellipsoids. All hydrogen atoms and a solvent molecule for **4b** were omitted for clarity. Only one molecule structure of **4b** is described for clarity.

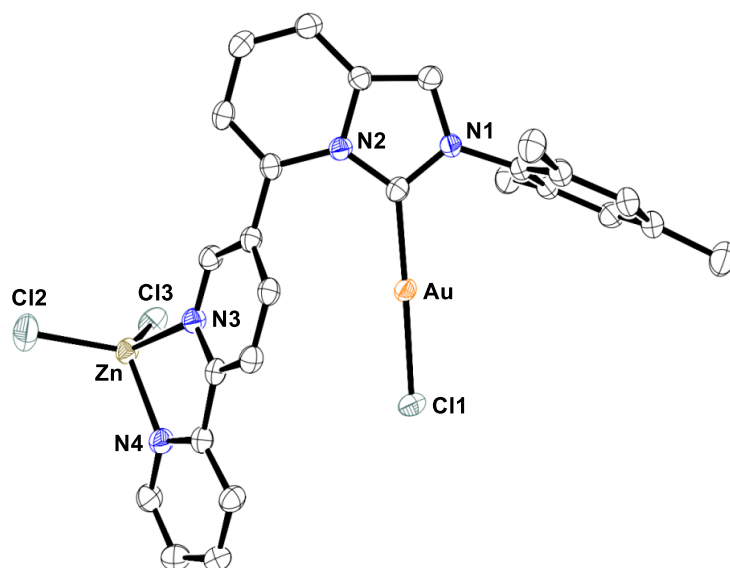


Figure S6. ORTEP drawing of **4a-ZnCl₂** showing 50% probability thermal ellipsoids. All hydrogen atoms and a solvent molecule were omitted for clarity.

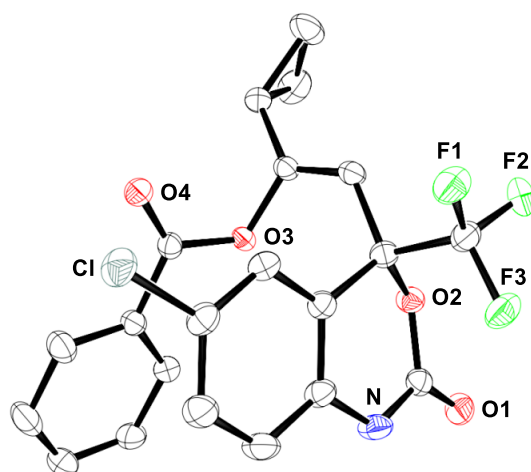


Figure S7. ORTEP drawing of **7o** showing 50% probability thermal ellipsoids. All hydrogen atoms were omitted for clarity.

Table S1. Crystal Data and Structure Refinement Parameters.

	4a	4b	4c	4a-ZnCl₂	8o
empirical formula	C ₂₆ H ₂₂ AuClN ₄	C ₁₂₇ H ₁₁₆ Au ₆ Cl ₈ N ₁₈	C ₂₁ H ₁₉ AuClN ₃	C ₂₆ H ₂₃ AuCl ₃ N ₄ O _{0.5} Zn	C ₂₁ H ₁₅ ClF ₃ NO ₄
CCDC number	2162186	2162187	2162188	2162189	2162190
formula weight	622.89	3359.77	545.81	768.17	437.79
crystal system	monoclinic	triclinic	triclinic	monoclinic	orthorhombic
space group	<i>C</i> 2/c (#15)	<i>P</i> -1 (#2)	<i>P</i> -1 (#2)	<i>P</i> 2 ₁ /n (#14)	<i>P</i> 2 ₁ 2 ₁ 2 (#18)
<i>a</i> , Å	39.666(3)	14.1737(4)	9.1748(5)	15.2947(3)	15.01990(10)
<i>b</i> , Å	8.0213(2)	14.7408(4)	10.3022(3)	6.74350(10)	13.59580(10)
<i>c</i> , Å	21.0820(17)	16.0059(3)	12.3271(7)	25.6181(4)	9.53730(10)
α , deg.	-	96.269(2)	81.020(4)	-	-
β , deg.	137.626(15)	102.010(2)	70.069(5)	98.874(2)	-
γ , deg.	-	107.747(2)	88.318(4)	-	-
<i>V</i> , Å ³	4520.8(10)	3061.33(14)	1081.59(10)	2610.62(8)	1947.59(3)
<i>Z</i>	8	1	2	4	4
<i>D</i> _{calcd} , g/cm ⁻³	1.830	1.822	1.676	1.954	1.493
radiation, mm ⁻¹	Mo-K α : 0.71073	Mo-K α : 0.71073	Mo-K α : 0.71073	Mo-K α : 0.71073	Cu-K α : 1.54184
<i>T</i> , K	123(2)	123(2)	123(2)	123(2)	123(2)
crystal size, mm	0.12 x 0.12 x 0.03	0.23 x 0.20 x 0.10	0.20 x 0.16 x 0.05	0.08 x 0.06 x 0.03	0.12 x 0.12 x 0.12
range for data collection (deg.)	5.466 to 58.738	4.236 to 58.68	4.004 to 58.77	5.154 to 58.756	8.772 to 152.38
no. of reflections measured	43008	60308	21519	27064	28474
unique data (<i>R</i> _{int})	5578 (0.0320)	14093 (0.0752)	5080 (0.0734)	5998 (0.0367)	4036 (0.0467)
data/restraints/parameters	5578 / 0 / 292	14093 / 0 / 739	5080 / 0 / 238	5998 / 0 / 331	4036 / 0 / 271
<i>R</i> 1 (<i>I</i> > 2.0 σ (<i>I</i>))	0.0197	0.0335	0.0292	0.0282	0.0265
<i>wR</i> 2 (<i>I</i> > 2.0 σ (<i>I</i>))	0.0398	0.0783	0.0649	0.0656	0.0686
<i>R</i> 1 (all data)	0.0249	0.0473	0.0348	0.0364	0.0273
<i>wR</i> 2 (all data)	0.0409	0.0817	0.0665	0.0693	0.0692
GOF on <i>F</i> ²	1.069	1.030	1.009	1.043	1.081
Flack parameter	-	-	-	-	-0.014(6)

a) $R1 = (\sum ||F_o| - |F_c||) / (\sum |F_o|)$ b) $wR2 = \{[\sum w(F_o^2 - F_c^2)^2] / [\sum w(F_o^4)]\}^{1/2}$

DFT Calculations

General Procedure

All geometry optimizations and single-point energy calculations were performed by Gaussian 16 package.¹⁴ The geometry optimizations of all structures were conducted at the M06 functional in conjunction with the SDD (for Au, Zn) and 6-31G(d) (for others) basis set. Frequency analyses were performed at the same level of theory for geometry optimizations, in which the thermal free energy corrections were provided. All the transition states have the single imaginary frequency, and all the optimized structures as minima have no imaginary frequency. The transition states were traced with intrinsic reaction coordinate (IRC) analyses by using Global Reaction Route Mapping (GRRM) program²⁸ to confirm the connection of the reaction pathway. Further single-point energy calculations were performed at the M06 functional in conjunction with the SDD (for Au, Zn) and 6-311+G(d,p) (for others) basis set with the solvation model (SMD: dichloroethane) to evaluate solution phase electronic energies. The solution phase Gibbs free energies (G_{sol}) at 298.15 K (25 °C) were obtained from $G_{\text{sol}} = E + G_{\text{corr}}$, wherein the solvation electronic energies (E) were given from single-point energy calculations at the M06/SDD,6-311+G(d,p)/SMD level and gas-phase thermal free energy corrections (G_{corr}) were given from frequency analyses at the M06/SDD,6-31G(d) level. For the purpose of discussion, relative Gibbs free energies (ΔG_{sol}) were calculated from $\Delta G_{\text{sol}} = \Sigma G_{\text{sol}}$ for products – ΣG_{sol} for reactants. 3D models of optimized structures were described by CYLview20.²⁹

Summary of Energies

Structure Name	solvation electronic energies [Hartree]	thermal free energy corrections [Hartree]	solution phase Gibbs free energies [Hartree]
Int-0	-1897.272255	0.533200	-1896.739055
Int-1	-2964.729909	0.726540	-2964.003369
TS₁₋₂	-2964.693914	0.729865	-2963.964049
Int-2	-2964.706453	0.728478	-2963.977975
Int-3	-3385.424418	0.834783	-3384.589635
TS₃₋₄	-3385.393848	0.838509	-3384.555339
Int-4	-3385.419439	0.841548	-3384.577891
Int-5	-3385.418770	0.836712	-3384.582058
TS₅₋₆	-3385.395153	0.832457	-3384.562696
Int-6	-3385.440278	0.842589	-3384.597689
6a·dimer	-841.372264	0.187654	-841.18461
Zn(OBz)₂	-1067.396753	0.161822	-1067.234931

References

- (1) Yamamoto, Y.; Gridnev, I. D.; Patil, N. T.; Jin, T. Alkyne activation with Brønsted acids, iodine, or gold complexes, and its fate leading to synthetic application. *Chem. Commun.* **2009**, 5075-5087.
- (2) Recent reviews, (a) Praveen, C. Carbophilic activation of π -systems via gold coordination: Towards regioselective access of intermolecular addition products. *Coord. Chem. Rev.* **2019**, 392, 1-34. (b) Cadierno, V. Metal-Catalyzed Synthesis and Transformations of β -Haloenol Esters. *Catalysts* **2020**, 10, 399. (c) Leung, C. H.; Baron, M.; Biffis, A. Gold-Catalyzed Intermolecular Alkyne Hydrofunctionalizations—Mechanistic Insights. *Catalysts* **2020**, 10, 1210. (d) González-Belman, O. F.; Brotons-Rufes, A.; Tomasini, M.; Falivene, L.; Caporaso, L.; Jiménez-Halla, J. O. C.; Poater, A. Towards Dual-Metal Catalyzed Hydroalkoxylation of Alkynes. *Catalysts* **2021**, 11, 704.
- (3) Examples for gold-catalyzed nucleophilic addition of carboxylic acids to non-activated alkynes, (a) Chary, B. C.; Kim, S. Gold(I)-Catalyzed Addition of Carboxylic Acids to Alkynes. *J. Org. Chem.* **2010**, 75, 7928-7931. (b) Wang, Y.; Wang, Z.; Li, Y.; Wu, G.; Cao, Z.; Zhang, L. A general ligand design for gold catalysis allowing ligand-directed anti-nucleophilic attack of alkynes. *Nat. Commun.* **2014**, 5, 3470. (c) Dupuy, S.; Gasperini, D.; Nolan, S. P. Highly Efficient Gold(I)-Catalyzed Regio- and Stereoselective Hydrocarboxylation of Internal Alkynes. *ACS Catal.* **2015**, 5, 6918-6921. (d) González-Liste, P. J.; García-Garrido, S. E.; Cadierno, V. Gold(I)-catalyzed addition of carboxylic acids to internal alkynes in aqueous medium. *Org. Biomol. Chem.* **2017**, 15, 1670-1679. (e) León, F.; González-Liste, P. J.; García-Garrido, S. E.; Arribas, I.; Rubio, M.; Cadierno, V.; Pizzano, A. Broad Scope Synthesis of Ester Precursors of Nonfunctionalized Chiral Alcohols Based on the Asymmetric Hydrogenation of α, β -Dialkyl-, α, β -Diaryl-, and α -Alkyl- β -aryl-vinyl Esters. *J. Org. Chem.* **2017**, 82, 5852-5867. (f) Francos, J.; Moreno-Narváez, M. E.; Cadierno, V.; Sierra, D.; Ariz, K.; Gómez, J. Gold(I) Complexes with Ferrocenylphosphino Sulfonate Ligands: Synthesis and Application in the Catalytic Addition of Carboxylic Acids to Internal Alkynes in Water. *Catalysts* **2019**, 9, 955. (g) Darmandeh, H.; Löffler, J.; Tzouras, N. V.; Dereli, B.; Scherpf, T.; Feichtner, K.-S.; Broeck, S. V.; Van Hecke, K.; Saab, M.; Cazin, C. S. J.; Cavallo, L.; Nolan, S. P.; Gessner, V. H. Au \cdots H-C Hydrogen Bonds as Design Principle in Gold(I) Catalysis. *Angew. Chem., Int. Ed.* **2021**, 60, 21014-21024.

- (4) Examples for gold-catalyzed nucleophilic addition of phenols to non-activated alkynes, (a) Kuram, M. R.; Bhanuchandra, M.; Sahoo, A. Gold-Catalyzed Intermolecular Hydrophenoxylation of Unactivated Internal Alkynes. *J. Org. Chem.* **2010**, *75*, 2247-2258. (b) Oonishi, Y.; Gómez-Suárez, A.; Martin, A. R.; Nolan, S. P. Hydrophenoxylation of Alkynes by Cooperative Gold Catalysis. *Angew. Chem., Int. Ed.* **2013**, *52*, 9767-9771. (c) Richard, M. E.; Fraccica, D. V.; Garcia, K. J.; Miller, E. J.; Ciccarelli, R. M.; Holahan, E. C.; Resh, V. L.; Shah, A.; Findeis, P. M.; Stockland, R. A. Acid, silver, and solvent-free gold-catalyzed hydrophenoxylation of internal alkynes. *Beilstein J. Org. Chem.* **2013**, *9*, 2002-2008. (d) Gómez-Suárez, A.; Oonishi, Y.; Martin, A. R.; Nolan, S. P. Scope and limitations of the dual-gold-catalysed hydrophenoxylation of alkynes. *Beilstein J. Org. Chem.* **2016**, *12*, 172-178. (e) Gómez-Suárez, A.; Oonishi, Y.; Martin, A. R.; Vummaleti, S. V. C.; Nelson, D. J.; Cordes, D. B.; Slawin, A. M. Z.; Cavallo, L.; Nolan, S. P.; Poater, A. On the Mechanism of the Digold(I)-Hydroxide-Catalysed Hydrophenoxylation of Alkynes. *Chem. Eur. J.* **2016**, *22*, 1125-1132. (f) Lazreg, F.; Guidone, S.; Gómez-Herrera, A.; Nahra, F.; Cazin, C. S. J. Hydrophenoxylation of internal alkynes catalysed with a heterobimetallic Cu-NHC/Au-NHC system. *Dalton. Trans.* **2017**, *46*, 2439-2444. (g) González-Belman, O. F.; Jiménez-Halla, J. O. C.; Nahra, F.; Cazin, C. S. J.; Poater, A. The role of the metal in the dual-metal catalysed hydrophenoxylation of diphenylacetylene. *Catal. Sci. Technol.* **2018**, *8*, 3638-3648. (h) Ramos, M.; Poater, J.; Villegas-Escobar, N.; Gimferrer, M.; Toro-Labbé, A.; Cavallo, L.; Poater, A. Phenoxylation of Alkynes through Mono- and Dual Activation Using Group 11 (Cu, Ag, Au) Catalysts. *Eur. J. Inorg. Chem.* **2020**, 1123-1134.
- (5) (a) Van Den Beuken, E. K.; Feringa, B. L. Bimetallic catalysis by late transition metal complexes. *Tetrahedron* **1998**, *54*, 12985-13011. (b) Park, J.; Hong, S. Cooperative bimetallic catalysis in asymmetric transformations. *Chem. Soc. Rev.* **2012**, *41*, 6931-6943. (c) Matsunaga, S.; Shibasaki, M. Recent advances in cooperative bimetallic asymmetric catalysis: dinuclear Schiff base complexes. *Chem. Commun.* **2014**, *50*, 1044-1057. (d) Xiong, N.; Zhang, G.; Sun, X.; Zeng, R. Metal-Metal Cooperation in Dinucleating Complexes Involving Late Transition Metals Directed towards Organic Catalysis. *Chin. J. Chem.* **2020**, *38*, 185-201.
- (6) Lewis acid-organic base cooperative catalysis with imidazo[1,5-*a*]pyridin-3-ylidene ligand has been developed for intramolecular nucleophilic addition of alkyne-tethered carboxylic acids: Rawat, V. K.; Higashida, K.; Sawamura, M. Use of Imidazo[1,5-

- a*]pyridin-3-ylidene as a Platform for Metal-Imidazole Cooperative Catalysis: Silver-Catalyzed Cyclization of Alkyne-Tethered Carboxylic Acids. *Adv. Synth. Catal.* **2021**, *363*, 1631-1637.
- (7) Iglesias-Sigüenza, J.; Izquierdo, C.; Díez, E.; Fernández, R.; Lassaletta, J. M. Chirality and catalysis with aromatic N-fused heterobicyclic carbenes. *Dalton. Trans.* **2016**, *45*, 10113-10117.
- (8) Examples of heterobimetallic complexes constructed by the combination of NHC and *N*-heteroaromatic ligands, (a) Rubio, M.; Jellema, E.; Siegler, M. A.; Spek, A. L.; Reek, J. N. H.; de Bruin, B. Supramolecular NHC ligands: on the influence of Zn^{II}-templates on the activity of Rh^I(cod) complexes in ‘carbene polymerization’. *Dalton. Trans.* **2009**, 8970-8976. (b) Strasser, C. E.; Catalano, V. J. “On–Off” Au(I)···Cu(I) Interactions in a Au(NHC)₂ Luminescent Vapochromic Sensor. *J. Am. Chem. Soc.* **2010**, *132*, 10009-10011. (c) Mondal, M.; Ranjeesh, T. K.; Gupta, S. K.; Choudhury, J. Labile coordination approach for the modulation of the electronic properties of ruthenium(II) and iridium(III) complexes within an “N-heterocyclic carbene (NHC)–pyridyl” dynamic platform. *Dalton. Trans.* **2014**, *43*, 9356-9362. (d) Bertrand, B.; Citta, A.; Franken, I. L.; Picquet, M.; Folda, A.; Scalcon, V.; Rigobello, M. P.; Gendre, P. L.; Casini, A.; Bodio, E. Gold(I) NHC-based homo- and heterobimetallic complexes: synthesis, characterization and evaluation as potential anticancer agents. *J. Biol. Inorg. Chem.* **2015**, *20*, 1005-1020. (e) Boselli, L.; Carraz, M.; Mazères, S.; Paloque, L.; González, G.; Benoit-Vical, F.; Valentin, A.; Hemmert, C.; Gornitzka, H. Synthesis, Structures, and Biological Studies of Heterobimetallic Au(I)–Ru(II) Complexes Involving N-Heterocyclic Carbene-Based Multidentate Ligands. *Organometallics* **2015**, *34*, 1046-1055. (f) Gatus, M. R. D.; Bhadbhade, M.; Messerle, B. A. Highly versatile heteroditopic ligand scaffolds for accommodating group 8, 9 & 11 heterobimetallic complexes. *Dalton. Trans.* **2017**, *46*, 14406-14419. (g) Kaub, C.; Lebedkin, S.; Li, A.; Kruppa, S. V.; Strebert, P. H.; Kappes, M. M.; Riehn, C.; Roesky, P. W. Bimetallic d¹⁰-Metal Complexes of a Bipyridine Substituted N-Heterocyclic Carbene. *Chem. Eur. J.* **2018**, *24*, 6094-6104. (h) Teng, Q.; Huynh, H. V. (Hetero)bimetallic and Tetranuclear Complexes of Pincer-Bridged N-Heterocyclic Carbene Ligands. *Organometallics* **2018**, *37*, 4119-4127. (i) Simler, T.; Möbius, K.; Müller, K.; Feuerstein, T. J.; Gamer, M. T.; Lebedkin, S.; Kappes, M. M.; Roesky, P. W. Mono- and Dinuclear Coinage Metal Complexes Supported by an Imino-

- Pyridine-NHC Ligand: Structural and Photophysical Studies. *Organometallics* **2019**, *38*, 3649-3661.
- (9) Using the reported procedure after modification, Carroll, J.; Woolard, H. G.; Mroz, R.; Nason, C. A.; Huo, S. Regiospecific Acylation of Cycloplatinated Complexes: Scope, Limitations, and Mechanistic Implications. *Organometallics* **2016**, *35*, 1313-1322.
- (10) Using the reported procedure after modification, Callado, A.; Gómez-Suárez, A.; Martín, A. R.; Slawin, A. M. Z.; Nolan, S. P. Straightforward synthesis of [Au(NHC)X] (NHC = *N*-heterocyclic carbene, X = Cl, Br, I) complexes. *Chem. Commun.* **2013**, *49*, 5541-5543.
- (11) General procedure of nucleophilic addition of carboxylic acids to alkynes: In a nitrogen-filled glove box, **4a** (5.0 mg, 0.008 mmol, 2 mol%) and NaBAR^F (7.1 mg, 0.008 mmol, 2 mol%) were placed in a screw vial containing a magnetic stirring bar. After addition of dry DCE (0.3 mL), the reaction mixture was stirred for 10 minutes. The resulting solution was filtered through a glass-fiber pad packed into a pipette, and the filtrate was added to Zn(acac)₂ (2.1 mg, 0.008 mmol, 2 mol%) and **6** (0.40 mmol, if boiling point of **6** is higher than 220 ° C) in a screw vial containing a magnetic stirring bar. After stirring for 30 minutes, all volatile compounds were removed under reduced pressure. **7** (0.48 mmol), **6** (0.40 mmol, if boiling point of **6** is lower than 220 ° C), and dry DCE (33 μ L) were added to the mixture, and the reaction vial was sealed with a screw-cap and removed from the glove box. After stirring at 80 ° C for 16 hours, the resulting mixture was quenched by passage through a short pad of silica. The crude mixture was purified by silica-gel column chromatography.
- (12) Ruthenium-catalyzed (*Z*)-selective *anti*-Markovnikov nucleophilic addition of carboxylic acids toward terminal alkynes was reported, in which ruthenium vinylidene complexes are proposed as the intermediates, Doucet, H.; Martin-Vaca, B.; Bruneau, C.; Dixneuf, P. H. General Synthesis of (*Z*)-Alk-1-en-1-yl Esters via Ruthenium-Catalyzed *anti*-Markovnikov *trans*-Addition of Carboxylic Acids to Terminal Alkynes. *J. Org. Chem.* **1995**, *60*, 7247–7255.
- (13) Purcell, K. F.; Stikeleather, J. A.; Brunk, S. D. Linear enthalpy-spectral shift correlations for 1,1,1,3,3,3-hexafluoro-2-propanol. *J. Am. Chem. Soc.* **1969**, *91*, 4019-4027.
- (14) Gaussian 16, Revision C.01, M. J. Frisch, G. W. Trucks, H. B. Schlegel, G. E. Scuseria, M. A. Robb, J. R. Cheeseman, G. Scalmani, V. Barone, G. A. Petersson, H. Nakatsuji, X. Li, M. Caricato, A. V. Marenich, J. Bloino, B. G. Janesko, R. Gomperts, B. Mennucci, H. P. Hratchian, J. V. Ortiz, A. F. Izmaylov, J. L. Sonnenberg, D. Williams-Young, F. Ding,

- F. Lipparini, F. Egidi, J. Goings, B. Peng, A. Petrone, T. Henderson, D. Ranasinghe, V. G. Zakrzewski, J. Gao, N. Rega, G. Zheng, W. Liang, M. Hada, M. Ehara, K. Toyota, R. Fukuda, J. Hasegawa, M. Ishida, T. Nakajima, Y. Honda, O. Kitao, H. Nakai, T. Vreven, K. Throssell, J. A. Montgomery, Jr., J. E. Peralta, F. Ogliaro, M. J. Bearpark, J. J. Heyd, E. N. Brothers, K. N. Kudin, V. N. Staroverov, T. A. Keith, R. Kobayashi, J. Normand, K. Raghavachari, A. P. Rendell, J. C. Burant, S. S. Iyengar, J. Tomasi, M. Cossi, J. M. Millam, M. Klene, C. Adamo, R. Cammi, J. W. Ochterski, R. L. Martin, K. Morokuma, O. Farkas, J. B. Foresman, and D. J. Fox, Gaussian, Inc., Wallingford CT, 2019.
- (15) Rawat, V. K.; Higashida, K.; Sawamura, M. Use of Imidazo[1,5-*a*]pyridin-3-ylidene as a Platform for Metal-Imidazole Cooperative Catalysis: Silver-Catalyzed Cyclization of Alkyne-Tethered Carboxylic Acids. *Adv. Synth. Catal.* **2021**, *363*, 1631–1637.
- (16) Dupuy, S.; Gasperini, D.; Nolan, S. P. Highly Efficient Gold(I)-Catalyzed Regio- and Stereoselective Hydrocarboxylation of Internal Alkynes. *ACS Catal.* **2015**, *5*, 6918–6921.
- (17) González-Liste, P. J.; García-Garrido, S. E.; Cadierno, V. Gold(I)-catalyzed addition of carboxylic acids to internal alkynes in aqueous medium. *Org. Biomol. Chem.* **2017**, *15*, 1670–1679.
- (18) Das, U. K.; Bhattacharjee, M. Synthesis and structure of [Ru(dppe)₂(CH₃CN)Cl][BPh₄] and its catalytic application to anti-Markovnikov addition of carboxylic acids to terminal alkynes. *J. Organomet. Chem.* **2012**, *700*, 78–82.
- (19) Chen, J.-F.; Li, C. Enol Ester Synthesis via Cobalt-Catalyzed Regio- and Stereoselective Addition of Carboxylic Acids to Alkynes. *Org. Lett.* **2018**, *20*, 6719–6724.
- (20) Nakamura, M.; Endo, K.; Nakamura, E. Indium-Catalyzed Addition of Active Methylene Compounds to 1-Alkynes. *J. Am. Chem. Soc.* **2003**, *125*, 13002–13003.
- (21) Oonishi, Y.; Gómez-Suárez, A.; Martin, A. R.; Nolan, S. P. Hydrophenoxylation of Alkynes by Cooperative Gold Catalysis. *Angew. Chem., Int. Ed.* **2013**, *52*, 9767–9771.
- (22) Lazreg, F.; Guidone, S.; Gómez-Herrera, A.; Nahra, F.; Cazin, C. S. J. Hydrophenoxylation of internal alkynes catalysed with a heterobimetallic Cu-NHC/Au-NHC system. *Dalton Trans.* **2017**, *46*, 2439–2444.

- (23) Gómez-Suárez, A.; Oonishi, Y.; Martin, A. R.; Nolan, S. P. Scope and limitations of the dual-gold-catalysed hydrophenoxylation of alkynes. *Beilstein J. Org. Chem.* **2016**, *12*, 172–178.
- (24) Sheldrick, G. M. SHTLXT-Integrated space-group and crystal-structure determination. *Acta Cryst.* **2015**, *A71*, 3–8.
- (25) Sheldrick, G. M. Crystal structure refinement with SHELXL. *Acta Cryst.* **2015**, *C71*, 3–8.
- (26) Dolomanov, O. V.; Bourhis, L. J.; Gildea, R. J.; Howard, J. A. K.; Puschmann, H. OLEX2: a complete structure solution, refinement and analysis program. *J. Appl. Crystallogr.* **2009**, *42*, 339–341.
- (27) ORTEP3: Farrugia, L. J. *J. Appl. Crystallogr.* **1997**, *30*, 565.
- (28) Global Reaction Route Mapping (GRRM) Program Version 17-A01, Produced by Satoshi Maeda, Yu Harabuchi, Yosuke Sumiya, Makito Takagi, Kimichi Suzuki, Kanami Sugiyama, Yuriko Ono, Miho Hatanaka, Yuto Osada, Tetsuya Taketsugu, Keiji Morokuma, Koichi Ohno.
- (29) CYLview20; Legault, C. Y., Université de Sherbrooke, 2020. (<http://www.cylview.org>)

Chapter 3

Nickel-catalyzed Homo-coupling of Aryl Ethers with Magnesium Anthracene Reductant

Abstract

Nickel-catalyzed reductive homo-coupling of aryl ethers has been achieved with $\text{Mg}(\text{anthracene})(\text{thf})_3$ as a readily available low-cost reductant. DFT calculations provided a rationale for the specific efficiency of the diorganomagnesium-type two-electron reducing agent. The calculations showed that the dianionic anthracene-9,10-diyl ligand reduces the two aryl ether substrates resulting in the homo-coupling reaction through supplying the electrons to the Ni-Mg bimetallic system to form organomagnesium nickel(0)-ate complexes, which cause two sequential C–O bond cleavage reactions. The calculations also showed cooperative actions of Lewis-acidic magnesium atoms and electron-rich nickel atoms in the C–O cleavage reactions.

Introduction

Homo-coupling of aryl halides is a straightforward method for preparing symmetrical biaryls as key building blocks of electronic materials, dyes, and biologically active compounds.¹ This reaction was first demonstrated by Ullmann in 1901 using copper as a stoichiometric reductant.² In the pursuit of better selectivity and reaction efficiency, a number of protocols using transition metal catalysts in addition to stoichiometric reductants has since been developed.^{3,4} While aryl halides and aryl sulfonates are common substrates for the homo-coupling reactions, extension of the scope of homo-coupling toward using aryl ethers, which are attractive substrates in terms of their ready availability from nature, is a formidable challenge at this moment. In this regard, Chatani and Tobisu reported the nickel-catalyzed homo-coupling of methoxyarenes using bis(neopentyl glycolato)diborane [B₂(nep)₂] as a reductant.⁵ This homo-coupling reaction consisted of two nickel-catalyzed reactions. One is the borylation of the methoxyarene substrate (ArOMe) to form the corresponding arylboronate [ArB(nep)], and the other is the subsequent Suzuki–Miyaura-type cross-coupling between the arylboronate and a second molecule of methoxyarene. A major issue for this transformation is the use of the expensive boron reagent B₂(nep)₂ as a stoichiometric reductant, generating costly waste.

Considering the potential of nickel catalysis in the development of efficient homo-coupling of aryl ethers and the well-demonstrated importance of Lewis-acidic cooperative participation of organometallic reagents in C–O bond cleavage by a nickel(0) species,^{6,7} the author focused on Mg(anthracene)(thf)₃ (**1**)^{8–11} as a potentially suitable reducing agent. Mg(anthracene)(thf)₃ is easily prepared from inexpensive magnesium powder and anthracene in THF (Figure 1).¹² This chapter describes nickel-catalyzed homo-coupling of aryl ethers using Mg(anthracene)(thf)₃ (**1**) as a stoichiometric reductant. The use of reductant **1** was crucial for the homo-coupling. Density functional theory (DFT) calculations suggested the occurrence of cooperative Ni–Mg bimetallic C–O bond activation through the formation of organomagnesium nickel(0)-ate complexes and Lewis acidic activation of the alkoxy leaving groups by ionized magnesium atoms.

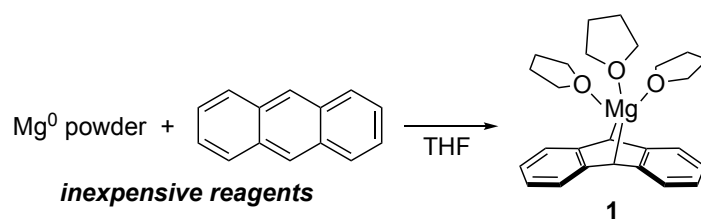


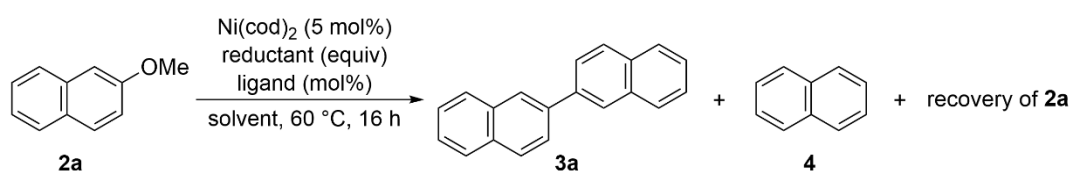
Figure 1. Preparation and a chemical structure of Mg(anthracene)(thf)₃ (**1**).

Result and Discussion

Specifically, the reaction of 2-methoxynaphthalene (**2a**) with an equimolar amount of Mg(anthracene)(thf)₃ (**1**) (**2a/1=1/1**) in the presence of a nickel-phosphine catalyst prepared *in situ* from Ni(cod)₂ (5 mol%) and tricyclohexylphosphine (20 mol%) in THF at 60 °C for 16 hours gave the desired homo-coupling product 2,2'-binaphthalene (**3a**) in 79% yield (Table 1, entry 1). This reaction formed a small amount of naphthalene (**4**, 5 %) as detected by ¹H NMR analysis of a crude mixture. The use of **1** was essential since **3a** was not obtained when other metal powder reductants such as magnesium, zinc, and manganese were used (entries 2-4). The reaction in the presence of a stoichiometric amount of Ni(cod)₂ without using an additional reductant did not cause the reaction of **2a** (entry 5). The use of a catalytic amount (10 mol%) of **1** with a stoichiometric amount of magnesium powder resulted in only 9% yield of **3a** (entry 6), indicating that the use of pre-formed Mg(anthracene)(thf)₃ (**1**) is essential.

Next, ligand effects were examined. When triphenylphosphine was employed as a ligand, **3a** was not obtained at all (entry 7). The use of 1,2-bis(dicyclohexylphosphino)ethane (dcype) as a peralkylbisphosphine ligand also caused no reaction (entry 8). While 1,3-dimesitylimidazol-2-ylidene (IMes) as a *N*-heterocyclic carbene ligand caused moderate catalytic activity to afford **3a** in 68% yield (entry 9), only a trace amount of **3a** was obtained with the more sterically demanding ligand 1,3-bis(2,6-diisopropylphenyl)imidazol-2-ylidene (IPr) (entry 10). Thus, tricyclohexylphosphine was selected as the optimal ligand. When the amount of tricyclohexylphosphine was reduced to 10 mol% (Ni/P=1/2), the catalytic activity was maintained to give **3a** in 80% yield (entry 11). However, further reduction of the amount of the ligand to 5 mol% (Ni/P=1/1) resulted in a decreased yield (69%, entry 12). The homo-coupling reaction of **2a** also occurred even in the absence of the phosphine ligand albeit with a lower yield (49%) of **3a** (entry 13). Heating the solution of **2a** and Mg(anthracene)(thf)₃ (**1**) in THF at 60 °C for 16 h in the absence of a nickel catalyst resulted in complete recovery of **2a**, indicating that direct reduction of **2a** with **1** did not occur under the reaction conditions (entry 14). The use of nickel(II) complex Ni(acac)₂ instead of Ni(cod)₂ led to decreased yield (20%, entry 15). Since it was reported that acetylacetonate ligand was replaced to η³-anthracenyl ligand in the reaction between [Ni(acac)Cp*] and **1**, the formation of such nickel anthracene complexes is the plausible reason for low catalytic activity of Ni(acac)₂ pre-catalyst.¹³ Cyclopentyl methyl ether (CPME), 1,4-dioxane, dimethoxyethane (DME), and toluene as a reaction solvent also gave the homo-coupling product albeit with lower yields (entries 16-19).

The use of an equimolar amount of the reductant **1** relative to **2a** was optimal for the homo-coupling of **2a** (Table 1, entries 1 and 11). Either an increase or a decrease in the relative amount of **1** caused a slight decrease in the homo-coupling efficiency; the use of 1.5 and 0.75 equivalents of **1** gave **3a** in 72% and 71% yields, respectively (Table 1, entries 20 and 21). The variation of the optimal reaction conditions (entry 11) by adding varying amounts of anthracene caused a significant decrease in the yield of the homo-coupling product **3a**, with 20 mol% and 50 mol% of anthracene giving **3a** in only 61% and 44% yields, respectively (entries 22 and 23). These inhibitory effects of anthracene suggest that anthracene generated *in situ* from **1** as the reaction proceeds may suppress the efficiency of nickel catalysis through anthracene-nickel π -coordination. This unfavorable interaction may be the cause of incomplete conversion of the starting material under the optimal conditions (entries 1, 11).

Table 1. Screening of Reaction Conditions^a

entry	reductant (equiv)	ligand (mol%)	solvent	yield of 3a [%] ^b	yield of 4 [%] ^b	recovery of 2a [%] ^b
1	1 (1.0 equiv)	PCy ₃ (20 mol%)	THF	79	5	14
2	Mg ⁰ (1.0 equiv)	PCy ₃ (20 mol%)	THF	0	1	97
3	Zn ⁰ (1.0 equiv)	PCy ₃ (20 mol%)	THF	0	trace	>99
4	Mn ⁰ (1.0 equiv)	PCy ₃ (20 mol%)	THF	0	trace	>99
5	Ni(cod) ₂ (1.0 equiv)	PCy ₃ (200 mol%)	THF	0	0	>99
6	1 (0.1 equiv)	PCy ₃ (20 mol%)	THF	9	1	88
	Mg ⁰ (1.0 equiv)					
7	1 (1.0 equiv)	PPh ₃ (20 mol%)	THF	0	3	94
8	1 (1.0 equiv)	dcype (10 mol%)	THF	0	0	>99
9	1 (1.0 equiv)	IMes (20 mol%)	THF	68	15	13
10	1 (1.0 equiv)	IPr (20 mol%)	THF	trace	2	95
11	1 (1.0 equiv)	PCy ₃ (10 mol%)	THF	80 (73) ^c	5	15
12	1 (1.0 equiv)	PCy ₃ (5 mol%)	THF	69	4	23
13	1 (1.0 equiv)	none	THF	49	4	45
14 ^d	1 (1.0 equiv)	PCy ₃ (20 mol%)	THF	0	0	>99
15 ^e	1 (1.0 equiv)	PCy ₃ (10 mol%)	THF	20	6	68
16	1 (1.0 equiv)	PCy ₃ (10 mol%)	CPME	62	5	29
17	1 (1.0 equiv)	PCy ₃ (10 mol%)	1,4-dioxane	62	2	28
18	1 (1.0 equiv)	PCy ₃ (10 mol%)	DME	15	1	83
19	1 (1.0 equiv)	PCy ₃ (10 mol%)	toluene	48	3	45
20	1 (1.5 equiv)	PCy ₃ (10 mol%)	THF	72	4	19
21	1 (0.75 equiv)	PCy ₃ (10 mol%)	THF	71	4	23
22	1 (1.0 equiv)	PCy ₃ (10 mol%)	THF	61	5	31
	anthracene (0.2 equiv)					
23	1 (1.0 equiv)	PCy ₃ (10 mol%)	THF	44	4	49
	anthracene (0.5 equiv)					

^a **2a** (0.1 mmol), reductant (xx equiv), Ni(cod)₂ (5 mol%), and ligand (yy mol%) in dry THF (0.5 mL) at 60 °C for 16 h. ^b Determined by ¹H NMR analysis using 1,3,5-trimethoxybenzene as an internal standard. ^c Isolated yield. ^d Without Ni(cod)₂. ^e Using Ni(acac)₂ instead of Ni(cod)₂.

Effect of Leaving Group

With the optimized conditions (Table 1, entry 11) in hand, the reactivity of various ethers derived from 2-naphthol was investigated (Figure 2). The leaving group had a strong impact on the reactivity. The yield of the homo-coupling product **3a** decreased in the order of increasing bulkiness of the leaving group (ethyl ether **2b**, 36 %; butyl ether **2c**, 19 %; isopropyl ether **2d**, 3 %). Methoxyethoxyethyl ether **2e** gave product **3a** in moderate yield (56 %), suggesting that the chelation of the leaving group to the ionized magnesium atom may have enhanced the reactivity, while no chelation effect was observed with methoxymethyl (MOM) ether **2f**, which gave **3a** in only 20% yield. Interestingly, a symmetrical diaryl ether 2,2'-oxydinaphthalene (**2g**) gave **3a**, which corresponds to the deoxygenation product, in 33% yield based on the molar amount of the used **2g**. This appeared, however, not to be a deoxygenation reaction but the homo-coupling of two aryl ether molecules (66% yield as the product of homo-coupling reaction) since 2-naphthol was observed in the crude product mixture in 79% yield. 2-Phenoxy-naphthalene (**2h**) was also applicable to the homo-coupling to afford **3a** in 43% yield in accompany with formation of phenol in 53% yield, in which C(naphthyl)–O bond was selectively reacted. The attempted reaction of carbamate **2i** resulted in decomposition of the starting material.

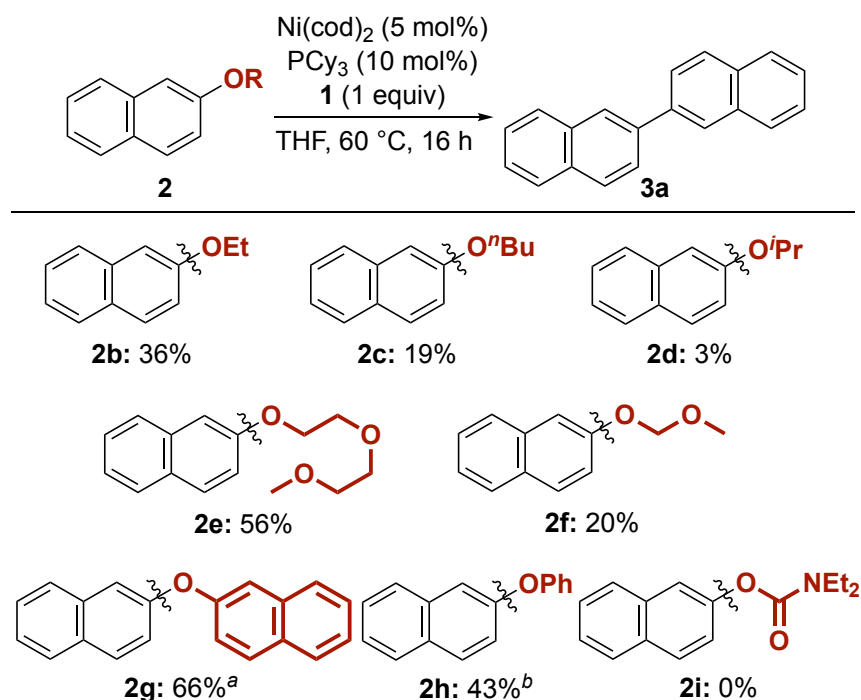


Figure 2. Effects of leaving groups. Substrate (0.1 mmol), **1** (0.1 mmol), $\text{Ni}(\text{cod})_2$ (5 mol%), and PCy_3 (10 mol%) in dry THF (0.5 mL) at 60 °C for 16 h. Yield was determined by ^1H NMR

analysis using 1,3,5-trimethoxybenzene as an internal standard. ^a 2-Naphthol was obtained in 79% yield. ^b Phenol was obtained in 53% yield.

Substrate Scope

Next, the scope and limitations of aryl methyl ethers were examined (Figure 3). 6-Hexyl-2-methoxynaphthalene (**2j**) and 1-((6-methoxynaphthalen-2-yl)piperidine (**2k**) gave the corresponding homo-coupling products in moderate yields (60% and 63%). Triarylamines **2l,m** and carbazole-substituted naphthyl ether **2n** served as substrates, and the desired products were obtained in 60%, 37%, and 35% yields, respectively. Interestingly, the methoxy groups on the aniline moieties of **2m** remained intact, resulting in a site-selective reaction at the naphthyl moiety. 2-Methoxy-9-methyl-9*H*-carbazole (**2o**) afforded the corresponding biscarbazole product in 19% yield. In the reaction of 2-methoxytriphenylene (**2p**), a non-negligible amount of triphenylene (22%) was produced as a reduction product, diminishing the yield of the desired homo-coupling product to 14%. 1-Methoxynaphthalene (**2q**) and 4-methoxybiphenyl (**2r**) were inert compounds for this protocol. The reaction of 6-methoxyquinoline (**2s**) and (*E*)-(3-methoxyprop-1-en-1-yl)benzene (**2t**) resulted in decomposition of the starting materials.

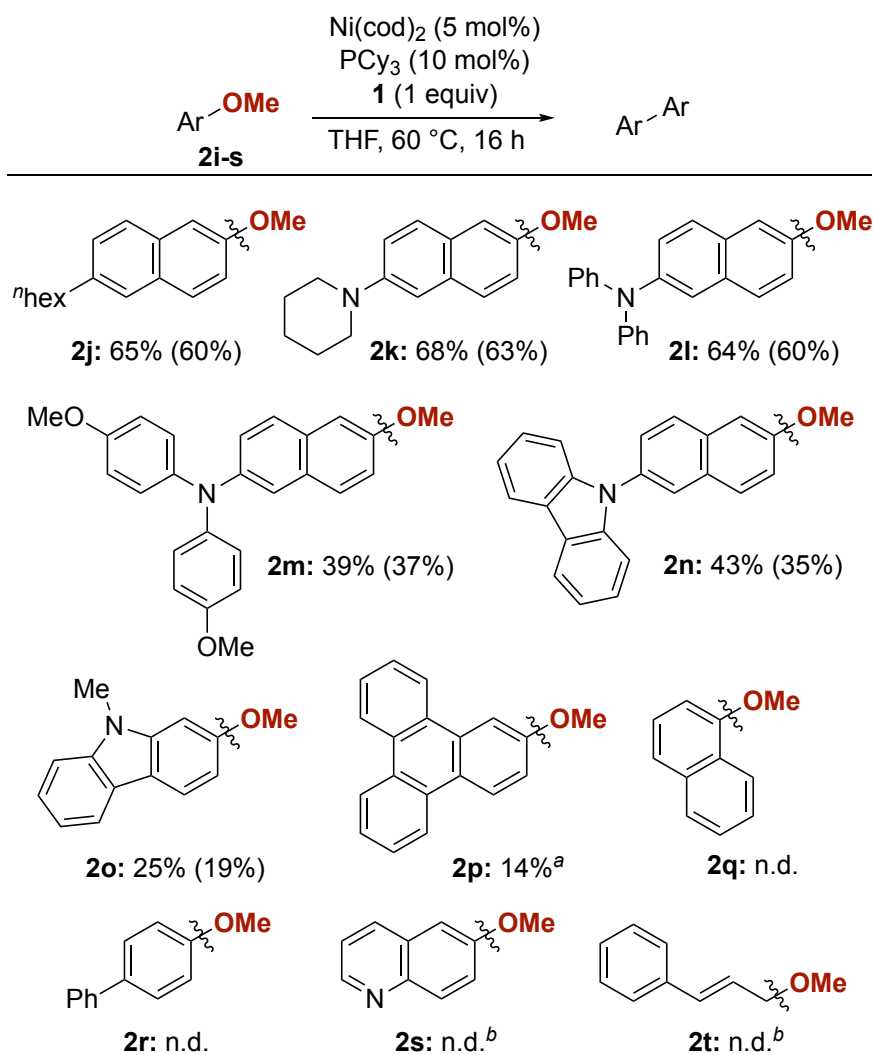
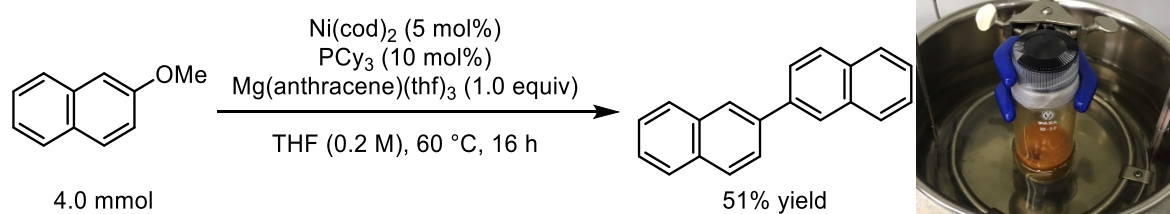


Figure 3. Scope and limitations. Substrate (0.1 mmol), **1** (0.1 mmol), Ni(cod)₂ (5 mol%), and PCy₃ (10 mol%) in dry THF (0.5 mL) at 60 °C for 16 h. Yield was determined by ¹H NMR analysis using 1,3,5-trimethoxybenzene as an internal standard. Isolated yield is shown in parenthesis. n.d.: Homo-coupling product was not detected in the crude product. ^a Triphenylene was obtained in 22% yield. ^b Complex mixture was observed.

To test the applicability of this reaction to large-scale synthesis, the homo-coupling of **2a** was conducted on a 4.0 mmol scale (Scheme 1). After the reaction, residual Mg(anthracene)(thf)₃ (**1**) was quenched with 1M HCl aqueous solution at 0 °C, and anthracene and residual **2a** were easily removed by Kugelrohr distillation at 150 °C (0.1 mmHg). The crude mixture was purified by silica-gel column chromatography to afford **3a** in 51% yield.

Scheme 1. Large-scale Experiment



To gain insight into the reaction mechanism, DFT calculations were conducted. It was reported that C–O bond cleavage with a nickel(0) complex through conventional oxidative addition requires a high activation energy.¹⁴ Harsh conditions are often required for nickel-catalyzed transformation of aryl ethers *via* C–O bond cleavage,⁶ with exception of the Kumada-Tamao-Corriu-type coupling of aryl ethers using Grignard reagents as a coupling partner that occur under much milder conditions in many cases.^{15,16} Regarding this issue, DFT calculation studies by Uchiyama and Wang suggested that *in situ* generation of nickel(0)-ate complexes from nickel(0) complexes and Grignard reagents would be the key for C–O bond cleavage.¹⁷ Based on this knowledge and the analogy between Grignard reagents and $\text{Mg}(\text{anthracene})(\text{thf})_3$ (**1**),⁹ I performed DFT calculations for nickel-catalyzed homo-coupling of 2-naphthyl methyl ether (**2a**) with **1** as a reductant, focusing on the nature of the nickel(0)-ate complexes and Lewis-acidic characters of the ionized magnesium atom.

The geometry optimization was carried out at the M06/lanl2dz (for Ni), 6-31G(d) (for others)/PCM(THF) level of theory, and additional single-point calculations were performed at the M06/SDD (for Ni), 6-311++G(d,p) (for others)/PCM(THF) level of theory.¹⁸ The obtained energy diagram is shown in Figure 4. Replacement of a THF molecule on the magnesium atom of **1** with 2-methoxynaphthalene (**2a**, shown in red) gives **Int-1**. Subsequent η^2 -coordination of 2-methoxynaphthalene at the C1–C2 unsaturated bond to $\text{Ni}(\text{PCy}_3)$ forms **Int-2**, which undergoes migration of the negatively charged 9-anthracenyl carbon atom from the magnesium atom to the nickel atom to form the more stable magnesium nickel(0)-ate complex **Int-3**. This key intermediate undergoes C–O bond cleavage with Lewis-acidic cooperative participation of the ionized magnesium atom with a reasonable energy barrier (**TS**_{3,4}, 12.1 kcal/mol) to give **Int-4**. As shown in Figure 5, this bimetallic C–O bond cleavage (**Int-3-TS**_{3,4}-**Int-4**) is accompanied by significant flattening of the anthracen-9,10-diyl ligand, which corresponds to electron release from the dianionic ligand to the nickel center. The author proposes that this electron release is the key for facile C–O cleavage. Moreover, he noticed that the nickel center

of the C–O cleavage product (**Int-4**) remains electron-rich due to this electron-releasing effect of the anthracene-9,10-diyl ligand. Figure 5b shows that the methoxy ligand is bound solely to the magnesium atom and that the 2-naphthyl ligand is also σ -bonded to the magnesium atom with π -coordination to the nickel atom. Next, **Int-4** undergoes replacement of another THF molecule on the magnesium atom with the second 2-methoxynaphthalene molecule (**2a**, shown in blue) to form **Int-5**. Energetically favorable dissociation of a neutral anthracene molecule accompanied by π -coordination of the second 2-methoxynaphthalene molecule to the nickel atom produces a new magnesium nickel(0)-ate complex (**Int-6**) with the release of energy as high as 24.2 kcal/mol. The second C–O cleavage proceeds again in bimetallic mode with an energy barrier of 11.9 kcal/mol to afford diaryl nickel(II) complex **Int-7**. Note that after this C–O cleavage the 2-naphthyl ligand originating from the first 2-methoxynaphthalene molecule loses its interaction with the magnesium atom, consequently forming a complete σ -bond with the nickel atom. Finally, reductive elimination of **Int-7** gives the biaryl product (**3a**) and a nickel(0) species, which then enters the second catalytic cycle (see Supporting Information for details of the calculations on the reductive elimination step). Thus, this computationally obtained reaction pathway illustrates the characteristic features of the Mg(anthracene)(thf)₃ (**1**) reductant, which forms electron-rich organomagnesium nickel(0)-ate complexes as key intermediates for the two sequential aryl ether C–O bond cleavage reactions.

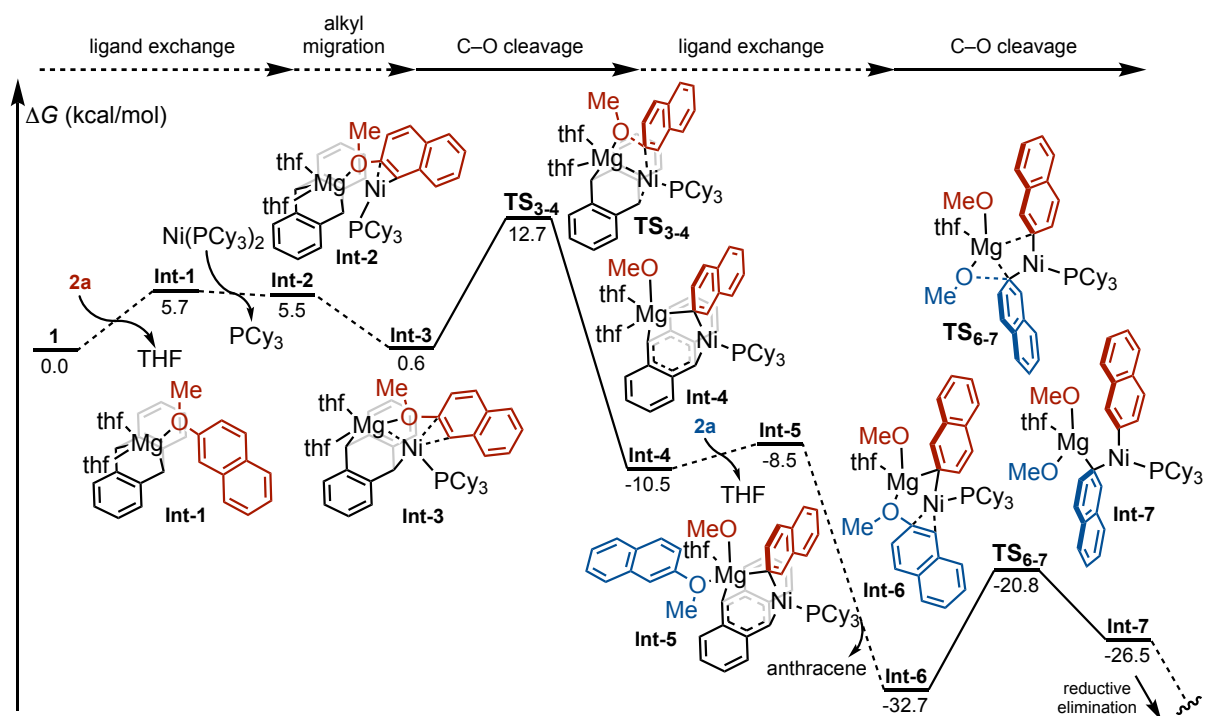


Figure 4. Energy diagram for homo-coupling of 2-methoxynaphthalene (**2a**) mediated by Mg(anthracene)(thf)₃ (**1**) and Ni(PCy₃)₂. Calculations were performed at M06/SDD (for Ni), 6-311++G(d,p) (for others)/PCM(THF)// M06/lanl2dz (for Ni), 6-31G(d) (for others)/PCM(THF) level of theory.

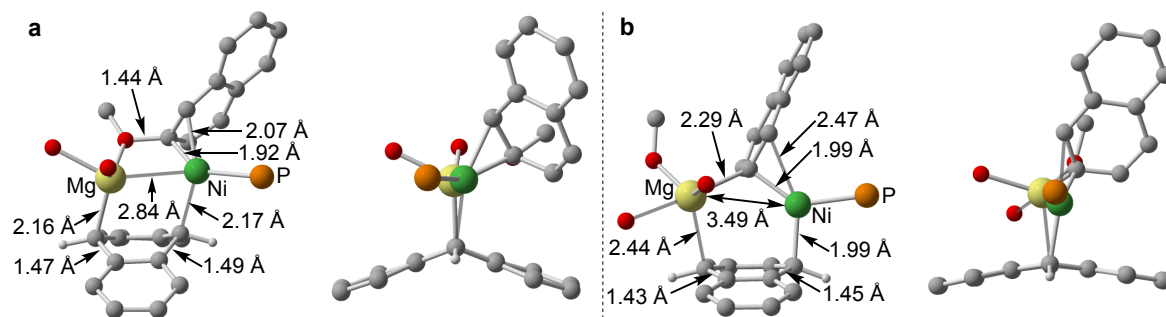


Figure 5. Structures of (a) **Int-3** and (b) **Int-4**. Hydrogen atoms, cyclohexyl groups on phosphorus atoms, and carbon frameworks of THF molecules are omitted for clarity

Conclusion

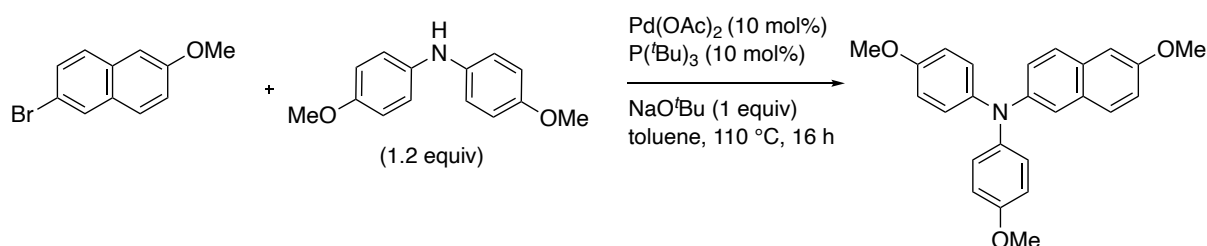
In summary, the author developed a nickel-catalyzed homo-coupling of aryl ethers with Mg(anthracene)(thf)₃ as a readily available low-cost reductant. DFT calculations provided the rationale for the specific efficiency of Mg(anthracene)(thf)₃ as a stoichiometric two-electron reductant. The dianionic anthracene-9,10-diyl ligand donates electrons to the Ni-Mg bimetallic system to form electron-rich magnesium nickel(0)-ate complexes. These cause two sequential aryl ether C–O bond cleavage reactions through cooperative actions of Lewis-acidic magnesium atoms and electron-rich nickel atoms.

Experimental Section

General

All air and moisture-sensitive reactions were operated using the standard Schlenk techniques or a glove box under nitrogen gas atmosphere. THF was dried and deoxygenated with a Grubbs column system (Glass Counter Solvent Dispensing System, Nikko Hansen & Co, Ltd.). Dry toluene, CPME, and MeOH were purchased from Kanto Chemical Co., Inc.. Dry 1,4-dioxane was purchased from FUJIFILM Wako Pure Chemical Corporation. Mg(anthracene)(thf)₃ was prepared according to the reported procedure,²⁰ and it was stored and treated in the nitrogen-filled glove box. ¹H NMR (400 MHz) and ¹³C{¹H} NMR (100 MHz) spectra were measured on JEOL ECZ-400S spectrometer. All ¹H NMR chemical shifts were reported in ppm (δ) relative to the chemical shifts of residual solvent resonances (CDCl₃ at δ 7.26 and DMSO-*d*₆ at δ 2.50). All ¹³C{¹H} NMR chemical shifts were reported in ppm (δ) relative to carbon resonances of CDCl₃ at δ 77.0 and DMSO-*d*₆ at δ 39.5. High resolution mass spectra were obtained with Thermo Fisher Scientific Exactive and JEOL JMS-T100GCv at the Instrumental Analysis Division, Equipment Management Center, Creative Research Institution, Hokkaido University. IR spectra were obtained on JASCO FT-IR-4600 spectrometer. Melting points were determined with OptiMelt MPA100 of Stanford Research Systems. Flash column chromatography was performed using silica gel (Wakogel FC-40, 0.020-0.040 mm >70%). Nickel catalyzed homo-coupling was conducted using EYELA RCH-1000 of TOKYO RIKAKIKAI CO, LTD as a heating reactor.

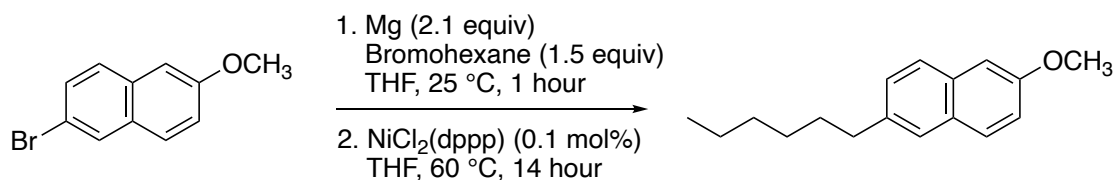
6-Methoxy-*N,N*-bis(4-methoxyphenyl)naphthalen-2-amine



In a nitrogen-filled glove box, 2-bromo-6-methoxynaphthalene (1.19 g, 5.0 mmol) was placed in a screw vial containing a magnetic stirring bar. A stock solution of Pd(OAc)₂ (112 mg, 0.5 mmol, 10 mol%) in dry toluene (3.0 mL) and P(^tBu)₃ (101.2 mg, 0.5 mmol, 10 mol%) in dry toluene (3.0 mL) was added subsequently into the screw vial. The orange colour reaction mixture was stirred for 2 minutes before addition of NaO^tBu (480.5 mg, 5.0 mmol, 1 equiv). Bis(4-methoxyphenyl)amine (1.38 g, 6 mmol, 1.2 equiv) was added to the resulting mixture. The remaining (9.0 mL) dry toluene was added to the mixture. The vial was sealed with screw cap and taken out from the glove box. After stirring at 110 °C for 16 hours, the resulting mixture was filtrated through the filter paper. Water was poured into the resulting solution, and aqueous layer was extracted with DCM. The combined organic layer was washed with brine, dried over Na₂SO₄, filtrated, and evaporated. The crude mixture was purified by silica-gel flush column chromatography (hexane/EtOAc=9/1) and was further crystallized with ethanol to afford the desired product as white solid (1.34 g, 3.47 mmol, 69% yield).

¹H NMR (CDCl₃, 400 MHz, 25 °C): 7.57 (d, *J* = 8.9 Hz, 1H), 7.46 (d, *J* = 9.8 Hz, 1H), 7.23 (s, 1H), 7.21 (dd, *J* = 8.8, 2.2 Hz, 1H), 7.07-7.04 (m, 6H), 6.85-6.80 (m, 4H), 3.90 (s, 3H), 3.81 (s, 6H). ¹³C{¹H} NMR (CDCl₃, 100 MHz, 25 °C): δ 156.4, 155.5, 144.7, 141.5, 130.1, 129.8, 128.2, 127.4, 125.9, 123.7, 118.8, 117.8, 114.6, 105.9, 55.5, 55.3.

2-Hexyl-6-methoxynaphthalene



Magnesium turnings (271 mg, 11 mmol, 2.1 equiv) and dry THF (8.0 mL) were placed in a 50 mL Schlenk flask under nitrogen atmosphere, and a few drop of dibromoethane was added to the mixture. Bromohexane (1.1 ml, 8.0 mmol, 1.5 equiv) was added dropwise to the reaction mixture for over 10 minutes, and the solution was stirred at room temperature for 1 hour. NiCl₂(dppp) (2.7 mg, 0.005mmol, 0.1 mol%) and 2-bromo-6-methoxynaphthalene (1.23 g, 5.2

mmol) were placed in a 50 mL flask, and the above solution of hexylmagnesium bromide was added into the flask through cannulation under nitrogen atmosphere. The reaction mixture was stirred at 60 ° C for 14 hours. After addition of cold water, the resulting mixture was extracted three times with EtOAc. The combined organic layer was washed with brine, dried over Na₂SO₄, and evaporated under reduced pressure. The residue was purified with a flash column chromatography (EtOAc/hexane = 1/50) to afford (723.2 mg, 3.66 mmol, 70% yield) as a white solid.

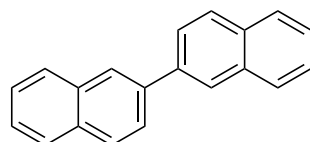
¹H NMR (CDCl₃, 400 MHz, 25 °C): 7.69-7.66 (m, 2H), 7.54 (s, 1H), 7.30 (dd, *J* = 8.3, 1.7 Hz, 1H), 7.13 (dd, *J* = 7.5, 2.5 Hz, 1H), 7.11 (s, 1H), 3.92 (s, 3H), 2.74 (t, *J* = 7.8 Hz, 2H), 1.71-1.65 (m, 2H), 1.39-1.25 (m, 6H), 0.90 (t, *J* = 7.0 Hz, 3H). ¹³C{¹H} NMR (CDCl₃, 100 MHz, 25 °C): δ 157.0, 138.1, 132.9, 129.1, 128.9, 127.9, 126.6, 126.1, 118.5, 105.6, 55.3, 35.9, 31.8, 31.4, 29.0, 22.6, 14.1.

General Procedure for the Nickel-catalyzed Homocoupling Reaction

In a nitrogen-filled glove box, an aryl ether (0.1 mmol) was placed in a screw vial containing stirring bar. Ni(cod)₂ (1.4 mg, 0.005 mmol, 5 mol%), PCy₃ (2.8 mg, 0.01 mmol, 10 mol%), Mg(anthracene)(thf)₃ (41.9 mg, 0.1 mmol, 1 equiv), and dry THF (0.5 mL) were added into the vial. The vial was sealed with a screw cap and taken out from the glove box. After stirring at 60 °C for 16 hours, the resulting mixture was cooled to room temperature and quenched with 1M HCl aq. In the case of amine compounds, the resulting mixture was neutralized with saturated NaHCO₃ aq. Organic layer was extracted with dichloromethane and passed through a short-pad of silica-gel. After addition of an internal standard, yield was determined by ¹H NMR analysis.

Isolation and Characterization of the Homo-coupled Products

2,2'-Binaphthalene (3a)⁵

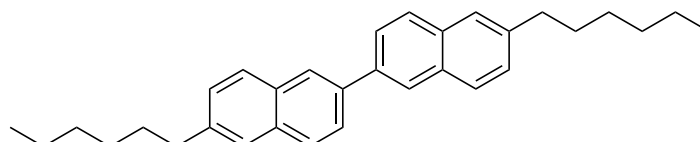


3a

A crude mixture was distilled to remove anthracene and 2-methoxynaphthalene (150 °C, 0.1 mmHg). Then, residual compounds were purified by silica-gel column chromatography (only

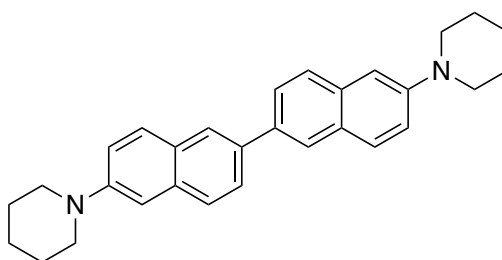
hexane). White solid (9.25 mg, 73% yield). $^1\text{H NMR}$ (CDCl_3 , 400 MHz, 25 °C): 8.18 (s, 2H), 7.98-7.93 (m, 4H), 7.92-7.88 (m, 4H), 7.56-7.49 (m, 4H). $^{13}\text{C}\{^1\text{H}\}$ NMR (CDCl_3 , 100 MHz, 25 °C): δ 138.4, 133.7, 132.7, 128.5, 128.2, 127.7, 126.3, 126.1, 126.0, 125.7. HRMS (EI) m/z calc. for $\text{C}_{20}\text{H}_{14}$ 254.10955 found 254.10891.

6,6'-Dihexyl-2,2'-binaphthalene⁵



A crude mixture was distilled to remove anthracene and 2-hexyl-6-methoxynaphthalene (150 °C, 0.1 mmHg). Then, residual compounds were purified by silica-gel column chromatography (only hexane). White solid (12.72 mg, 60% yield). $^1\text{H NMR}$ (CDCl_3 , 400 MHz, 25 °C): δ 8.12 (s, 2H), 7.90-7.83 (m, 6H), 7.65 (s, 2H), 7.38 (dd, $J = 8.5, 1.6$ Hz, 2H), 2.80 (t, $J = 7.7$ Hz, 4H), 1.77-1.69 (m, 4H), 1.41-1.30 (m, 12H), 0.90 (t, $J = 7.0$ Hz, 6H). $^{13}\text{C}\{^1\text{H}\}$ NMR (CDCl_3 , 100 MHz, 25 °C): δ 140.7, 137.7, 132.8, 132.2, 128.04, 127.95, 126.1, 125.7, 36.2, 31.8, 31.3, 29.0, 22.6, 14.1. HRMS (EI) m/z calc. for $\text{C}_{32}\text{H}_{38}$ 422.29735 found 422.29680.

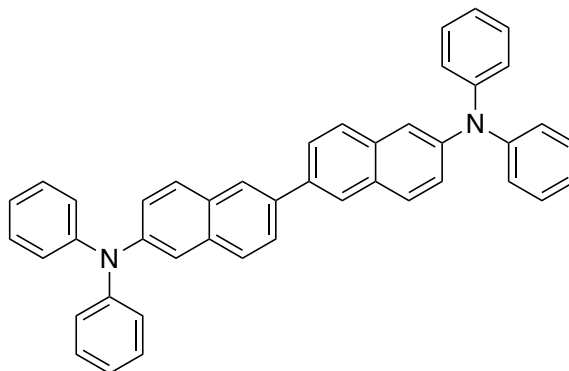
6,6'-Di(piperidin-1-yl)-2,2'-binaphthalene



A crude mixture was purified by silica-gel column chromatography (EtOAc/hexane=3/100 to 1/10). Light brown solid (13.25 mg, 63% yield). mp: 175°C (decomp.). IR (ATR, v/cm^{-1}): 2931 m, 2854 w, 2806 w, 1626 w, 1591 s, 1448 w, 1387 w, 1202 s, 1112 m, 926 m, 871 s, 802 m, 666 m, 630 w. $^1\text{H NMR}$ (CDCl_3 , 400 MHz, 25 °C): δ 8.01 (s, 2H), 7.80-7.75 (m, 6H), 7.31 (dd, $J = 8.9, 2.3$ Hz, 2H), 7.16 (d, $J = 2.1$ Hz, 2H), 3.29 (t, $J = 5.4$ Hz, 8H), 1.82-1.74 (m, 8H), 1.68-1.60 (m, 4H). $^{13}\text{C}\{^1\text{H}\}$ NMR (CDCl_3 , 100 MHz, 25 °C): δ 150.1, 135.9, 133.8, 128.8, 128.6,

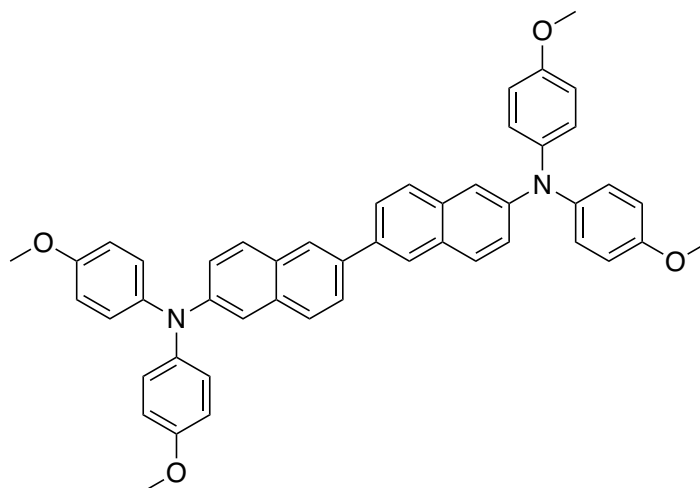
127.1, 125.8, 125.1, 120.4, 110.1, 50.9, 25.9, 24.4. HRMS (ESI⁺) m/z calc. for C₃₀H₃₃N₂ 421.26383 found 421.26361.

***N*⁶,*N*⁶,*N*^{6'},*N*^{6'}-Tetraphenyl-[2,2'-binaphthalene]-6,6'-diamine**



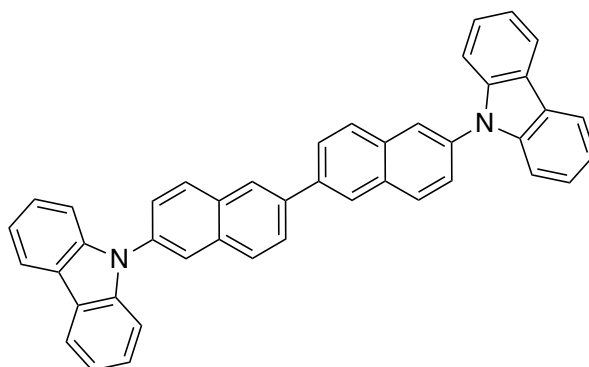
A crude mixture was purified by washing with EtOH. Light green solid (17.60 mg, 60% yield). **mp**: 245-247 °C. **IR** (ATR, v/cm⁻¹): 3026 w, 1628 w, 1585 m, 1485 m, 1377 w, 1265 m, 1171 w, 876 m, 750 s, 692 s, 661 m, 613 w. **¹H NMR** (CDCl₃, 400 MHz, 25 °C): δ 8.06 (s, 2H), 7.79 (d, *J* = 9.2 Hz, 2H), 7.78 (dd, *J* = 6.8, 1.6 Hz, 2H), 7.69 (d, *J* = 8.8 Hz, 2H), 7.45 (d, *J* = 2.0 Hz, 2H), 7.33-7.27 (m, 10H), 7.16 (dd, *J* = 7.6, 1.2 Hz, 8H), 7.06 (tt, *J* = 7.2, 1.2 Hz, 4H). **¹³C{¹H} NMR** (CDCl₃, 100 MHz, 25 °C): δ 147.7, 145.6, 137.0, 133.5, 130.2, 129.3, 129.1, 127.5, 126.0, 125.4, 124.8, 124.4, 123.0, 119.8. **HRMS** (APCI) m/z calc. for C₄₄H₃₃N₂ 589.26383 found 589.26422.

***N*⁶,*N*⁶,*N*^{6'},*N*^{6'}-Tetrakis(4-methoxyphenyl)-[2,2'-binaphthalene]-6,6'-diamine¹⁹**



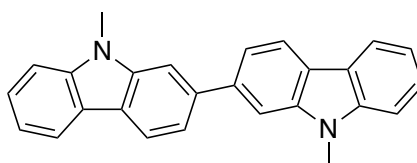
A crude mixture was purified by silica-gel column chromatography (Et₂O/hexane=1/20 to 1/5). Pale yellow solid (13.15 mg, 37% yield). ¹H NMR (DMSO-*d*₆, 400 MHz, 25 °C): δ 8.15 (s, 2H), 7.81-7.79 (m, 4H), 7.67 (d, *J* = 8.8 Hz, 2H), 7.11-7.04 (m, 12H), 6.93 (d, *J* = 9.2 Hz, 8H), 3.75 (s, 12H). ¹³C{¹H} NMR (DMSO-*d*₆, 100 MHz, 25 °C): δ 155.8, 146.3, 140.2, 134.9, 133.3, 129.1, 128.8, 127.1, 126.6, 125.4, 124.6, 121.9, 115.0, 114.2, 55.2. HRMS (EI) *m/z* calc. for C₄₈H₄₀N₂O₄ 708.29881 found 708.29908.

6,6'-Di(9*H*-carbazol-9-yl)-2,2'-binaphthalene



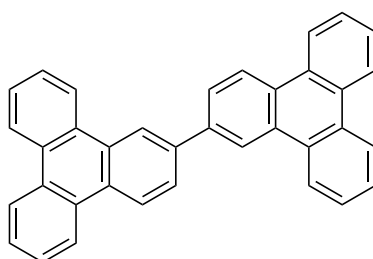
A crude mixture was purified by washing with EtOH. Light brown solid (10.13 mg, 35% yield). **mp**: 270 °C (decomp.). **IR** (ATR, *v*/cm⁻¹): 2920 w, 2852 w, 2224 w, 1749 m, 1657 m, 1599 w, 1331w, 1126 s, 1043 m, 849 m, 596 m, 548 s. ¹H NMR (CDCl₃, 400 MHz, 25 °C): δ 8.36 (s, 2H), 8.21-8.19 (m, 6H), 8.13 (d, *J* = 2.0 Hz, 2H), 8.09-8.03 (m, 4H), 7.76 (dd, *J* = 6.4, 2.0 Hz, 2H), 7.52 (d, *J* = 8.0 Hz, 4H), 7.45 (dt, *J* = 7.0, 0.8 Hz, 4H), 7.33 (dt, *J* = 7.0, 0.8 Hz, 4H). ¹³C{¹H} NMR (CDCl₃, 100 MHz, 25 °C): δ 141.0, 138.8, 135.5, 133.3, 132.7, 130.2, 128.6, 126.6, 126.2, 126.0, 125.9, 125.1, 123.5, 120.4, 120.1, 109.8. HRMS (ESI⁺) *m/z* calc. for C₄₄H₂₉N₂ 585.23253 found 585.23249.

9,9'-Dimethyl-9*H*,9'*H*-2,2'-bicarbazole⁵



A crude mixture was purified by silica-gel column chromatography (Et₂O/hexane=1/20 to 1/5). White solid (3.51 mg, 19% yield). **¹H NMR** (CDCl₃, 400 MHz, 25 °C): δ 8.19 (dd, *J* = 8.0, 0.5 Hz, 2H), 8.14 (dt, *J* = 7.8, 0.9 Hz, 2H), 7.73 (d, *J* = 1.1 Hz, 2H), 7.64 (dd, *J* = 8.1, 1.5 Hz, 2H), 7.51 (t, *J* = 7.6 Hz, 2H), 7.44 (d, *J* = 8.0 Hz, 2H), 7.29-7.25 (m, 2H), 3.95 (s, 6H). **¹³C{¹H} NMR** (CDCl₃, 100 MHz, 25 °C): δ 141.6, 141.5, 140.2, 125.6, 122.6, 121.9, 120.5, 120.3, 119.1, 119.0, 108.4, 107.4, 29.2. **HRMS** (EI) *m/z* calc. for C₂₆H₂₀N₂ 360.16265 found 360.16214.

2,2'-bitriphenylene²¹



Yield was determined by only ¹H NMR analysis due to small amount of the product. **¹H NMR** (CDCl₃, 400 Hz, 25 °C) δ 9.07 (d, *J* = 1.6 Hz, 2H), 8.87-8.84 (m, 2H), 8.81 (d, *J* = 8.8 Hz, 2H), 8.75-8.70 (m, 6H), 8.12 (dd, *J* = 8.8, 1.6 Hz, 2H), 7.75-7.71 (m, 8H).

DFT Calculations

General Information

All geometry optimizations and single-point calculations were performed by Gaussian 16 package.²² The geometry optimizations as well as frequency calculations of all structures were conducted at the M06 functional²³ in conjunction with the lanl2dz (for nickel) and 6-31G(d) (for other elements) basis set. The integral equation formalism polarizable continuum model (IEFPCM) was introduced to evaluate the effects of solvent (THF).²⁴ All the transition states have the single imaginary frequency, and these transition states were traced with intrinsic reaction coordinate (IRC) analyses by the use of Global Reaction Route Mapping (GRRM) program²⁵ to describe the reaction pathway. Additional single-point calculations including frequency calculations were performed at the M06 functional in conjunction with the SDD (for nickel) and 6-311++G(d,p) (for other elements) basis set with IEFPCM (THF) based on geometries obtained through the method described as above. For describing energy diagram in the main text, the relative energies were corrected for the Gibbs free energies and given in kcal/mol. The structures of intermediates and transition states were described by CYLview20, as shown in the following.²⁶

Summary of Energies

Structure Name	Electronic Energies (EE) [Hartree]	EE + Zero-point Energy [Hartree]	EE + Thermal Free Energy Correction [Hartree]
1	-1436.452658	-1435.909002	-1435.967065
Int-1	-1704.260871	-1703.654732	-1703.717925
Int-2	-2922.068019	-2920.982114	-2921.068871
Int-3	-2922.078597	-2920.992023	-2921.076698
TS₃₋₄	-2922.057908	-2920.972627	-2921.057295
Int-4	-2922.092283	-2921.007061	-2921.094320
Int-5	-3189.903576	-3188.757232	-3188.851001
Int-6	-2650.691190	-2649.738844	-2649.820381
TS₆₋₇	-2650.668003	-2649.718408	-2649.801500
Int-7	-2650.675480	-2649.725621	-2649.810563
Int-8	-1987.916950	-1987.167516	-1987.236092
TS₈₋₉	-1987.913298	-1987.164460	-1987.232214
Int-9	-1987.973924	-1987.222995	-1987.289043
2a	-500.167380	-499.989528	-500.024112
THF	-232.351887	-232.236425	-232.264243
Ni(PCy₃)₂	-2264.581415	-2263.624352	-2263.696294
PCy₃	-1046.778060	-1046.300213	-1046.345640
anthracene	-539.226434	-539.034401	-539.069113

References

- (1) (a) Vasconcelos, S. N. S.; Reis, J. S.; De Oliveira, I. M.; Balfour, M. N.; Stefani, H. A. *Tetrahedron* **2019**, *75*, 1865-1959. b) Hassan, J.; Sévignon, M.; Gozzi, C.; Schulz, E.; Lemaire, M. *Chem. Rev.* **2002**, *102*, 1359-1469.
- (2) (a) Ullmann, F.; Bielecki, J. *Chem. Ber.* **1901**, *34*, 2174–2185. (b) Ullmann, F.; Meyer, G. M.; Loewenthal, O.; Gilli, E. *Justus Liebigs Ann. Chem.* **1904**, *332*, 38-81.
- (3) Recent reports on nickel-catalyzed homo-coupling reactions; (a) Qiu, H.; Shuai, B.; Wang, Y.-Z.; Liu, D.; Chen, Y.-G.; Gao, P.-S.; Ma, H.-X.; Chen, S.; Mei, T.-S. *J. Am. Chem. Soc.* **2020**, *142*, 9872-9878. (b) Rahil, R.; Sengmany, S.; Gall, E. L.; Léonel, E. *Synthesis* **2018**, *50*, 146-154. (c) Lv, L.; Qiu, Z.; Li, J.; Liu, M.; Li, C.-J. *Nat. Commun.* **2018**, *9*, 4739. (d) Liu, Y.; Xiao, S.; Qi, Y.; Du, F. *Chem. Asian J.* **2017**, *12*, 673-678. (e) Guo, L.; Huang, C.; Liu, L.; Shao, Z.; Tong, Y.; Hou, H.; Fan, Y. *Cryst. Growth Des.* **2016**, *16*, 4926-4933. (f) Maddaluno, J.; Durandetti, M. *Synlett* **2015**, *26*, 2385-2388. (g) Yamamoto, T. *Appl. Organometal. Chem.* **2014**, *28*, 598-604.
- (4) Recent reports on palladium-catalyzed homo-coupling reactions; (a) Schroeter, F.; Lerch, S.; Strassner, T. *Org. Process Res. Dev.* **2018**, *22*, 1614-1621. (b) Lakshmidēvi, J.; Appa, R. M.; Naidu, B. R.; Prasad, S. S.; Sarma, L. S.; Venkateswarlu, K. *Chem. Commun.* **2018**, *54*, 12333-12336. (c) Zhong, S.; Chen, M.; Liu, G.; Sun, C.; Liu, W. *Appl. Organometal. Chem.* **2017**, *31*, e3705. (d) Huang, Y.; Liu, L.; Feng, W. *Chemistry Select* **2016**, *3*, 630-634.
- (5) Nakamura, K.; Tobisu, M.; Chatani, N. *Org. Lett.* **2015**, *17*, 6142-6145.
- (6) (a) Tobisu, M.; Chatani, N. *Acc. Chem. Res.* **2015**, *48*, 1717-1726. (b) Zeng, H.; Qiu, Z.; Domínguez-Huerta, A.; Hearne, Z.; Chen, Z.; Li, C.-J. *ACS Catal.* **2017**, *7*, 510-519. (c) Qiu, Z.; Li, C.-J. *Chem. Rev.* **2020**, *120*, 10454-10515.
- (7) (a) Yu, D.-G.; Li, B.-J.; Zheng, S.-F.; Guan, B.-T.; Wang, B.-Q.; Shi, Z.-J. *Angew. Chem., Int. Ed.* **2010**, *49*, 4566-4570. (b) Sergeev, A. G.; Hartwig, J. F. *Science* **2011**, *332*, 439-443. (c) Liu, X.; Hsiao, C.-C.; Kalvet, I.; Leiendecker, M.; Guo, L.; Schoenebeck, F.; Rueping, N. *Angew. Chem., Int. Ed.* **2016**, *55*, 6093-6098. (d) Yang, Z.-K.; Wang, D.-Y.; Minami, M.; Ogawa, H.; Ozaki, T.; Saito, T.; Miyamoto, K.; Wang, C.; Uchiyama, M. *Chem. Eur. J.* **2016**, *22*, 15693-15699. (e) Kelley, P.; Edouard, G. A.; Lin, S.; Agapie, T. *Chem. Eur. J.* **2016**, *22*, 17173-17176.
- (8) The chemical structure of **1** was discussed; (a) Bogdanović, B.; Liao, S.; Mynott, R.; K. Schlichte, K.; Westeppe, U. *Chem. Ber.* **1984**, *117*, 1378-1392. (b) Engelhardt, L. M.; Harvey, S.; Raston, C. L.; White, A. H. *J. Organometallic. Chem.* **1988**, *341*, 39-51.

- (9) For a variety of chemical properties of **1**, see; (a) Bogdanović, B. *Acc. Chem. Res.* **1988**, *21*, 261-267. (b) Bogdanović, B.; Janke, N.; Kinzelmann, H.-G. *Chem. Ber.* **1990**, *123*, 1507-1515.
- (10) For reducing ability of **1** toward organic compounds, see; (a) Bogdanović, B.; Schlichte, K.; Westeppe, U. *Chem. Ber.* **1988**, *121*, 27-32. (b) Raston, C. L.; Salem, G. *J. Chem. Soc., Chem. Commun.* **1984**, 1702-1703. (c) Harvey, S.; Junk, P. C.; Raston, C. L.; Salem, G. *J. Org. Chem.* **1988**, *53*, 3134-3140. (d) Velian, A.; Cummins, C. C. *J. Am. Chem. Soc.* **2012**, *134*, 13978-13981.
- (11) For reducing ability of **1** toward metal reagents, see; (a) Bönnemann, H.; Bogdanović, B.; Brinkmann, R.; He, D.-W.; Spliethoff, B. *Angew. Chem., Int. Ed.* **1983**, *22*, 728. (b) Scholz, J.; Thiele, K.-H.; *J. Organomet. Chem.* **1986**, *314*, 7-11. (c) Stanger, A.; Vollhardt, K. P. C. *Organometallics* **1992**, *11*, 317-320. (d) Aleandri, L. E.; Bogdanović, B.; Dürr, C.; Hockett, S. C.; Jones, D. J.; Kolb, U.; Lagarden, M.; Rozière, J.; Wilczok, U. *Chem. Eur. J.* **1997**, *3*, 1710-1718. (e) Hatnean, J. A.; Beck, R.; Borrelli, J. D.; Johnson, S. A. *Organometallics* **2010**, *29*, 6077-6091.
- (12) For a large-scale preparation of **1**, see; Transue, W. J.; Velian, A.; Nava, M.; García-Iriepa, C.; Temprado, M.; Cummins, C. C. *J. Am. Chem. Soc.* **2017**, *139*, 10822-10831.
- (13) Schneider, J. J.; Wolf, D.; Denninger, U.; Goddard, R.; Krüger, C. *J. Organometallic Chem.* **1999**, *579*, 139-146.
- (14) (a) Cornella, J.; Gómez-Bengoa, E.; Martin, R. *J. Am. Chem. Soc.* **2013**, *135*, 1997-2009. (b) Uthayopas, C.; Surawatanawong, P. *Dalton. Trans.* **2019**, *48*, 7817-7827.
- (15) The first report of Kumada-Tamao-Corriu-type coupling of aryl ethers; Wenkert, E.; Michelotti, E. L.; Swindell, C. S. *J. Am. Chem. Soc.* **1979**, *101*, 2246-2247.
- (16) Recent reports of Kumada-Tamao-Corriu-type coupling of aryl ethers; (a) Ambre, R.; Yang, H.; Chen, W.-C.; Yap, G. P. A.; Jurca, T.; Ong, T.-G. *Eur. J. Inorg. Chem.* **2019**, 3511-3517. (b) Ghorai, D.; Loup, J.; Zannoni, G.; Ackermann, L. *Synlett* **2019**, *30*, 429-432. (c) Yang, Z.-K.; Xu, N.-X.; Takita, R.; Muranaka, A.; Wang, C.; Uchiyama, M. *Nat. Commun.* **2018**, *9*, 1587. (d) Wang, T.-H.; Ambre, R.; Wang, Q.; Lee, W.-C.; Wang, P.-C.; Liu, Y.; Zhao, L.; Ong, T.-G. *ACS Catal.* **2018**, *8*, 11368-11376. (e) Harkness, G. J.; Clarke, M. L. *Catal. Sci. Technol.* **2018**, *8*, 328-334.
- (17) (a) Ogawa, H.; Minami, H.; Ozaki, T.; Komagawa, S.; Wang, C.; Uchiyama, M. *Chem. Eur. J.* **2015**, *21*, 13904-13908. (b) Kojima, K.; Yang, Z.-K.; Wang, C.; Uchiyama, M. *Chem. Pharm. Bull.* **2017**, *65*, 862-868.
- (18) Details of calculations are described in Experimental section.

- (19) Huang, K.-L.; Zou, J.-H.; Liu, J.-Z.; Jin, G.; Li, J.-B.; Yao, S.-L.; Peng, J.-B.; Cao, Y.; Zhu, X.-H. *Org. Electron.* **2018**, *58*, 139-144.
- (20) Transue, W. J.; Velian, A.; Nava, M.; Iriepa, C.-G.; Temprado, M.; Cummins, C. C. *J. Am. Chem. Soc.* **2017**, *139*, 10822-10831.
- (21) Ramakrishna, J.; Karunakaran, L.; Paneer, S. V. K.; Chennamkulam, A. M.; Subramanian, V.; Dutta, S.; Venkatakrishnan, P. *Eur. J. Org. Chem.* **2020**, 662-673.
- (22) Gaussian 16, Revision C.01, M. J. Frisch, G. W. Trucks, H. B. Schlegel, G. E. Scuseria, M. A. Robb, J. R. Cheeseman, G. Scalmani, V. Barone, G. A. Petersson, H. Nakatsuji, X. Li, M. Caricato, A. V. Marenich, J. Bloino, B. G. Janesko, R. Gomperts, B. Mennucci, H. P. Hratchian, J. V. Ortiz, A. F. Izmaylov, J. L. Sonnenberg, D. Williams-Young, F. Ding, F. Lipparini, F. Egidi, J. Goings, B. Peng, A. Petrone, T. Henderson, D. Ranasinghe, V. G. Zakrzewski, J. Gao, N. Rega, G. Zheng, W. Liang, M. Hada, M. Ehara, K. Toyota, R. Fukuda, J. Hasegawa, M. Ishida, T. Nakajima, Y. Honda, O. Kitao, H. Nakai, T. Vreven, K. Throssell, J. A. Montgomery, Jr., J. E. Peralta, F. Ogliaro, M. J. Bearpark, J. J. Heyd, E. N. Brothers, K. N. Kudin, V. N. Staroverov, T. A. Keith, R. Kobayashi, J. Normand, K. Raghavachari, A. P. Rendell, J. C. Burant, S. S. Iyengar, J. Tomasi, M. Cossi, J. M. Millam, M. Klene, C. Adamo, R. Cammi, J. W. Ochterski, R. L. Martin, K. Morokuma, O. Farkas, J. B. Foresman, and D. J. Fox, Gaussian, Inc., Wallingford CT, 2019.
- (23) Zhao, Y.; Truhlar, D. G. *Theor. Chem. Account* **2008**, *120*, 215–241.
- (24) Cancès, E.; Mennucci, B.; Tomasi, J. *J. Chem. Phys.* **1997**, *107*, 3032-3041.
- (25) Global Reaction Route Mapping (GRRM) Program Version 17-A01, Produced by Satoshi Maeda, Yu Harabuchi, Yosuke Sumiya, Makito Takagi, Kimichi Suzuki, Kanami Sugiyama, Yuriko Ono, Miho Hatanaka, Yuto Osada, Tetsuya Taketsugu, Keiji Morokuma, Koichi Ohno.
- (26) CYLview20; Legault, C. Y., Université de Sherbrooke, 2020 (<http://www.cylview.org>).

Publications

- (1) Rawat, V. K.; Higashida, K.; Sawamura M. *Adv. Synth. Catal.*, **2021**, *363*, 1631-1637.
- (2) Rawat, V. K.; Higashida, K.; Sawamura M. *ACS Catal.*, **2022**, *12*, 8325-8330.
- (3) Rawat, V. K.; Higashida, K.; Sawamura M. *Synthesis*, **2021**, *53*, 3397-3403.

Acknowledgement

I genuinely deliberate my enormous dignity and the broad sensation of honour towards my project guide Prof. Masaya Sawamura and Dr. Kosuke Higashida. Their outstanding direction consequences in the form of fruitful works. I am incredibly blessed to get a teacher alike them towards the work liberty they have granted to me throughout the project. I am immensely appreciative towards them to me and wish to have the moment and thank to them from core of my heart for conferring me towards the organometallic catalysis subject and moral beliefs of life.

I also appetite to have the moment to deliberate my genuine gratitude towards my labmates and other staffs in the lab (Dr. Yohei Shimizu and Dr. Yusuke Masuda) for their constant guidance and beneficial suggestions all over the project regime. I am also explicit acknowledgement headed for JICA (Japan International Cooperation Agency) for their sponsorship throughout my doctoral research by providing financial assistance and research grant aid.

At the end, I explicit honour towards my parents and family members for their constant affection and assistance for in pursuance something phenomenal in my life.